In Vitro and In Vivo Activities of *Allium*-derived Alk(en)ylmercaptocysteines

by

Bryan Quoc Le

A dissertation submitted in partial fulfillment of

the requirements for the degree of

Doctor of Philosophy

(Food Science)

at the

University of Wisconsin-Madison

2020

Date of final oral examination: 8/12/2020

The dissertation is approved by the following members of the Final Oral Committee:

Kirk L. Parkin, Professor, Food Science

Bradley W. Bolling, Associate Professor, Food Science

Jan Peter van Pijkeren, Associate Professor, Food Science

Judith Burstyn, Professor, Chemistry

In Vitro and In Vivo Activities of *Allium*-derived Alk(en)ylmercaptocysteines

Bryan Quoc Le

Under the supervision of Professor Kirk L. Parkin and Professor Bradley W. Bolling

At the University of Wisconsin-Madison

Consumption of *Allium* vegetables has been demonstrated to reduce inflammation and oxidative stress, and their healthful properties are associated with their metabolism to hydrogen sulfide (H_2S). This dissertation was carried out with the goal of evaluating the H_2S-releasing potential related to the biological effects of *Allium*-derived mercaptocysteines (CySSR). Additional goals of this dissertation were to investigate the biological mechanisms of action for the anti-inflammatory properties of CySSR and the effect of onion-derived *S*-1-propenylmercaptocysteine (CySSPe) on an obese mouse model.

CySSA (*S*-allylmercaptocysteine) and CySSPe were found to produce hydrogen sulfide (H_2S) when reacted with cysteine or glutathione (GSH), with CySSPe generating 10-fold higher levels of H_2S compared to CySSA when reacted with GSH *in chemico*. Inhibition of H_2S-evolving enzymes cystathionine β-synthase (CBS) and cystathionine γ-lyase (CSE) in macrophage cells reduced H_2S output (15% and 31%, respectively) following CySSPe treatment. GSH depletion in macrophage cells resulted in a 36% reduction in H_2S after CySSPe treatment.

Nrf2 was found to be upregulated by CySSR in LPS-activated macrophage cells in a time and dose-dependent manner. Furthermore, CySSPe treatment induced the upregulation of cysteine glutamate ligase (CGL) and glutathione-S-transferase P (GSTP) protein expression, whereas CySSA treatment induced heme oxygenase 1 (HO-1) upregulation. Nrf2 silencing by

small interference RNA (siRNA) reversed CySSR-mediated inhibition of nitric oxide (NO) output.

NO production in activated macrophage cells was suppressed by CySSPe and CySSA through inhibition of the IKK signaling pathway (100% and 93% relative effect, respectively). CySSPe exhibited a reduction in NO output through the p38 signaling pathway (67% relative to IKK). The TAK1 signaling pathway was not a major contributor to the CySSR-dependent suppression of NO output by RAW 264.7 cells.

CySSPe treatment of obese mice resulted in a reduction in liver triglycerides, increased total hepatic GSH, and suppressed elevated levels of pro-inflammatory cytokines IL-6, IL-1β, and TNF-α in the liver, and IL-6 and TNF-α in the plasma. However, treatment with CySSPe did not exhibit changes to liver enzyme function, cholesterol profile, adipokine levels, or morphometric measurements. Overall, CySSPe exhibited some protection against obesity-associated inflammation in mice possibly through the transient formation of persulfides and release of H_2S.

Acknowledgements

I would like to take this opportunity to express my gratitude to the many people who provided me the support and opportunity to complete my PhD studies here at the University of Wisconsin-Madison.

My Ph.D. adviser Prof. Kirk Parkin for his ongoing encouragement and guidance for all these years during my studies. I am grateful he provided me the opportunity to complete my degree under his supervision.

My Ph.D. committee members, Prof. Jan-Peter van Pjikeren, Prof. Brad Bolling, and Prof. Judith Burstyn for their thoughts, suggestions and direction, and for allowing me to use their laboratory space, equipment, and supplies.

Special thanks to Dr. Restituto Tocmo, for helping me learn all the techniques and protocols, providing me suggestions, and for the interesting discussions. I would also like to acknowledge members of the Bolling Lab, Dr. Derek Martin, Dr. Ruisong Pei, Matthew Dorris, Junhyo Cho, Jonathan Valdez, Kelley Putt, Xiaocao (Grace) Liu, Serena Wu, for their kindness, friendship, and willingness to listen to my presentations. I would like to acknowledge members of the van Pijkeren Lab, Dr. Jee-Hwan Oh and Laura Alexander, for their help and support with the animal studies. I would also like to thank Dr. Martha Vestling for her help on mass spectrometry analysis and Dr. Heike Hofstetter on NMR spectroscopy.

I would like to thank my mother, father, and sister, and who always encouraged me to strive for academic and professional excellence. I would also like to thank my parents-in-law for their ongoing encouragement. And I would like to especially acknowledge the support and encouragement of my wife, Yvonne Le, who has always been there for me during my Ph.D. studies.

Table of Contents

List of Figures

List of Equations

List of Tables

Chapter 1

Literature Review

1.1 Introduction

Dietary modification is a potential strategy to prevent the pathogenesis of chronic lifestyle diseases such as breast (1,3), colorectal (2,3) and prostate cancers (4), obesity (5,6), diabetes (7,8), and cardiovascular diseases (9-11). It is estimated that a third of all cancer deaths could be prevented through dietary intervention (12). Indeed, there is increasing epidemiological evidence that the consumption of fruits and vegetables leads to reduced risk of these chronic diseases. In a review of approximately 200 studies that examined the impact of fruit and vegetable consumption on lung, colon, breast, stomach, pancreas, and other cancers, a statistically significant protective effect was found (13). Additionally, frequency of fruit and vegetable intake is inversely associated with cardiovascular risk, possibly due to their low energy density and the synergistic effects of nutrients from whole fruit and vegetables (14). An analysis of data from the Canadian Community Health Survey revealed a significant and negative association between BMI and fruit and vegetable consumption (15). Moreover, results from an analysis of data from the Nurses' Health Study and the Health Professionals' Follow-Up Study (HPFS) over 10 years showed a protective relationship between fruit and vegetable intake against risk of ischemic stroke, especially cruciferous and green leafy vegetables (16). Increased consumption of plant-based foods may be an effective strategy for reducing the incidence of these diseases.

Phytochemicals are non-nutritive substances in fruit and vegetable tissue that confer health-protective benefits in humans and include phenolics, vitamins, alkaloids, phytosterols, carotenoids, and organosulfur compounds. The mechanisms by which these phytochemicals affect biological systems are varied and dependent on the cellular and molecular events underlying the progression of each disease. Phytochemicals can affect relevant physiological

processes by serving as substrates for biochemical reactions, inhibitors of enzymatic reactions, sequestrants of toxic compounds, ligands for cell surface receptors, conjugation substrates with key molecular elements, and activators of transcription factors (17). Additional mechanisms include scavenging of radical oxygen species (ROS) and modification of redox status through activation of transcriptional factors involved in these processes (18). Many phytochemicals exhibit a combination of these mechanisms which can work in concert, and the synergistic effects between phytochemicals are well-documented (19, 20).

Organosulfur compounds are largely found in a subset of vegetables that include members of *Brassica* and *Allium*. Many organosulfur compounds are the product of rapid enzyme-driven reactions that normally serve to defend plant tissue against herbivores, microorganisms, and parasites. For example, disrupted broccoli (*Brassica oleracea*) tissues enzymatically generate isothiocyanates, which have a repellant effect against pests. Similarly, when garlic (*Allium sativum*) tissue is disrupted, the relatively potent antimicrobial and irritating organosulfur derivative, allicin, is rapidly released and protects the plant against bacteria, molds, viruses, parasites, and animals (21). While toxic and irritating to other organisms, these organosulfur compounds are the primary source of flavor for these vegetables and their consumption by humans is common. Additionally, the healthful properties of these vegetables are largely tied to the production of the unique organosulfur molecules generated during raw tissue maceration, such as during chewing, chopping, or crushing. The biological properties of the organosulfur compounds produced by *Allium* vegetables, specifically cysteine conjugated derivatives, will be explored in this dissertation.

1.2 Allium Vegetables

While most *Allium* plants have little to no economic significance, the edible *Allium* vegetables that include onion, garlic, chives, leeks, and shallots are highly recognized and used as food. Onions and garlic are the most consumed *Allium* vegetable in the United States, with the horticultural production of onions second only to tomatoes globally (22). Historically, garlic and onion have been used worldwide as a traditional medicinal herb to treat a wide range of diseases and conditions (23). Garlic and onion have been employed to treat bacterial, viral, fungal, and parasitic infections, hypertension, bronchitis, poor digestion, fevers, and fatigue. Studies have shown that dietary consumption of these *Allium* vegetables leads to a decreased incidence of a variety of disease states, including gastric, prostate, and lung cancers (24-26), cardiovascular disease (27-29), and chronic kidney disease (29).

The beneficial properties exhibited by *Allium* vegetables are derived from the organosulfur compounds generated from bruised or cut tissues through an enzymatically-driven process (30). The enzyme involved in these rapid chemical reactions is alliinase, which is found in all *Allium* vegetables sequestered in bundle sheath cells. Alliinase acts on a class of non-proteinogenic amino acids known as cysteine sulfoxides, which are found in mesophyll cells separated from the enzyme and are combined following tissue injury. The products of the reaction are alk(en)ylsulfenic acids, which quickly self-condense and dehydrate to form a mixture of symmetrical and asymmetrical thiosulfinates. Thiosulfinates are relatively unstable organosulfur compounds that readily break down to form a wide variety of secondary products, including disulfides, trisulfides, sulfines, ajoene, zweibelanes, and other sulfur-containing derivatives (30-36).

1.3 Allium-Derived Organosulfur Compounds

Sulfur is largely absorbed and metabolized by *Alliums* in the form of sulfates found in the soil (37). Through $^{35}SO_4^{2-}$ labeled studies, it was found that inorganic sulfate is first assimilated in plants through reduction to inorganic sulfide, then converted to cysteine in the chloroplasts. The cysteine is subsequently converted to γ-glutamylcysteine, which undergoes alkylation with various substrates and oxidase-catalyzed oxidation to form alkyl or alk(en)yl derivatives (30). The γ-glutamylcysteine is cleaved by γ-glutamyl transpeptidase and generates the corresponding *S*-alk(en)yl-L-cysteine sulfoxide (ACSO) derivative.

1.3.1 *S*-Alk(en)yl-L-Cysteine Sulfoxides

Cysteine sulfoxides are non-proteinogenic amino acids found abundantly in the cytoplasm of *Allium* vegetable cells. ACSO are the main source of sulfur in these plants and are largely responsible for the wide variety of organosulfur compounds generated from *Alliums*. *Allium* spp. are composed of between 1 – 5% dry weight of these sulfur-containing ACSOs (30). The four main ACSOs found abundantly in *Allium* spp. are *S*-methyl-, *S*-propyl-, *S*-allyl-, and *S*-(*E*)-1-propenyl-L-cysteine *S*-oxides, with some minor amounts of *S*-ethyl-L-cysteine *S*-oxides (30,38). Garlic contains approximately 300 to 500 mg ACSO/100 g tissue, while onion contains less ACSO at 100 to 200 mg ACSO/100 g tissue (38). The cysteine sulfoxide derivative structures and corresponding concentrations vary widely range across *Allium* vegetables. Seasonal variation and climate similarly affect cysteine sulfoxide composition, with colder climates reducing levels of *S*-methyl cysteine sulfoxide (MCSO) (30). Saturated alkyl-derivatives MCSO and *S*-propyl cysteine sulfoxide (PCSO) are found at lower concentrations compared to unsaturated cysteine sulfoxides in nearly all *Allium* vegetables. *S*-allyl cysteine sulfoxide (2-PeCSO) is the major cysteine sulfoxide found in garlic, whereas *S*-*trans*-1-propenyl

cysteine sulfoxide (1-PeCSO) is largely found in onion. Garlic has been reported to contain 305 mg 2-PeCSO/100 g tissue and onion 98 to 131 mg 1-PeCSO/100g tissue (38).

1.3.2 Alliinase Enzyme Activity

Alliin lyase (EC 4.4.1.4.) is a pyridoxal 5'-phosphate dependent enzyme responsible for the degradation of ACSO and was first identified by Stoll and Seebeck in 1951 (39). Alliin lyase, or alliinase, cleaves ACSO amino acids to form an alk(en)ylsulfenic acid and ammonium pyruvate as products. Garlic tissue soluble protein is composed of nearly 10% alliinase while the total soluble protein in onion tissues is composed of 6% onion alliinase. The alliinase isoform found in garlic is a dimer composed of two 51.5 kDa glycoprotein subunits with 6% carbohydrate composition (40).

Alliinase enzymes exhibit differential activities across the *Allium* genus. The alliinase isoform from garlic exhibits a pH optimum of 6.5 (40). The alliinase found in onion tissue has a mass of 51.2 kD and maximal activity at pH 7.4-8.8 depending on substrate, with high specificity for S-propyl-cysteine sulfoxide (41,42). 2-PeCSO and MCSO were degraded by the onion alliinase at a lower rate. Onion alliinase was more recently shown to act most preferentially on 1-PeCSO, followed by 2-PeCSO, ECSO, and MCSO (43). Alliinase levels differ markedly based on time spent in post-harvest storage and source of garlic, which modulates the level of organosulfur compounds generated during the enzymatic action on cysteine sulfoxides. High concentrations of reaction product reversibly inhibit alliinase activity (40). Alliinase is irreversibly inactivated at pH 3 or below, which includes the acidic environment of the stomach, and above pH 9 (30). As such, organosulfur products of alliinase activity are not produced in the body after consumption but must be produced exogenously prior to consumption, unless *Allium*

tissue materials are enterically coated in commercial supplement products to protect the alliinase enzyme from the acidic conditions of the stomach.

1.3.3 Thiosulfinates and Their Properties

Intact cloves and bulbs from *Alliums* do not contain the volatile organosulfur compounds responsible for the flavor, pungency, and bioactivity exhibited by these vegetables. Sulfenic acids are unstable products formed from the action of alliinase on cysteine sulfoxides upon tissue disruption. The structural R-groups found on the cysteine sulfoxides determine the structure of the sulfenic acid and their properties. All sulfenic acids readily condense to form thiosulfinates and water. Sulfenic acids bearing the same structural groups ($R_1 = R_2$) will form homologous thiosulfinates, whereas sulfenic acids of different structural groups ($R_1 \neq R_2$) form heterologous thiosulfinates, a property that has been previously exploited to capture and trap unstable sulfenic acids **(Fig. 1.1)** (44).

Allylsulfenic acid is the main product of alliinase on garlic-derived ACSO and will quickly condense to form diallyl thiosulfinate, or allicin. Allicin is the major thiosulfinate of garlic and has been extensively studied for its biological properties both *in vivo* and *in vitro*. The reported amount of allicin in fresh, raw garlic preparations is 3.1 mg/g (31). However, other minor heterologous thiosulfinates are simultaneously generated from this process due to the presence of some MCSO in garlic tissues, including the two heterologous isomeric allyl methyl thiosulfinates (R_1 = Allyl, R_2 = Methyl or R_1 = Methyl, R_2 = Allyl). Similar permutations are formed in other *Allium* vegetables due to the variety of cysteine sulfoxide derivatives found in varying concentrations in their tissues (30, 43).

The stability of thiosulfinates is a function of structure, pH, temperature, and the presence of biological material. Synthetic thiosulfinates in chemical media are relatively stable. The order

Figure 1.1. Chemical Structures of Thiosulfinates, *S*-Alk(en)ylmercaptocysteines, and *S*-Alk(en)ylmercaptoglutathiones (44).

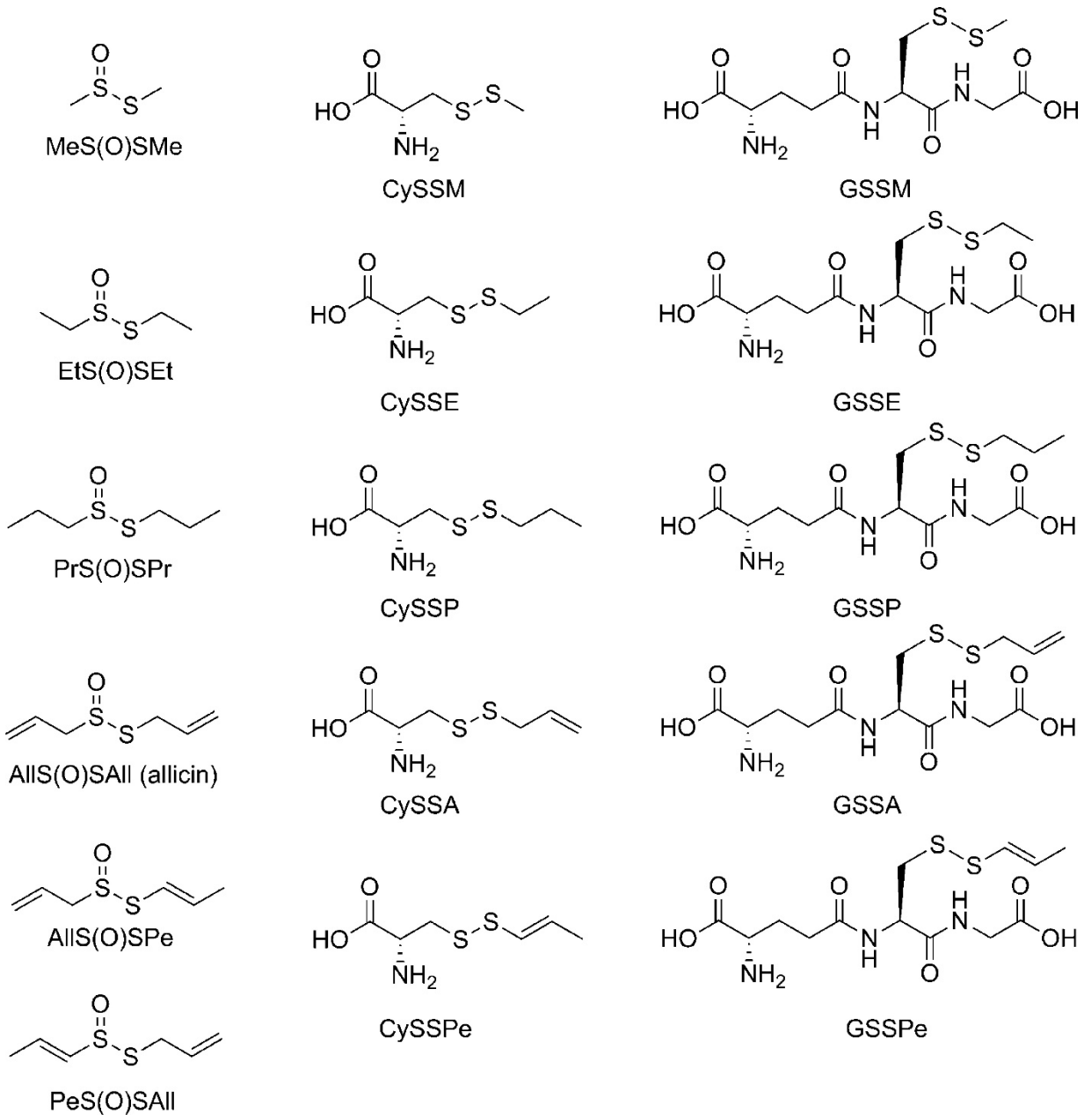

of stability for symmetrical thiosulfinates is propyl > ethyl > methyl > allyl (45). Thiosulfinates possessing saturated groups (methyl, ethyl, propyl) remain quite stable at room temperature and acidic pH levels between 1.2 and 5.5 in 0.1 M Tris buffer, with calculated half-lives of several months. Allyl-bearing thiosulfinates possess lower stability and have a half-life of approximately 3 to 7 weeks in the same conditions. However, the stability of thiosulfinates drops markedly with increasing pH, with neutral conditions leading to half-lives on the order of days and alkaline conditions leading to half-lives on the order of hours (45). At temperatures at and above 40 ºC, thiosulfinates are prone to rapid decomposition and decay within approximately 0.1 to 10 hours at 80 ºC (45). The mechanism by which thiosulfinates decompose in chemical environments is driven either by disproportionation into disulfide and thiosulfonate species or base-mediated hydrolysis (30, 45-47). Allicin is especially prone to cycloelimination reactions that generate allylic disulfides, trisulfides, ajoene, and vinyl dithiins (30). Base-mediated decomposition of thiosulfinates is induced by nucleophilic attack of hydroxyl groups on either sulfur group and produces the corresponding disulfide and sulfinate ions (45,47). Thiosulfinates are even less stable in disrupted *Allium* tissues, and readily generate organosulfur byproducts within hours of tissue maceration, which may be driven by the presence of endogenous thiols, enzymes, and other components (32).

Thiosulfinates are rapidly metabolized in blood and their presence is short lived *in vivo*. Allicin is not detectable after it is incubated in blood for 5 min (48). Allicin is even less stable in the blood cell fraction, where it is rapidly degraded after 3 minutes, whereas allicin is slowly degraded in the plasma fraction with an estimate half-life of 50 minutes, suggesting red blood cells are predominantly responsible for its quick degradation. Thiosulfinates are lipid soluble and can freely transverse the cell membrane into the cytoplasm, where they react with intracellular

cysteine and glutathione to form *S*-alk(en)ylmercaptocysteine and *S*-alk(en)ylmercaptoglutathione derivatives (Figure 1.1) (49,50). The conjugation reaction is pH dependent, with increasing pH correlated with increased formation of the mercapto product (50). One mechanism of action by which thiosulfinates affect biological systems is through covalent modification of functional sulfhydryl groups found in proteins involved in cell signaling or biocatalysis. Physiologically relevant proteins possessing free thiol residues can be inhibited through reaction with thiosulfinates. Rabinov et al. tested this property by incubating allicin with papain, a protease possessing a cysteine residue within its active site at residue position 25 and required for its proteolytic properties (51). Allicin has been shown to react to free thiol groups in the whey protein β-lactoglobulin and form a stable allylmercapto adduct at Cys^{121} (52,53). More recently, a global analysis of allicin-induced protein modifications in *Escherichia coli* was shown to occur in 73 individual proteins and generate *S*-allylmercapto-modified cysteine residues with inhibition of multiple enzymes (54). In human Jurkat cells, allicin modifies 332 proteins in the cell proteome, disrupting cytoskeletal elements tubulin, actin, cofilin, and filamin, heat shock proteins, and several glycolytic enzymes (55).

While nearly all other sulfenic acids can condense to form thiosulfinates, thiosulfinates bearing 1-propenyl groups are challenging to generate and isolate due to their greater instability compared to other thiosulfinates. The dominant cysteine sulfoxide found in onion, 1-PeCSO, undergoes an additional enzymatic reaction unique to onion and some other *Alliums*. 1-PeCSO is first cleaved to form the corresponding 1-propenylsulfenic acid through the action of alliinase, followed by rapid conversion to propanethial *S*-oxide (PTSO) via the lachrymatory factor synthase (LFS) activity found endogenously in onion tissues (56). The remaining 1-propenylsulfenic acid can either self-condense to form the di-1-propenyl thiosulfinate, which

rapidly undergoes electrocyclic rearrangement to generate zwiebelanes and other cyclic derivatives, or condense with other sulfenic acids, including garlic-derived allyl and methyl sulfenic acids, to generate heterologous thiosulfinates (31,36,43). While 1-propenyl thiosulfinates and other 1-propenyl-containing analogues make up 45% of all organosulfur species generated from crushed onion, the previously mentioned competing reactions rearrange most of these groups to other molecular species that lack the 1-propenyl moiety (31).

Onions genetically silenced for LFS are unable to convert the 1-propenylsulfenic to PTSO, and instead generate a surplus pool of 1-propenylsulfenic acid molecules (57). Two molecules of 1-propenylsulfenic first condense to form the transient di-1-propenyl thiosulfinate, which rapidly converts to 5,6-dimethyl-2-oxa-3,7-dithiabicycloheptane. An additional 1-propenylsulfenic acid further condenses with the compound to produce the novel asymmetric thiosulfinate, cepathiolane, as the dominant product. Cepathiolanes exhibit similar bioactivity to other thiosulfinates and inhibit COX-1 and α-glucosidase activity. However, their reactivity with reduced thiols and thiol-bearing proteins has not yet been explored.

1.3.4 *S*-Alk(en)ylmercaptocysteines

The rapid metabolism of allicin, with a half-life of less than 1 min, suggests thiosulfinates are not the major biologically relevant species that contribute to the healthful properties of *Allium* species (48,58,59). Thiosulfinates can react with endogenous sulhydryl moieties such as cysteine, glutathione, coenzyme A, lipoic acid, and thiol-containing proteins in the cell to form mercapto-derivatives (60). The reaction of allicin with cysteine was first described by Cavallito and co-workers in 1944 (61). When combined with cysteine or cysteine-bearing compounds, other thiosulfinates have been shown to produce *S*-alk(en)ylmercaptocysteines (CySSR) and their corresponding derivatives (44,50). For example,

when allicin is reacted with the main intracellular antioxidant glutathione, present at high concentrations of 2-10 mM, the product formed is *S*-allylmercaptoglutathione (GSSA) (50).

Mercaptocysteines exhibit several healthful properties reminiscent of their thiosulfinate precursors, including anti-inflammation (62-64), anti-oxidation (50,62,65-68), and anticarcinogenesis (69-73). The majority of these studies on mercaptocysteines have focused on the garlic-derived CySSA due to its ease of synthesis and stability. Mercaptocysteines exert their biological effects through multiple potential mechanisms. CySSA modifies reduced sulfhydryl groups through thiol-disulfide exchange to form the allylmercapto moiety in a similar fashion as allicin (50). Enzymes papain and alcohol dehydrogenase, which possess sulfhydryl groups in their active sites, exhibit inhibited enzymatic activity after incubation with CySSA. However, while other saturated mercaptocysteine derivatives have similar thiol-disulfide exchange properties, the unsaturated homologues CySSA and CySSPe possess more potent bioactivities compared to these saturated analogues (62,63,68), which suggests there are other mechanisms by which these mercaptocysteines exert their bioactivities that involve their unsaturated R-groups. Additionally, these biological properties occur at the micromolar range in vitro, whereas cytosolic glutathione concentration is ten- to one hundred-fold higher. Thiolation by mercaptocysteines, as the only mechanism of action, would be transient in cellular systems, as thiolated enzymes would be quickly restored to their active form in the presence of endogenous glutathione.

To date, few studies have been conducted to investigate the bioactive potential of the onion-derived CySSPe. Studies investigating the bioactivity of CySSPe have shown CySSPe is more potent than all other mercaptocysteines (62,63,68,72,73). One reason behind the paucity of experimental data regarding the activity of CySSPe in comparison to its isomer, CySSA, is due

to the challenge of isolating its precursors, the 1-propenyl sulfenic acid and thiosulfinate derivatives. As previously mentioned, 1-propenyl sulfenic acid is rapidly exhausted from onion tissue samples through conversion into syn-propanethiol-S-oxide, the lachrymatory factor of onions, via lachrymatory factor synthase while the homologous di-1-propenyl thiosulfinate rapidly cyclizes to form zwiebelanes and related cyclic species (30). Our laboratory has developed an enriched tissue method for generating and isolating CySSPe by trapping and stabilizing the 1-propenyl sulfenic acid in an asymmetric thiosulfinate through the co-generation of allyl sulfenic acid from garlic tissues, and subsequent reaction with cysteine to produce the desired compound (44). The facile preparation of CySSPe has opened the opportunity to study this elusive derivative in greater detail.

1.4 Properties and Health Benefits of *S*-Alk(en)ylmercaptocysteines

1.4.1 Metabolism

Mercaptocysteines have several potential metabolic fates. If the mercaptocysteines are absorbed into the bloodstream following digestion of thiosulfinates with thiol-rich proteins or generated in the extracellular space as a result of conjugation of absorbed thiosulfinates with endogenous thiols in blood, they are imported into cells via the system L neutral amino acid transporter (74). Following uptake, RAW 264.7 macrophage cells treated with garlic-derived CySSA dose-dependently release free thiol allyl mercaptan for up to 3 hours (62). Glutaredoxin (Grx) has previously been shown to be involved in the catalytic reduction of disulfide bonds involving glutathione conjugates (62,75). When cells were pre-treated with cadmium chloride, a specific inhibitor of Grx, it was found that thiol generation from CySSA was inhibited (62).

CySSA has been shown to be rapidly metabolized under several biological conditions. CySSA possesses a half-life of 3 minutes in whole blood and generates allyl mercaptan nearly

stoichiometrically (62). In human subjects, CySSA is metabolized to allyl methyl sulfide (AMS), with a maximum metabolite concentration reached at 3.3 ± 1.1 hours and time at which half the maximum concentration remains at 8.8 ± 0.7 hours after consumption (76). AMS is further metabolized by liver cytochrome P450 enzymes to allyl methyl sulfoxide and allyl methyl sulfone, and detectable in rat plasma and liver tissues (77). A pharmacokinetic study of CySSA in male rats demonstrated that CySSA had a mean residence time of 4.36 minutes and half-life of 3.81 minutes after being injected into the rats at a concentration of 25 mg/kg (78).

β-Lyase reactions are another potential pathway by which mercaptocysteines are metabolized. Studies investigating the direct enzymatic transformation of mercaptocysteine derivatives revealed that these compounds are substrates of glutamine transaminase K (GTK), L-amino acid oxidase, cystathionine β-synthase (CBS) and cystathionine γ-lyase (CSE) (79). The bulk of activity on mercaptocysteines in rat-liver cytosol is through CSE, and inhibition of CSE with propargylglycine results in diminished β-lyase activity towards derivatives CySSA, *S*-propylmercapto-L-cysteine, and *S*-penta-1,3-dienylmercapto-L-cysteine. Other studies have shown purified CSE from rat liver does not act on methyl or ethyl-containing mercaptocysteine derivatives, but only cysteine conjugates with alk(en)yl leaving group moeity larger than two carbons (79,80).

Both CBS and CSE are involved in the generation of persulfides by effectively catalyzing β-elimination reactions from cystine to form cysteine hydropersulfide (CySSH) (81). Persulfides are highly reactive sulfur intermediates that are especially nucleophilic, reducing, and demonstrate high redox activity. As mercaptocysteines are disulfides that act as substrates for CBS and CSE, the bioactivity of mercaptocysteines may be mediated by their enzymatic conversion to the corresponding alk(en)yl persulfide. Murine hepatocytes treated with μM doses

of CySSPe showed elevated levels of the persulfidated form of the thiol-bearing transcriptional regulator Keap1, suggesting CySSPe is metabolized to a persulfide derivative that rapidly exchanges with the thiols attached to Keap1 **(Fig. 1.2)** (68). Additionally, the levels of hydrogen sulfide (H_2S), a metabolic byproduct of persulfide exchange, were elevated when hepatocytes were treated with CySSPe. These elevated H_2S levels were diminished when the cells were pretreated with either the CSE inhibitor, propargylglycine, or CBS inhibitor, aminooxyacetic acid, which suggests these two enzymes are involved in the generation of H_2S from mercaptocysteines.

1.4.2 Inhibitory Properties

Mercaptocysteines can undergo thiol-disulfide exchange with thiol-bearing proteins with roles in redox signaling and metabolism. By modifying key thiols groups involved in catalysis or maintaining conformational structure, mercaptocysteines can inhibit physiological relevant proteins. Both CySSA and the allylic glutathione conjugate, GSSA, modify the sulfhydryl group in the $NADP^+$ binding site of papain and deactivate its proteolytic activity at Cys^{25} (51). After 2.5 hours of incubation with papain, 9 mM GSSA reduced enzymatic activity to 20%. Similarly, 2.9 mM GSSA incubated with alcohol dehydrogenase inhibited the enzyme 30% after 1 hour through binding with Cys^{203}. Studies investigating the effect of garlic-derived organosulfur compounds found that CySSA exhibited inhibitory activity against cholesterol synthesis in hepatocytes harvested from male Sprague-Dawley rats (82). The incorporation levels of acetate as a substrate of cholesterol synthesis in hepatocytes were measured using radioactively labeled sodium [2-^{14}C] acetate after 4 hours treatment with CySSA and [2-^{14}C] acetate incorporation was found to be inhibited by 7 to 17%. CySSA was also found to moderately inhibit histone deacetylase activity in murine erythroleukemia cells in the low

Figure 1.2. Putative persulfidation mechanism by CySSPe (68).

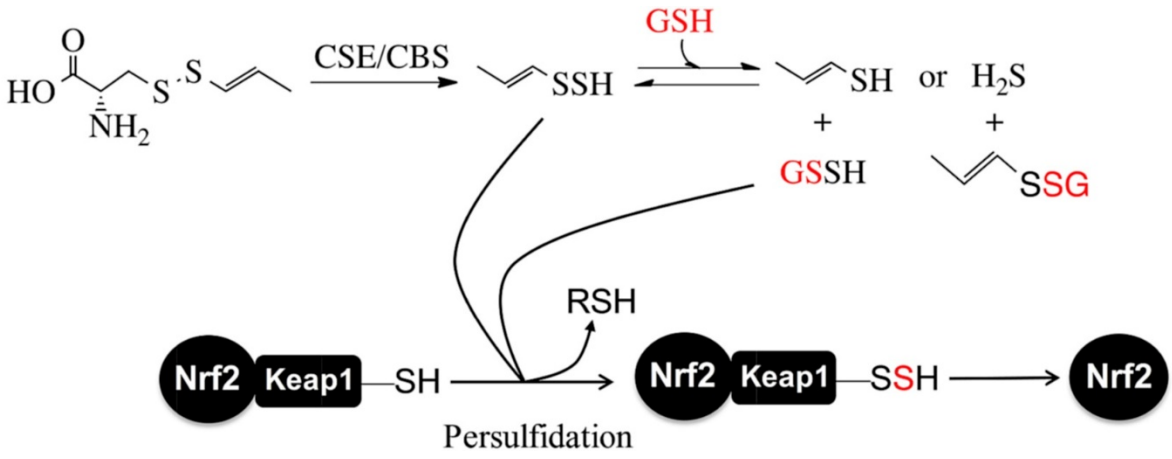

micromolar range (83).

1.4.3 Anti-Inflammation

Long-term inflammation is involved in the etiology of several chronic diseases, including cancer, obesity, and cardiovascular and gastrointestinal diseases (84). *Allium*-derived mercaptocysteines, especially CySSA and CySSPe, possess potent anti-inflammatory properties. Mercaptocysteines are *in vitro* inhibitors of pro-inflammatory cytokines and mediators, such as nitric oxide (NO), inducible nitric oxide synthase (iNOS), tumor necrosis factor α (TNF-α), interleukin 1β (IL-1β), and interleukin 6 (IL-6) in lipopolysaccharide (LPS)-activated RAW 264.7 murine macrophage cells (44,62,63). Additionally, mercaptocysteines CySSA and CySSPe modulate the nuclear factor-κB (NF-κB)-dependent inflammatory signaling pathway by inhibiting phosphorylation of key transcriptional regulatory enzyme complex IκB kinase α/β (IKKα/β) and downregulating the NF-κB p65 subunit. Furthermore, the protein expression of nuclear factor κB inhibitor α (IκBα), which sequesters NF-κB proteins in the cytosol and blocks transcriptional activation of the inflammatory response, is upregulated in the presence of CySSA and CySSPe (63). In these studies, it is important to note CySSPe exhibited more potent anti-inflammatory properties compared to CySSA and other prevalent *Allium* mercaptocysteines (methyl, ethyl, propyl).

Garlic-derived mercaptocysteine, CySSA, has been shown to exhibit anti-inflammatory effects *in vivo* as well. CySSA ameliorates acute lung injury induced with LPS by inhibiting the inflammatory response via NF-κB. CySSA at 10 to 60 mg/kg was administered intragastrically to mice 30 minutes after intra-tracheal LPS challenge, which alleviated histological changes such as inflammatory cell infiltration, interstitial and alveolar edema, and alveolar hemorrhage in the liver (85). Furthermore, CySSA treatment dose-dependently suppressed LPS-induced expression

of pro-inflammatory cytokines TNF-α, IL-1β, and IL-6, protein expression of inflammatory mediators iNOS, COX-2, NF-κB p65, and NF-κB phosphorylation, IκBα phosphorylation, and IκBα degradation. A study on the effects of intraperitoneal CySSA injection (single injection, 200 mg/kg) on a non-alcoholic fatty liver disease *in vivo* rat model reported CySSA treatment reduced TNF-α, IL-1β, iNOS, SOCS3, and COX-2 mRNA transcription and TNF-α, SOCS3, and IL-1β protein expression in rat liver tissue (86).

CySSA previously demonstrated protective effects against carbon tetrachloride (CCl_4)-induced inflammation in mice (87). Intraperitoneal injection of CySSA at 200 mg/kg (single injection) reduced TNF-α, IL-1β, iNOS, and COX-2 mRNA expression, and IL-1β and COX-2 protein expression. Additionally, NF-κB p50 and p65 activity was attenuated by CySSA treatment. CySSA treatment also reduced TNF-α, IL-1β, and IL-6 cytokine levels in mice co-treated with posaconazole, an antifungal with adverse intestinal inflammatory effects (88). While CySSA has been well-evaluated for its *in vivo* bioactivities, the anti-inflammatory properties of the onion-derived CySSPe have not yet been studied *in vivo*. It would be interesting to evaluate if the enhanced *in vitro* bioactivities previously observed for CySSPe translate to more potent anti-inflammatory effects in animal models of inflammation such as inflammatory bowel disease, Crohn's disease, rheumatoid arthritis, and obesity.

1.4.4 Anticarcinogenic Properties

Mercaptocysteines have shown apoptotic and anti-proliferative properties in several cancer cell lines, including breast, thyroid, colon, gastric, and gastric cancer cell lines (60,69-73,83,89-107). The action of CBS and CSE on mercaptocysteines generates reactive persulfides, which may act on redox-sensitive proteins involved in cytoprotective and anti-proliferative processes (60,81). Studies comparing synthetic S-cysteinyl analogues containing disulfide with

monosulfinic moieties showed that monosulfinic analogues possess marginal inhibitory effects against prostate carcinomas, and the bioactivity of mercaptocysteines was dependent on the existence of the disulfide bond (89). CySSA exhibits differential IC_{50} values ranging from 50-200 μM in gastric cancer (95), colon cancer (69,70), and erythroleukemia cell lines (91). Prostate cancer cell lines remain tolerant of elevated CySSA levels, retaining greater than 80% cell viability up to 300 μM (96). In human colon cancer cells, CySSA induces apoptosis by increasing caspase-3-like activity, which is accompanied by induction of c-Jun N-terminal kinase (JNK) activity, cell cycle arrest at G2/M, and a marked increase in glutathione (69,71). CySSA has been shown to inhibit cell migration and division in MCF-7 breast cancer cells by inducing cell cycle arrest at G0/G1 phase and triggering the mitochondrial apoptosis pathway through activation of Bax, caspase-9, and caspase-3 (99).

CySSA possesses antiproliferative effects and impedes polyamine synthesis of putrescine and spermine in human prostate carcinoma cells (LNCaP), most likely by reacting directly with the thiol found in Cys^{70} and Cys^{360} on ornithine decarboxylase (89). Furthermore, CySSA modulates the expression of androgen-responsive biomarkers, prostate specific antigen (PSA) and prostate specific membrane antigen (PSMA), in this carcinoma cell line, with PSA concentrations decreased compared to control while PSMA increased with CySSA treatment over 6 days (92). CySSA also enhanced testosterone catabolism over the 6-day incubation period in both LNCaP and androgen-independent PC-3 cell lines. Additionally, CySSA has been shown to act on PC-3 prostate cancer cells by inhibiting cancer cell invasion and motility through the restoration of E-cadherin expression (93) and suppresses PC-3 tumor growth *in vivo* (94).

Mercaptocysteines augment anticarcinogenic properties in combination with selenium, which also possesses potent chemopreventative properties (72,73). Synergistic combinations of

CySSA or CySSPe with selenite as a selenium source affect the phosphoinositide-3-kinase/protein kinase B (PI3K/Akt) signal transduction pathway involved in survival by inhibiting PI3K and reducing Akt levels, which reduced proliferation in MCF-7 cells (72). In estrogen receptor negative (ER^-) MDA breast cancer cell line, CySSR in combination with selenite increased levels of phosphorylated-JNK, the activated form of JNK and one of the signaling protein kinases involved in apoptotic events (73). The mechanism of this synergistic effect may involve the importing of mercaptocysteines into the cell, followed by subsequent β-elimination via CBS or CSE to persulfides that independently act on redox-sensitive proteins involved in apoptosis combined with glutaredoxin and thioredoxin reductase-dependent reduction of CySSR to free thiols. The reduced thiols are then exported out of the cell and can activate selenite by reducing the selenium compound to cytotoxic H_2Se (73).

1.4.5 Antioxidant Effects and Nrf2-Keap1 Upregulation

The cellular defense system against xenobioitics and oxidative stress involves the activation of the nuclear factor erythroid 2-related factor 2 (Nrf2) transcriptional signaling pathway (108). Nrf2 is normally inactivated in the cytosol by the action of repressor protein Kelch-like erythroid cell-derived protein 1 (Keap1) **(Fig. 1.3)**. Keap1 binds to Nrf2 to form the Keap1-Nrf2 complex and controls the level of Nrf2 present in the cytosol by promoting the ubiquination of Nrf2 via the ubiquitin proteasome pathway. Keap1 is a thiol-rich protein, with 27 cysteine residues in human Keap1. These thiol groups are highly sensitive to oxidative stress and can be modified by several electrophiles and oxidants. Five cysteine residues (C151, C257, C273, C288, and C297) serve a functional role by altering Keap1 conformation following modification (109). With the Keap1 repressor inactivated, newly synthesized Nrf2 proteins are free to translocate to the nucleus and bind to the antioxidant response element (ARE), which

Figure 1.3 Nrf2-Keap1 signaling pathway (109).

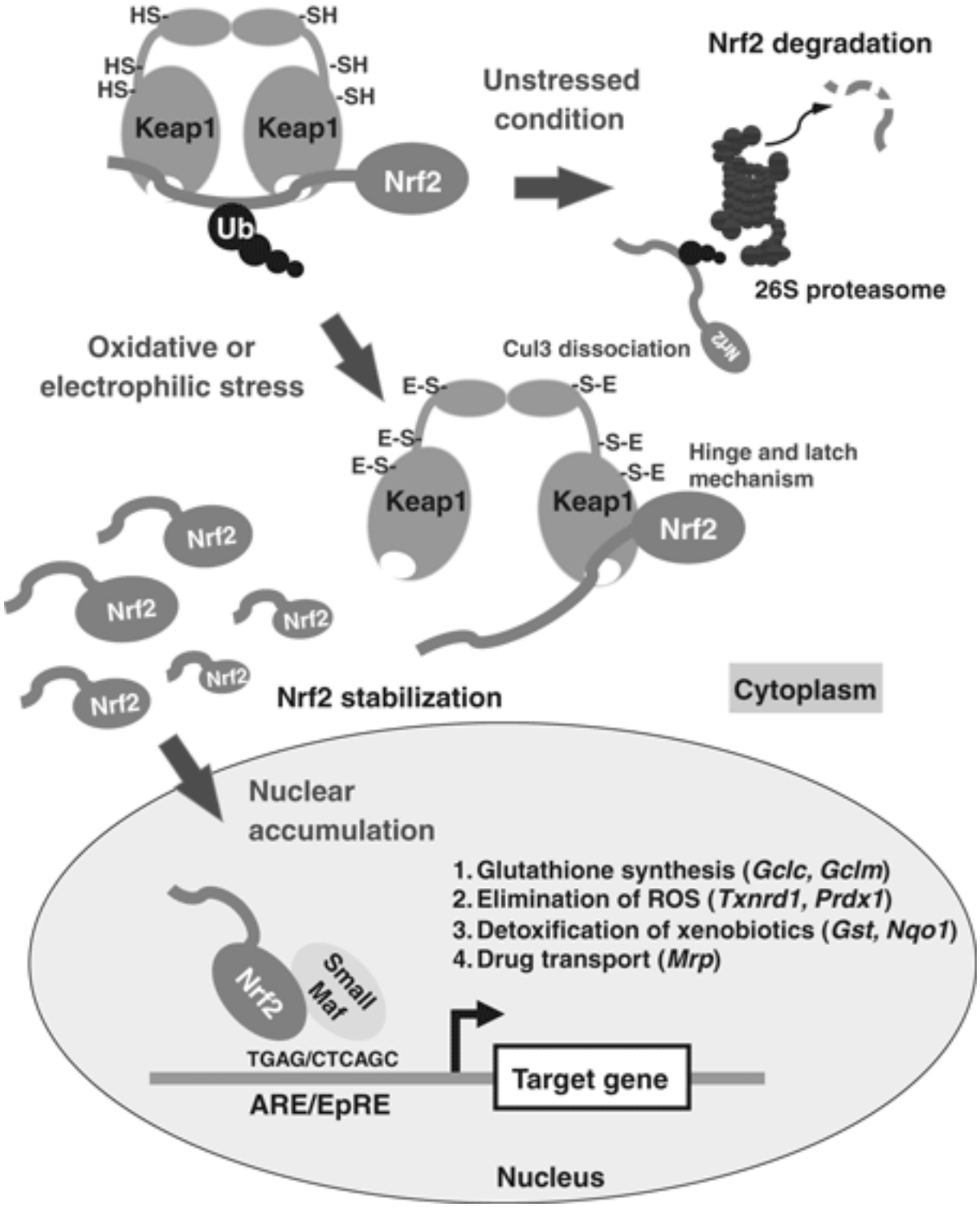

activates the expression of Nrf2-associated gene products including NAD(P)H quinone oxidoreductase 1 (NQO1), heme oxygenase 1 (HO-1), glutamate-cysteine ligase (GCL), and glutathione S transferase (GST). The production of glutathione (GSH), one of the primary endogenous antioxidants in cells, is enhanced by Nrf2 activation through the upregulation of GCL, as GCL is involved in the rate-limiting step of GSH biosynthesis.

CySSR has been shown to upregulate the expression of Nrf2 and its target genes *in vitro*. In previous studies, unsaturated mercaptocysteines CySSA and CySSPe enhanced NQO1 activity in Hepa1c1c7 murine hepatocytes (44,62,110) and CySSA and CySSPe also increased GCLc protein expression in RAW 264.7 macrophage cells (63). CySSPe was found to increase antioxidant proteins Nrf2, NQO1, HO-1, and GCL catalytic subunit (GCLc) in murine hepatocytes (68). The upregulation of NQO1 and HO-1 by CySSPe was found to be Nrf2-dependent, as pre-treatment of the hepatocytes with Nrf2 small interference RNA (siRNA) reduced protein expression of NQO1 and HO-1. CySSPe also exhibited potent antioxidant effects against oxidant tert-butyl hydroperoxide (t-BHP) and restored GSH levels and cell viability in murine hepatocytes following t-BHP challenge. Both CySSA and CySSPe enhanced intracellular cysteine and GSH levels, and quenched LPS-induced oxidative stress in macrophages (63). CySSPe treatment of the hepatocytes elevated levels of persulfidated Keap1. Persulfidation is a post-translational modification to thiol groups through the addition of a sulfhydryl group to the cysteine residue and is known to deactivate Keap1 (and subsequently activate Nrf2), which may be one of the mechanisms by which CySSPe exerts its antioxidant effects (68,111).

CySSA has been shown to exhibit antioxidant characteristics both *in vitro* and *in vivo.* CySSA previously demonstrated radical scavenging activity and reduced malondialdehyde

(MDA) concentration in t-BHP-induced lipid peroxidation of liver microsomes (66). GSSA, the GSH analogue of CySSA, has been shown to quench hydroxyl radical spin adducts and dose-dependently reduce lipid peroxide production in fetal brain slices under iron-induced oxidative stress (50). CySSA reduced cytochrome P450 2E1 (CYP2E1) protein, catalase (CAT) and glutathione peroxidase (GPx) mRNA, and nitrotyrosine and MDA formation in a non-alcoholic fatty liver disease *in vivo* mouse model (86). CySSA also decreased levels of CYP2E1 protein, and CAT, GPx, and superoxide dismutase (SOD) mRNA in mice undergoing CCl_4-induced hepatic oxidative stress (87). CySSA attenuates MDA formation and increases SOD levels in posaconazole-induced oxidation in mice (88). Furthermore, CySSA exerts protective effects in cisplatin nephrotoxicity in rats by reducing MDA and increasing GSH content. CySSA also upregulates Nrf2 and NQO1 and downregulates pro-inflammatory COX-2. In an LPS-induced model of acute lung injury in mice, CySSA treatment dose-dependently increased GSH, Nrf2, HO-1, and NQO1 levels, SOD activity, and reduced MDA levels (64).

1.5 Hydrogen Sulfide and Persulfides as Mediators of Mercaptocysteine Bioactivity

Hydrogen sulfide (H_2S) is the third gasotransmitter, after nitric oxide and carbon monoxide, that exerts biological activities including antioxidation (113), anti-inflammation (114), antiproliferation (115), cardioprotection (116,117), and vasodilation (118). The physiological effects of H_2S was first demonstrated by Kimura and co-workers in 1996 (119) to serve a modulatory role in the mammalian nervous system. Since then, H_2S has gained significant research interest for its potential role in a variety of physiological and pathological processes. Endogenous H_2S is generated from three enzymes involved in the transsulfuration pathway, CBS, CSE, and mercaptopyruvate sulfurtransferase (3MST), which largely act on L-cysteine, L-homocysteine, L-cystine, and other L-cysteine derivatives to form H_2S (120). The

rate of H_2S released is dependent on substrate. For example, CBS generates H_2S 23 times faster in the presence of L-homocysteine with L-cysteine than L-cysteine alone (121). Additionally, the expression of each of the three enzymes varies, and so their relative contribution to H_2S production is tissue dependent (122), with CBS and MST generating H_2S mainly in the nervous system while CSE primarily forms H_2S in hepatic and cardiovascular tissues (122-124).

The signaling mechanisms by which H_2S affect biological processes is not yet clear but may involve persulfidation of proteins and oxidized thiols. H_2S undergoes sulfhydration with disulfides to form highly reactive persulfides. There is growing evidence that suggests persulfides (RSSH) are a transient intermediate that primarily exerts bioactivity in situ, and that H_2S is a byproduct of these persulfidation reactions (81). Persulfides are reactive sulfur species with both strong nucleophilic and weak electrophilic character, as the outer sulfur can attack alkylating compounds and either the inner or outer sulfurs atoms can undergo exchange with a nucleophile such as another thiol (120). Persulfides possess higher reactivity than their thiol analogues. For example, persulfidated albumin protein exhibits 20-fold increase reactivity compared to the original thiol form of albumin (125). However, persulfides spontaneously degrade through disproportionation reactions to form free thiols, polysulfides, and H_2S, and so persulfides are short-lived *in vitro*.

1.5.1 Roles in *Allium* Organosulfur Chemistry

H_2S is one of the byproducts of *Allium* organosulfur metabolism. Benavides et al. demonstrated that diallyl disulfide, a decomposition product of allicin, generated H_2S when added to human red blood cells (RBCs) and its H_2S output is dependent on both endogenous and exogenous GSH concentration (118). Addition of biologically relevant thiols to RBCs increased H_2S concentration, with GSH exhibiting the most H_2S induction, while addition of GSH-

quenching alkylating agents iodoacetic acid (IAA) and iodoacetamide (IAM) attenuated H_2S release. Onion-derived CySSPe is metabolized *in vitro* to H_2S in Hepa1c1c7 hepatocytes, with peak H_2S formation in the first 2 hours (68). Hepatocytes pretreated with CSE and CBS inhibitors resulted in a reduction in H_2S. Similarly, hepatocytes pretreated with both alkylating agent diethyl maleimide (DEM) and GSH synthesis inhibitor buthionine sulphoximine (BSO) exhibited a 70% reduction in H_2S output, which suggests GSH is involved in these H_2S-generating reactions.

H_2S is both a product of persulfide decay and reactant in the formation of persulfides. Dissolved H_2S readily reacts with oxidized sulfur species found in the biological milieu, such as disulfides, sulfenic acids, and thiosulfinates, to form persulfides. These persulfides can further react with endogenous reduced thiol species, including cysteine and glutathione, or reduced thiols in proteins to release H_2S as a marker of persulfide exchange. When cystine (CySSCys) is reacted with enzymes CBS and CSE, the persulfide, CySSH, is formed and little or no H_2S is detected (81), suggesting H_2S is primarily a byproduct of persulfide degradation through exchange reactions with endogenous thiols. While H_2S plays a role in organosulfur metabolism, studies suggest persulfides could be the primary mediators of *Allium* organosulfur bioactivity. Previous studies have shown mercaptocysteines CySSA, *S*-propylmercapto-L-cysteine, and *S*-penta-1,3-dienylmercapt-L-cysteine are all substrates of CBS and CSE and undergo β-elimination (60). The presumed fragment of this elimination reaction is a persulfide, as cystine, which is structurally analogous to mercaptocysteines, is known to generate cysteine hydropersulfide from β-lyase activity. Hepatocytes incubated with 50 μM CySSPe exhibit elevated levels of Keap1 persulfide, a product of persulfide exchange between the Keap1 native form and GSH persulfides (GSSH) in the cytosolic milieu presumably generated from CySSPe

degradation and subsequent GSH exchange (68). The addition of 50 μM NaHS, an H_2S donor and persulfide generator, increased Keap1 persulfide levels to same degree. Keap1 persulfidation has been previously shown to activate the Nrf2 antioxidant pathway and is one mechanism by which mercaptocysteines exert their antioxidant effects (68,126).

1.5.2 Mechanisms of Action

Protein persulfides formed from *S*-sulfhydration of protein cysteine residues has been proposed as a mechanism by which H_2S mediates cell signaling, rather than H_2S reacting directly with ROS (127). While H_2S is unable to sulfhydrate reduced thiols, H_2S can post-translationally modify oxidized cysteine residues such as those in the sulfenic acid or disulfide state to form a persulfide product. Persulfides share similar characteristics with thiols, disulfides, peroxides, and sulfenic acids (129). Cysteine persulfides within proteins themselves are quite unstable and are readily reduced by intracellular GSH or antioxidant enzymes, or intramolecularly displaced by a vicinal cysteine. The end-product is a regenerated H_2S and disulfide. The formation of the short-lived persulfide has been shown to activate enzymes and proteins *in vitro* (129).

Sulfhydration of an important cysteine residue and subsequent formation of its persulfide form can enhance its nucleophilicity over the original thiol. For example, gain of function has been observed in persulfide forms of glyceraldeyde 3-phosphate dehydrogenase (127), malate dehydrogenase (130), and MAP kinase kinase 1 (MEK-1), which phosphorylates and activates mitogen-activated protein kinase (MAPK) member extracellular signal-regulated kinase 2 (ERK2) (131). Key transcriptional regulators Hsp70 (132), NF-κB (133), and Nrf2 (134) have been shown to be activated by the formation of persulfides on these proteins and their associated regulatory elements. Loss of function by persulfide formation has also been reported in proteins such as papain (135), tyrosine aminotransferase (136), and phosphatase PTP1B (137).

1.5.3 Antioxidant Effects

While persulfides are transient intermediates, they possess several interesting antioxidant properties. The dissociation energy for the S-H bond is lower for persulfides than thiols at 70 kcal/mol compared to 92 kcal/mol (138) and the rate constant for hydrogen atom donation is one order of magnitude higher for protonated persulfides compared its protonated thiol analogue (139), which make persulfides good one-electron reductants. GSSH generated from the action of glutathione reductase on GSSSG scavenges ~17 times more hydrogen peroxide (H_2O_2) than GSH alone (81). These reactivities play an important role in biological settings. The antioxidant activity of GSH is normally mediated by enzymes such as GST and GSH-dependent peroxidases, otherwise, GSH reacts relatively poorly with electrophilic oxidants such as H_2O_2. On the other hand, persulfide analogue GSSH has strong antioxidant properties and can scavenge H_2O_2 without enzymatic assistance.

H_2S and its generated persulfides also exhibit antioxidant properties by mediating the upregulation of signaling pathways involved in cellular defenses. NaHS, an H_2S donor, *S*-sulfhydrates the inhibitory protein Keap1 in HEK-239 cell cultures modified to overexpress the Keap1 protein at Cys^{151} to generate the persulfidated Keap1 form, which stimulates Nrf2 translocation and upregulates antioxidant proteins (111). In the human gastric epithelial cell line GES-1, 100 μM NaHS protects cells from reactive oxygen species after initiating ischemia-like conditions by increasing Keap1 *S*-sulfhydration and promoted Nrf2 nuclear translocation (140). *S*-sulfhydration of Keap1, Nrf2 translocation, and HO-1 upregulation is also exhibited in peritoneal macrophages following treatment with H_2S donor, GYY4137 (141). Preincubation of cells with Na_2S increases endogenous cysteine persulfide levels with concomitant increase in GSH, nuclear Nrf2, and NQO1 levels (142). In diabetic mice with induced myocardial ischemia-

reperfusion injury, 7 days of H_2S injection, in the form of 0.1 mg/kg Na_2S, reduced lipid hydroperoxide formation and increased nuclear Nrf2 expression, NQO1 and HO-1 protein expression in cardiac tissue (143). Na_2S treatment activates Erk1/2, a MAPK signaling protein which removes Bach1, a stress responsive transcription factor that competes with Nrf2 for ARE-promoter binding, from the nucleus.

1.5.4 Pro- and Anti-Inflammatory Properties

The NF-κB family of proteins are a group of transcriptional regulators best known for their involvement in inflammation, immunity, and carcinogenesis (144). Dysregulation of NF-κB signaling leads to prolonged inflammation, which is linked to several disease states (145). The canonical NF-κB signaling pathway involves the binding of exogenous bacterial lipoproteins and lipopolysaccharides to the pattern-recognition receptors Toll-like receptors (TLRs), including TLR2 and TLR4, at the surface of macrophages and other immune cells (146,147). Upon stimulation, TLRs dimerize and undergo a conformation change that recruits essential adaptor protein myeloid differentiation factor 88 (MyD88) and NADPH oxidase 4 (NOX4) (148), followed by recruitment of interleukin-1 receptor-associated kinase 4 (IRAK4) and phosphorylation of IRAK1 **(Fig. 1.4)** (63). The protein complex recruits and activates tumor necrosis factor receptor (TNFR)-associated factor 6 (TRAF6), a ubiquitin protein ligase (149). TRAF6 can then polyubiquitinate IKK-γ for targeted degradation, which recruits TGF-β activate kinase 1 (TAK1). TAK1 subsequently phosphorylates IKK-β and induces the release of transcriptional regulator NF-κB, which is tightly controlled by IκB inhibitory proteins that sequesters NF-κB dimer proteins in the cytosol. The released NF-κB dimers are then free to translocate into the nucleus and initiate downstream expression of pro-inflammatory cytokines and other inflammatory gene products (150). TAK1 activation also leads to signal induction

Figure 1.4. Metabolism and effect of mercaptocysteines on NF-κB signaling (63). Solid lines represent pathways and elements supported by literature and dash lines represent pathways and elements that remain to be determined.

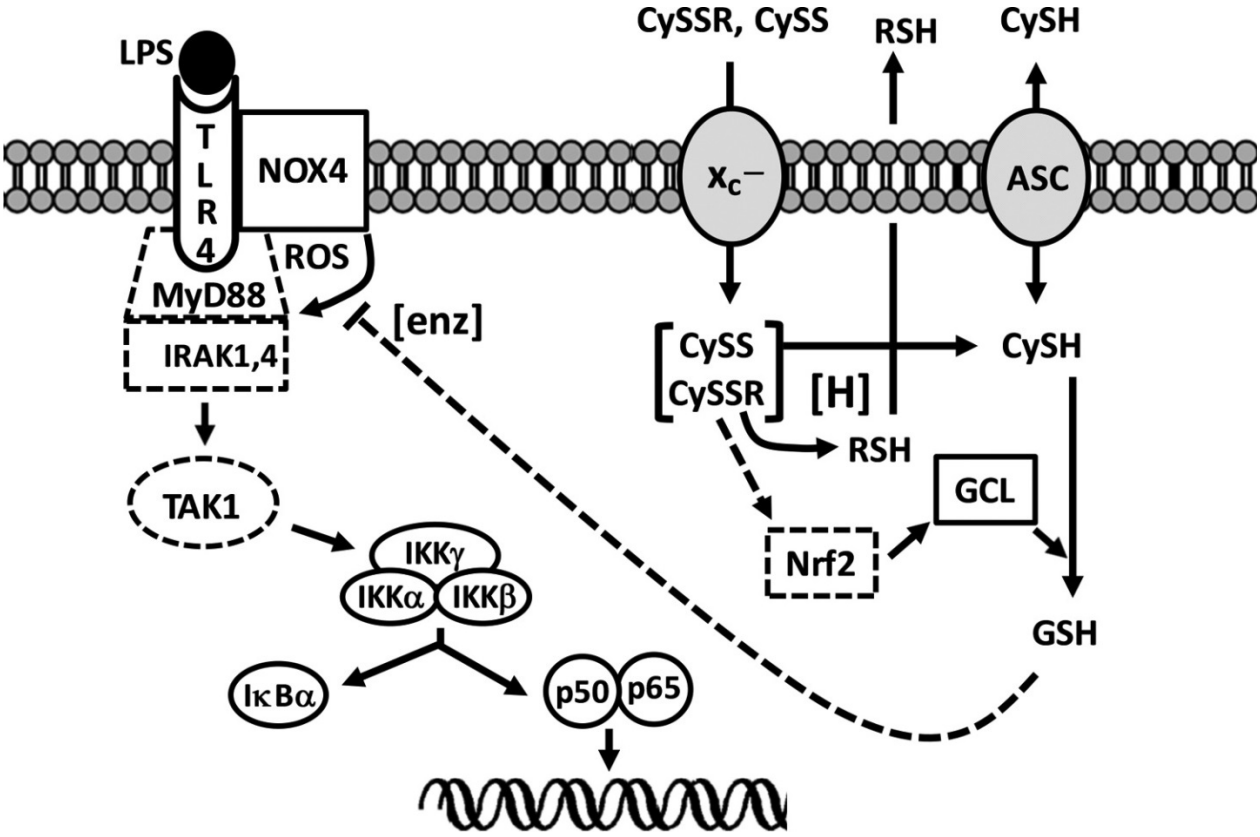

through the MAP kinase pathway including kinases JNK, ERK, and p38 MAPK pathways, which activates the activator protein 1 (AP-1) transcription factors that also mediates pro-inflammatory cytokine expression (151).

Reports on the effects of H_2S and its involvement in persulfide formation on inflammation offer conflicting results. Post-translational modification by *S*-sulfhydration of the p65 subunit of NF-κB at cysteine-38 activates the pro-inflammatory NF-κB and promotes its binding to coactivator ribosomal protein S3 (133). However, H_2S donors have been shown to exhibit anti-inflammatory properties *in vitro*. H_2S inhibits NF-κB activation and subsequent iNOS expression and NO production in LPS-activated macrophages (152). In microglia cells, H_2S inhibits upregulation of iNOS expression, NO production, and pro-inflammatory cytokine expression after inflammatory induction with an endotoxin, partially mediated by the suppression of p38 MAPK phosphorylation by H_2S (153). Slow-releasing H_2S donor GYY-4137 dose-dependently inhibits NO production, and TNF-α and IL-1β expression in endotoxin-pretreated RAW 264.7 cells, whereas fast-releasing H_2S donor NaHS enhanced the output of these NF-κB-regulated inflammatory mediators (154). The effect of H_2S on NF-κB could be biphasic and dependent on concentration, with low concentrations activating NF-κB while high concentrations inhibiting NF-κB.

1.6 Chronic Inflammation and Oxidative Stress in Obesity

Changes in lifestyle and diet in the last several decades have resulted in an increase in the incidence of obesity across the world and is considered one of the largest public health challenges for the United States (155). Obesity is a chronic disease in which excessive energy consumption results in excessive growth of adipose tissues, generally through overconsumption of high-energy nutrients, such as sugars and fats, combined with lack of exercise (156).

Comorbid conditions associated with obesity include type 2 diabetes mellitus, colon cancer, hypertension, cardiovascular disease, osteoarthritis, gallbladder disease, and sleep apnea (157). Obesity also increases mortality amongst those suffering from the condition (157).

1.6.1 Obesity and Adipose Tissue

Two types of adipose tissue exist in humans. Brown adipose tissue possesses abundant mitochondria and are responsible for activating and regulating thermogenesis via the uncoupling protein-1 (UCP-1), while white adipose tissues are primarily responsible for excess fat storage (158). White adipose tissue is a heterogenous mixture of several cell types, including macrophages, adipocytes, and fibroblasts. Excessive consumption of sugar and fats induces adipose tissues hypertrophy, hyperplasia and reduction in insulin receptors (159,160). More beta-3 adrenergic receptors are displayed by adipocytes, which initiates a pro-inflammatory cycle between adipocytes and monocytes.

Several adipocyte-derived cell signaling molecules, known as adipokines or adipocytokines, are important for maintaining the homeostasis of several physiological processes. Leptin is an appetite-regulating hormone produced by adipose tissue in proportion to its size and nutritional content (161). Leptin serves as a metabolic signal for energy sufficiency, as levels decline with weight loss (162). Leptin also acts on macrophages and increases proinflammatory cytokine production, which activates other immune cells and promotes vascular inflammation (163). Elevated circulating leptin levels are associated with common forms of obesity. Adiponectin, a hormone that regulates the metabolism of glucose and lipids with anti-inflammatory activity, is expressed at reduced levels during increasing adiposity (164). Adiponectin also regulates the liver by inhibiting gluconeogenic liver enzymes and glucose release while stimulating glucose use and fatty acid oxidation.

Other adipokines interact with cell types associated with the immune system. TNF-α is produced by adipocytes, monocytes, and lymphocytes, and is involved in the systemic inflammatory response (165,166). The presence of elevated TNF- α concentrations decreases insulin sensitivity in adipose tissues by inhibiting insulin signaling via induction of serine phosphorylation of the insulin receptor (167). Additionally, TNF-α downregulates anti-inflammatory adiponectin and activates the NF-κB-dependent inflammatory state in adipose tissue, inducing atherogenesis. IL-6 is an additional pro-inflammatory cytokine found to be elevated in obese subjects and produced by both adipocytes and macrophages (168). The elevated levels of inflammatory markers by both adipose tissue and recruited immune cells initiates chronic low-grade inflammation that exacerbates the condition through the release of ROS and other oxidative byproducts.

1.6.2 Obesity and Oxidative Stress

Obesity and chronic oxidative stress are closely linked. Oxidative stress is a state in which there is a net imbalance of ROS and the endogenous antioxidant systems in the body are overwhelmed, which leads to pathophysiological conditions (169). Normally, the oxidative products generated from energy metabolism and other physiological processes are neutralized by the native antioxidant capacity in cells. However, obesity creates an overaccumulation of oxidants that have deleterious effects on the redox status in the tissues and organs affected by the condition (170). The high concentration of oxidative products affect cell signaling, cell metabolism, and other cellular activities. Obesity has been reported to induce systemic oxidative stress and dysregulation of adipokine production (158). Additionally, diets high in carbohydrates and fat reduces antioxidant defense biomarkers and increase oxidative stress and inflammation (171).

One mechanism implicated in the initiation of oxidative stress in obesity involves mitochondrial dysfunction. Excessive quantities of high calorie macromolecules are processed through the Kreb's cycle and oxidative metabolism in the mitochondria. As the major source of cellular ROS generation, the mitochondrial electron transport chain normally generates ROS through incomplete electron transfer to oxygen (172). Adipocyte mitochondria must metabolize excess free fatty acids, which further causes mitochondrial uncoupling and increases ROS. In turn, these mitochondrial ROS signals trigger macrophages to produce proinflammatory cytokines that further activate the inflammatory response and subsequent release oxidative products in neighboring adipocytes (173).

NADPH oxidases (NOX) are a family of membrane-bound enzyme complexes that transfer electrons from NADPH to oxygen. In the process, they generate superoxide and are a source of non-mitochondrial ROS. One member of the NOX family, NOX4, is upregulated by hypoxia (174), TNF-α and other inflammatory cytokines (175), and endoplasmic-reticulum stress (176). NOX4 is also transiently activated in mouse models that are challenged with a high-fat, high-sugar diet (177). However, NOX4-deficient mice display a predisposition towards diet-induced obesity as well which suggests NOX4 plays a complex homeostatic role in the pathogenesis of obesity.

Long-term persistence of obesity depletes antioxidant sources over time. The activity of antioxidant enzymes SOD and GPx are lowered in obese male individuals compared to health subjects (178). Levels of antioxidants GSH, vitamin E, and β-carotene in the serum are also decreased in obesity (179,180). Plasma, liver, and brain lipoperoxide concentrations were higher in obese rats compared lean rats (181). Additionally, hepatic vitamin A concentrations and liver GPx activity was lower in the obese versus lean rats.

1.6.3 Obesity and Inflammation

Epidemiological and experimental studies have linked obesity and inflammation for some time (155,158,161,182). The enlargement of adipocytes through excessive nutrient intake initiates adipogenesis, the process of preadipocyte maturation to mature adipocytes that secrete a large amount of inflammatory adipokines, such as TNF-α, IL-6, resistin, MCP-1, PAI-1, and leptin (158,161). Reciprocally, obesity is linked to a decrease in anti-inflammatory adipokines, including adiponectin and interleukin 10. Glucose and fat intake activate transcription factors NF-κB (183), activating protein-1 (AP-1), and early growth response-1 (EGR1) (184). Fat storage also induces adipose tissue hypoxia, which leads to adipocyte necrosis and the recruitment of macrophages and other immune cells (185). Additionally, the release of chemokines such as MCP-1 initiated by high lipid intake locally recruits monocytes to activated adipocytes. Overexpression of MCP-1 in transgenic mice was sufficient to induce macrophage recruitment and insulin resistance (186). These combined factors induce a perpetual state of low-grade inflammation as adipocytes continue to release pro-inflammatory adipokines in response to inflammatory signaling from macrophage cells.

Inflammatory signaling enhances the insulin resistance of adipocytes. The NF-κB pathway and JNK pathway are two transcription factor-signaling pathways linked to the pro-inflammatory effects of obesity and insulin resistance. Both pathways are activated via the toll-like receptors (TLRs), which can be activated by the presence of fatty acids and links the immune system with lipid concentration (187). Hypertrophic growth of adipocytes gives rise to increased ROS and endoplasmic reticulum stress, additional factors that activate the NF-κB and JNK pathways (170,188). Inhibition of NF-κB in liver or macrophages through overexpression of inhibitory protein IκBα or deletion of activating kinase IKKβ reduces concurrent insulin

resistance and inflammatory gene expression in mice fed an HFD (189). The insulin resistance of mice heterozygous for IKKβ ($IKK\beta^{+/-}$) that were crossed with obese mice or fed with an HFD was attenuated (190). Additionally, chemical inhibitors of JNK activity and JNK1 knockout increase insulin sensitivity in insulin resistant mice (190,191).

1.6.4 The Effect of Allium-Derived Compounds on Obesity

Mice fed a high-fat diet (HFD) supplemented with 2% or 4% powdered garlic displayed a reduction in body weight gain, liver mass weight, and epididymal fat tissue in a dose dependent manner compared to the HFD control group (192). Additionally, the HFD group given 4% garlic exhibited a dramatic 78% reduction in epididymal fat, approaching the level of the standard diet group. Significant reductions in plasma triglycerides (45-55%), total cholesterol (52-58%), and low-density lipoprotein (LDL) cholesterol (68-71%) were observed. The high-density lipoprotein (HDL) cholesterol was elevated by 1.9- to 2.2-fold in the garlic supplemented groups. Reductions in gene expression implicated in fat accumulation in epididymal fat tissues, including peroxisome proliferator-activated receptor γ (PPARγ), acetyl CoA carboxylase (ACC), adipose specific fatty acid binding protein (aP2), and glycerol-3-phosphate dehydrogenase (GPDH), was exhibited by the garlic supplemented groups. Gene expression levels were decreased between 27 to 58% across the different gene products. In an open label, comparative study conducted on patients with type 2 diabetes and obesity, patients were either given the control anti-diabetic drug metformin alone or metformin supplemented with 250 mg garlic capsules for 12 weeks (193). The group given both metformin and garlic capsules showed a significant decrease in serum total cholesterol, triglycerides, and LDL cholesterol and increase in HDL cholesterol compared to the group given metformin alone following the study.

Another study conducted by Yang et al. (194) to evaluate the effects of garlic and onion oil on rats fed an HFD demonstrated that garlic oil had a stronger anti-obesity and hypolipidemic effect compared to onion oil. Following 60 days of treating Sprague-Dawley rats with steam distilled garlic and onion oil, they reported a reduction in body weight, epididymal fat, perirenal fat pad, and adipose tissue ratio in the rats treated with garlic and onion oil. Additionally, an increase in liver mass was found in both garlic and onion oil-treated rats. Triglycerides, total cholesterol, and LDL cholesterol were lower while HDL cholesterol was higher in the treatment groups. Interestingly, the rats treated with a higher dose concentration of onion oil yielded an increase or no change in some biomarker levels compared to lower doses of onion oil, as opposed to garlic oil, which lowered biomarker levels dose-dependently. Garlic oil exhibited a stronger suppression of obesity biomarkers except serum triglycerides, which was more strongly suppressed by onion oil. Rats fed garlic and onion oil had strongly reduced inflammatory cell infiltration compared with the HFD group.

Zucker diabetic fatty (ZDF) rats treated with 3% or 5% onion extract exhibited lowered liver mass, adipose tissue, fasting blood glucose, homeostatic model assessment of insulin resistance (HOMA-IR), and serum insulin compared to control (195). The onion oil-fed rat groups also showed lowered total cholesterol, triglycerides, and free fatty acids. However, there were mixed results for HDL and LDL cholesterol. The 3% dose reduced HDL levels whereas 5% onion extract returned HDL to control levels, while the 3% dose increased LDL levels and the 5% dose only slightly increased LDL levels. Additionally, rat white preadipocyte cell differentiation was suppressed by onion extract and onion-component S-methyl cysteine sulfoxide in a dose-dependent manner. These findings show that crude extracts of onion, which contain a variety of organosulfur compounds, possess anti-obesity properties.

Allicin, the bioactive principle of garlic, has been shown to improve cardiovascular, diabetic, and obesity biomarkers in animal models. Male Sprague-Dawley rats fed a fructose-enriched diet supplemented with allicin, which led to a significant attenuation in weight gain compared to the control (196). In HFD-induced obese mice, allicin ameliorated weight gain and increased HDL cholesterol (197). White adipose tissue, brown adipose tissue, and epididymal tissue samples from the allicin-treated mice yielded an increase in expression levels of lipolysis, mitochondria, thermogenesis, and insulin signaling pathway-related genes, whereas adipokine-related gene expression was decreased. Furthermore, allicin suppressed expression of lipogenesis and lipid transport genes. Mice treated with allicin also exhibited increased oxygen expenditure and glucose utilization rate in brown adipose tissue (198).

Conjugated transformation products of *Allium* thiosulfinates and thiol-containing agents possess anti-obesity properties. The hybrid therapeutic agent, allylmercaptocaprotril, is a conjugated hybrid of allicin and the antihypertensive drug captotril. In a rat model of metabolic syndrome, spontaneously hypertensive, obese (SHROB) rats treated with allylmercaptocaptotril exhibited a significant reduction in body weight, serum glucose, triglycerides, and free fatty acids compared to those treated with the unconjugated captotril or the control (191). The allylmercaptocaptotril-treated rat group had lower blood pressure than control and captotril-treated groups (199). A rat model of non-alcoholic fatty liver disease (NAFLD) induced through a high fat diet was treated with allicin-derived cysteine conjugate, S-allylmercaptocysteine (SAMC) (86). SAMC restored mRNA expression of antioxidant enzymes glutathione peroxidase (GPx) and catalase (CAT), which were downregulated during the progression of NAFLD. SAMC treatment reduced serum free fatty acids and the formation of malondialdehyde (MLA).

SAMC also reduced pro-inflammatory IL-1β protein levels, TNF-α protein levels, and TNF-α, IL-1β, iNOS, and COX-2 mRNA expression levels in liver tissues.

1.7 Dissertation Rationale

Chronic lifestyle diseases like cardiovascular disease, cancer, and obesity are a growing source of morbidity and mortality worldwide. *Allium* vegetables exert protective properties against these diseases. Many of the health benefits associated with *Allium* vegetables stem from the organosulfur metabolites generated from the enzymatic reaction between endogenous cysteine sulfoxides and alliinase. Thiosulfinates have been documented to exert many biological effects and are the most abundant organosulfur compounds in freshly macerated *Allium* tissues and are most likely the bioactive component (or progenitor thereof) of *Alliums.* That said, thiosulfinates are highly unstable in biological systems with a short half-life in the presence of thiol groups and biological milieu. For example, allicin, the major thiosulfinate of garlic, is absorbed by the bloodstream within 5 minutes of administration (48). Thiosulfinates are readily permeable through cell lipid membranes and can readily react with reduced thiol groups to form asymmetric mercaptocysteines, the putative secondary metabolite of *Allium* vegetables that exerts biological activity in tissues (49). Other organosulfur compounds derived from *Alliums*, such as disulfides and trisulfides, similarly generate asymmetric mercaptocysteines in the presence of thiols.

H_2S, a gasotransmitter with pleiotropic effects, has been found to be a metabolic product of *Allium* organosulfurs (68,118). H_2S demonstrates cytoprotective properties against carcinogenesis, oxidative stress and inflammation, and evidence shows H_2S exerts its biological effects through the formation of persulfides with oxidized cysteine and cystine cellular components (116,126). Mercaptocysteines are also metabolized directly into persulfides and

generate H_2S as a byproduct of thiol-disulfide exchange with the persulfide analogue (68). In either case, the H_2S-producing properties of mercaptocysteines is an important metabolic biomarker of mercaptocysteine bioactivity. One of the objectives of this dissertation was to examine the H_2S-releasing capacity of mercaptocysteines in the presence of cysteine and glutathione and in macrophage cells to determine if endogenous thiols and H_2S-releasing enzymes are involved in the production of H_2S as a mediator of the anti-inflammatory and antioxidant properties exhibited by these compounds.

Previous studies have demonstrated the biological potency of mercaptocysteines *in vitro*. Mercaptocysteines have been shown to exert anti-inflammatory properties through the inactivation and downregulation of the inflammatory transcriptional regulator NF-κB and associated regulatory proteins involved in the inflammatory signal (64). Mercaptocysteines, especially the onion-derived 1-propenylmercaptocysteine (CySSPe), inhibit the production of downstream inflammatory cytokines TNF-α, IL-1β, and IL-6 in activated macrophage cells and deactivate inflammatory transcriptional regulator NF-κB. Other inflammatory mediators downregulated by mercaptocysteines include iNOS and its product NO. Mercaptocysteines have also been shown to upregulate antioxidant machinery *in vitro*. Nrf2 is an important transcriptionally regulator of the phase II enzyme response to pro-oxidants and xenobiotics. Nrf2-associated enzymes quinone oxidoreductase (NQO1), heme oxygenase (HO-1), and glutamate cysteine ligase (GCL) are all similarly upregulated by the mercaptocysteines in murine hepatocytes (69). However, some of these anti-oxidative effects of mercaptocysteines have not yet been demonstrated in macrophages, which could be one mechanism by which mercaptocysteines attenuate the inflammatory response in these cells. A secondary objective of this dissertation is to investigate if mercaptocysteines upregulate Nrf2/ARE antioxidant enzymes

in LPS-activated cultured macrophage cells and determine if Nrf2 is a mediator of the anti-inflammatory properties exhibited by mercaptocysteines through a redox mechanism.

Allium mercaptocysteines have been shown to exert anti-inflammatory effects in macrophages through the blockade of specific elements of the canonical NF-κB inflammatory signaling pathway (63). The NF-κB signaling pathway is initiated by the binding of LPS with receptor TLR4, which recruits several adaptor proteins that activate TAK1 (150). TAK1 is an upstream kinase of NF-κB as well as the family of MAP kinases that include JNK, p38, and ERK (151). MAPK proteins also play a role in regulating inflammatory and stress responses and may be another pathway that mercaptocysteines act upon in exerting their anti-inflammatory effects. H_2S donors have previously been shown to inhibit p38 as a mechanism by which H_2S inhibits inflammation (153). It is also yet unclear whether mercaptocysteines inhibit the NF-κB signal at points upstream or downstream of TAK1. Therefore, an additional objective of this dissertation is to evaluate if mercaptocysteines inhibit NO release as a biomarker of inflammatory by modulating the TAK1 and the MAP kinase network.

While onion derivative CySSPe exert more potent bioactivity than garlic-based *S*-allylmercaptocysteine (CySSA), much of the 1-propenylmercapto equivalents in onion is lost through conversion of 1-propenylsulfenic acids to the volatile lachrymatory factor PTSO and cyclized non-thiosulfinate byproducts that cannot conjugate with biological thiols to form stable CySSPe (30,36). These rapid enzymatic and intramolecular processes limit the utility of onions as a source of health-promoting organosulfur compounds for the production and development of functional foods or pharmaceutical agents. As such, there are few studies evaluating the biological activity of CySSPe, and none that have assessed the effect of CySSPe on *in vivo* models of disease. To address this challenge, our laboratory has developed a simple tissue

homogenate method to produce the CySSPe onion-derivative in quantities suitable for cellular and animal studies (44). Given the anti-inflammatory and anti-oxidative effects previously mentioned suggest mercaptocysteines could be effective agents for attenuating the progression of diseases that involve inflammation and oxidative stress, such as obesity, another objective of this dissertation research is to be evaluate if CySSPe ameliorates obesity through the reduction of obese mouse weight and triglycerides, and modulates serum lipid biochemistry, liver function enzymes, and pro-inflammatory cytokines in a mouse model of obesity.

Several healthful properties of *Allium* vegetables are linked to the metabolic formation of mercaptocysteines *in situ* following consumption. The properties of garlic-derived conjugate CySSA have been previously well-characterized both *in vitro* and *in vivo* due to its ease of synthesis, high stability, and association with aged garlic extract (AGE) supplements. However, the discovery of CySSPe as a similar or more potent bioactive agent than CySSA and its straight-forward synthesis initiated a series of studies to better understand the biological properties of this onion-derived conjugate (44,62,63,68,72,73,110). These outlined studies were designed to evaluate the possible mechanisms behind the bioactivity of *Allium* mercaptocysteines, especially CySSPe, and the potential of CySSPe for ameliorating the effects of obesity *in vivo*.

1.8 References

1. Prentice, R.L. et al. Low-Fat Dietary Pattern and Risk of Invasive Breast Cancer. *JAMA*. **2006**, *295*, 629-642.

2. Beresford, S.A.A. et al. Low-Fat Dietary Pattern and Risk of Colorectal Cancer. *JAMA.* **2006,** *295*, 643-654.

3. Prentice, R.L. et al. Low-Fat Dietary Pattern and Cancer Incidence in the Women's Health Initiative Dietary Modification Randomized Clinical Trial. *JAMA*. **2007**, *99*, 1534-1543.

4. Parsons, J.K., Newman, V.A., Mohler, J.L., Pierce, J.P., Flatt, S., Marshall, J. Dietary Modification in Patients with Prostate Cancer on Active Surveillance: A Randomized, Multicentre Feasibility Study. *BJU Int.* **2008**, *101*, 1227-1231.

5. Epstein, L.H., Gordy, C.C., Raynor, H.A., Beddome, M., Kilanowski, C.K., Paluch, R. Increasing Fruit and Vegetable Intake and Decreasing Fat and Sugar Intake in Families at Risk for Childhood Obesity. *Obesity* **2001**, *9*, 171-178.

6. He, K., Hu, F.B., Colditz, G.A., Manson, J.E., Willett, W.C., Liu, S. Changes in Intake of Fruits and Vegetables in Relation to Risk of Obesity and Weight Gain Among Middle-Aged Women. *Int. J. Obes.* **2004**, *28*, 1569-1574.

7. Bazzano, L.A., Serdula, M., Liu, S. Prevention of Type 2 Diabetes by Diet and Lifestyle Modification. *J. Am. Coll. Nutr.* **2005**, *24*, 310-319.

8. Ramachadran, A., Snehalatha, C., Mary, S., Mukesh, B., Bhaskar, A.D., Vijay, V. The Indian Diabetes Prevention Programme Shows That Lifestyle Modification and Metformin Prevent Type 2 Diabetes in Asian Indian Subjects with Impaired Glucose Tolerance (IDPP-1). *Diabetologia* **2006**, *49*, 289-297.

9. Gardener, H., Wright, C.B., Gu, Y., Demmer, R.T., Boden-Albala, B., Elkind, M.S., Sacco, R.L., Scarmeas, N. Mediterranean-Style Diet and Risk of Ischemic Stroke, Myocardial Infarction, and Vascular Death: The Northern Manhattan Study. *Am. J. Clin. Nutr.* **2011**, *91*, 1458-1464.

10. Estruch, R., Ros, E., Salas-Salvadó, J., Covas, M.I., Corella, D., Arós, F., Gómez-Gracia, E., Ruiz-Gutiérrez, V., Fiol., M., Lapetra, J., Lamuela-Raventos, R.M., Serra-Majem, L., Pintó, X., Basora, J., Muñoz, M.A., Sorlí, J.V., Martínez, J.A., Martínez-González, M.A. Primary Prevention of Cardiovascular Disease with a Mediterranean Diet. *N. Engl. J. Med.* **2013**, *368*, 1279-1290.

11. Lau, K.-K., Wong, Y.-K., Chan, Y.-H., Li, O.-Y., Lee, P.Y.-S., Yuen, G.G., Wong, Y.-K., Tong, S., Wong, D., Chan, K.-H., Cheung, R.T.-K., Siu, C.-W., Ho, S.-L., Tse, H.-F. Mediterranean-Style Diet is Associated with Reduced Blood Pressure Variability and

Subsequent Stroke Risk in Patients with Coronary Artery Disease. *Am. J. Hypertens.* **2015**, *28*, 501-507.

12. Doll, R., Peto, R. The Causes of Cancer: Quantitative Estimates of Avoidable Risks of Cancer in the United States Today. *J. Natl. Cancer Inst.* **1981**, *66*, 1191-1308.

13. Block, G., Patterson, B., Subar, A. Fruits, Vegetables, and Cancer Prevention: A Review of the Epidemiological Evidence. *Nutr. Cancer* **1992**, *18*, 1-29.

14. Bazzano, L.A., He, J., Ogden, L.G., Loria, C.M., Vupputuri, S., Leann, M., Whelton, P.K. Fruit and Vegetable Intake and Risk of Cardiovascular Disease in US Adults: The First National Health and Nutrition Examination Survey Epidemiologic Follow-Up Study. *Am. J. Clin. Nutr.* **2002**, *76*, 93-99.

15. Azagba, S., Sharaf, M.F. Fruit and Vegetable Consumption and Body Mass Index: A Quantile Regression Approach. *J. Prim. Care Community Health* **2012**, *3*, 210-220.

16. Joshipura, K.J., Ascherio, A., Manson, J.E., Stampfer, M.J., Rimm, E.B., Speizer, F.E., Hennekens, C.H., Spiegelman, D., Willett, W.C. Fruit and Vegetable Intake in Relation to Risk of Ischemic Stroke. *JAMA*. **1999**, *282*, 1233-1239.

17. Dillard, C.J., German, J.B. Phytochemicals: Nutraceuticals and Human Health. *J. Sci. Food Agric.* **2000**, *80*, 1744-1756.

18. Surh, Y.-J., Kundu, J.K., Na, H.-K., Lee, J.-S. Redox-Sensitive Transcription Factors as Prime Targets for Chemoprevention with Anti-Inflammatory and Antioxidative Phytochemicals. *J. Nutr.* **2005***, 135*, 2993S-3001S.

19. Liu, R.H. Potential Synergy of Phytochemicals in Cancer Prevention: Mechanism of Action. *J. Nutr.* **2004**, *134*, 3579S-3485S.

20. Jacobs, D.R., Steffen, L.M. Nutrients, Foods, and Dietary Patterns as Exposures in Research: A Framework for Food Synergy. *Am. J. Clin. Nutr.* **2003***, 78*, 508S-513S.

21. Mirelman, D., Ankri, S. Antimicrobial Properties of Allicin from Garlic. *Microb. Infect.* **1999**, *1*, 125-129.

22. Griffiths, G., Trueman, L., Crowther, T., Thomas, B., Smith, B. Onions – A Global Benefit to Health. *Phytother. Res.* **2002***, 16*, 603-615.

23. Rivlin, R.S. Historical Perspective on the Use of Garlic. *J. Nutr.* **2001***, 131*, 951S-954S.

24. Turati, F., Pelucchi, C., Guercio, V., Vecchia, C.L., Galeone, C. Allium Vegetable Intake and Gastric Cancer: A Case-Control Study and Meta-Analysis. *Mol. Nutr. Food Res.* **2015**, *59*, 171-179.

25. Hsing, A.W., Chokkalingam, A.P., Gao, Y.-T., Madigan, M.P., Deng, J., Gridley, G., Fraumeni, J.F. Allium Vegetables and Risk of Prostate Cancer: A Population-Based Study. *J. Natl. Cancer Inst.* **2002**, *94*, 1648-1651.

26. Jin, Z.-Y., Wu, M., Han, R.-Q., Zhang, X.-F., Wang, X.-S., Liu, A.-M., Zhou, J.-Y., Lu, Q.-Y., Zhang, Z.-F., Zhao, J.-K. Raw Garlic Consumption as a Protective Factor for Lung Cancer, a Population-Based Case-Control Study in a Chinese Population. *Cancer Prev. Res.* **2013**, *6*, 711-718.

27. Bordia, A., Verma, S.K., Srivastava, K.C. Effect of Garlic (Allium sativum) on Blood Lipids, Blood Sugar, Fibrinogen and Fibrinolytic Activity in Patients with Coronary Artery Disease. *Prostag. Leukotr. Ess.* **1998**, *58*, 267-263.

28. Blekkenhorst, L.C., Bondonno, C.P., Lewis, J.R., Devine, A., Zhu, K. Lim, W.H., Woodman, R.J., Beilin, L.J., Prince, R.L., Hodgson, J.M. Cruciferous and Allium Vegetable Intakes are Inversely Associated with 15-Year Atherosclerotic Vascular Disease Deaths in Older Adult Women. *J. Am. Heart Assoc.* **2017**, *6*, 1-15.

29. Zahra, B., Parvin, M., Momenan, A.A., Feridoun, A. Allium Vegetable Intakes and the Incidence of Cardiovascular Disease, Hypertension, Chronic Kidney Disease, and Type 2 Diabetes in Adults: A Longitudinal Follow-Up Study. *J. Hypertens.* **2017**, *35*, 1909-1916.

30. Block, E. The Organosulfur Chemistry of the Genus *Allium* – Implications for the Organic Chemistry of Sulfur. *Angew. Chem. Int. Ed.* **1992**, *31*, 1135-1178.

31. Block, E., Putman, D., Zhao, S.H. *Allium* Chemistry: GC-MS Analysis of Thiosulfinates and Related Compounds from Onion, Leek, Scallion, Shallot, Chive, and Chinese Chive. *J. Agric. Food Chem.* **1992**, *40*, 2431-2438.

32. Block, E., Naganathan, S., Putman, D., Zhao, S.H. *Allium* Chemistry: HPLC Analysis of Thiosulfinates from Onion, Garlic, Wild Garlic (Ramsoms), Leek, Scallion, Shallot, Elephant (Great-Headed) Garlic, Chive, and Chinese Chive. Uniquely High Allyl to Methyl Ratios in Some Garlic Samples. *J. Agric. Food Chem.* **1992**, *40*, 2418-2430.

33. Block, E., Ahmad, S., Catalfamo, J.L., Jain, M.K., Apitz-Castro, R. Antithrombotic Organosulfur Compounds from Garlic: Structural, Mechanistic, and Synthetic Studies. *J. Am. Chem. Soc.* **1986**, *108*, 7045-7055.

34. Block, E., O'Connor, J. The Chemistry of Alkyl Thiosulfinate Esters. VII. Mechanistic Studies and Synthetic Applications. *J. Am. Chem. Soc.* **1974**, *96*, 3929-3944.

35. Block, E., Bayer, T., Naganathan, S., Zhao, S.H. *Allium* Chemistry: Synthesis and Sigmatropic Rearrangements of Alk(en)yl 1-Propenyl Disulfide *S*-Oxides from Cut Onion and Garlic. *J. Am. Chem. Soc.* **1996**, *118*, 2799-2810.

36. Bayer, T., Wagner, H., Block, E., Grisoni, S., Zhao, S.H., Neszmelyi, A. Zwiebelanes: Novel Biologically Active 2,3-Dimethyl-5,6-dithiabicyclo[2.1.1]hexane 5-Oxides from Onion. *J. Am. Chem. Soc.* **1989**, *8*, 3085-3086.

37. Lancaster, J.E., Shaw, M.L. γ-Glutamyl Peptides in the Biosynthesis of *S*-Alk(en)yl-L-Cysteine Sulphoxides (Flavour Precursors) in *Allium*. *Phytochemistry* **1989**, *2*, 455-460.

38. Thomas, D.J., Parkin, K.L. Quantification of Alk(en)yl-L-Cysteine Sulfoxides and Related Amino Acids in Alliums by High-Performance Liquid Chromatography. *J. Agric. Food Chem.* **1994**, *42*, 1632-1638.

39. Stoll, A., Seebeck, E. Chemical Investigations on Alliin, the Specific Principle of Garlic. *Adv. Enzymol. Relat. Subj. Biochem.* **1951**, *11*, 377-400.

40. Rabinkov, A., Zhu, X.Y., Grafi, G., Galili, G., Mirelman, D. Alliin Lyase (Alliinase) from Garlic (Allium sativum). Biochemical Characterization and cDNA Cloning. *Appl. Biochem. Biotechnol.* **1994**, *48*, 149-171.

41. Schwimmer, S., Mazelis, M. Characterization of Alliinase of *Allium cepa* (Onion). *Arch. Biochem. Biophys.* **1963**, *100*, 66-73.

42. Tobkin, H.E., Mazelis, M. Alliin Lyase: Preparation and Characterization of the Homogenous Enzyme from Onion Bulbs. *Arch. Biochem. Biophys.* **1979**, *193*, 150-157.

43. Shen, C., Parkin, K.L. In Vitro Biogeneration of Pure Thiosulfinates and Propanethial-*S*-oxide. *J. Agric. Food Chem.* **2000**, *48*, 6254-6260.

44. Zhang, G., Parkin, K.L. A Tissue Homogenate Method to Prepare Gram-Scale *Allium* Thiosulfinates and Their Disulfide Conjugates with Cysteine and Glutathione. *J. Agric. Food Chem.* **2013**, *61*, 3030-3038.

45. Shen, C., Xiao, H., Parkin, K.L. In Vitro Stability and Chemical Reactivity of Thiosulfinates. *J. Agric. Food Chem.* **2002**, *50*, 2644-2651.

46. Moore, T.L., O'Connor, D.E. The Reaction of Methanesulfenyl Chloride with Alkoxides and Alcohols. Preparation of Aliphatic Sulfenate and Sulfinate Esters. *J. Org. Chem.* **1966**, *31*, 3587-3592.

47. Kice, J.L., Rogers, T.E. Mechanism of the Alkaline Hydrolysis of Aryl Thiosulfinates and Thiolsulfonates. *J. Am. Chem. Soc.* **1974**, *96*, 8009-8015.

48. Freeman, F. & Kodera, Y. Garlic Chemistry: Stability of *S*-(2-Propenyl)-2-Propene-1-sulfinothioate (Allicin) in Blood, Solvents, and Simulated Physiological Fluids. *J. Agric. Food Chem.* **1995**, *43*, 2332-2338.

49. Miron, T., Rabinkov, A., Mirelman, D., Wilchek, M., Weiner, L. The Mode of Action of Allicin: Its Ready Permeability Through Phospholipid Membranes May Contribute to Its Biological Activity. *Biochim. Biophys. Acta Biomembr.* **2000**, *1463*, 20-30.

50. Rabinkov, A., Miron, T., Mirelman, D., Wilchek, M., Glozman, S., Yavin, E. & Weiner, L. *S*-Allylmercaptoglutathione: The Reaction Product of Allicin with Glutathione Possesses SH-Modifying and Antioxidant Properties. *BBA-Mol. Cell Res.* **2000**, *1499*, 144-153.

51. Rabinkov, A., Miron, T., Konstantinovski, L, Wilchek, M., Mirelman, D., Weiner, L. The Mode of Action of Allicin: Trapping of Radicals and Interaction with Thiol Containing Proteins. *Biochim. Biophys. Acta.* **1998**, *179*, 233-244.

52. Wilde, S.C., Keppler, J.K., Palani, K., Schwarz, K. β-Lactoglobulin as Nanotransporter – Part I: Binding of Organosulfur Compounds. *Food Chem.* **2016**, *197*, 1015-1021.

53. Wilde, S.C., Treitz, C., Keppler, J.K., Koudelka, T., Palani, K., Tholey, A., Rawel, H.M., Scharz, K. β-Lactoglobulin as Nanotransporter – Part II: Characterization of the Covalent Protein Modification by Allicin and Diallyl Disulfide. *Food Chem.* **2016**, *197*, 1022-1029.

54. Müller, A., Eller, J., Albrecht, F., Prochnow, P., Kuhlmann, K., Bandow, J.E., Slusarenko, A.J., Leichert, L.I.O. Allicin Induces Thiol Stress in Bacteria Through *S*-Allylmercapto Modification of Protein Cysteines. *J. Biol. Chem.* **2016**, *291*, 11477-11490.

55. Gruhlke, M.C.H., Antelmann, H., Bernhardt, J., Kloubert, V., Rink, L., Slusarenko, A.J. The Human Allicin-Proteome: *S*-Thioallylation of Proteins by the Garlic Defence Substance Allicin and Its Biological Effects. *Free Rad. Biol. Med.* **2019**, *131*, 144-153.

56. Imai, S., Tsuge, N., Tomotake, M., Nagatome, Y., Sawada, H., Nagata, T., Kumagai, H. An Onion Enzyme That Makes the Eyes Water. *Nature* **2002**, *419*, 685.

57. Aoyagi, M., Kamoi, T., Kato, M., Sasako, H., Tsuge, N., Imai, S. Structure And Bioactivity of Thiosulfinates Resulting from Suppression of Lachrymatory Factor Synthase in Onion. *J. Agric. Food Chem.* **2011**, 59, 10893-10900.

58. Lawson, L.D., Wang, Z.J. Pre-Hepatic Fate of the Organosulfur Compounds Derived from Garlic (Allium Sativum). *Planta Med.* **1993**, *59*, A688.

59. Lawson, L.D., Block, E. Comments on Garlic Chemistry: Stability Of *S*-(2-Propenyl) 2-Propene-1-sulfinothioate (Allicin) In Blood, Solvents, and Simulated Physiological Fluids. *J. Agric. Food Chem.* **1997**, *45*, 542-542.

60. Pinto, J.T., Krasnikov, B.F., Cooper, A.J.L. Redox-Sensitive Proteins are Potential Targets of Garlic-Derived Mercaptocysteine Derivatives. *J. Nutr.* **2006**, *136*, 835S-841S.

61. Cavallito, C.J., Buck, J.S., Suter, C.M. Allicin, the Antibacterial Principle of *Allium sativum*. II. Determination of the Chemical Structure. *J. Am. Chem. Soc.* **1944**, *66*, 1952-1954.

62. Zhang, G. & Parkin, K.L. S-Alk(en)ylmercaptocysteine: Chemical Synthesis, Biological Activities, and Redox-Related Mechanism. *J. Agric. Food Chem.* **2013**, *61*, 3030-3038.

63. Tocmo, R. & Parkin, K. S-Alk(en)ylmercaptocysteine Suppresses LPS-Induced Pro-inflammatory Responses in Murine Macrophages through Inhibition of NF-κB Pathway and Modulation of Thiol Redox Status. *Free Rad. Biol. Med.* **2018**, *129*, 548-558.

64. Mo, M., Li, S., Dong, Z., Li, C., Sun, Y., Li, A., Zhao, Z. S-Allylmercaptocysteine Ameliorates Lipopolysaccharide-Induced Acute Lung Injury in Mice by Inhibiting Inflammation and Oxidative Stress via Nuclear Factor Kappa B and Keap1/Nrf2 Pathways. *Int. Immunopharmacol.* **2020**, *81*, 1-10.

65. Sumiyoshi, H., Wargovich, M.J. Chemoprevention of 1,2-Dimethylhydrazine-Induced Colon Cancer in Mice by Naturally Occurring Organosulfur Compounds. *Canc. Res.* **1990**, *50*, 5084-5087.

66. Imai, J., Ide, N., Nagae, S., Moriguchi, T., Matsuura, H., Itakura, Y. Antioxidant and Radical Scavenging Effects of Aged Garlic Extract and Its Constituents. *Planta Med.* **1994**, *60*, 417-420.

67. Ide, N., Nelson, A.B., Lau, B.H.S. Aged Garlic Extract and Its Constituents Inhibit Cu^{+}-Induced Oxidative Modification of Low Density Lipoprotein. *Planta Med.* **1997**, *63*, 263-264.

68. Tocmo, R., Parkin, K. S-1-Propenylmercaptocysteine Protects Murine Hepatocytes Against Oxidative Stress via Persulfidation of Keap1 and Activation of Nrf2. *Free Rad. Biol. Med.* **2019**, *143*, 164-175.

69. Shirin, H., Pinto, J.T., Kawabata, Y., Soh, J.-W., Delohery, T., Moss, S.F., Murty, V., Rivlin, R.S., Holt, P.R. & Weinstein, I.B. Antiproliferative Effects of S-Allylmercaptocysteine on Colon Cancer Cells When Tested Alone or in Combination with Sulindac Sulfide. *Cancer Res.* **2001**, *61*, 725-731.

70. Xiao, D., Pinto, J.T., Soh, J.W., Deguchi, A., Gundersen, G.G., Palazzo, A.F., Yoon, J.T., Shirin, H. & Weinstein, I.B. Induction of Apoptosis by the Garlic-Derived Compound S-Allylmercaptocysteine (SAMC) is Associated with Microtubule Depolymerization and c-Jun NH_2-Terminal Kinase 1 Activation. *Cancer Res.* **2003**, *63*, 6825-6837.

71. Xiao, D., Pinto, J.T., Gundersen, G.G. & Weinstein, I.B. Effects of a Series of Organosulfur Compounds on Mitotic Arrest and Induction of Apoptosis in Colon Cancer Cells. *Mol. Cancer Ther.* **2005**, *4*, 1388-1398.

72. Zhang, W., Xiao, H., Parkin, K.L. Apoptosis in MCF-7 Breast Cancer Cells Induced by S-Alkenylmercaptocysteine (CySSR) Species Derived from Allium Tissues in Combination with Sodium Selenite. *Food Chem. Toxicol.* **2014**, *68*, 1-10.

73. Zhang, W., Tocmo, R., Parkin, K.L. Synergistic Effects of S-Alkenylmercaptocysteine (CySSR) Species Derived from Allium Tissue and Selenium on Inducing Apoptosis in ER^- Breast Cancer Cells. *J. Funct. Foods* **2020**, *65*, 1-11.

74. Ishii, T., Bannai, S., Sugita, Y. Mechanism of Growth Stimulation of L1210 Cells by 2-Mercaptoethanol *in Vitro*. *J. Biol Chem.* **1981**, *256*, 12387-12392.

75. Ren, Q. Thiosulfinate Manipulation in Allium Tissues and Biological Effects of Thiosulfinates on Cells In Vitro. *Ph.D. Dissertation, University of Wisconsin-Madison* (2006).

76. Lawson, L.D. & Wang, Z.J. Allicin and Allicin-Derived Garlic Compounds Increase Breath Acetone through Allyl Methyl Sulfide: Use in Measuring Allicin Bioavailability. *J. Agric. Food Chem.* **2005**, *53*, 1974-1983.

77. Germain, E., Auger, J., Ginies, C., Siess, M.H., Teyssier, C. *In Vivo* Metabolism of Diallyl Disulphide in the Rat: Identification of Two New Metabolites. *Xenobiotica* **2002**, *32*, 1127-1138.

78. Yang, M., Dong, Z., Jiang, X., Zhao, Z., Zhang, J., Cao, X., Zhang, D. Determination of S-Allylmercaptocysteine in Rat Plasma by LC-MS/MS and Its Application to a Pharmacokinetics Study. *J. Chromatogr. Sci.* **2018**, *56*, 396-402.

79. Cooper, A.J.L., Pinto. J.T. Aminotransferase, L-Amino Acid Oxidase, and β-Lyase Reactions Involving L-Cysteine *S*-Conjugates Found in Allium Extracts: Relevance to Biological Activity? *Biochem. Pharmacol.* **2005**, *69*, 209-220.

80. Cooper, A.J.L., Bruschi, S.A., Anders, M.W. Toxic Halogenated Cysteine S-Conjugates and 3 Targeting of Mitochondrial Enzymes of Energy Metabolism. *Biochem. Pharmacol.* **2002**, *64*, 553-563.

81. Ida, T., Sawa, T., Ihara, H., Tsuchiya, Y., Watanabe, Y., Kumagai, Y., Suematsu, M., Motohashi, H., Fujii, S., Matsunaga, T., Yamamoto, M., Ono, K. Devarie-Baez, N.O., Xian, M., Fukuto, J.M., Akaike, T. Reactive Cysteine Persulfides and S-Polythiolation Regulate Oxidative Stress and Redox Signaling. *Proc. Natl. Acad. Sci. USA* **2014**, *111*, 7606-7611.

82. Liu, L., Yeh, Y.-Y. Inhibition of Cholesterol Biosynthesis by Organosulfur Compounds Derived from Garlic. *Lipids* **2000**, *35*, 197-203.

83. Lea, M.A., Rasheed, M., Randolph, V.M., Khan, F., Shareef, A., desBordes, C. Induction of Histone Acetylation and Inhibition of Growth of Mouse Erythroleukemia Cells by S-Allylmercaptocysteine. *Nutr. Cancer* **2002**, *43*, 90-102.

84. Medzhitov, R. Origin and Physiological Roles of Inflammation. *Nature* **2008**, *454*, 428-435.

85. Mo, M., Li, S., Dong, Z., Li, C., Sun, Y., Li, A., Zhao, Z. S-Allylmercaptocysteine Ameliorates Lipopolysaccharide-Induced Acute Lung Injury in Mice by Inhibiting Inflammation and Oxidative Stress via Nuclear Factor Kappa B and Keap1/Nrf2 Pathways. *Int. Immunopharmacol.* **2020**, *81*, 1-10.

86. Xiao, J., Ching, Y.P, Liong, E.C., Nanji, A.A., Fung, M.L., Tipoe, G.L. Garlic-Derived S-Allylmercaptocysteine is a Hepato-Protective Agent in Non-Alcoholic Fatty Liver Disease In Vivo Animal Model. *Eur. J. Nutr.* **2013**, *52*, 179-191.

87. Xiao, J., Liong, E.C., Ling, M.-T., Ching, Y.-P., Fung, M.-L., Tipoe, G.L. S-Allylmercaptocysteine Reduces Carbon Tetrachloride-Induced Hepatic Oxidative Stress and Necroinflammation via Nuclear Factor Kappa B-Dependent Pathways in Mice. *Eur. J. Nutr.* **2012**, *51*, 323-333.

88. Yang, L., Yang, M., Li, S., Zhao, Z. S-Allylmercaptocysteine Attenuates Posaconazole-Induced Adverse Effects in Mice through Antioxidation and Anti-Inflammation. *Int. Immunopharmacol.* **2018**, *58*, 9-14.

89. Pinto. J.T., Qiao, C., Xing, J., Rivlin, R.S., Protomastro, M.L., Weissler, M.L., Tao, Y., Thaler, H., Heston, W.D. Effects of Garlic Thioallyl Derivatives on Growth, Glutathione Concentration, and Polyamine Formation of Human Prostrate Carcinoma Cells in Culture. *Am. J. Clin. Nutr.* **1997**, *66*, 398-405.

90. Sigounas, G., Hooker, J., Anagnostou, A., Steiner, M. S-Allylmercaptocysteine Inhibits Cell Proliferation and Reduces the Viability of Erythroleukemia, Breast, and Prostate Cancer Cell Lines. *Nutr. Cancer* **1997**, *27*, 186-191.

91. Sigounas, G., Hooker, J.L., Li, W., Anagnostous, A., Steiner, M. S-Allylmercaptocysteine, a Stable Thioallyl Compound, Induces Apoptosis in Erythroleukemia Cell Lines. *Nutr. Cancer* **1997**, *28*, 153-159.

92. Pinto, J.T., Qiao, C., Xing, J., Suffoletto, B.P., Schubert, K.B., Rivlin, R.S., Huryk, R.F., Bacich, D.J., Heston, W.D. Alterations of Prostate Biomarker Expression and Testosterone Utilization in Human LNCaP Prostatic Carcinoma Cells by Garlic-Derived S-Allylmercaptocysteine. *Prostate* **2000**, *45*, 304-314.

93. Chu, Q., Ling, M.T., Feng, H., Cheung, H.W., Tsao, S.W., Wang, X., Wong, Y.C. A Novel Anticancer Effect of Garlic Derivatives: Inhibition of Cancer Cell Invasion through Restoration of *E-Cadherin* Expression. *Carcinogenesis* **2006**, *27*, 2180-2189.

94. Howard, E.W., Ling, M.T., Chua, C.W., Cheung, H.W., Wang, X., Wong, Y.C. Garlic-Derived S-Allylmercaptocysteine is a Novel In Vivo Antimetastatic Agent for Androgen-Independent Prostate Cancer. *Clin. Cancer Res.* **2007**, *13*, 1847-1856.

95. Lee, Y. Induction of Apoptosis by S-Allylmercapto-L-Cysteine, a Biotransformed Garlic Derivative, on a Human Gastric Cancer Cell Line. *Int. J. Mol. Med.* **2008**, *21*, 765-770.

96. Howard, E.W., Lee, D.T., Chiu, Y.T., Chua, C.W., Wang, X., Wong, Y.C. Evidence of a Novel Docetaxel Sensitizer, Garlic-Derived S-Allylmercaptocysteine, as a Treatment Option for Hormone Refractory Prostate Cancer. *Int. J. Cancer* **2008**, *122*, 1941-1948.

97. Lee, Y., Kim, H., Lee, J., Kim, K. Anticancer Activity of S-Allylmercapto-L-Cysteine on Implanted Tumor of Human Gastric Cancer Cell. *Biol. Pharm. Bull.* **2011**, *34*, 677-681.

98. Yan, J.Y., Tian, F.M., Hu, W.N., Zhang, J.H., Cai, H.F., Li, N. Apoptosis of Human Gastric Cancer Cells Line SGC 7901 Induced by Garlic-Derived Compound S-Allylmercaptocysteine (SAMC). *Eur. Rev. Med. Pharmacol. Sci.* **2013**, *17*, 745-751.

99. Zhang, H., Wang, K., Lin, G., Zhao, Z. Antitumor Mechanisms of S-Allyl Mercaptocysteine for Breast Cancer Therapy. *BMC Complement. Altern. Med.* **2014**, *270*, 1-12.

100. Tong, D., Qu, H., Meng, X., Jiang, Y., Liu, D., Ye, S., Chen, H., Jin, Y., Fu, S., Geng, J. S-Allylmercaptocysteine Promotes MAPK Inhibitor-Induced Apoptosis by Activating the TGF-β Signaling Pathway in Cancer Cells. *Oncol. Rep.* **2014**, *32*, 1124-1132.

101. Zhang, Y., Li, H.Y., Zhang, Z.H., Bian, H.L., Lin, G. Garlic-Derived Compound S-Allylmercaptocysteine Inhibits Cell Growth and Induces Apoptosis via the JNK and p38 Pathways in Human Colorectal Carcinoma Cells. *Oncol. Lett.* **2014**, *8*, 2591-2596.

102. Liu, Y., Yan, J., Han, X., Hu, W. Garlic-Derived Compound S-Allylmercaptocysteine (SAMC) is Active Against Anaplastic Thyroid Cancer Cell Line 8305C (HPACC). *Technol. Health Care* **2015**, *23*, S89-S93.

103. Wu, J., Zhao, S., Zhang, J., Qu, X., Jiang, X., Zhong, Z., Zhang, F., Wong, Y., Chen, H. Over-Expression of Survivin is a Factor Responsible for Differential Responses of Ovarian Cancer Cells to S-Allylmercaptocysteine (SAMC). *Exp. Mol. Pathol.* **2016**, *100*, 294-302.

104. Wang, K., Wang, Y., Qi, Q., Zhang, F., Zhang, Y., Zhu, X., Liu, G., Luan, Y., Zhao, Z., Cai, J., Cao, J., Li, S. Inhibitory Effects of S-Allylmercaptocysteine Against Benzo(a)pyrene-Induced Precancerous Carcinogenesis in Human Lung Cells. *Int. Immunopharmacol.* **2016**, *34*, 37-43.

105. Zhu, X., Jiang, X., Li, A., Sun, Y., Liu, Y., Sun, X., Feng, X., Li, S., Zhao, Z. S-Allylmercaptocysteine Suppresses the Growth of Human Gastric Cancer Xenographs Through Induction of Apoptosis and Regulation of MAPK and PI3K/Akt Signaling Pathways. *Biochem. Biophys. Res. Commun.* **2017**, *491*, 821-826.

106. Li, S., Yang, G., Zhu, X., Cheng, L., Sun, Y., Zhao, Z. Combination of Rapamycin and Garlic-Derived S-Allylmercaptocysteine Induces Colon Cancer Cell Apoptosis and Suppresses Tumor Growth in Xenograft Nude Mice Through Autophagy/p62/Nrf2 Pathway. *Oncol. Rep.* **2017**, *38*, 1637-1644.

107. Yi, L.V., Kwok-Fai, S.O., Nai-Kei, W., Jia, X. Anti-Cancer Activities of *S*-Allylmercaptocysteine from Aged Garlic. *Chin. J. Nat. Medicines.* **2019**, *17*, 43-49.

108. Kansanen, E., Kuosmanen, S.M., Leinonen, H., Levonen, A.-L. The Keap1-Nrf2 Pathway: Mechanisms of Activation and Dysregulation in Cancer. *Redox Biol.* **2013**, *1*, 45-49.

109. Taguchi, K., Motohashi, H., Yamamoto, M. Molecular Mechanisms of the Keap1-Nrf2 Pathway in Stress Response and Cancer Evolution. *Gene Cells* **2011**, *16*, 123-140.

110. Zhang, G., Li, B., Lee, C.-H., Parkin, K.L. Cysteine and Glutathione Mixed-Disulfide Conjugates of Thiosulfinates: Chemical Synthesis and Biological Activities. *J. Agric. Food Chem.* **2010**, *58*, 1564-1571.

111. Yang, G., Zhao, K., Ju, Y., Mani, S., Cao, Q., Puukila, S., Khaper, N., Wu, L., Wang, R. Hydrogen Sulfide Protects Against Cellular Senescence via S-Sulfhydration of Keap1 and Activation of Nrf2. *Antioxid. Redox Signal.* **2013**, *18*, 1906-1919.

112. Zhu, X., Jiang, X., Li, A., Zhao, Z., Li, S. *S*-Allylmercaptocysteine Attenuates Cisplatin-Induced Nephrotoxicity Through Suppression of Apoptosis, Oxidative Stress, and Inflammation. *Nutrients* **2017**, *9*, 1-16.

113. Kimura, Y., Kimura, H. Hydrogen Sulfide Protects Neurons from Oxidative Stress. *FASEB J.* **2004**, *18*, 1-16.

114. Li, L., Bhatia, M., Zhu, Y.Z., Zhu, Y.C., Ramnath, R.D., Wang, Z.J., Anuar, F.B.M., Whiteman, M., Salto-Tellez, M., Moore, P.K. Hydrogen Sulfide is a Novel Mediator of Lipopolysaccharide-Induced Inflammation in the Mouse. *FASEB J.* **2005**, *19*, 1-17.

115. Lee, Z.W., Zhou, J., Chen, C.-S., Zhao, Y., Tan, C.-H., Li, L., Moore, P.K., Deng, L.-W. The Slow-Releasing Hydrogen Sulfide Donor, GYY4137, Exhibits Novel Anti-Cancer Effects *In Vitro* and *In Vivo*. *PLoS One* **2011**, *6*, 1-7.

116. Lefer, D.J. A New Gaseous Signaling Molecule Emerges: Cardioprotective Role of Hydrogen Sulfide. *Proc. Natl. Acad. Sci. U.S.A.* **2007**, *104*, 17907-17908.

117. Calvert, J.W., Jha, S., Gundewar, S., Elrod, J.W., Ramachandran, A., Pattillo, C.B., Kevil, C.G., Lefer, D.J. Hydrogen Sulfide Mediates Cardioprotection through Nrf2 Signaling. *Circ. Res.* **2009**, *105*, 365-374.

118. Benavides, G.A., Squadrito, G.L., Mills, R.W., Patel, H.D., Isbell, T.S., Patel, R.P., Darley-Usmar, V.M., Doeller, J.E., Kraus, D.W. Hydrogen sulfide mediates the vasoactivity of garlic. *Proc. Natl. Acad. Sci. U.S.A.* **2007**, *104*, 17977-17982.

119. Abe, K., Kimura, H. The Possible Role of Hydrogen Sulfide as an Endogenous Neuromodulator. *J. Neurosci*. **1996**, *16*, 1066-1071.

120. Cao, X., Ding, L., Xie, Z., Yang, Y., Whiteman, M., Moore, P.K., Bian, J.-S. A Review of Hydrogen Sulfide Synthesis, Metabolism, and Measurement: Is Modulation of Hydrogen Sulfide a Novel Therapeutic for Cancer? *Antioxid. Redox Signal.* **2018**, *31*, 1-38.

121. Singh, S., Padovani, D., Leslie, R.A., Chiku, T., Banerjee, R. Relative Contributions of Cystathionine Beta-Synthase and Gamma-Cystathionase to H_2S Biogenesis via Alternative Trans-Sulfuration Reactions. *J. Biol. Chem.* **2009**, *284*, 22457-22466.

122. Kabil, O., Vitvitsky, V., Xie, P., Banerjee, R. The Quantitative Significance of the Transsulfuration Enzymes for H_2S Production in Murine Tissues. *Antioxid. Redox Signal.* **2011**, *15*, 363-372.

123. Yang, G., Wu, L., Jiang, B., Yang, W., Qi, J., Cao, K., Meng, Q., Mustafa, A.K., Mu, W., Zhang, S., Snyder, S.H., Wang, R. H2S as a Physiologic Vasorelaxant: Hypertension in Mice with Deletion of Cystathionine Gamma-Lyase. *Science* **2008**, *322*, 587-590.

124. Shibuya, N., Tanaka, M., Yoshida, M., Ogasawara, Y., Togawa, T., Ishii, K., Kimura, H. 3-Mercaptoypyruvate Sulfurtransferase Produces Hydrogen Sulfide and Bound Sulfane Sulfur in the Brain. *Antioxid. Redox Signal.* **2009**, *11*, 703-714.

125. Cuevasanta, E., Lange, M., Bonanata, J., Coitiño, E.L., Ferrer-Sueta, G., Filipovic, M.R., Alvarez, B. Reaction of Hydrogen Sulfide with Disulfide and Sulfenic Acid to Form the Strongly Nucleophilic Persulfide. *J. Biol. Chem.* **2015**, *290*, 26866-26880.

126. Kasamatsu, S., Nishimura, A., Morita, M., Matsunaga, T., Hamid, H.A., Akaike, T. Redox Signaling Regulated by Cysteine Persulfide and Protein Polysulfidation. *Molecules* **2016**, *21*, 1-10.

127. Mustafa, A.K., Gadalla, M.M., Sen, N., Kim, S., Mu, W., Gazi, S.K., Barrow, R.K., Yang, G., Wang, R., Snyder, S.H. H_2S Signals Through Protein S-Sulfhydration. *Sci. Signal*. **2009**, *2*, 1-15.

128. Kabil, O., Banerjee, R. Redox Biochemistry of Hydrogen Sulfide. *J. Biol. Chem.* **2010**, *285*, 21903-21907.

129. Cuevasanta, E., Mollër, M.N., Alvarez, B. Biological Chemistry of Hydrogen Sulfide and Persulfides. *Arch. Biochem. Biophys.* **2017**, *617*, 9-25.

130. Agró, A.F., Mavelli, I., Cannella, C., Federici, G. Activation of Porcine Heart Mitochondrial Malate Dehydrogenase by Zero Valence Sulfur and Rhodanese. *Biochem. Biophys. Res. Commun.* **1976**, *68*, 553-560.

131. Zhao, K., Ju, Y., Li, S., Altaany, Z., Wang, R., Yang, G. S-Sulfhydration of MEK1 Leads to PARP-1 Activation and DNA Damage Repair. *EMBO Rep.* **2014**, *15*, 792-800.

132. Zhang, D., Macinkovic, I., Devarie-Baez, N.O., Pan, J., Park, C.-M., Carroll, K.S., Filipovic, M.R., Xian, M. Detection of Protein S-Sulfhydration by a Tag-Switch Technique. *Angew. Chem. Int. Ed. Engl.* **2014**, *53*, 575-581.

133. Sen, N., Paul, B.D., Gadalla, M.M., Mustafa, A.K., Sen, T., Xu, R., Kim. S., Snyder, S.H. Hydrogen Sulfide-Linked Sulhydration of NF-κB Mediates Its Antiapoptotic Actions. *Mol. Cell* **2012**, *45*, 13-24.

134. Yang, G., Zhao, K., Ju, Y., Mani, S., Cao, Q., Puukila, S., Khaper, N., Wu, L., Wang, R. Hydrogen Sulfide Protects Against Cellular Senescence via *S*-Sulfhydration of Keap1 and Activation of Nrf2. *Antioxid. Redox Signal.* **2013**, *18*, 1906-1919.

135. Francoleon, N.E., Carrington, S.J., Fukuto, J.M. The Reaction of H(2)S with Oxidized Thiols: Generation of Persulfides and Implications to H(2)S Biology. *Arch. Biochem. Biophys.* **2011**, *516*, 146-153.

136. Hargrove, J.L. Persulfide Generated from L-Cysteine Inactivates Tyrosine Aminotransferase. Requirement for a Protein with Cysteine Oxidase Activity and Gamma-Cystathionase. *J. Biol. Chem.* **1988**, *263*, 17262-17269.

137. Krishnan, N., Fu, C., Pappin, D.J., Tonks, N.K. H_2S-Induced Sulfhydration of the Phosphatase PTP1B and Its Role in the Endoplasmic Reticulum Stress Response. *Sci. Signal.* **2011**, *4*, 1-12.

138. Benson, S.W. Thermochemistry and Kinetics of Sulfur-Containing Molecules and Radicals. *Chem. Rev.* **1978**, *78*, 23-35.

139. Everett, S.A., Folkes, L.K., Wardman, P., Asmus, K.D. Free-Radical Repair by a Novel Perthiol: Reversible Hydrogen Transfer and Perthiyl Radical-Formation. *Free Radic. Res.* **1994**, *20*, 387-400.

140. Guo, C., Liang, F.L., Masood, W.S., Yan, X. Hydrogen Sulfide Protected Gastric Epithelial Cells from Ischemia/Reperfusion Injury by Keap1 S-Sulfhydration, MAPK

Dependent Anti-Apoptosis and NF-κB Dependent Anti-Inflammation Pathway. *Eur. J. Pharmacol.* **2014**, *725*, 70-78.

141. Xie, L., Gu, Y., Wen, M., Zhao, S., Wang, W., Ma, Y., Meng, G., Han, Y., Wang, Y., Liu, G., Moore, P.K., Wang, X., Wang, H., Zhang, Z., Yu, Y., Ferro, A., Huang, Z., Ji, Y. Hydrogen Sulfide Induces Keap1 S-Sulfhydration and Suppresses Diabetes-Accelerated Atherosclerosis via Nrf2 Activation. *Diabetes* **2016**, *65*, 3171-3184.

142. Koike, S., Nishimoto, S., Ogasawara, Y. Cysteine Persulfides and Polysulfides Produced by Exchange Reactions with H_2S Protect SH-SY5Y Cells from Methylglyoxal-Induced Toxicity Through Nrf2 Activation. *Redox Biol.* **2017**, *12*, 530-539.

143. Peake, B.F., Nicholson, C.K., Lambert, J.P., Hood, R.L., Amin, H., Amin, S., Calvert, J.W. Hydrogen Sulfide Preconditions the *db/db* Diabetic Mouse Heart Against Ischemia-Reperfusion Injury by Activating Nrf2 Signaling in an Erk-Dependent Manner. *Am. J. Physiol. Heart Circ. Physiol.* **2013**, *309*, 1214-1224.

144. Yamamoto, Y., Gaynor, R.B. Role of the NF-kB Pathway in the Pathogenesis of Human Disease States. *Curr. Mol. Med.* **2001**, *1*, 287-296.

145. Hunter, P. The Inflammation Theory of Disease. *EMBO Rep.* **2012**, *13*, 968-970.

146. Chow, J.C., Young, D.W., Golenbock, D.T., Christ, W.J. Gusovsky, F. Toll-Like Receptor-4 Mediates Lipopolysaccharide-Induced Signal Transduction. *J. Biol. Chem.* **1999**, *274*, 10689-10692.

147. Aliprantis, A.O., Yang, R.-B., Weiss, D.S., Godowski, P., Zychlinsky, A. The Apoptotic Signaling Pathway Activated by Toll-like Receptor-2. *EMBO J.* **2000**, *19*, 3325-3336.

148. Vaure, C., Liu, Y. A Comparative Review of Toll-Like Receptor 4 Expression and Functionality in Different Animal Species. *Front. Immunol.* **2014**, *5*, 1-15.

149. Cao, Z., Xiong, J., Takeuchi, M., Kurama, T., Goeddel, D.V. TRAF6 is a Signal Transducer for Interleukin-1. *Nature* **1996**, *383*, 443-446.

150. Israël, A. The IKK Complex, a Central Regulator of NF-κB Activation. *Cold Spring Harb. Perspect. Biol.* **2010**, *2*, 1-14.

151. Wang, C., Deng, L., Hong, M., Akkaraju, G.R., Inoue, J.-I., Chen, Z.J. TAK1 is a Ubiquitin-Dependent Kinase of MKK and IKK. *Nature* **2001**, *412*, 346-351.

152. Oh, G.-S., Pae, H.-O., Lee, B.-S., Kim, B.-N., K., J.-M., Kim, H.-R., Jeon, S.B., Jeon, W.K., Chae, H.-J., Chung, H.-T. Hydrogen Sulfide Inhibits Nitric Oxide Production and Nuclear Factor-κB via Heme Oxygenase-1 Expression in RAW 264.7 Macrophages Stimulated with Lipopolysaccharide. *Free Rad. Biol. Med.* **2006**, *41*, 106-119.

153. Hu, L.F., Wong, P.T., Moore, P.K., Bian, J.S. Hydrogen Sulfide Attenuates Lipopolysaccharide-Induced Inflammation by Inhibition of p38 Mitogen-Activated Protein Kinase in Microglia. *J. Neurochem.* **2007**, *100*, 1121-1128.

154. Whiteman, M., Li, L., Rose, P., Tan, C.-H., Parkinson, D.B., Moore, P.K. The Effect of Hydrogen Sulfide Donors on Lipopolysaccharide-Induced Formation of Inflammatory Mediators in Macrophages. *Antioxid. Redox Signal.* **2010**, *12*, 1147-1154.

155. Ogden, C.L., Yanovski, S.Z., Carroll, M.D., Flegal, K.M. The Epidemiology of Obesity. *Gastroenterology* **2007**, *132*, 2087-2102.

156. Spiegelman, B.M., Flier, J.S. Obesity and the Regulation of Energy Balance. *Cell* **2001**, *104*, 531-543.

157. Schelbert, K.B. Comorbidities of Obesity. *Prim. Care* **2009**, *36*, 271-285.

158. Fantuzzi, G. Adipose Tissue, Adipokines, and Inflammation. *J. Allergy Clin. Immunol.* **2005**, *115*, 911-919.

159. Muir, L.A., Neeley, C.K., Meyer, K.A., Baker, N.A., Brosius, A.M., Washabaugh, A.R., Varban, O.A., Finks, J.F., Zamarron, B.F., Flesher, C.G., Chang, J.S. Adipose Tissue Fibrosis, Hypertrophy, and Hyperplasia: Correlations with Diabetes in Human Obesity. *Obesity* **2016**, *24*, 597-605.

160. Schenk, S., Saberi, M. and Olefsky, J.M. Insulin Sensitivity: Modulation by Nutrients and Inflammation. *J. Clin. Invest.* **2008**, *118*, 2992-3002.

161. Kershaw, E.E., Flier, J.S. Adipose Tissue as an Endocrine Organ. *J. Clin. Endocrinol.* **2004**, *89*, 2548-2556.

162. Myers, M.G., Cowley, M.A., Münzberg, H. Mechanisms of Leptin Action and Leptin Resistance. *Annu. Rev. Physiol.* **2008**, *70*, 537-556.

163. Abella, V., Scotece, M., Conde, J., Pino, J., Gonzalez-Gay, M.A., Gomez-Reino, J.J., Mera, A., Lago, F., Gómez, R., Gualillo, O. Leptin in the Interplay of Inflammation, Metabolism and Immune System Disorders. *Nat. Rev. Rheumatol.* **2017**, *13*, 100-109.

164. Turer, A.T., Scherer, P.E. Adiponectin: Mechanistic Insights and Clinical Implications. *Diabetologia* **2012**, *55*, 2319-2326.

165. Blaser, H., Dostert, C., Mak, T.W., Brenner, D. TNF and ROS Crosstalk in Inflammation. *Trends Cell Biol.* **2016**, *26*, 249-261.

166. Hoareau, L., Bencharif, K., Rondeau, P., Murumalla, R., Ravanan, P., Tallet, F., Delarue, P., Cesari, M., Roche, R., Festy, F. Signaling Pathways Involved in LPS Induced TNFalpha Production in Human Adipocytes. *J. Inflamm.* **2010**, *7*, 1-12.

167. Hotamisligil, G.S., Murray, D.L., Choy, L.N., Spiegelman, B.M. Tumor Necrosis Factor Alpha Inhibits Signaling from the Insulin Receptor. *Proc. Natl. Acad. U.S.A.* **1994**, *91*, 4854-4858.

168. Park, E.J., Lee, J.H., Yu, G.Y., He, G., Ali, S.R., Holzer, R.G., Österreicher, C.H., Takahashi, H., Karin, M. Dietary and Genetic Obesity Promote Liver Inflammation And Tumorigenesis by Enhancing IL-6 and TNF Expression. *Cell* **2010**, *140*, 197-208.

169. Sies, H. Physiological Society Symposium: Impaired Endothelial and Smooth Muscle Cell Function in Oxidative Stress. *Exp. Physiol.* **1997**, *82*, 291-295.

170. Furukawa, S., Fujita, T., Shimabukuro, M., Iwaki, M., Yamada, Y., Nakajima, Y., Nakayama, O., Makishima, M., Matsuda, M., Shimomura, I. Increased Oxidative Stress in Obesity and Its Impact on Metabolic Syndrome. *J. Clin. Invest.* **2004**, *114*, 1752-1761.

171. Beltowski, J., Wojcicka, G., Gorny, D., Marciniak, A. The Effect of Dietary-Induced Obesity on Lipid Peroxidation, Antioxidant Enzymes and Total Plasma Antioxidant Capacity. *J. Physiol. Pharmacol.* **2000**, *51*, 883-896.

172. Bournat, J.C., Brown, C.W. Mitochondrial Dysfunction in Obesity. *Curr. Opin. Endocrinol. Diabetes Obes.* **2010**, *17*, 446-452.

173. Bulua, A.C., Simon, A., Maddipati, R., Pelletier, M., Park, H., Kim, K.Y., Sack, M.N., Kastner, D.L., Siegel, R.M. Mitochondrial Reactive Oxygen Species Promote Production of Proinflammatory Cytokines and are Elevated in TNFR1-Associated Periodic Syndrome (TRAPS). *J. Exp. Med.* **2011**, *208*, 519-533.

174. Zhang, M., Brewer, A.C., Schröder, K., Santos, C.X., Grieve, D.J., Wang, M., Anilkumar, N., Yu, B., Dong, X., Walker, S.J., Brandes, R.P., Shah, A.M. NADPH Oxidase-4 Mediates Protection Against Chronic Load-Induced Stress in Mouse Hearts by Enhancing Angiogenesis. *Proc. Natl. Acad. Sci. U.S.A.* **2010**, *107*, 18121-18126.

175. Moe, K.T., Aulia, S., Jiang, F., Chua, Y.L., Koh, T.H., Wong, M.C., Dusting, G.J. Differential Upregulation of Nox Homologues of NADPH Oxidase by Tumor Necrosis Factor-Alpha in Human Aortic Smooth Muscle and Embryonic Kidney Cells. *J. Cell Mol. Med.* **2006**, *10*, 231-239.

176. Zhang, K., Kaufman, R.J. From Endoplasmic-Reticulum Stress to the Inflammatory Response. *Nature* **2008**, *454*, 455-462.

177. Hartigh, L.J.D., Omer, M., Goodspeed, L., Wang, S., Wietecha, T., O'Brien, K.D., Han, C.Y. Adipocyte-Specific Deficiency of NADPH Oxidase 4 Delays the Onset of Insulin Resistance and Attenuates Adipose Tissue Inflammation in Obesity. *Arterioscler. Thromb. Vasc. Biol.* **2017**, *37*, 466-475.

178. Ozata, M., Mergen, M., Oktenli, C., Aydin, A., Sanisoglu, S.Y., Bolu, E., Yilmaz, M.I., Sayal, A., Isimer, A., Ozdemir, I.C. Increased Oxidative Stress and Hypozincemia in Male Obesity. *Clin. Biochem.* **2002**, *35*, 627-631.

179. Decsi, T., Molnár, D., Koletzko, B. Reduced Plasma Concentrations of Alpha-Tocopherol and Beta-Carotene in Obese Boys. *J. Pediatr.* **1997**, *130*, 653-655.

180. Salazar, D.E., Sorge, C.L., Jordan, S.W., Corcoran, G.B. Obesity Decreases Hepatic Glutathione Concentrations and Markedly Potentiates Allyl Alcohol-Induced Periportal Necrosis in the Overfed Rat. *Int. J. Obes. Relat. Metab. Disord.* **1994**, *18*, 25-33.

181. Capel, I.D., Dorrell, H.M. Abnormal Antioxidant Defence in Some Tissues of Congenitally Obese Mice. *Biochem. J.* **1984**, *219*, 41-49.

182. Rodríguez-Hernández, H., Simental-Mendía, L.E., Rodríguez-Ramírez, G., Reyes-Romero, M.A. Obesity and Inflammation: Epidemiology, Risk Factors, and Markers of Inflammation. *Int. J. Endocrinol.* **2013**, *2013*, 1-11.

183. Dhindsa, S., Tripathy, D., Mohanty, P., Ghanim, H., Syed, T., Aljada, A., Dandona, P. Differential Effects of Glucose and Alcohol on Reactive Oxygen Species Generation and Intranuclear Nuclear Factor-κB in Mononuclear Cells. *Metabolism* **2004**, *53*, 330-334.

184. Aljada, A., Ghanim, H., Mohanty, P., Syed, T., Bandyopadhyay, A., Dandona, P. Glucose Intake Induces an Increase in Activator Protein 1 and Early Growth Response 1 Binding Activities, in the Expression of Tissue Factor and Matrix Metalloproteinase in Mononuclear Cells, and in Plasma Tissue Factor and Matrix Metalloproteinase Concentrations. *Am. J. Clin. Nutr*. **2004**, *80*, 51-57.

185. Trayhurn, P. Hypoxia and Adipose Tissue Function and Dysfunction in Obesity. *Physiol. Rev.* **2013**, *93*, 1-21.

186. Kamei, N., Tobe, K., Suzuki, R., Ohsugi, M., Watanabe, T., Kubota, N., Ohtsuka-Kowatari, N., Kumagai, K., Sakamoto, K., Kobayashi, M., Yamauchi, T. Overexpression of Monocyte Chemoattractant Protein-1 in Adipose Tissues Causes Macrophage Recruitment and Insulin Resistance. *J. Biol. Chem.* **2006**, *281*, 26602-26614.

187. Shi, H., Kokoeva, M.V., Inouye, K., Tzameli, I., Yin, H., Flier, J.S. TLR4 Links Innate Immunity and Fatty Acid–Induced Insulin Resistance. *J. Clin. Invest.* **2006**, *116*, 3015-3025.

188. Özcan, U., Cao, Q., Yilmaz, E., Lee, A.H., Iwakoshi, N.N., Özdelen, E., Tuncman, G., Görgün, C., Glimcher, L.H., Hotamisligil, G.S. Endoplasmic Reticulum Stress Links Obesity, Insulin Action, and Type 2 Diabetes. *Science* **2004**, *306*, 457-461.

189. Arkan, M.C., Hevener, A.L., Greten, F.R., Maeda, S., Li, Z.W., Long, J.M., Wynshaw-Boris, A., Poli, G., Olefsky, J., Karin, M.IKK-β Links Inflammation to Obesity-Induced Insulin Resistance. *Nat. Med.* **2005**, *11*, 191-198.

190. Yuan, M., Konstantopoulos, N., Lee, J., Hansen, L., Li, Z.W., Karin, M., Shoelson, S.E. Reversal of Obesity-and Diet-Induced Insulin Resistance With Salicylates or Targeted Disruption of IKKβ. *Science* **2001**, *293*, 1673-1677.

191. Hundal, R.S., Petersen, K.F., Mayerson, A.B., Randhawa, P.S., Inzucchi, S., Shoelson, S.E., Shulman, G.I. Mechanism by Which High-Dose Aspirin Improves Glucose Metabolism in Type 2 Diabetes. *J. Clin. Invest.* **2002**, *109*, 1321-1326.

192. Kim, M.J., Kim, H.K. Effect of Garlic on High Fat Induced Obesity. *Acta Biol. Hung.* **2011**, *62*, 244-254.

193. Kumar, R., Chhatwal, S., Arora, S., Sharma, S., Singh, J., Singh, N., Bhandari, V., Khurana, A. Antihyperglycemic, Antihyperlipidemic, Anti-inflammatory and Adenosine Deaminase–Lowering Effects of Garlic in Patients with Type 2 Diabetes Mellitus with Obesity. *Diabetes Metab. Syndr. Obes.* **2013**, *6*, 49-56.

194. Yang, C., Li, L., Yang, L., Lǔ, H., Wang, S., Sun, G. Anti-Obesity and Hypolipidemic Effects of Garlic Oil and Onion Oil in Rats Fed a High-Fat Diet. *Nutr. Metab*. **2018**, *15*, 1-8.

195. Yoshinari, O., Shiojima, Y., Igarashi, K. Anti-Obesity Effects of Onion Extract in Zucker Diabetic Fatty Rats. *Nutrients* **2012**, *4*, 1518-1526.

196. Elkayam, A., Mirelman, D., Peleg, E., Wilchek, M., Miron, T., Rabinkov, A., Oron-Herman, M., Rosenthal, T. The Effects of Allicin on Weight in Fructose-Induced Hyperinsulinemic, Hyperlipidemic, Hypertensive Rats. *Am. J. Hypertens.* **2003**, *16*, 1053-1056.

197. Shi, X.E., Zhou, X., Chu, X., Wang, J., Xie, B., Ge, J., Guo, Y., Li, X., Yang, G. Allicin Improves Metabolism in High-Fat Diet-Induced Obese Mice by Modulating the Gut Microbiota. *Nutrients* **2019**, *11*, 2909-2923.

198. Zhang, C., He, X., Sheng, Y., Xu, J., Yang, C., Zheng, S., Liu, J., Li, H., Ge, J., Yang, M., Zhai, B. Allicin Regulates Energy Homeostasis Through Brown Adipose Tissue. *iScience* **2020**, *23*, 1-16.

199. Ernsberger, P., Johnson, J.L., Rosenthal, T., Mirelman, D., Koletsky, R.J. Therapeutic Actions of Allylmercaptocaptopril and Captopril in a Rat Model of Metabolic Syndrome. *Am. J. Hypertens.* **2007**, *20*, 866-874.

Chapter 2

The Hydrogen Sulfide-Releasing Properties of *S*-Alk(en)ylmercaptocysteines

2.1 Abstract

Allium mercaptocysteines are secondary organosulfur metabolites that exhibit anti-inflammatory and antioxidant properties. The hypothesis of the study was that mercaptocysteines release of hydrogen sulfide (H_2S), a gaseous signaling molecule, in the presence of thiols and H_2S-evolving enzymes. The aim of the present work was to characterize the H_2S-releasing properties of the isomeric garlic-derived *S*-allylmercaptocysteine (CySSA) and onion-derived *S*-1-propenylmercaptocysteine (CySSPe) *in chemico* and *in vitro*. CySSPe released 10-fold more H_2S than CySSA in the presence of glutathione over 24 h. CySSA generated H_2S in a time and dose-dependent manner in the presence of cysteine or glutathione. RAW 264.7 macrophage cells pretreated with CySSPe generated up to 15-fold more H_2S than CySSA and reached maximum H_2S levels after 2 h. CySSA did not exhibit H_2S release significantly above control. Chemical inhibition of cystathionine β-synthase (CBS) and cystathionine γ-lyase (CSE) in macrophage cells resulted in a reduction in H_2S output (15% and 31%, respectively) following treatment with CySSPe. Combined chemical binding of glutathione and inhibition of glutathione synthesis in the cells resulted in a 36% reduction in H_2S after CySSPe treatment. Therefore, mercaptocysteines are glutathione and enzyme-dependent H_2S donors, and may exert their biological activities through H_2S and related persulfides.

2.2 Introduction

Garlic (*Allium sativum*) and onion (*Allium cepa*) are the two most widely consumed *Allium* vegetables worldwide. The traditional medicinal properties of garlic and onion have been known for thousands of years in ancient Greek, Indian, and Chinese culture, and have been used in to treat wounds, promote healing, improve blood circulation, and reduce inflammation (1). The organosulfur compounds generated from these vegetables are associated with multiple biological activities, including antioxidant, anticarcinogenic, anti-inflammatory, and cardioprotective effects (2–4). However, the exact structure-activity relationship between these compounds and their elicited bioactive effects is still ambiguous.

Recently, the ability of organosulfur compounds to serve as H_2S donors under physiological conditions has received significant research attention (5). H_2S is considered a third endogenous gaseous signaling molecule in addition to nitric oxide and carbon monoxide (6). H_2S confers several physiological functions, including antioxidation, anti-inflammation, vasodilation, synaptic transmission, and angiogenesis (5,7). The therapeutic properties of H_2S have been well-studied, and several synthetic and natural donors of this gaseous compound have been identified as potential therapeutic compounds (5). Organosulfur compounds from garlic, namely diallyl disulfide (DADS) and diallyl trisulfide (DATS), have been shown to exert their healthful properties through the release of H_2S *in vitro* and in animal-based studies (8,9). For example, the vasoactivity of garlic is primarily mediated by the H_2S generated from garlic-derived polysulfides through their reaction with the endogenous thiol glutathione (GSH) (7).

Garlic and onion organosulfur compounds are generated from the enzymatic release of sulfenic acid from endogenous cysteine sulfoxides. Sulfenic acids readily dimerize to form thiosulfinates, which react with nucleophiles or decay to other organosulfur compounds such as

DADS, DATS, ajoene, and vinyldithiins (10). The bioavailability of allicin, the major thiosulfinate of crushed garlic, is up to 80% in humans and allicin has been found to be quickly metabolized in human blood and rodents to form allyl mercaptan in less than 1 minute (11). High concentrations of allicin administered through crushed fresh garlic or synthetic allicin solutions result in no detectable levels of allicin in blood, urine, or stool (12,13). Thiosulfinates rapidly react with endogenous reduced thiol groups, such as cysteine or GSH, to form stable mercaptocysteines (14). The onion-derived mercaptocysteine, *S*-1-propenylmercaptocysteine (CySSPe), has been shown to generate H_2S when incubated with murine hepatocytes (15).

H_2S is generated in cells through the action of cystathionine beta-lyase (CBS) and cystathionine gamma-synthase (CSE) on cysteine and cysteine-containing substrates (16,17). Given the mechanism by which these enzymes act on cysteine derivatives, it is believed alkenylmercaptocysteine derivatives yield persulfide, a potential sulfur sulfane intermediate that exerts the biological effects of *Allium*-derived mercaptocysteines by modifying protein function through its action on the key cysteinyl residues in signaling proteins (18). The formation of persulfides in enzymes and proteins has been shown to accelerate or deactivate their activity (19,20). CySSA, the allicin cysteine conjugation product, is a more effective substrate for β-lyase activity than its endogenous substrate, cysteine (21). Additionally, treatment of Hepa1c1c7 murine cells with CySSPe, the onion-derived isomer, yielded the persulfidated Keap1, a highly reactive S-sulfhydration product of the Keap1 sequestering protein of the Keap1-Nrf2 cytoprotective signaling pathway (15). However, persulfides are highly unstable and readily decompose to H_2S following thiol-disulfide exchange with GSH and other biologically relevant thiols. H_2S may be a marker of persulfide formation as well as a direct bioactive agent (22). Given that the H_2S-releasing capacity of organosulfur compounds is dependent on concentration

and chemical structure, it is necessary to examine how physiologically relevant conditions affect the H_2S-releasing potential of mercaptocysteines as a marker of persulfide formation.

There is a lack of data regarding the H_2S-releasing properties of *Allium* mercaptocysteines in chemical and cell culture environments, and the comparative H_2S production between different mercaptocysteines. The objective of this study was to characterize the H_2S-releasing potential of garlic and onion-derived mercaptocysteines to better understand their chemical fate in cellular and chemical systems.

2.3 Materials and Methods

2.3.1 Chemicals and General Procedures

All chemicals were obtained from Millapore Sigma (Burlington, MA, USA) unless otherwise noted. All solvents used for extraction or HPLC analysis were purchased from Fisher Scientific (Hampton, NH, USA) or Millapore Sigma. Garlic and onion were purchased from a local grocery store in Madison, WI. Analytical HPLC was conducted using 250 x 4.6 mm, 5 µM, Discovery C18 column (Supelco, Bellefonte, PA, USA) on an Ultimate 3000 HPLC System (Thermo Fisher Scientific, Madison, WI, USA) equipped with a diode array detector. Semi-preparative HPLC was carried out using a 250 x 21.2 mm, 5 µM, Discovery C18 (Supelco, Bellefonte, PA) on a Reveleris Prep purification system (Grace Co., Columbia, MD).

2.3.2 Preparation and Isolation of Mercaptocysteines

Five hundred grams of white onions were halved and heated in the microwave (700 W) for 5 to 8 minutes, then allowed to cool to room temperature. The onion tissue was homogenized with 50 g peeled fresh garlic and 100 mL deionized water for 1 minute at 4 ºC. The homogenized mixture was left to incubate at room temperature for 1 hr. After the incubation period, the

mixture was filtered through cheesecloth and extracted three times with 50 mL $CHCl_3$. The organic phase was separated, collected, and dried over anhydrous $MgSO_4$.

Approximately 1.0 g L-cysteine hydrochloride hydrate was dissolved in 10 mL MeOH and the solution was added dropwise to the thiosulfinate-enriched $CHCl_3$ solution. The solution was stirred and allowed to react over 30 to 45 minutes at 20-22 ºC. The solvent was removed under vacuum using a rotary evaporator, and the residue was re-dissolved in phosphate buffered saline (PBS) buffer and the pH re-adjusted to 2.1 - 2.2. CySSA and CySSPe were each isolated and purified from the crude mixture using a fractionator on a 250 x 21.2 mm, 5 µM, Discovery C18 on a Reveleris Prep purification system. Elution was conducted with MeOH/H_2O (30:70) with 0.5% acetic acid at a flow rate of 10 mL/min with detection at 254 nm. The corresponding fractions were collected, evaporated under vacuum to remove excess methanol, and freeze-dried to give two white solid powders for CySSA and CySSPe. HPLC, MS, and ^1H and ^{13}C NMR analyses were conducted to confirm the identity of the products **(Appendix A.2.)**, which corresponded with previously collected spectral data (23-25).

2.3.3 Cell Culture Protocols

Murine macrophage RAW 264.7 cells (ATCC® TIB-71) were obtained from ATCC (Manassas, VA). Cell cultures were maintained in 75-cm^2 tissue culture flasks in phenol red-free Dulbecco's Modified Eagle Medium (DMEM, Invitrogen) supplemented with 10% fetal bovine serum (FBS), streptomycin (100 µg/mL), penicillin (100 U/mL), and incubated at 37 ºC with 5% CO_2 humidified atmosphere. Cells (80-90% confluence) were sub-cultured every 2 to 3 days, passaging at a 1:10 split ratio and cell passages 5 to 16 were used for all experiments to reduce phenotype and genotype drift. The medium was replaced with fresh DMEM medium containing test compounds and the cells were incubated for 24 h.

2.3.4 Preparation of Flasks for H_2S Trapping

H_2S released from incubation in cell-free conditions was detected using 50 mL cell culture flasks that had been preset with a layer of zinc-agar as previously described (26). In brief, agar (1% w/v, DOT Scientific, Burton, MI) was prepared, autoclaved (20 min at 120 ºC), and kept at 60 ºC until use. Twenty mL of 45 mM zinc acetate (1% w/v) were first added to 100 mL of sterilized agar, and then 4.5 mL of 3 M NaOH (12% w/v). The solution was stirred, and 5 mL of the mixture was immediately applied to the inside of each flask on one side. The flasks were allowed to set in horizontal position overnight. Once the zinc-agar layer had solidified, the flasks were ready for incubation experiments.

2.3.5 Chemical Incubations with CySSA and CySSPe

Solutions of L-cysteine hydrochloride or glutathione were prepared by dissolving the solids in PBS buffer (pH = 7.0) to give a working concentration of 20 mM and degassed with N_2 gas for 15 min. The solutions of L-cysteine or glutathione were added to each of the zinc-agar flasks on the side void of agar to give the desired final concentration (250, 500, or 1000 μM). To the flasks were added aqueous buffered solutions of CySSA and CySSPe to give a final concentration of 500 μM. The solutions were thoroughly mixed, and the flasks were capped with a 14/20 rubber septum. The mixtures were allowed to incubate over 6 – 48 h in the dark. A blank vehicle control was included to establish a baseline measurement.

2.3.6 Detection of H_2S from Chemical Incubations

The H_2S produced from the chemical incubation reactions were trapped in the form of zinc sulfide in the agar layer and assayed as follows (26). After the incubation period, the media was aspirated from the flasks and care was taken to avoid disturbing the agar layer. The flasks were rotated 180º to position the agar layer down, and the agar was treated *in situ* with the

methylene blue assay (27). Two mL of *N,N*-dimethyl-*p*-phenylenediamine chloride (N,N-dpd, 40 mM in 7.2 M HCl) was added and the flask was gently rocked to create a uniform layer and incubated at 20-22 ºC for 10 min. Afterwards, 400 µL $FeCl_3$ (Thermofisher Scientific, Madison, WI; 30 mM in 1.2 M HCl) was added and mixed with the N,N-dpd. After 20 min incubation, the contents of the flask were thoroughly mixed and 200 µL aliquots were transferred to a 96-well microtiter plate. The absorbance of the mixture was measured at 670 nm with a UV-Visible SpectraMax spectrophotometer (Molecular Devices, San Jose, CA). The sulfide concentration was calculated against a standard curve that was generated using the zinc-agar trap culture flasks. The standard curve was generated by incubating flasks containing NaHS solutions (0 – 200 µM) for 1 h at 20-22 ºC and the agar layer was subjected to the same *in situ* methylene blue assay previously described. A blank vehicle control was included to establish a baseline measurement.

2.3.7 Detection of H_2S from Cell Culture Incubations

RAW 264.7 cells were cultured in phenol red-free Dulbecco's modified Eagle's medium (DMEM, Invitrogen, Carlsbad, CA) supplemented with 10% FBS, streptomycin (100 µg/mL), and penicillin (100 U/mL) at 37 ºC in 5% CO_2 in a 96-well plates (2 x 10^4 cells per well) for 24 h. The medium was then replaced with fresh medium containing mercaptocysteine test compounds, and the plates were incubated for 0.5 – 3 h. In another series of experiments, the cells were pretreated with PAG (5 mM), an inhibitor of the CSE enzyme, or AOAA (0.5 mM), an inhibitor of CBS for 1 h prior to the addition of test compounds. A 100 µL sample was removed from the culture supernatant of each well and treated with 100 µL zinc acetate/NaOH (1%/3% wt/vol). Subsequently, 25 µL of *N,N*-dimethyl-p-phenylenediamine sulfate (20 mM) in HCl (7.2 M) and 25 µL of $FeCl_3$ (30 mM) in HCl (1.2 M) were added, and the optical

absorbance of the solutions was measured after incubating for 20 min at a wavelength of 670 nm with a UV-Visible SpectraMax spectrophotometer.

2.3.8 Statistical Analysis

Statistical analyses were performed using SigmaPlot 13 software (Systat Software, Inc., San Jose, CA). Results were expressed as mean values ± SD of at least three independent experiments. Difference in the means were evaluated by one-way ANOVA followed by Tukey's HSD test, and differences of $P \leq 0.05$ were considered significant.

2.4 Results

2.4.1 Effects of reduced thiols on hydrogen sulfide production of mercaptocysteines

CySSA incubated with cysteine or glutathione and CySSPe incubated with glutathione generated significant levels of H_2S *in chemico* **(Fig. 2.1)**. CySSPe incubated with glutathione generated 47.8-fold more H_2S versus cysteine with CySSPe over 24 hours. CySSPe treated with glutathione produced 10-fold and 12.7-fold more H_2S compared to CySSA with glutathione or cysteine, respectively. The presence of 500 μM cysteine and glutathione increased H_2S output when incubated with CySSA over 48 hours **(Fig. 2.2)**. Increasing concentrations of reduced thiols with 500 μM CySSA increased H_2S released, with the combination of glutathione and CySSA exhibiting higher H_2S output than cysteine and CySSA at 1000 μM **(Fig. 2.3)**.

2.4.2 Effects of mercaptocysteines on hydrogen sulfide evolution *in vitro*

Given that mercaptocysteines yielded H_2S when combined with endogenous thiol glutathione, and the potential role played by H_2S in antioxidant and anti-inflammatory cell signaling, the ability of mercaptocysteines was further evaluated to generate H_2S in RAW 264.7 macrophage cells. Treatment of cells with CySSPe yielded H_2S in a dose-dependent manner over

the range evaluated **(Fig. 2.4)**. H_2S production was maximal 2 h following treatment **(Fig. 2.5)**. However, CySSA only generated <1 μM of H_2S over the same concentration and time range.

2.4.3 Effect of glutathione depletion on hydrogen sulfide output *in vitro*

Pre-treatment of RAW 264.7 cells with glutathione-depleting agent diethyl maleate (DEM) and either of the two mercaptocysteines retained cell viability near 100% **(Fig. 2.6)**. Combinations of DEM, glutathione synthesis inhibitor buthionine sulfoximine (BSO) and each of the two mercaptocysteines retained cell viability of >80%. CySSPe treatment increased H_2S levels 3.2-fold **(Fig. 2.7)**. Following DEM or DEM and BSO-dependent glutathione depletion and treatment with CySSPe, H_2S production was moderately reduced **(Fig. 2.7)**.

2.4.4 Effect of CBS and CSE inhibition on hydrogen sulfide output *in vitro*

Pre-treatment of macrophages with CBS inhibitor aminooxyacetic acid (AOAA) at 0.5 mM or CSE inhibitor propargylglycine (PAG) at 5 mM retained cell viabilities of >90% **(Fig. 2.8)**. Cells treated with CySSPe alone exhibited 2.5-fold more H_2S levels compared to untreated cells **(Fig. 2.9)**. Following pre-incubation with PAG or AOAA inhibitors and treatment with CySSPe, H_2S levels were decreased compared to CySSPe treatment alone.

2.5 Discussion

H_2S has been shown to be an important gaseous mediator in cellular physiology and pathology. To that end, the levels of H_2S released from the major mercaptocysteine species derived from *Allium* extracts was measured under various physiologically relevant conditions. H_2S was generated from major *Allium* mercaptocysteines CySSA and CySSPe in the presence of endogenous thiols cysteine and glutathione. In previous work, organosulfur compound DADS from garlic generated H_2S when directly reacted with glutathione (8). This H_2S-releasing potential of DADS is an important property involved in the mechanism by which DADS exerts

vasorelaxation in cardiac tissue. Other *Allium* organosulfur compounds have been shown to generate H_2S in a thiol-dependent manner. For example, DATS rapidly releases H_2S when mixed with glutathione and its bioactivity is partly attributed to this H_2S output (8,22,28).

Herein CySSPe was reported to produce a higher amount of H_2S than CySSA in the presence of glutathione alone over 24 h. Additionally, CySSM, another major *Allium*-derived mercaptocysteine, did not exhibit H_2S-releasing properties when mixed with either cysteine or glutathione in the same time frame. To our knowledge, there have been no other reports that demonstrate production of H_2S by the direct reaction of CySSPe with GSH in cell-free environments. The heightened H_2S output of CySSPe relative to both CySSA and CySSM is notable given the higher biological potency sometimes exhibited by CySSPe compared to these other mercaptocysteines. CySSPe has been shown to exert higher quinone reductase (QR)-inducing activity in hepatocytes versus CySSA and CySSM (24,25). CySSPe has also been shown to downregulate inflammatory signaling and the production of inflammatory mediators in activated murine macrophage cells more strongly compared to CySSA (29). These enhanced bioactivities may be attributable to the higher H_2S-donor properties associated with CySSPe.

The H_2S-donor properties of CySSPe has been previously demonstrated in hepatocytes (15). However, the comparative H_2S output between CySSPe and its isomer CySSA was not yet reported. CySSPe was shown to generate H_2S in macrophage cells several-fold higher than CySSA in a time and dose-dependent manner. In contrast, cells did not release significant levels of H_2S following the addition of CySSA within 3 hours.

Interestingly, increasing the concentration of reduced thiols raised the amount of H_2S evolved from CySSA *in chemico*. Furthermore, increasing the time of incubation increased the H_2S output from the reaction between CySSA and thiols over a 48 h time frame. H_2S release

from allyl disulfide-containing compounds is driven by thiol attack on the α-carbon of the allyl moiety, which is kinetically slow and only minor amounts of H_2S are formed from these compounds when reacted with glutathione (22). The direct reaction of excess thiols with allylic disulfides under physiological conditions has been previously demonstrated but requires 24 h to reach 56% completion (30). Other processes, such as the direct import of cysteine conjugates by cystine-specific and L system (leucine and related neutral amino acids) transporters followed by glutaredoxin (Grx)-dependent reduction to the corresponding mercaptan derivative and cysteine are more rapid **(Fig. 2.10)** (25). Within 3 h, more than one-third of added mercaptocysteine equivalents are reduced to mercaptan in CySSA-treated macrophage cells.

Cysteine is the main endogenous precursor of H_2S biosynthesis. However, cysteine alone is a poor H_2S donor and requires the presence of homocysteine to generate H_2S at physiologically relevant rates (16). Therefore, the ability of mercaptocysteines to donate cysteine equivalents alone is not sufficient to account for the elevated H_2S output by these compounds. Several cysteine derivatives are known H_2S donors with promising therapeutic properties in biological systems. *S*-propargyl-cysteine is a common H_2S donor that upregulates antioxidant proteins and attenuates inflammation in a H_2S-dependent manner (31,32). *S*-propyl-L-cysteine and *S*-allyl-L-cysteine are additional cysteine-containing H_2S donors that modulate antioxidant defenses in rats (31). The protective effects of these cysteine derivatives are attenuated upon the addition of CSE inhibitor, PAG, which suggests the H_2S-releasing properties and biological activities of these cysteine derivatives is dependent on the action of this enzyme (31,32).

In contrast, the H_2S output was only modestly reduced by the addition of inhibitors for either H_2S-generating enzymes CBS or CSE in macrophage cells, possibly because these enzymes were inhibited at limited levels, or other enzymes are involved, such as H_2S-generating

enzyme 3-mercaptopyruvate sulfurtransferase (3-MST). The presence of glutathione is a component of CySSPe metabolism to H_2S, shown by the 36% reduction in H_2S output following glutathione depletion and chemical inhibition of glutathione synthesis in macrophages. In hepatocytes, pretreatment of cells with BSO and DEM lowered H_2S output by 87%. Indeed, glutathione has been shown here to non-enzymatically release H_2S from both CySSA and CySSPe but appears to be more facile for CySSPe (15).

H_2S may be a byproduct of and marker for the more reactive persulfide in addition to serving as a bioactive mediator (33). Previous research in our laboratory demonstrated that the addition of CySSPe to hepatocytes generates the persulfidated Keap1 protein, a product of persulfide formation and exchange (15). Given that inhibition of CSE and CBS enzymes results in lowered H_2S output after the addition of CySSPe, mercaptocysteines may be directly metabolized by these enzymes to produce cysteine persulfide. CySSA and its saturated propyl analogue CySSP are known substrates of the β-lyase enzymes found in rat liver cytosol (18). Given the structural similarity of CySSPe to these mercaptocysteine analogues, CySSPe is likely to be a substrate of these enzymatic activities as well.

The present study suggests that glutathione reacts with CySSPe directly as one potential pathway by which H_2S is formed and generates higher quantities of H_2S than CySSA in the same time frame. While glutathione can react with allyl disulfides, such as CySSA, to form H_2S, the process is hampered by the poor reactivity of nucleophiles onto the α-carbon of allyl group (22,30). A potential mechanism by which glutathione may react with CySSPe and generate more H_2S than the corresponding reaction with CySSA is through a Michael addition-elimination reaction **(Fig. 2.11)**. In studies on glutathione-sensitive cleavable linkers containing vinyl sulfide-containing moieties, glutathione or other thiol undergoes Michael addition to these

chemical structures, leading to the cleavage of the unsaturated bond and formation of the *S*-vinyl glutathione conjugate with the concomitant release of the thiol-containing residue at physiological pH (34-36). Similarly, GSH may attack the vinyl carbon of the 1-propenyl moiety of CySSPe adjacent to the disulfide, giving rise to a dithioacetal. The dithioacetal would subsequently decompose to a cysteine persulfide and *S*-1-propenyl glutathione conjugate **(Fig. 2.11)**. The unstable cysteine persulfide product would readily release H_2S upon reaction with an additional GSH molecule. Given the role and reactivity of persulfides in biological signaling, more in-depth investigations into the chemical fate of CySSPe in the presence of reduced thiols as a possible GSH-sensitive persulfide donor is warranted.

In conclusion, the current study provided evidence that CySSA and CySSPe produce H_2S in a thiol-dependent manner. CySSPe showed the most potent H_2S-releasing properties both *in vitro* and *in chemico*, which is correlated with the higher biological activity demonstrated by CySSPe compared to other mercaptocysteines. Both direct reaction with glutathione and intracellular metabolism are important pathways by which mercaptocysteines are degraded to persulfides and subsequently H_2S, which may have potential health-conferring benefits against oxidative stress and inflammatory injury. Further work is necessary to understand how the H_2S-releasing properties of mercaptocysteines affect their biological activities and the role played by H_2S and related progenitors in activating or inhibiting relevant signaling pathways, such as cytoprotective Nrf2 or inflammatory NF-κB. Additionally, confirming the formation of persulfide, as the intermediate metabolic precursor to H_2S release, from the activity of CBS, CSE, or glutathione on mercaptocysteines would provide insight into the role of persulfides in the bioactivity exhibited by these compounds.

2.6 Figures and Tables

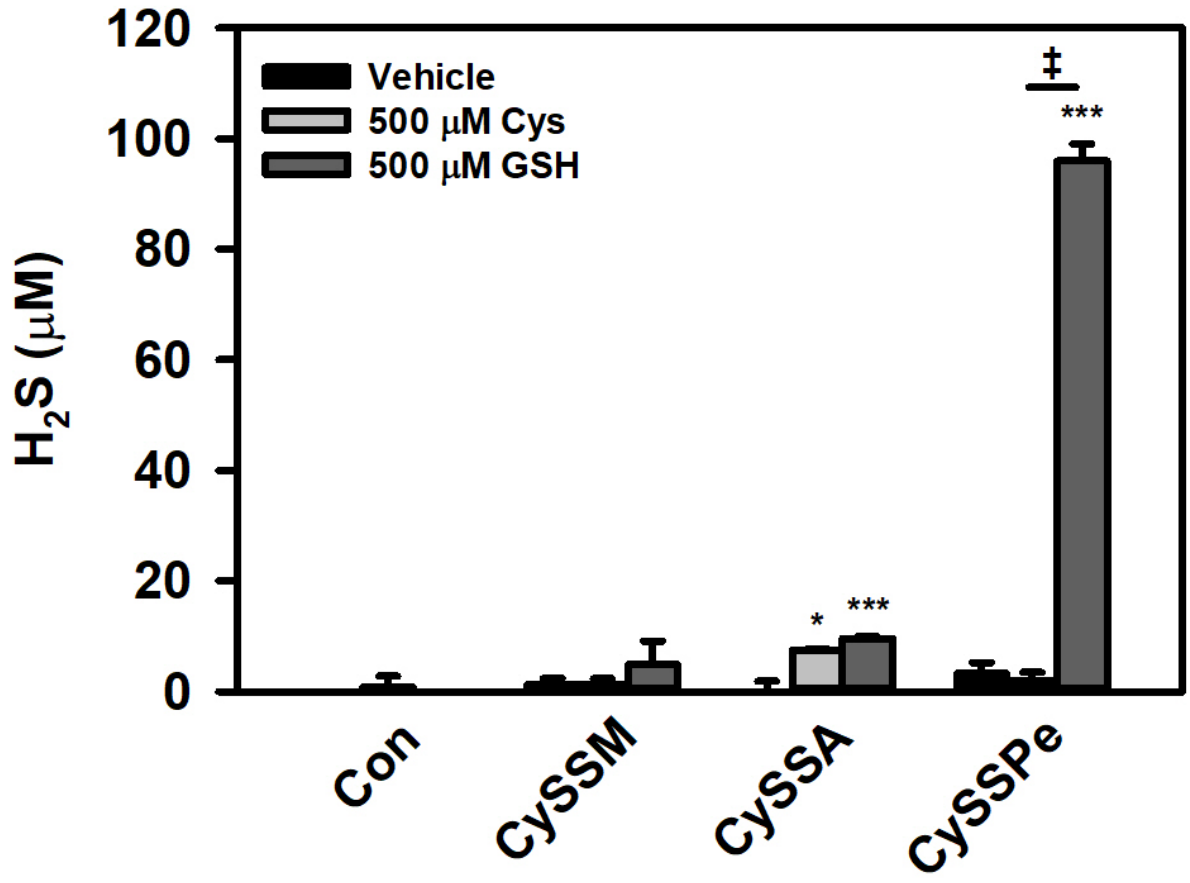

Figure 2.1. H_2S production by *Allium* mercaptocysteines in cell-free environments. Compounds treated with vehicle alone, 500 μM cysteine (Cys) in vehicle, or 500 μM glutathione (GSH) over 24 hours. Vehicle is 10 mM phosphate buffered saline (PBS) at pH 7.4. Statistical significance was determined by one-way ANOVA with Tukey's post-test. * = $P < 0.05$, *** = $P < 0.001$ vs control, bars bearing ‡ = $P < 0.001$.

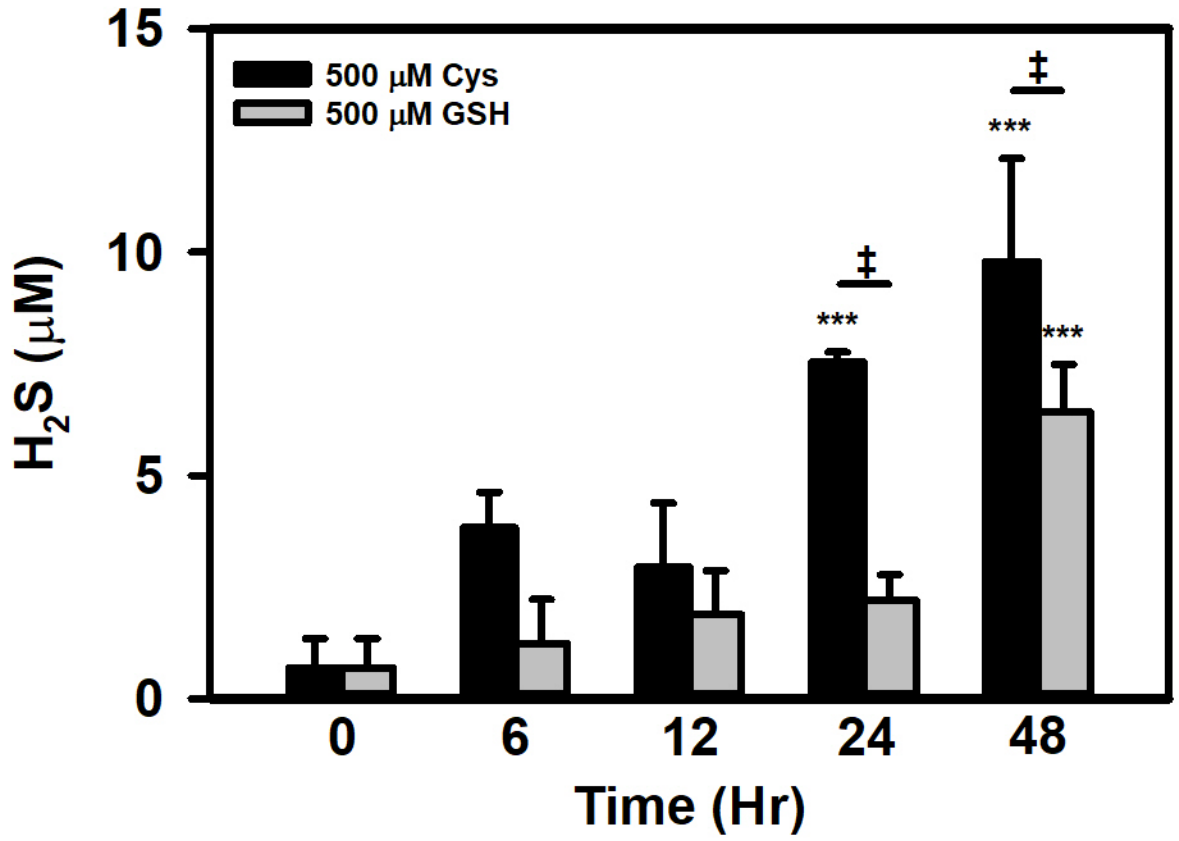

Figure 2.2. Time course of H_2S production by CySSA treated with Cys or GSH. CySSA was treated with 500 μM cysteine (Cys) or 500 μM glutathione (GSH) in 10 mM PBS at pH 7.4 over a 48-h period. Statistical significance was determined by one-way ANOVA with Tukey's post-test. *** = $P < 0.001$ vs control, bars bearing ‡ = $P < 0.001$.

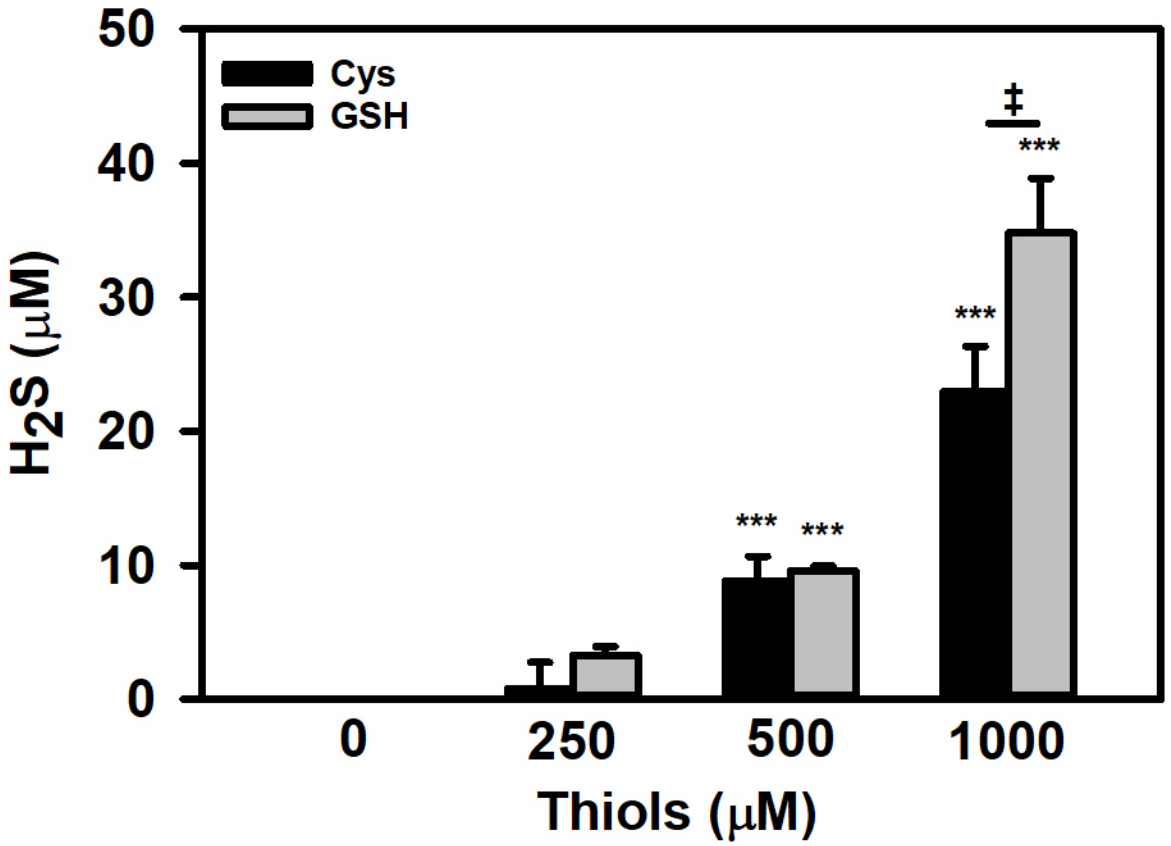

Figure 2.3. H_2S production by CySSA treated with varied concentrations of Cys or GSH. CySSA was treated with Cys or GSH (0-1000 μM) in 10 mM PBS at pH 7.4 after 24 h. Statistical significance was determined by one-way ANOVA with Tukey's post-test. *** = $P < 0.001$ vs control, bars bearing ‡ = $P < 0.001$.

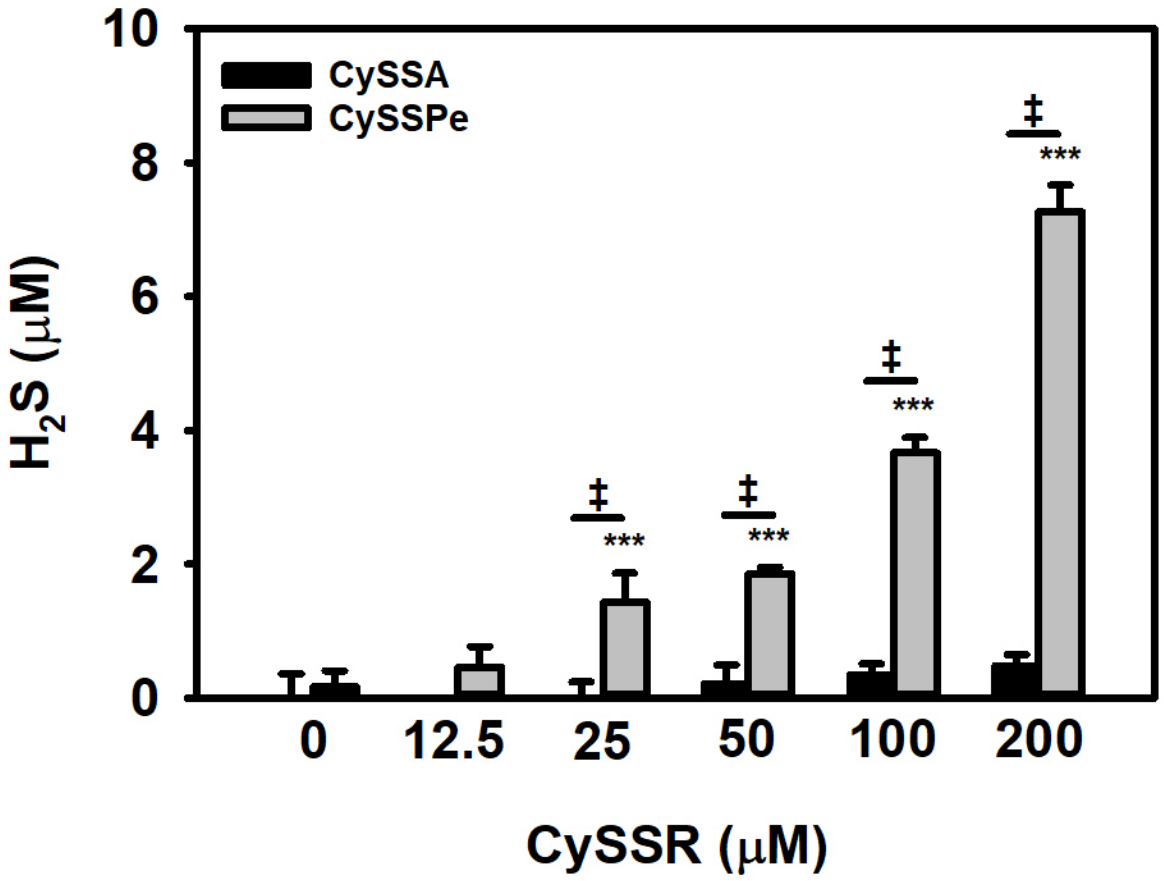

Figure 2.4. Dose-response curve of H_2S released by RAW 264.7 cells pretreated with CySSR. Cells were pretreated with CySSA or CySSPe (0-200 μM) for 2 h. Statistical significance was determined by one-way ANOVA with Tukey's post-test. *** = $P < 0.001$ vs [CySSR] = 0, bars bearing ‡ = $P < 0.001$.

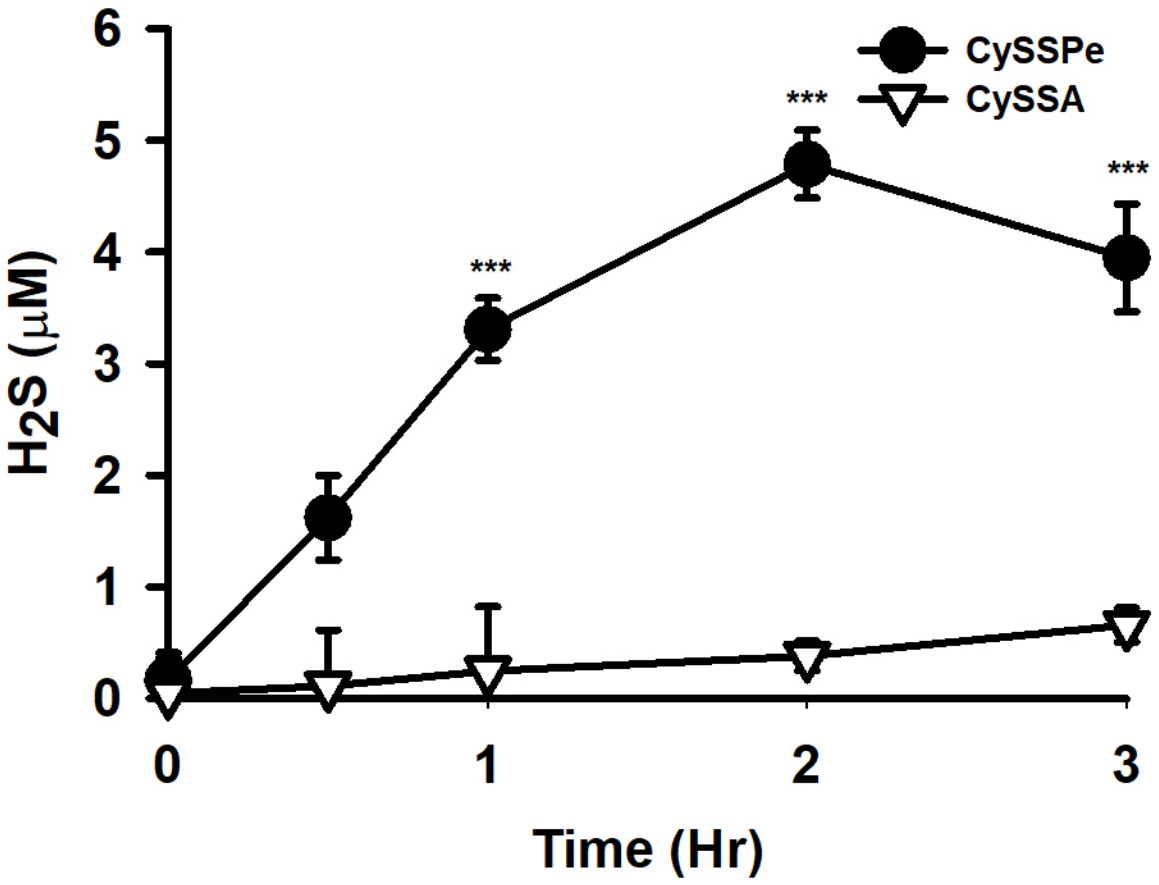

Figure 2.5. Time course of H_2S released by RAW 264.7 cells pretreated with CySSR. Cells were pretreated with 100 μM CySSA or 100 μM CySSPe over a 3-h period. Statistical significance was determined by one-way ANOVA with Tukey's post-test. *** = $P < 0.001$ vs Time = 0 hr.

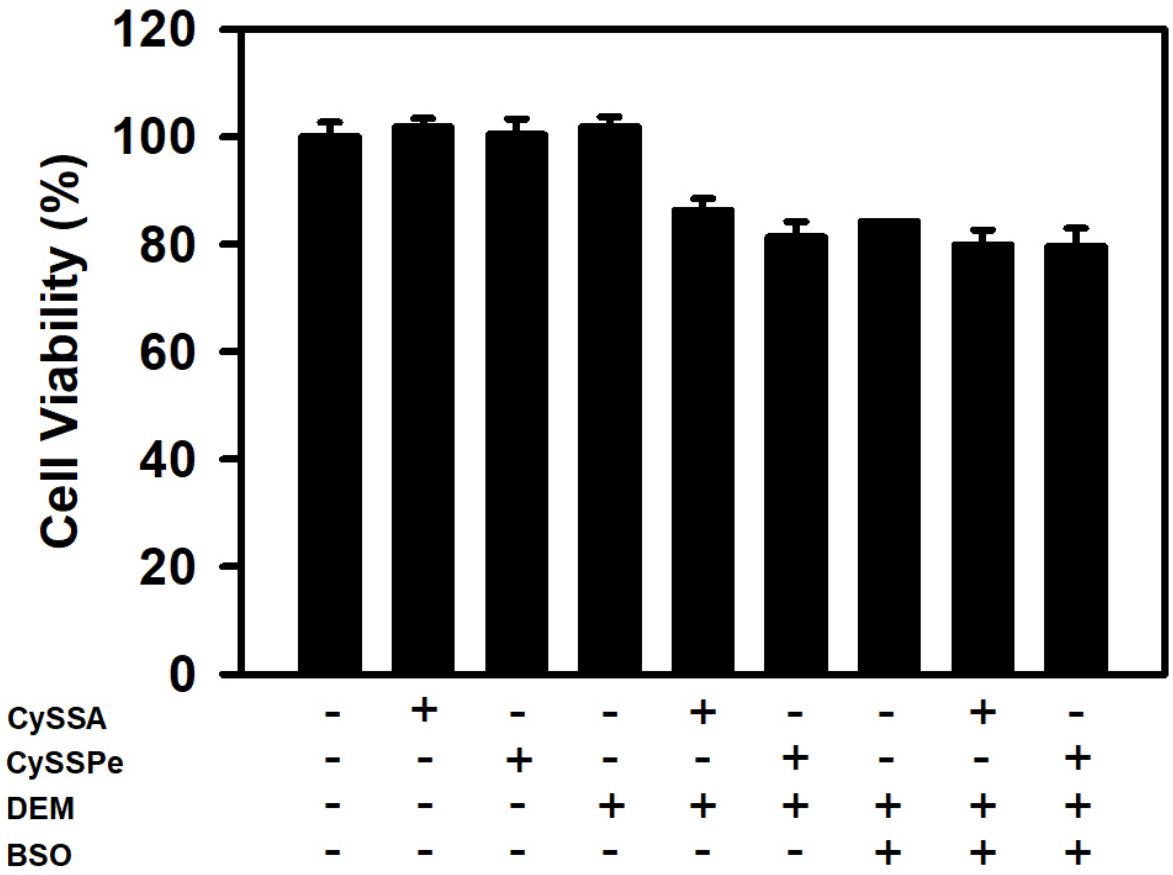

Figure 2.6. Cell viabliities of RAW 264.7 cells pretreated with GSH depleters and CySSR. Cells were pretreated with PBS vehicle, 10 mM DEM for 40 minutes prior, or 200 µM BSO for 18 h and 10 mM DEM for 40 minutes prior to incubation with 200 µM CySSA or 200 µM CySSPe for 2 h.

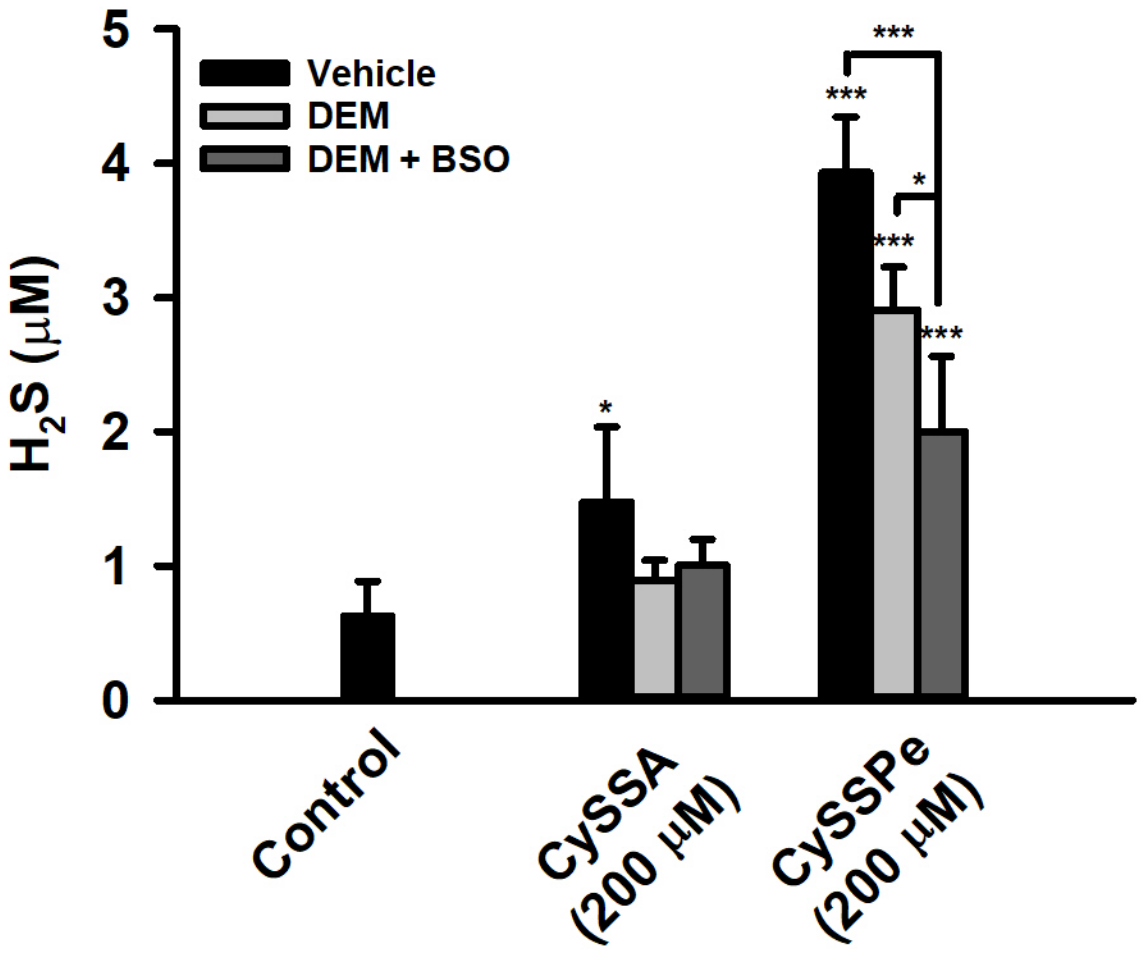

Figure 2.7. Relative H_2S release by RAW 264.7 cells pretreated with GSH depleters and CySSR. Cells were pretreated with 10 mM DEM for 40 minutes prior, or 200 μM BSO for 18 h and 10 mM DEM for 40 minutes prior to incubation with 200 μM CySSA or 200 μM CySSPe for 2 h. H_2S levels were normalized to control. Statistical significance was determined by one-way ANOVA with Tukey's post-test. * = $P < 0.05$, ** = $P < 0.01$, *** = $P < 0.001$ vs control.

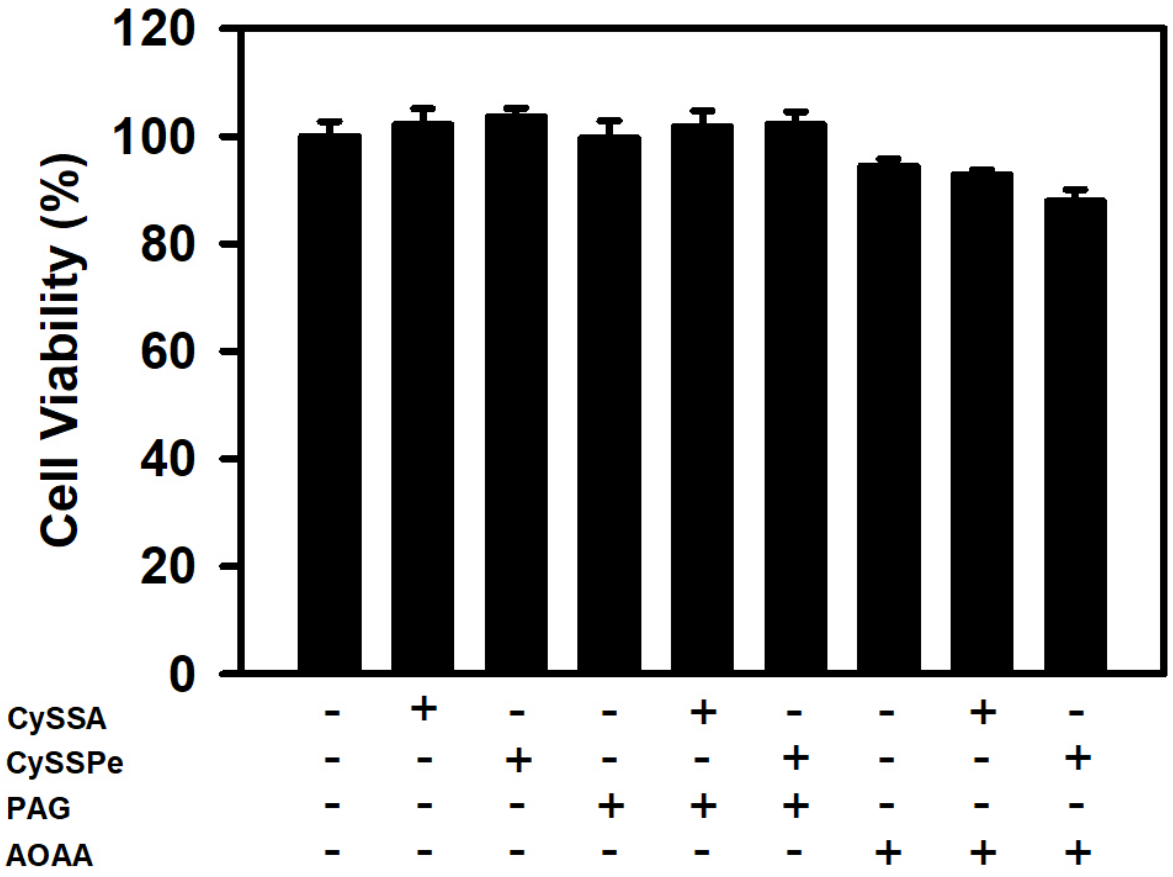

Figure 2.8. Cell viabliities of RAW 264.7 cells pretreated with CBS/CSE inhibitors and CySSR. Cells were pretreated with PBS vehicle, 5 mM PAG, or 0.5 mM AOAA for 4 h prior to incubation with 200 μM CySSA or 200 μM CySSPe for 2 h.

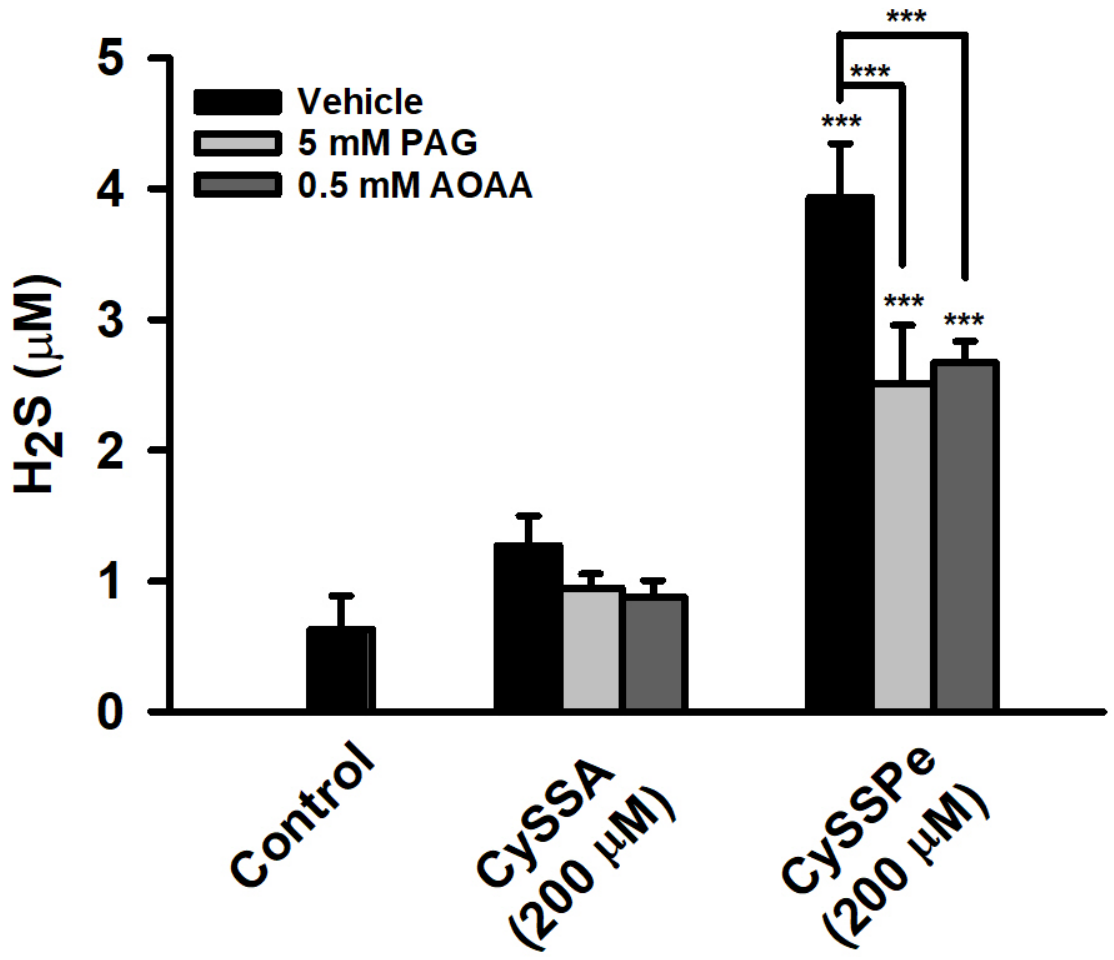

Figure 2.9. Relative H_2S release by RAW 264.7 cells pretreated with CBS/CSE inhibitors and CySSR. Cells were pretreated with PBS vehicle, 5 mM PAG, or 0.5 mM AOAA for 4 h prior to incubation with 200 μM CySSA or 200 μM CySSPe for 2 h. H_2S levels were normalized to control. Statistical significance was determined by one-way ANOVA with Tukey's post-test. *** = $P < 0.001$ vs control.

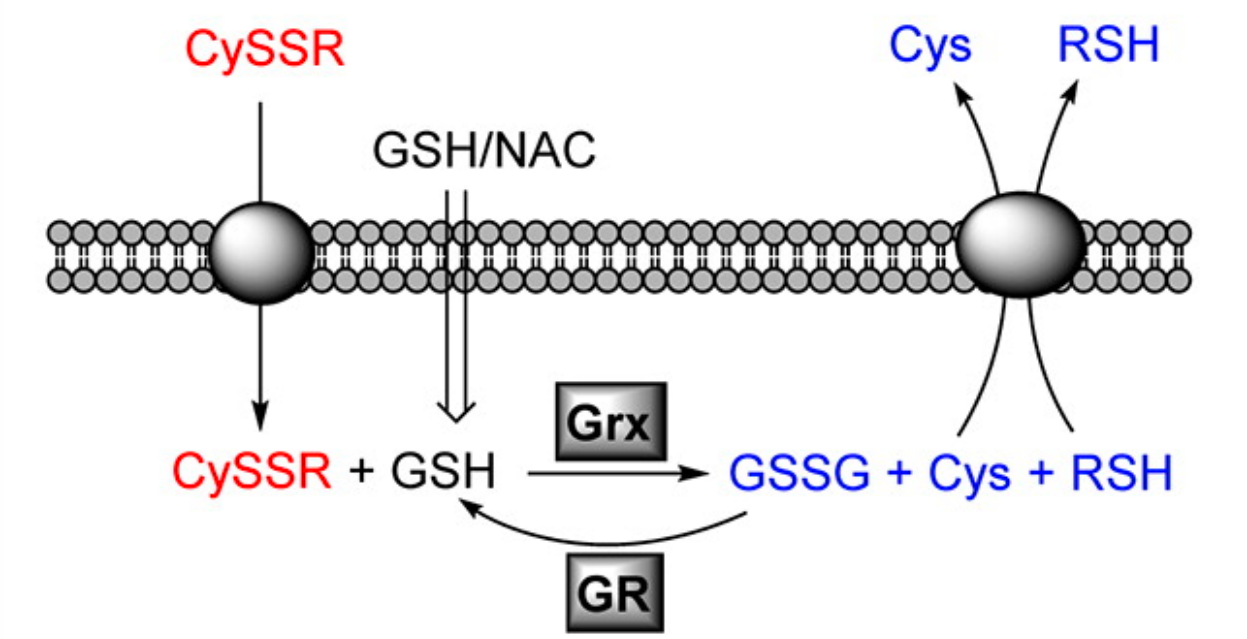

Figure 2.10. Mechanism of CySSR cell importation and reduction by Grx/GR. Mercaptocysteines are imported by cystine-specific and L system transporters and reduced by glutaredoxin via a glutathione-dependent mechanism. Both cysteine and the corresponding alkenyl mercaptan is exported from the cell (25).

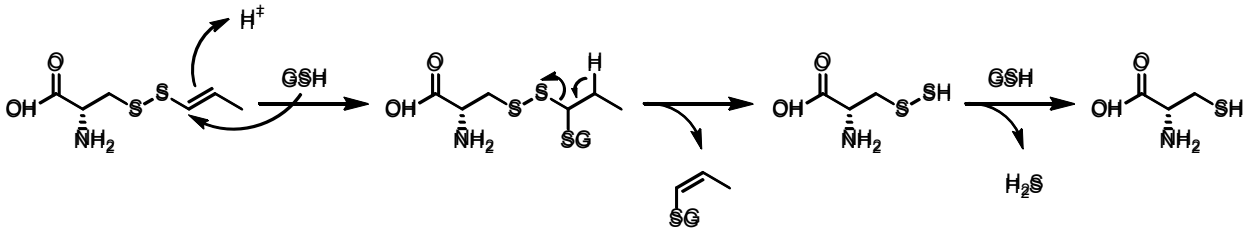

Figure 2.11. Michael addition-elimination mechanism as pathway for persulfide formation and H_2S by CySSPe treated with GSH. H_2S is subsequently generated through a thiol-disulfide exchange with an additional glutathione molecule.

2.7 References

1. Block, E. Antithrombotic Agent of Garlic: A Lesson From 5000 Years of Folk Medicine. In *Folk Medicine: The Art and the Science*. Steiner, R. P., Ed.; American Chemical Society: Washington, DC, 1986; pp 125-137.

2. Thomson, M., Ali, M. Garlic [Allium Sativum]: A Review of Its Potential Use as an Anti-Cancer Agent. *Curr. Canc. Drug Targets* **2003**, *3*, 67-81.

3. Kendler, B.S. Garlic (*Allium Sativum*) and Onion (*Allium Cepa*): A Review of Their Relationship to Cardiovascular Disease. *Prev. Med.* **1987**, *16*, 670-685.

4. Griffiths, G., Trueman, L., Crowther, T., Thomas, B., Smith, B. Onions–a Global Benefit to Health. *Phytother. Res.* **2002**, *16*, 603-615.

5. Wallace, J.L., Wang, R. Hydrogen Sulfide-Based Therapeutics: Exploiting a Unique but Ubiquitous Gasotransmitter. *Nat. Rev. Drug Discov.* **2015**, *14*, 329-345.

6. Szabo, C. Gasotransmitters In Cancer: From Pathophysiology to Experimental Therapy. *Nat. Rev. Drug Discov.* **2016**, *15*, 185-203.

7. Li, L., Rose, P., Moore, P.K. Hydrogen Sulfide and Cell Signaling. *Annu. Rev. Pharmacol. Toxicol.* **2011**, *51*, 169-187.

8. Benavides, G.A., Squadrito, G.L., Mills, R.W., Patel, H.D., Isbell, T.S., Patel, R.P., Darley-Usmar, V.M., Doeller, J.E., Kraus, D.W. Hydrogen Sulfide Mediates the Vasoactivity of Garlic. *Proc. Natl. Acad. Sci. U.S.A.* **2007**, *104*, 17977-17982.

9. Predmore, B.L., Kondo, K., Bhushan, S., Zlatopolsky, M.A., King, A.L., Aragon, J.P., Bennett Grinsfelder, D., Condit, M.E., Lefer, D.J. The Polysulfide Diallyl Trisulfide Protects the Ischemic Myocardium by Preservation of Endogenous Hydrogen Sulifde and Increasing Nitric Oxide Bioavailability. *Am. J. Physiol. Heart Circ. Physiol.* **2012**, *302*, H2410-H2418.

10. Block, E. The Organosulfur Chemistry of the Genus *Allium* – Implications for the Organic Chemistry of Sulfur. *Angew. Chem. Int. Ed.* **1992**, *31*, 1135-1178.

11. Lawson, L.D., Wang, Z.J. Allicin and Allicin-Derived Garlic Compounds Increase Breath Acetone through Allyl Methyl Sulfide: Use in Measuring Allicin Bioavailability. *J. Agric. Food Chem.* **2005**, *53*, 1974-1983.

12. Lawson, L.D., Ransom, D.K., Hughes, B.G. Inhibition of Whole Blood Platelet Aggregation by Compounds in Garlic Clove Extracts and Commercial Garlic Products. *Thromb. Res*. **1992**, *65*, 141-156.

13. Lawson, L.D. Garlic: A Review of Its Medicinal Effects and Indicated Active Compounds. In *Phytomedicines of Europe: Chemistry and Biological Activity*; Lawson, L.D., Bauer, R., Eds.; ACS Symposium Series 691; American Chemical Society: Washington, DC, 1998; pp 176-209.

14. Rabinkov, A., Miron, T., Mirelman, D., Wilchek, M., Glozman, S., Yavin, E., Weiner, L. S-Allylmercaptoglutathione: The Reaction Product of Allicin with Glutathione Possesses SH-Modifying and Antioxidant Properties. *BBA-Mol. Cell Res*. **2000**, *1499*, 144-153.

15. Tocmo, R., Parkin, K. *S*-1-Propenylmercaptocysteine Protects Murine Hepatocytes Against Oxidative Stress via Persulfidation Of Keap1 and Activation of Nrf2. *Free Rad. Biol. Med*. **2019**, *143*, 164-175.

16. Chen, X., Jhee, K.-H., Kruger, W.D. Production of The Neuromodulator H_2S by Cystathionine B-Synthase via the Condensation of Cysteine and Homocysteine. *J. Biol. Chem*. **2004**, *279*, 52082-52086.

17. Stipanuk, M.H., Beck, P.W. Characterization of the Enzymic Capacity for Cysteine Desulphhydration in Liver and Kidney of the Rat. *Biochem. J.* **1982**, *206*, 267-277.

18. Pinto, J.T., Krasnikov, B.F., Cooper, A.J.L. Redox-Sensitive Proteins are Potential Targets of Garlic-Derived Mercaptocysteine Derivatives. *J. Nutr*. **2006**, *136*, 835S-841S.

19. Mustafa, A.K., Gadalla, M.M., Sen, N., Kim, S., Mu, W., Gazi, S.K., Barrow, R.K., Yang, G., Wang, R., Snyder, S.H. H_2S Signals through Protein *S*-Sulfhydration. **2009**, *Sci. Signal*. *2*, 1-15.

20. Yang, G., Zhao, K., Ju, Y., Mani, S., Cao, Q., Puukila, S., Khaper, N., Wu, L., Wang, R. Hydrogen Sulfide Protects Against Cellular Senescence via *S*-Sulfhydration of Keap1 and Activation of Nrf2. *Antioxid. Redox Signal*. **2013**, *18*, 1906-1919.

21. Cooper, A.J.L., Pinto, J.T. Aminotransferase, L-Amino Acid Oxidase and B-Lyase Reactions Involving L-Cysteine *S*-Conjugates Found in Allium Extracts: Relevance to Biological Activity? *Biochem. Pharmacol*. **2005**, *69*, 209-220.

22. Liang, D., Wu, H., Wong, M.W., Huang, D. Diallyl Trisulfide is a Fast H_2S Donor, but Diallyl Disulfide Is a Slow One: The Reaction Pathways and Intermediates of Glutathione with Polysulfides. *Org. Lett*. **2015**, *17*, 4196-4199.

23. Rabinkov, A., Miron, T., Konstantinov, L., Wilchek, M., Mirelman, D., Weiner, L. The Mode of Action of Allicin: Trapping of Radicals and Interaction with Thiol Containing Proteins. *BBA-Gen. Subjects* **1998**, *1379*, 233-244.

24. Zhang, G., Parkin, K.L. A Tissue Homogenate Method To Prepare Gram-Scale *Allium* Thiosulfinates and Their Disulfide Conjugates with Cysteine and Glutathione. *J. Agric. Food Chem*. **2013**, *61*, 3030-3038.

25. Zhang, G., Parkin, K.L. *S*-Alk(en)ylmercaptocysteine: Chemical Synthesis, Biological Activities, and Redox-Related Mechanism. *J. Agric. Food Chem*. **2013**, *61*, 3030-3038.

26. Kartha, R.V., Zhou, J., Hovde, L.B., Cheung, B.W.Y., Schröder, H. Enhanced Detection of Hydrogen Sulfide Generated in Cell Culture Using an Agar Trap Method. *Anal. Biochem*. **2012**, *423*, 102-108.

27. Zhu, Y.Z., Wang, Z.J., Ho, P., Loke, Y.Y., Zhu, Y.C., Huang, S.H., Tan, C.S., Whiteman, M., Lu, J., Moore, P.K. Hydrogen Sulfide and Its Possible Role in Myocardial Ischemia in Experimental Rats. *J. Appl. Physiol.* **2007**, *102*, 261-268.

28. Zhang, F., Jin, H., Wu, L., Shao, J., Zhu, X., Chen, A., Zheng, S. Diallyl Trisulfide Suppresses Oxidative Stress-Induced Activation of Hepatic Stellate Cells Through Production of Hydrogen Sulfide. *Oxid. Med. Cell. Longev*. **2017**, *17*, 1-13.

29. Tocmo, R., Parkin, K. S-Alk(en)ylmercaptocysteine Suppresses LPS-Induced Pro-Inflammatory Responses in Murine Macrophages Through Inhibition of NF-Kb Pathway and Modulation of Thiol Redox Status. *Free Rad. Biol. Med*. **2018**, *129*, 548-558.

30. Ruddraraju, K.V., Parsons, Z.D., Lewis, C.D., Gates, K.S. Allylation and Alkylation of Biologically Relevant Nucleophiles by Diallyl Sulfides. *J. Org. Chem*. **2017**, *82*, 776-780.

31. Wang, Q., Wang, X.-L., Liu, H.-R., Rose, P., Zhu, Y.-Z. Protective Effects of Cysteine Analogues on Acute Myocardial Ischemia: Novel Modulators of Endogenous H_2S Production. *Antioxid. Redox Signal*. **2010**, *12*, 1155-1165.

32. Pan, L.-L., Liu, X.-H., Gong, Q.-H., Zhu, Y.-Z. *S*-Propargyl-Cysteine (SPRC) Attenuated Lipopolysaccharide-Induced Inflammatory Response in H9C2 Cells Involved in a Hydrogen Sulfide-Dependent Mechanism. *Amino Acids* **2011**, *41*, 205-215.

33. Ida, T., Sawa, T., Ihara, H., Tsuchiya, Y., Watanabe, Y., Kumagai, Y., Suematsu, M., Motohashi, H., Fujii, S., Matsunaga, T., Yamamoto, M., Ono, K. Devarie-Baez, N.O., Xian, M., Fukuto, J.M., Akaike, T. Reactive Cysteine Persulfides and S-Polythiolation Regulate Oxidative Stress and Redox Signaling. *Proc. Natl. Acad. Sci. USA* **2014**, *111*, 7606-7611.

34. Shiu, H.-Y., Chan, T.-C., Ho, C.-M., Liu, Y., Wong, M.-K., Che, C.-M. Electron-Deficient Alkynes as Cleavable Reagents for the Modification of Cysteine-Containing Peptides in Aqueous Medium. *Chem. Eur. J.* **2009**, *15*, 3839-3850.

35. Leriche, G., Chisholm, L., Wagner, A. Cleavable Linkers in Chemical Biology. *Bioorg. Med. Chem*. **2012**, *20*, 571-582.

36. Qiu, J., Cheng, R., Zhang, J., Sun, H., Deng, C., Meng, F., Zhong, Z. Glutathione-Sensitive Hyaluronic Acid-Mercaptopurine Prodrug Linked via Carbonyl Vinyl Sulfide: A Robust and CD44-Targeted Nanomedicine for Leukemia. *Biomacromolecules* **2017**, *18*, 3207-3214.

Chapter 3

S-Alk(en)ylmercaptocysteines Upregulate Phase II Detoxification Enzymes in Activated RAW 264.7 Murine Macrophage Cells

3.1 Abstract

The *Allium*-derived cysteine derivatives, S-alkenylmercaptocysteine (CySSR), have been found to exert cytoprotective activities. The objective of this study was to investigate if CySSR upregulate nuclear factor erythroid 2-related factor Nrf2 and Nrf2-linked phase II enzymes in *E. coli* lipopolysaccharide (LPS)-activated RAW 264.7 macrophage cells and their relationship with the anti-inflammatory effects of CySSR previously observed. Both treatments with *S*-allylmercaptocysteine (CySSA) and *S*-1-propenylmercaptocysteine (CySSPe) increased levels of Nrf2. CySSPe upregulated phase II detoxification enzymes glutamate cysteine ligase (GCL) and glutathione S-transferase P (GSTP), whereas CySSA induced expression of heme oxygenase 1 (HO-1). Silencing Nrf2 mRNA translation by Nrf2-siRNA attenuated the inhibitory effect of both CySSA and CySSPe on nitric oxide (NO) release. These results show that CySSR modulate the Nrf2 signaling pathway and exert anti-inflammatory effects partially through an Nrf2-dependent process in activated macrophages. However, further work is needed to clarify the precise molecular relationships between Nrf2 and Nrf2-associated proteins and their effect on the inflammatory state.

3.2 Introduction

Inflammation is an immune response to a variety of noxious stimuli, such as cytokines, nitric oxide, microbial cell wall products, and oxidative products (1). Lipopolysaccharide (LPS) is a Gram-negative bacterial cell wall component that activates the inflammatory response by binding to the Toll-like receptor 4-myeloid differentiation factor 2 (TLR4-MD-2) complex, which further initiates a signaling cascade down to nuclear factor-kappa B (NF-κB) (2). NF-κB is a major transcriptional regulator of inflammatory signaling and is involved in the upregulation of inflammatory cytokines, prostaglandins, and nitric oxide (NO) through inducible nitric oxide synthase (iNOS) (3). Reactive oxygen species (ROS) are also produced as an antimicrobial defense and signaling agent by immune cells (4). Dysregulation of this response can lead to the excessive formation of ROS, resulting in oxidative stress and chronic inflammatory response.

Oxidative stress occurs when an imbalance in ROS overwhelms the native antioxidant capacity of cells and tissues, resulting in oxidative damage to lipids, proteins, and DNA and disruption of normal cellular processes (5). Overwhelming cellular damage can lead to pathophysiological states that further lead to chronic disorders if not resolved. Together, oxidative stress and chronic inflammation are involved in the etiology of a host of diseases including cancer (6), cardiovascular diseases (7), and obesity (8). Dietary compounds and diet-based interventions that can restore redox homeostasis and reduce inflammation may help reduce the risk of these diseases.

The nuclear factor-erythroid 2 p45-related factor 2 (Nrf2) is a major protein transcriptional regulator in the cellular antioxidant and phase II detoxification defense system (9). Nrf2 functions by binding to the promoter region of Nrf2 target genes, known as the antioxidant response element (ARE), which regulates a battery of genes involved in

detoxification and antioxidation (10). Nrf2 is normally kept deactivated in the cytosol by the associated binding of the inhibitory Kelch-like ECH-associated protein-1 (Keap1). Keap1 targets Nrf2 for polyubiquitination by the Cullin3-Keap1- E3 ligase complex to maintain low basal levels of Nrf2 (11). However, under stressed conditions, Keap1 is inhibited, and dissociated or newly synthesized Nrf2 can freely translocate to the nucleus (12), where it initiates the transcription of ARE-associated phase II detoxifying enzymes (13).

Allium species are commercially important vegetable products cultivated for their sensory, culinary, and purported medicinal properties (14). Many of these distinct properties are tied to the organosulfur compounds generated from crushed or sliced cloves or bulbs. Most organosulfur compounds are derived from the thiosulfinates formed after the alliinase-dependent degradation of the *S*-alk(en)ylcysteine sulfoxides present in the storage compartments of *Allium* tissues (14). However, thiosulfinates exhibit poor stability in vitro and vivo (14-16), with a reported half-life of <1 min in blood (14), and readily decompose into other organosulfur compounds.

Thiosulfinates rapidly react with endogenous thiol-containing compounds, including glutathione and cysteine, to form *S*-alk(en)ylmerccaptocysteines (CySSR) and related analogues (17,18). CySSRs are stable compounds and the unsaturated forms possess potent bioactivity in vitro (17). The major thiosulfinate formed from garlic, allicin, reacts with cysteine to form *S*-allylmercaptocysteine (CySSA), which has been extensively studied for its anti-inflammatory, antioxidant, and anti-tumorigenesis effects (17,19-22). The bioactivities of the CySSPe onion-derived isomer, however, has not been well-characterized due to the difficulty in obtaining the compound and its thiosulfinate precursor. Alliinase reaction product, 1-propenylsulfenic acid, is rapidly converted to propanethial *S*-oxide by lachrymatory factor synthase, found abundantly in

onion tissues (23). Additionally, the symmetric thiosulfinate dimer of 1-propenylsulfenic acid, di-1-propenyl thiosulfinate, rapidly cyclizes to form zwiebelanes and other organosulfur compounds (24,25). Our laboratory has developed an enriched tissue homogenate protocol to generate purified CySSPe (18), and previous studies have revealed CySSPe exhibits more potent anti-inflammatory and antioxidant activities compared to CySSA (17,18,26). Both CySSRs have been shown to inhibit key regulatory elements of the NF-κB inflammatory pathway in lipopolysaccharide (LPS)-activated macrophage through a glutathione-dependent mechanism, with CySSPe exerting more potent effects versus CySSA (26). Additionally, evidence suggests CySSPe activates Nrf2 as well as Nrf2-associated detoxification gene products and enzymes through a persulfide-dependent mechanism in hepatocytes (27).

To better elucidate the molecular mechanisms linking the anti-inflammatory and anti-oxidative properties of CySSR, the present research study investigated the effects of CySSR on the Nrf2 and ARE-coded phase II enzymes in LPS-activated RAW 264.7 cells, and their role in attenuating the inflammatory response.

3.3 Materials and Methods

3.3.1 Chemicals and General Procedures

LPS (*E. coli* serotype O127:B8), dimethyl sulfoxide (DMSO), dithiothreitol, and bovine serum albumin (BSA) were purchased from Millipore Sigma (Burlington, MA, USA). Enhanced chemiluminescent reagent Clarity Western ECL substrate was purchased from Bio-Rad Laboratories (Hercules, CA, USA). Nrf2 (16396-1-AP), GCLc (12601-1-AP), HO-1 (10701-1-AP), GSTP1 (15902-1-AP), and β-actin (60008-1-lg) antibodies, and anti-rabbit IgG, horseradish peroxidase (HRP)-conjugated (SA00001-2) and anti-mouse IgG-HRP (SA00001-1) secondary antibodies were purchased from ProteinTech (Rosemont, IL, USA). All other chemicals were

obtained from Millapore Sigma unless otherwise noted. All solvents used for extraction or HPLC analysis were purchased from Fisher Scientific (Hampton, NH) or Millapore Sigma. Garlic and onion were purchased from a local grocery store in Madison, WI. Analytical HPLC was conducted using 250 x 4.6 mm, 5 μM, Discovery C18 column (Supelco, Bellefonte, PA) on an Ultimate 3000 HPLC System (Thermo Fisher Scientific, Madison, WI) equipped with a diode array detector. Semi-preparative HPLC was carried out using a 250 x 21.2 mm, 5 μM, Discovery C18 (Supelco, Bellefonte, PA) on a Reveleris Prep purification system (Grace Co., Columbia, MD).

3.3.2 Preparation and Isolation of Mercaptocysteines

Mercaptocysteines were prepared as previously discussed with modifications (26). Briefly, 500 g of white onions were halved and heated in the microwave for 5 min (700 W), then allowed to cool to room temperature. The onion tissue was homogenized with 50 g peel fresh garlic and 100 mL deionized water for 1 minute at 4 ºC. The homogenized mixture was left to incubate at room temperature for 1 h. After the incubation period, the mixture was filtered through cheesecloth and extracted with $CHCl_3$. The organic phase was separated, collected, and dried over anhydrous $MgSO_4$.

The solvent was evaporated under a stream of nitrogen gas until an oily residue remained of crude thiosulfinates. The crude material was resuspended in 10 mL of ddH_2O and reacted with 0.5 to 1.0 g of cysteine-hydrochloride hydrate for 30 min with stirring. The solution was filtered through a 0.2 μm filter and separated using a Reveleris® Prep purification system. Separation was conducted on a 25 cm x 21.2 mm, 5 μM Discovery® C18 column with isocratic elution using MeOH/H_2O (30:70) at a flow rate of 12 mL/min over 25 min. Peak resolution was monitored by UV (254 and 210 nm). Isolated fractions were combined and slowly evaporated under vacuum at

25 ºC to remove excess methanol. The remaining aqueous solution was frozen at -20 ºC, then freeze dried over three days. Isolated solid compounds were analyzed by HPLC and identified by their ^{1}H NMR, ^{13}C NMR, and MS spectra **(Appendix A.2)**, as previously reported (17,18).

3.3.3 Cell Culture Protocols

Murine macrophage RAW 264.7 cells (ATCC® TIB-71) were obtained from ATCC (Manassas, VA). Cell cultures were maintained in 75-cm^2 tissue culture flasks in phenol red-free Dulbecco's Modified Eagle Medium (DMEM, Invitrogen) supplemented with 10% fetal bovine serum (FBS), streptomycin (100 µg/mL), penicillin (100 U/mL), and incubated at 37ºC with 5% CO_2 humidified atmosphere. Cells (80-90% confluence) were subcultured every 2 to 3 days, passaging at a 1:10 split ratio and cell passages 5 to 16 were used for all experiments. The medium was replaced with fresh DMEM medium containing test compounds and the cells were incubated for 24 h.

3.3.4 Small Interfering RNA Nrf2 Silencing

Murine macrophage RAW 264.7 cells were seeded in a 96-well plate and incubated for 24 h at 37 ºC with 5% CO_2 humidified atmosphere. A siRNA diluted duplex solution was prepared by diluting 80 µL of Nrf2 siRNA duplex (Santa Cruz Biotechnology, Dallas, TX) in 1 mL serum-free Opti-MEM® medium (Thermo Fisher Scientific, Madison, WI). 80 µL siRNA Transfection Reagent (Santa Cruz Biotechnology, Dallas, TX) was diluted in 1 mL Opti-MEM® medium. The two solutions were combined and allowed to incubate for 15 min at room temperature. The combined solution was further diluted with 8 mL Opti-MEM® medium. DMEM medium was aspirated from the 96-well plate, washed once with 200 µL Opti-MEM® medium, and replaced with 200 µL of the diluted siRNA transfection reagent mixture. The cells were incubated for 6 h at 37 ºC with 5% CO_2 humidified atmosphere.

3.3.5 Griess Nitric Oxide Assay in LPS-Activated Macrophage Cells

RAW 264.7 cells were grown for 24 h in 96-well plates (2 x 10^4 cells per well) in 200 µL of phenol red-free DMEM supplemented with 10% FBS, streptomycin (100 µg/mL), penicillin (100 U/mL), and incubated at 37 ºC with 5% CO_2 humidified atmosphere. The medium was then replaced with fresh medium containing test compounds and 1 µg/mL lipopolysaccharide (LPS), and plates were incubated for an additional 24 h. A 100 µL sample was removed from the culture supernatant of each well and mixed with an equal amount of fresh prepared Griess reagent, incubated for 10 min, and then the absorbance at 540 nm was measured with a Spectra Max Absorbance microplate reader (Molecular Devices, Sunnyvale, CA).

Duplicate 96-well plates were prepared to measure cell viability and facilitate relative nitric oxide production calculations. The medium from the duplicate microplate was aspirated and 100 µL of 3-(4,5-dimethylthiazol-2-yl)-2,5-diphenyltetrazolium bromide (MTT) (0.2% in 2% EtOH) was added to each well and incubated for 4 h in a humidified atmosphere at 37 ºC and 5% CO_2. The MTT solution was aspirated from the wells of the microplate and replaced with 50 µL anhydrous DMSO. The microplate was allowed to incubate at room temperature for 15 min. The microplate was shaken for 5 min and the absorbance was measured at 570 – 590 nm using a Spectra Max Absorbance microplate reader. The absorbance values of the blanks were subtracted from the control and treated sample wells.

3.3.6 Immunoblot Analysis

RAW 264.7 cells were cultured in 5 mL medium in 60 mm plates (5 x 10^5 cells) for 24 h. then the medium was decanted, replaced with fresh medium containing samples and the cells were incubated for another 24 h. After treatment, the cells were washed with cold PBS, 100 µL cell lysis buffer with protease inhibitor (10x) was added to each plate. The cells were detached

from the plate by scraping with a rubber spatula, the cell lysates were incubated on ice for 30 min, and then centrifuged at 14,000 x g at 4 ºC for 5 min. The protein concentration in the supernatant was determined by a protein assay kit (Bio-Rad, Hercules, CA). Each sample with an equal amount of protein was mixed with loading buffer, loaded on a 10% Tris-HCl SDS-PAGE gel (Bio-Rad, Hercules, CA), and run initially at 80 V for 10-20 min then increased to 120 V. The proteins were transferred onto a nitrocellulose membrane (Bio-Rad, Hercules, CA) by electroblotting. The nitrocellulose membrane was blocked with 5% skim milk solution in Tris-Buffered Saline Tween-20 (TBST) buffer for 1 h at room temperature, washed 3 times with TBST buffer, then incubated with primary antibodies overnight at 4 ºC. After hybridization with primary antibodies, the membranes were washed with TBST buffer three times, then incubated with secondary horseradish peroxidase (HRP) antibodies for 1 h at room temperature and washed with TBST buffer 3 times. Blots were developed by treatment with a 1:1 ratio luciferin and hydrogen peroxide chemiluminescent Clarity™ substrates (Bio-Rad, Hercules, CA), and images were captured using a ChemiDoc™ Touch Imaging System (Bio-Rad, Hercules, CA). The intensities were quantified by densitometric analysis using Image J Analysis (Bio-Rad, Hercules, CA).

3.3.7 Statistical Analysis

Statistical analyses were performed using SigmaPlot 13 software (Systat Software, Inc., San Jose, CA). Results were expressed as mean values ± SD of at least three replicates. Difference in the means were evaluated by one-way ANOVA followed by Tukey's HSD test, and differences of $P \leq 0.05$ were deemed significant.

3.4 Results & Discussion

In this study, the mechanisms of action by which *Allium*-derived CySSR species, CySSPe and CySSA, confer their antioxidant effects were evaluated in activated RAW 264.7 murine macrophage cells. A previous study from our laboratory demonstrated that both CySSA and CySSPe inhibited the NF-κB-dependent inflammatory response through the upregulation of GCL and glutathione, products of the Nrf2 signaling pathway, in LPS-stimulated RAW 264.7 cells (26). Additionally, previous work in Hepa1c1c7 murine cells revealed onion-derived CySSPe provides cytoprotection against oxidative stress via activation of Nrf2 and the subsequent upregulation of ARE-coded antioxidant and detoxification products HO-1, GCL, NQO1, and GSH (27). Together, these studies offer evidence that Nrf2 is a key regulator element conferring CySSR cytoprotective bioactivity. However, it remains unclear if Nrf2 signaling is directly involved in the anti-inflammatory properties exhibited by CySSR. Thus, this study was conducted to evaluate the role played by CySSR-induced Nrf2 activation in modulating inflammation in LPS-activated RAW 264.7 cells.

Exposure of LPS-activated RAW 264.7 cells to both CySSA and CySSPe elevated levels of Nrf2 proteins in cell lysates in a dose and time-dependent manner (**Fig. 3.1-3.4**). Here, cells were activated with LPS for 24 h and then treated with CySSR to evaluate the Nrf2 response following inflammatory challenge. CySSA treatment at 40 μM in LPS-activated cells increased relative Nrf2 protein levels 89% compared to cells untreated with LPS (control) **(Fig. 3.1.)**. CySSPe treatment at 40 μM in LPS-activated cells increased relative Nrf2 protein levels 54% compared to control **(Fig. 3.2)**. Cells treated with 25 μM CySSA reached a maximum of Nrf2 protein expression of 3.5-fold after 1 h treatment compared to control **(Fig. 3.3.)**. Cells reached a peak in relative Nrf2 protein levels following 1 h treatment with 25 μM CySSPe at a 2.1-fold increase compared to control **(Fig. 3.4.)**. The higher relative Nrf2 protein expression exhibited by

the “0 h” time point after treatment with CySSA **(Fig. 3.3)** compared to the “0 h” time point after treatment with CySSPe **(Fig 3.4)** may be due to minor impurities remaining in the sample and inconsistencies in sample preparation. In a previous study, Nrf2 was activated in Hepa1c1c7 cells within 1 h, with a rapid accumulation of nuclear Nrf2 within the first 30 min (27). These results suggest CySSR exhibit a rescuing effect on inflammation through Nrf2 activation.

Interestingly, CySSPe exerted a less potent increase in Nrf2 levels compared to CySSA when cells were pretreated with LPS for 24 h. Previous work showed CySSPe possesses more potent inhibitory activities against elements of the NF-κB signaling cascade and downstream inflammatory mediators than CySSA in RAW 264.7 cells that were pre-treated with CySSR 2 h prior to brief LPS activation for 5 min (26). The longer LPS activation time-period of 24 h in this study versus the 5 min LPS activation in the previous study may have accounted for the reversal in potency between these two mercaptocysteines. COX-2 and NF-κB-specific DNA complex formation continue to increase up to the 24 h time point following LPS treatment (28). iNOS expression and NO concentrations has been shown to increase and remain elevated at the 10 h time point after LPS stimulation in RAW 264.7 cells (29). NO reacts with cysteine-rich proteins by forming S-nitrosothiol species, which preferentially react with H_2S and persulfides (30). H_2S and persulfides evolved from CySSPe may have rapidly reacted with NO and nitrosylated species prior to interacting with Keap1 and other thiol-rich signaling proteins, and thus result in an attenuated effect on Nrf2 upregulation compared to CySSA.

Nrf2 controls the transcription of more than 200 target gene products, with several involved in the phase II cytoprotective system that confers cytoprotection against oxidative stress and xenobiotics (31). CySSA and CySSPe differentially affected the upregulation of Nrf2-dependent enzymes GCLc, HO-1, and GSTP. GCLc reached maximum upregulation 6 h after

treatment with CySSPe with a 19% increase in relative protein level versus control **(Fig. 3.5.)**. HO-1 protein expression was stimulated by CySSA and reached a peak of a 2.5-fold increase over control HO-1 levels after 6 h **(Fig. 3.6.)**. However, CySSPe decreased HO-1 levels (~33%) of LPS-stimulated cells at time 0 h down to control levels after 6 h. Similar to GCLc, GSTP was upregulated in activated cells by CySSPe treatment by ~21% versus control (**Fig. 3.7)**.

GCL was also previously found to be strongly upregulated by exposure of RAW 264.7 cells to CySSR (26). GCL is an important rate-limiting enzyme that regulates the biosynthesis of glutathione through the catalyzed formation of γ-glutamylcysteine from L-glutamate and L-cysteine. Upregulation of GCL, especially its catalytic subunit (GCLc), is associated with the increase and maintenance of cellular glutathione levels, which protects cells from oxidative damage and xenobiotic compounds (32). CySSR significantly increased glutathione in RAW 264.7 cells and served as the protective mediator against oxidative stress induced by LPS (26). CySSPe also increased cellular glutathione in Hepa cells and protected cells from tert-butylhydroxyperoxide (tBHP)-induced oxidative stress in a glutathione-dependent manner (27). Glutathione serves as a substrate for other ARE-linked antioxidant enzymes as well, including thioredoxins, peroxiredoxin, glutaredoxin, glutathione peroxidase (GPx), and glutathione reductase (GR) (33). The reaction rates of enzyme-catalyzed reactions between glutathione and reactive oxygen species or electrophiles is several magnitudes higher than with glutathione or other low molecular weight thiol alone, and so the presence of antioxidant enzymes is essential to carry out an effective defense against these species (34). GSTP is one member of the glutathione-S-transferase superfamily that is also transcriptionally regulated by Nrf2 and protects cells from oxidative damage by catalyzing the conjugation of glutathione to exogenous

electrophilic compounds (35). Evidence of GCL and GSTP upregulation by CySSPe further supports an Nrf2 and glutathione-dependent mechanism of cytoprotection by CySSPe.

Nrf2-siRNA was used to knock down Nrf2 expression in RAW 264.7 cells to evaluate the effect Nrf2 has on NO output as a biomarker of inflammation. Neither siRNA treatment nor CySSA or CySSPe treatments affected cell viability, with all treatments exhibiting cell viabilities greater than 98% relative to control **(Fig. 3.8)**. Pretreatment of macrophage cells with Nrf2-siRNA led to a moderate restoration of NO output after activation with LPS and co-treatment with CySSA or CySSPe **(Fig. 3.9)**. Nrf2 and NF-κB pathways are known to be interconnected pathways, as cells lacking Nrf2 show more pronounced NF-κB activity, oxidative and nitrosative stress, and cytokine production (36). Nrf2 silencing of hepatocytes was previously shown to attenuate the protective effects of CySSPe against tBHP-induced oxidative stress (27). Nrf2 has also been shown to suppress the inflammatory response in macrophage cells via blockade of proinflammatory cytokine production (37). Nrf2 activation by diallyl disulfide (DADS) has also been demonstrated to suppress the carbon tetrachloride (CCl_4)-induced inflammatory response and reduce elevated levels of NF-κB, COX-2, TNF-α, and iNOS in rats in an Nrf2-dependent fashion (38). Nrf2 is a major pathway that regulates antioxidant and anti-inflammatory gene expression, and this work suggests inhibition of LPS-induced inflammation by CySSR is partially mediated by Nrf2.

This study demonstrated that CySSR activation of Nrf2 inhibits the LPS/NF-κB-dependent release of NO. These findings provide a mechanistic link between the Nrf2 and NF-κB signaling pathways explored in previous work regarding the anti-inflammatory effects of CySSR exhibited in activated macrophage cells mediated by inhibition of the NF-κB pathway (26) and antioxidant properties of CySSR exhibited in hepatocytes mediated by Nrf2 activation

(27). Additionally, as discussed in chapter 2 and previous work (27), the Nrf2-activating features of CySSR, especially CySSPe, may be through the metabolic and glutathione-dependent formation of H_2S and/or persulfides. Nrf2 and NF-κB are known to exhibit functional cross-talk (36). Nrf2 activity has been shown to downregulate NF-κB nuclear accumulation mediated through downstream Nrf2 gene products such as HO-1. On the other hand, NF-κB activity increases the production of oxidative and nitrosative species, which modulates the redox status activates Nrf2. Other kinase signaling pathways, including the p38 and ERK1/2 mitogen-activated protein kinase (MAPK) pathway, exhibits cross-talk with Nrf2 and play a regulatory role in the expression of HO-1 (39). The ability of CySSR to modulate these other pathways warrants additional investigation.

Given the role played by NF-κB in initiating and sustaining inflammation in chronic diseases such as obesity (40) or gastric cancer (41), determining the role played by Nrf2 and Nrf2-linked enzymes including HO-1, GCLc, GPx, and GR in suppressing NF-κB-dependent inflammatory responses could provide further knowledge of the mechanism by which CySSR exert their beneficial effects in *in vivo* models of these diseases. Furthermore, the modulating effect of CySSR on Nrf2 and these Nrf2-associated gene products could be evaluated *in vivo* following treatment with CySSR. The ability of CySSR to maintain redox homeostasis by upregulating glutathione-dependent antioxidant enzymes that counteract elevated intracellular ROS levels, such as peroxiredoxin, sulfiredoxin, and GPx, as a mechanism of inhibiting ROS-dependent NF-κB signaling was an original goal of this study and should be further explored both *in vitro* and *in vivo*.

3.5 Figures and Tables

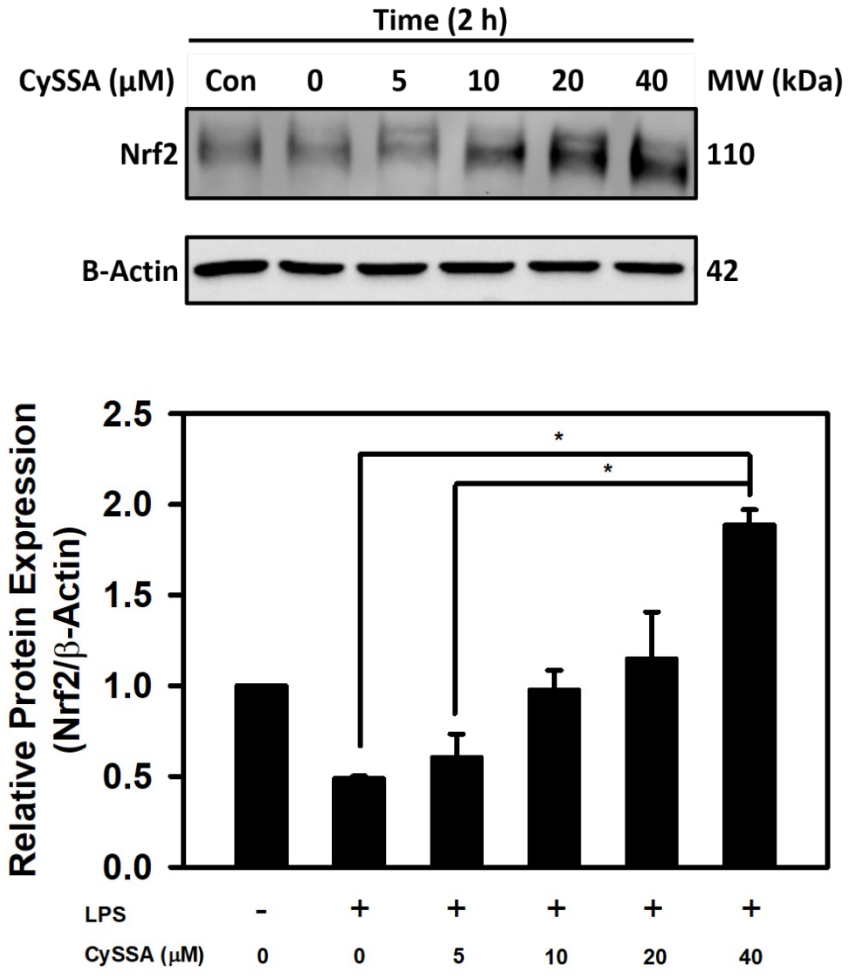

Figure 3.1. Dose-response curve and Western blot analysis of Nrf2 upregulation by CySSA in LPS-stimulated RAW 264.7 cells. Cells were pretreated with 1 μg/mL LPS for 24 h and treated with CySSA (0-40 μM) for 2 h. Cells were lysed and immunoblotted with anti-Nrf2 and anti-*β*-actin antibodies. Relative protein densities were normalized to *β*-actin and untreated RAW 264.7 cells (control). The blots shown are representatives of three independent experiments. Statistical significance was determined by one-way ANOVA with Tukey's post-test. * = $P < 0.05$

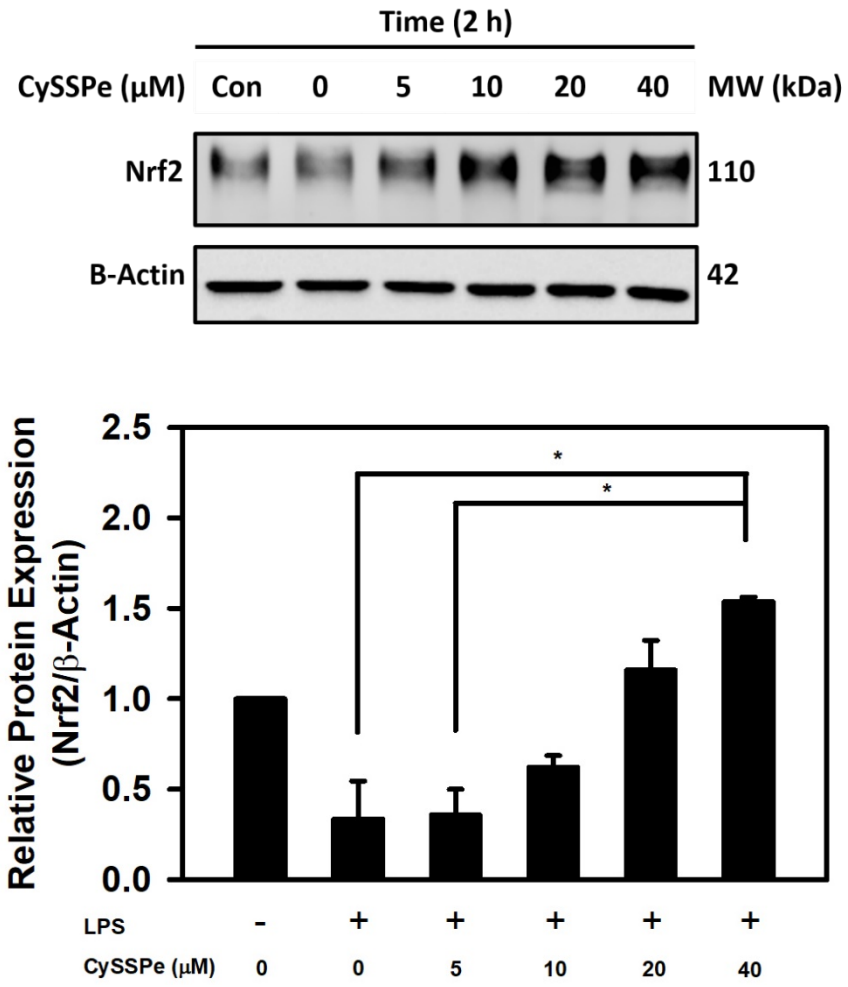

Figure 3.2. Dose-response curve and Western blot analysis of Nrf2 upregulation by CySSPe in LPS-stimulated RAW 264.7 cells. Cells were pretreated with 1 μg/mL LPS for 24 h and treated with CySSPe (0-40 μM) for 2 h. Cells were lysed and immunoblotted with anti-Nrf2 and anti-*β*-actin antibodies. Relative protein densities were normalized to *β*-actin and untreated RAW 264.7 cells (control). The blots shown are representatives of three independent experiments. Statistical significance was determined by one-way ANOVA with Tukey's post-test. * = $P < 0.05$

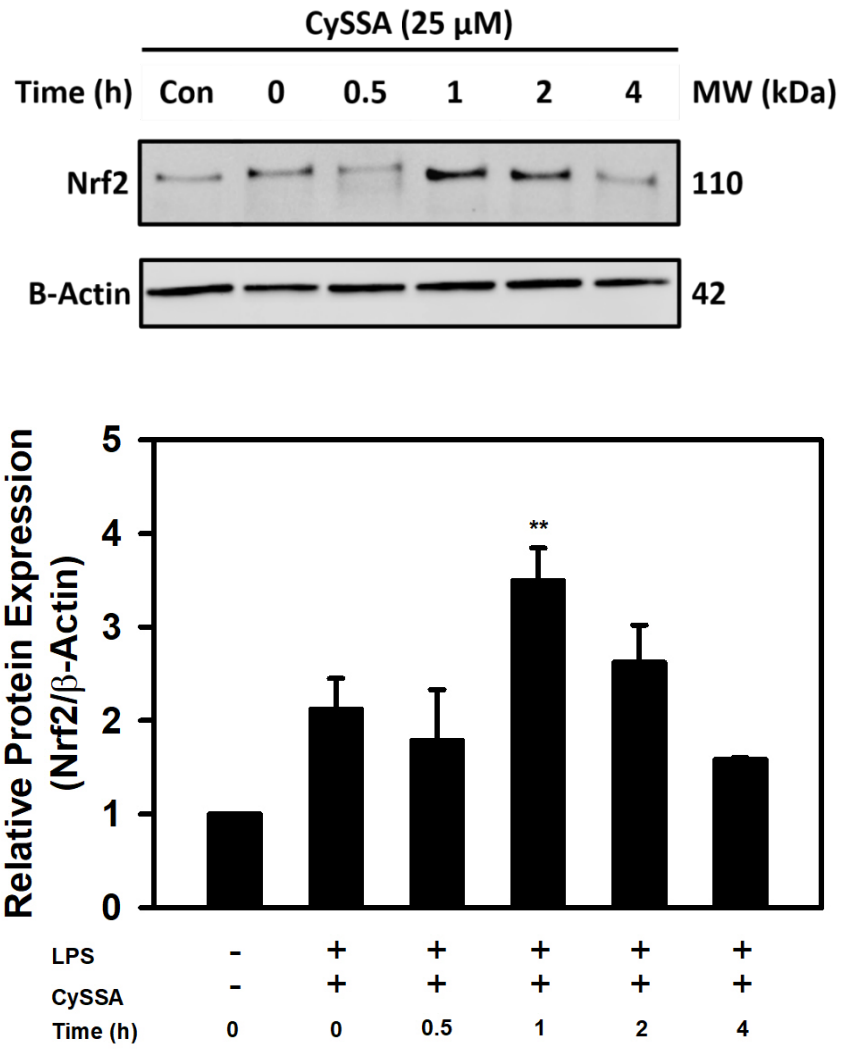

Figure 3.3. Time course and Western blot analysis of Nrf2 upregulation by CySSA in LPS-stimulated RAW 264.7 cells. Cells were pretreated with 1 μg/mL LPS for 24 h and treated with 25 μM CySSA over a 4-h period. Cells were lysed, proteins collected at each time point, and immunoblotted with anti-Nrf2 and anti-*β*-actin antibodies. Relative protein densities were normalized to *β*-actin and untreated RAW 264.7 cells (control). The blots shown are representatives of three independent experiments. Statistical significance was determined by one-way ANOVA with Tukey's post-test. ** = $P < 0.01$ compared to control.

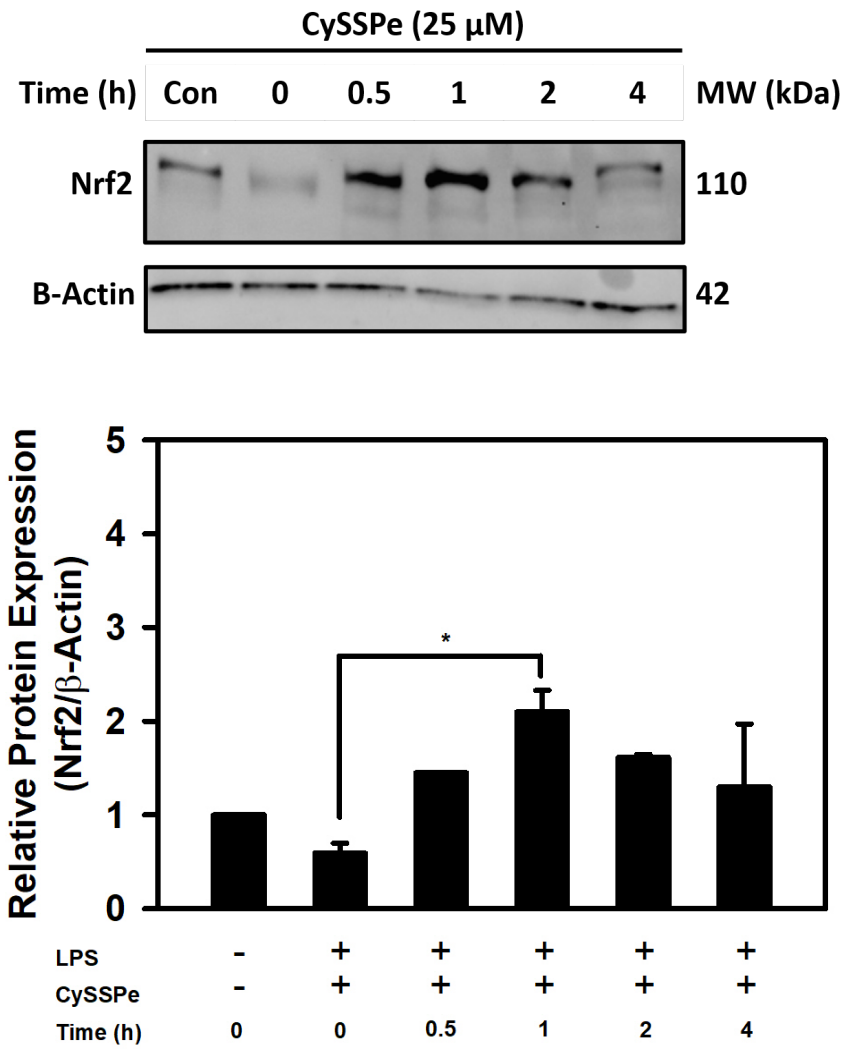

Figure 3.4. Time course and Western blot analysis of Nrf2 upregulation by CySSPe in LPS-stimulated RAW 264.7 cells. Cells were pretreated with 1 µg/mL LPS for 24 h and treated with 25 µM CySSPe over a 4-h period. Cells were lysed, proteins collected at each time point, and immunoblotted with anti-Nrf2 and anti-*β*-actin antibodies. Relative protein densities were normalized to *β*-actin and untreated RAW 264.7 cells (control). The blots shown are representatives of three independent experiments. Statistical significance was determined by one-way ANOVA with Tukey's post-test. * = $P < 0.05$

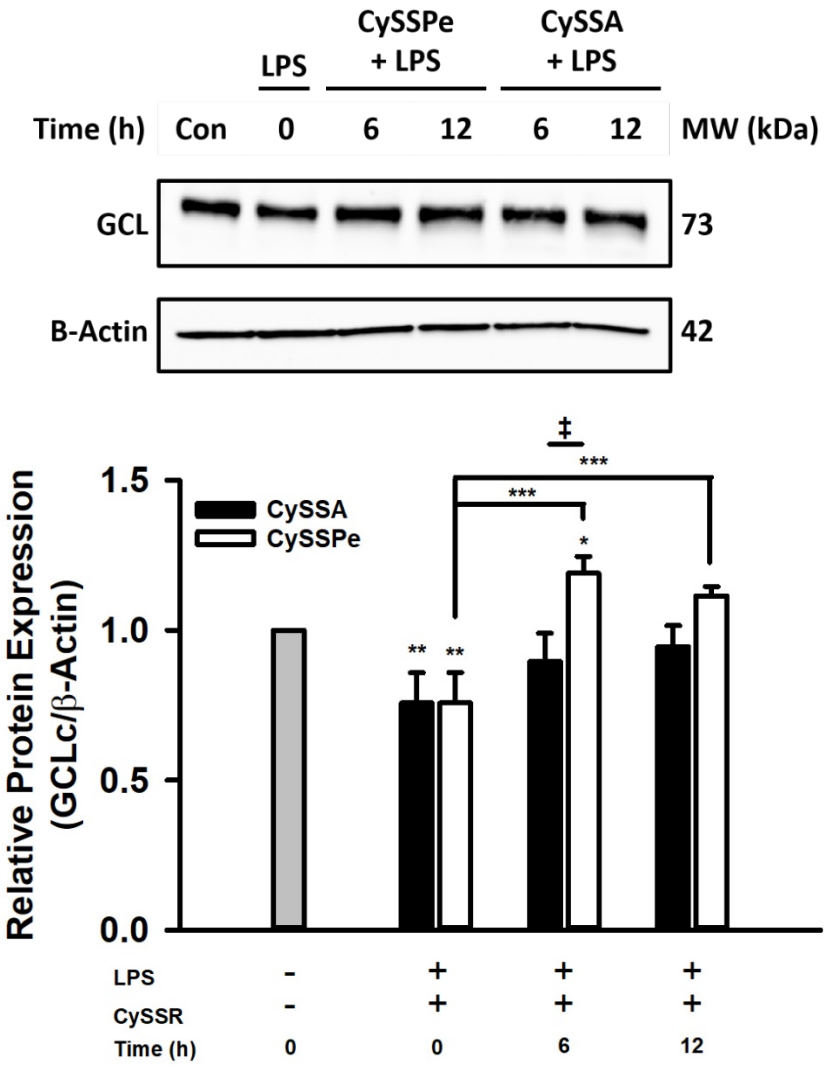

Figure 3.5. Western blot analysis of GCL upregulation by CySSR in LPS-stimulated RAW 264.7 cells. Cells were pretreated with 1 μg/mL LPS for 24 h and treated with 25 μM CySSA or CySSPe over a 12-h period. Cells were lysed, proteins collected at each time point, and immunoblotted with anti-GCLc and anti-*β*-actin antibodies. Relative protein densities were normalized to *β*-actin and untreated RAW 264.7 cells (control). The blots shown are representatives of three independent experiments. Statistical significance was determined by one-way ANOVA with Tukey's post-test. * = $P < 0.05$ and ** = $P < 0.01$ (versus control), *** = $P < 0.001$. Bars bearing ‡ = $P < 0.001$.

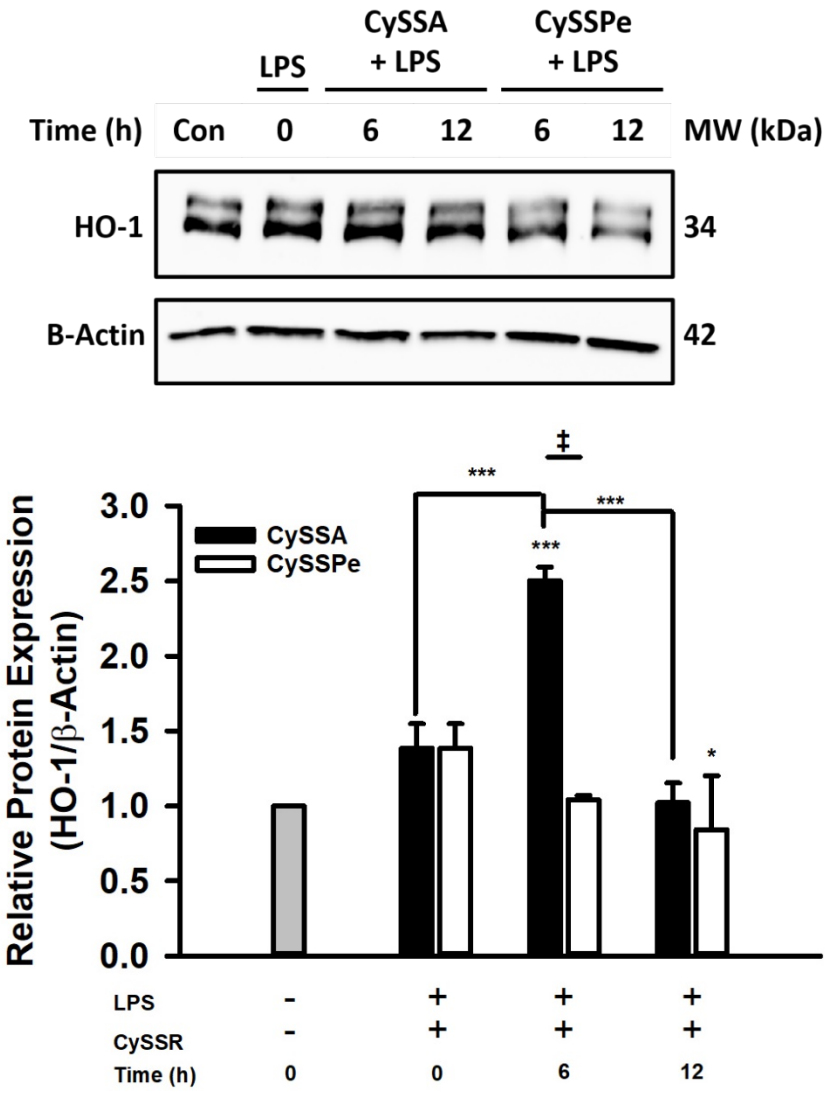

Figure 3.6. Western blot analysis of HO-1 upregulation by CySSR in LPS-stimulated RAW 264.7 cells. Cells were pretreated with 1 μg/mL LPS for 24 h and treated with 25 μM CySSA or CySSPe over a 12-h period. Cells were lysed, proteins collected at each time point, and immunoblotted with anti-HO-1 and anti-*β*-actin antibodies. Relative protein densities were normalized to *β*-actin and untreated RAW 264.7 cells (control). The blots shown are representatives of three independent experiments. Statistical significance was determined by one-way ANOVA with Tukey's post-test. * = $P < 0.05$ (versus control), *** = $P < 0.001$. Bars bearing ‡ = $P < 0.001$.

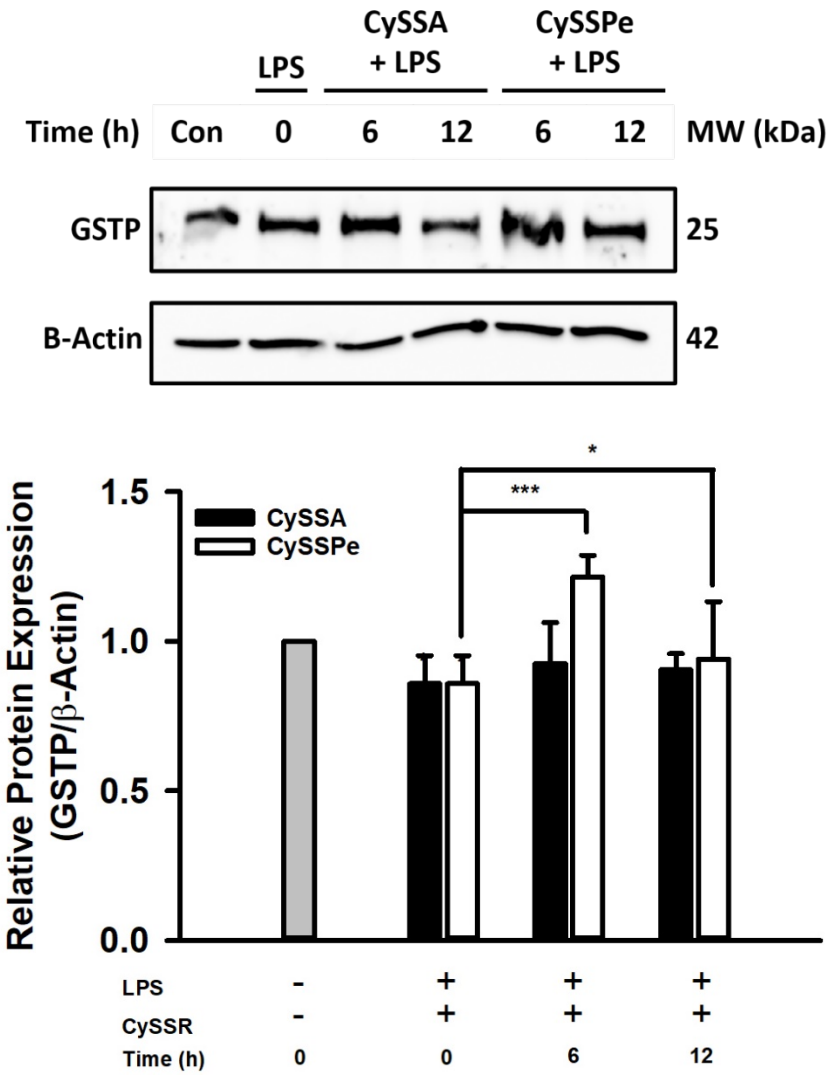

Figure 3.7. Western blot analysis of GSTP upregulation by CySSR in LPS-stimulated RAW 264.7 cells. Cells were pretreated with 1 μg/mL LPS for 24 h and treated with 25 μM CySSA or CySSPe over a 12-h period. Cells were lysed, proteins collected at each time point, and immunoblotted with anti-GSTP and anti-*β*-actin antibodies. Relative protein densities were normalized to *β*-actin and untreated RAW 264.7 cells (control). The blots shown are representatives of three independent experiments. Statistical significance was determined by one-way ANOVA with Tukey's post-test. * = $P < 0.05$ and *** = $P < 0.001$ versus control.

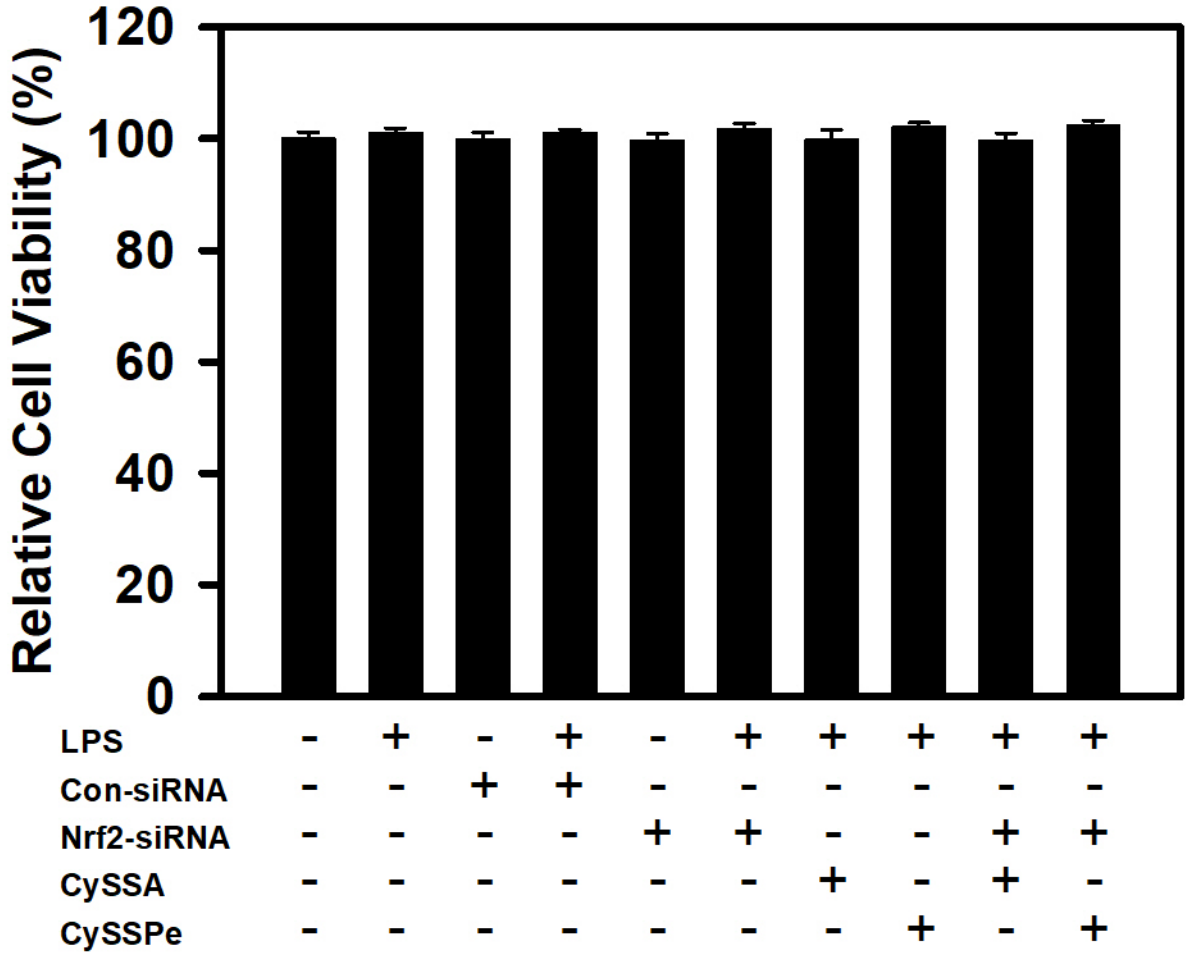

Figure 3.8. Cell viabilities of RAW 264.7 cells transfected with Nrf2 siRNA and treated with CySSR. Cells were transfected with or without scrambled siRNA or Nrf2-siRNA for 24 h followed by pretreatment with or without 1 μg/mL LPS for 24 h. Cells were then incubated with or without 25 μM CySSA or CySSPe for 24 h.

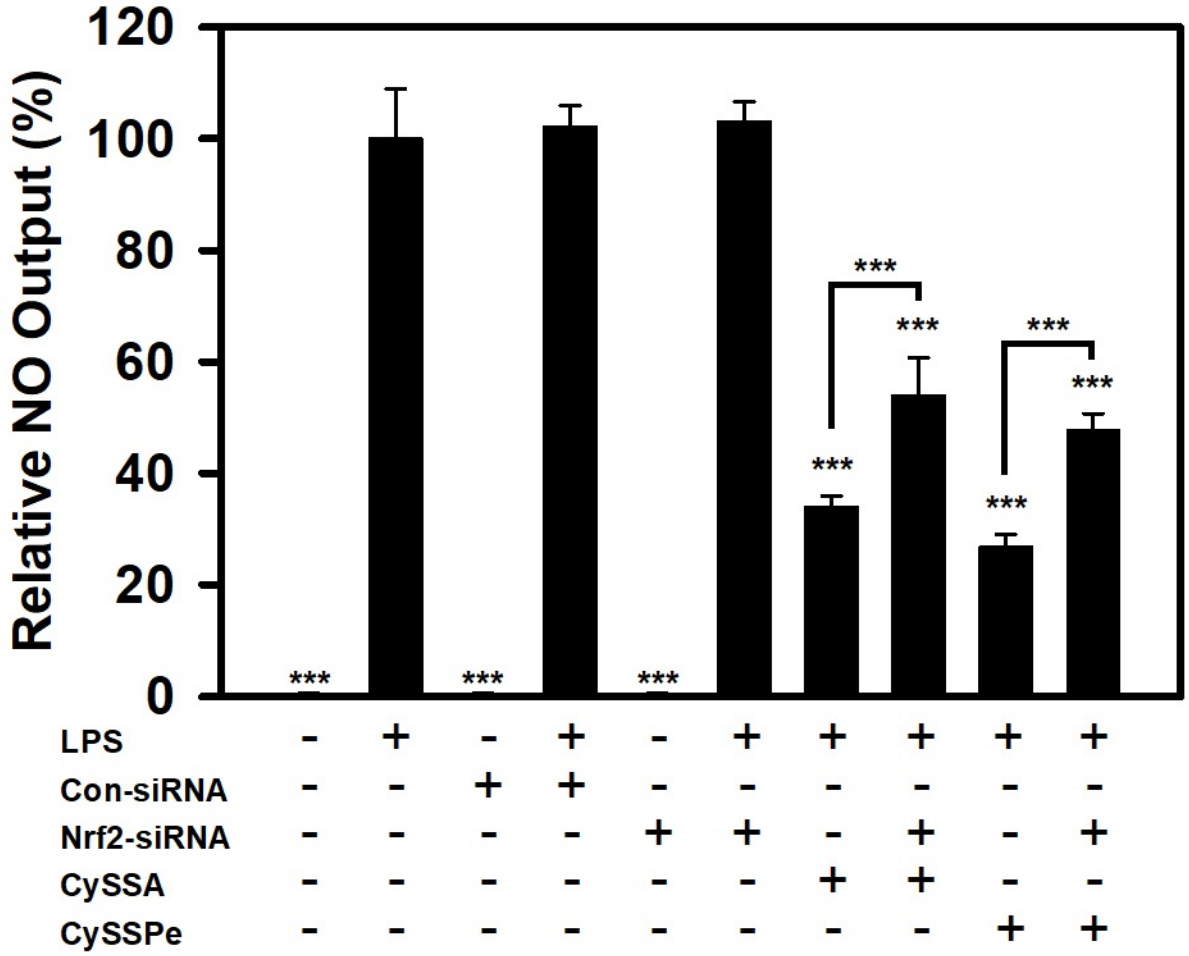

Figure 3.9. NO output of RAW 264.7 cells transfected with Nrf2 siRNA and treated with CySSR. RAW 264.7 cells were transfected with or without scrambled siRNA or Nrf2-siRNA for 24 h followed by pretreatment with or without 1 μg/mL LPS for 24 h. Cells were then incubated with or without 25 μM CySSA or CySSPe for 24 h. NO % set relative to LPS-treated cells. Statistical significance was determined by one-way ANOVA with Tukey's post-test. *** = $P < 0.001$ versus LPS-treated cells.

3.6 References

1. Medzhitov, R. Origin and Physiological Roles of Inflammation. *Nature* **2008**, *454*, 428-435.

2. Lu, Y.-C., Yeh, W.-C., Ohashi, P.S. LPS/TLR4 Signal Transduction Pathway. *Cytokine* **2008**, *42*, 145-151.

3. Liu, T., Zhang, L., Joo, D., Sun, S.-C. NF-κB Signaling in Inflammation. *Nat. Immunol.* **2017**, *18*, 851-860.

4. Mittal, M., Siddiqui, M.R., Tran, K., Reddy, S.P., Malik, A.B. Reactive Oxygen Species in Inflammation and Tissue Injury. *Antioxid. Redox Signal*. **2014**, *20*, 1126-1167.

5. Sies, H., Berndt, C., Jones, D.P. Oxidative Stress. *Annu. Rev. Biochem*. **2017**, *86*, 715-748.

6. Federico, A., Morgillo, F., Tuccillo, C., Ciardiello, F., Loguercio, C. Chronic Inflammation and Oxidative Stress in Human Carcinogenesis. *Int. J. Canc*. **2007**, *121*, 2381-2386.

7. Siti, H.N., Kamisah, Y., Kamsiah, J. The Role of Oxidative Stress, Antioxidants, and Vascular Inflammation in Cardiovascular Disease. *Vascul. Pharmacol*. **2015**, *71*, 40-56.

8. Fernández-Sánchez, A., Madrigal-Santillán, E., Bautista, M., Esquivel-Soto, J., Morales-González, Á., Esquivel-Chirino, C., Durante-Montiel, I., Sánchez-Rivera, G., Valadez-Vega, C., Morales-González, J.A. Inflammation, Oxidative Stress, and Obesity. *Int. J. Mol. Sci*. **2011**, *12*, 3117-3132.

9. Bellezza, I., Giambanco, I., Minelli, A., Donato, R. Nrf2-Keap1 Signaling in Oxidative and Reductive Stress. *BBA-Mol. Cell Res*. **2018**, *1865*, 721-733.

10. Raghunath, A., Sundarraj, K., Nagarajan, R., Arfuso, F., Bian, J., Kumar, A.P., Sethi, G., Perumal, E. Antioxidant Response Elements: Discovery, Classes, Regulation and Potential Applications. *Redox Biol*. **2018**, *17*, 297-314.

11. Dinkova-Kostova, A.T., Kostov, R.V., Canning, P. Keap1, the Cysteine-Based Mammalian Intracellular Sensor for Electrophiles and Oxidants. *Arch. Biochem. Biophys*. **2017**, *617*, 84-93.

12. Baird, L., Llères, D., Swift, S., Dinkova-Kostova, A.T. Regulatory Flexibility in the Nrf2-Mediated Stress Response is Conferred by Conformational Cycling of the Keap1-Nrf2 Protein Complex. *Proc. Natl. Acad. Sci. USA* **2013**, *110*, 15259-15264.

13. Itoh, K., Chiba, T., Takahashi, S., Ishii, T., Igarashi, K., Katoh, Y., Oyake, T., Hayashi, N., Satoh, K., Hatayama, I., Yamamoto, M., Nabeshima, Y. An Nr2-Small Maf

Heterodimer Mediates the Induction of Phase II Detoxifying Enzyme Genes Through Antioxidant Response Elements. *Biochem. Biophys. Res. Commun.* **1997**, *236*, 313-322.

14. Block, E. The Organosulfur Chemistry of The Genus *Allium* – Implications for the Organic Chemistry of Sulfur. *Angew. Chem. Int. Ed.* **1992**, *31*, 1135-1178.

15. Lawson, L.D. Garlic: A Review of its Medicinal Effects and Indicated Active Compounds. In *Phytomedicines of Europe: Chemistry and Biological Activity*; Lawson, L.D., Bauer, R., Eds.; ACS Symposium Series 691; American Chemical Society: Washington, DC, 1998; pp 176-209.

16. Shen, C., Xiao, H., Parkin, K.L. In Vitro Stability and Chemical Reactivity of Thiosulfinates. *J. Agric. Food Chem.* **2002**, *50*, 2644-2651.

17. Zhang, G., Parkin, K.L. *S*-Alk(en)ylmercaptocysteine: Chemical Synthesis, Biological Activities, and Redox-Related Mechanism. *J. Agric. Food Chem.* **2013**, *61*, 3030-3038.

18. Zhang, G., Parkin, K.L. A Tissue Homogenate Method to Prepare Gram-Scale *Allium* Thiosulfinates and Their Disulfide Conjugates with Cysteine and Glutathione. *J. Agric. Food Chem.* **2013**, *61*, 3030-3038.

19. Xiao, J., Liong, E.C., Ling, M.-T., Ching, Y.-P., Fung, M.-L., Tipoe, G.L. *S*-Allylmercaptocysteine Reduces Carbon Tetrachloride-Induced Hepatic Oxidative Stress and Necroinflammation via Nuclear Factor Kappa B-Dependent Pathways in Mice. *Eur. J. Nutr.* **2012**, *51*, 323-333.

20. Shirin, H., Pinto, J.T., Kawabata, Y., Soh, J.-W., Delohery, T., Moss, S.F., Murty, V., Rivlin, R.S., Holt, P.R., Weinstein, I.B. Antiproliferative Effects Of *S*-Allylmercaptocysteine on Colon Cancer Cells When Tested Alone or in Combination with Sulindac Sulfide. *Cancer Res.* **2001**, *61*, 725-731.

21. Xiao, D., Pinto, J.T., Soh, J.W., Deguchi, A., Gundersen, G.G., Palazzo, A.F., Yoon, J.T., Shirin, H., Weinstein, I.B. Induction of Apoptosis by the Garlic-Derived Compound *S*-Allylmercaptocysteine (SAMC) is Associated with Microtubule Depolymerization and c-Jun NH_2-Terminal Kinase 1 Activation. *Cancer Res.* **2003**, *63*, 6825-6837.

22. Pedraza-Chaverrí, J., Barrera, D., Maldonado, P.D., Chirino, Y.I., Macías-Ruvalcaba, N.A., Medina-Campos, O.N., Castro, L., Salcedo, M.I., Hernández-Pando, R. *S*-Allylmercaptocysteine Scavenges Hydroxyl Radical and Singlet Oxygen *In Vitro* and Attenuates Gentamicin-Induced Oxidative and Nitrosative Stress and Renal Damage *In Vivo*. *BMC Clin. Pharmacol.* **2004**, *4*, 1-13.

23. Silvaroli, J.A., Pleshinger, M.J., Banerjee, S., Kiser, P.D., Golczak, M. Enzyme that Makes You Cry-Crystal Structure of Lachrymatory Factor Synthase from *Allium cepa*. *ACS Chem. Biol.* **2017**, *12*, 2296-2304.

24. Bayer, T., Wagner, H., Block, E., Grisoni, S., Zhao, S.H., Neszmelyi, A. Zwiebelanes: Novel Biologically Active 2,3-Dimethyl-5,6-dithiabicyclo[2.1.1]hexane 5-Oxides from Onion. *J. Am. Chem. Soc.* **1989**, *8*, 3085-3086.

25. Aoyagi, M., Kamoi, T., Kato, M., Sasako, H., Tsuge, N., Imai, S. Structure and Bioactivity of Thiosulfinates Resulting from Suppression of Lachrymatory Factor Synthase in Onion. *J. Agric. Food Chem.* **2011**, *59*, 10893-10900.

26. Tocmo, R., Parkin, K. S-Alk(en)ylmercaptocysteine Suppresses LPS-Induced Pro-Inflammatory Responses in Murine Macrophages Through Inhibition of NF-Kb Pathway and Modulation of Thiol Redox Status. *Free Rad. Biol. Med.* **2018**, *129*, 548-558.

27. Tocmo, R., Parkin, K. *S*-1-Propenylmercaptocysteine Protects Murine Hepatocytes Against Oxidative Stress via Persulfidation of Keap1 and Activation of Nrf2. *Free Rad. Biol. Med.* **2019**, *143*, 164-175.

28. Chen, C.-C., Chiu, K.-T., Sun, Y.-T., Chen, W.-C. Role of the Cyclic AMP-Protein Kinase A Pathway in Lipopolysaccharide-Induced Nitric Oxide Synthase Expression in RAW 264.7 Macrophages. *J. Biol. Chem.* **1999**, *274*, 31559-31564.

29. Jacobs, A.T., Ignarro, L.J. Lipopolysaccharide-Induced Expression of Interferon-β Mediates the Timing of Inducible Nitric-Oxide Synthase Induction in RAW 264.7 Macrophages. *J. Biol. Chem.* **2001**, *276*, 47950-47957.

30. Bianco, C.L., Chavez, T.A., Sosa, V., Saund, S.S., Nguyen, Q.N.N., Tantillo, D.J., Ichimura, A.S., Toscano, J.P., Fukuto, J.M. The Chemical Biology of the Persulfide (RSSH)/Perthiyl (RSS·) Redox Couple and Possible Role in Biological Redox Signaling. *Free Radic. Biol. Med.* **2016**, *101*, 20-31.

31. Hayes, J.D., Dinkova-Kostova, A.T. The Nrf2 Regulatory Network Provides an Interface Between Redox and Intermediary Metabolism. *Trends Biochem. Sci.* **2014**, *39*, 199-218.

32. Zhang, H., Liu, H., Zhou, L., Yuen, J., Forman, H.J. Temporal Changes in Glutathione Biosynthesis During the Lipopolysaccharide-Induced Response of THP-1 Macrophages. *Free Rad. Biol. Med.* **2017**, *113*, 304-310.

33. Shaw, P., Chattopadhyay, A. Nrf2-ARE Signaling in Cellular Protection: Mechanism of Action and the Regulatory Mechanisms. *J. Cell. Physiol.* **2020**, *235*, 3119-3130.

34. Aldini, G., Altomare, A., Baron, G., Vistoli, G., Carini, M., Borsani, L., Sergio, F. N-Acetylcysteine as an Antioxidant and Disulphide Breaking Agent: The Reasons Why. *Free Rad. Res.* **2018**, *52*, 751-762.

35. Yin, Z., Ivanov, V.N., Habelhah, H., Tew, K., Ronai, Z. Glutathione *S*-Transferase p Elicits Protection against H_2O_2-induced Cell Death via Coordinated Regulation of Stress Kinases. *Canc. Res.* **2000**, *60*, 4053-4057.

36. Wardyn, J.D., Ponsford, A.H., Sanderson, C.M. Dissecting Molecular Cross-Talk Between Nrf2 and NF-Kb Response Pathways. *Biochem. Soc. Trans.* **2015**, *43*, 621-626.

37. Kobayashi, E.H., Suzuki, T., Funayama, R., Nagashima, T., Hayashi, M., Sekine, H., Tanaka, N., Moriguchi, T., Motoahashi, H., Nakayama, K., Yamamoto, M. Nrf2 Suppresses Macrophage Inflammatory Response by Blocking Proinflammatory Cytokine Transcription. *Nat. Comm.* **2016**, *7*, 1-14.

38. Lee, I.-C., Kim, S.-H., Baek, H.-S., Moon, C., Kang, S.-S., Kim, S.-H., Kim, Y.-B., Shin, I.-S., Kim, J.-C. The Involvement of Nrf2 in the Protective Effects of Diallyl Disulfide on Carbon Tetrachloride-Induced Hepatic Oxidative Damage and Inflammatory Response in Rats. *Food Chem. Toxicol.* **2014***, 63*, 174-185.

39. Naidu, S., Vijayan, V., Santoso, S., Kietzmann, T., Immenschuh, S. Inhibition and Genetic Deficiency of p38 MAPK Up-Regulates Heme Oxygenase-1 Gene Expression via Nrf2. *J. Immunol.* **2009**, *182*, 7048-7057.

40. Carlsen, H., Haugen, F., Zadelaar, S., Kleemann, R., Kooistra, T., Drevon, C.A., Blomhoff, R. Diet-Induced Obesity Increases NF-κB Signaling in Reporter Mice. *Genes Nutr.* **2009**, *4*, 215-222.

41. Sokolva, O., Naumann, M. NF-κB Signaling in Gastric Cancer. *Toxins* **2017**, *9*, 1-22.

Chapter 4

The Role of Mitogen-Activated Protein Kinases in the Anti-Inflammatory Effects of *S*-Alk(en)ylmercaptocysteines on Stimulated Macrophage Cells

4.1 Abstract

S-alk(en)ylmercaptocysteines, especially the onion-derived *S*-1-propenylmercaptocysteine (CySSPe), exhibit potent anti-inflammatory properties. The aim of this study was to explore the regulatory effect of *Allium* mercaptocysteines on key elements of the inflammatory signaling through NF-κB and mitogen-activated protein kinase (MAPK) pathways in activated macrophage cells. RAW 264.7 cells were treated with single and multiple combinations of chemical inhibitors of kinases IKKα/β, p38, JNK, and TAK1 alongside vehicle, *S*-allylmercaptocysteine (CySSA), or *S*-1-propenylmercaptocysteine (CySSPe). The nitric oxide (NO) output from these treated cells was assayed as a biomarker of inflammation. NO output was strongly suppressed by CySSA and CySSPe through inhibition of the IKKα/β signaling pathway (93% and 100% relative effect, respectively), with diminished effects on the p38 signaling pathway (67% relative effect). CySSA exhibits pro-inflammatory effect through JNK (-12% relative effect). Combined partial inhibition of p38, JNK, and TAK1 resulted in a blockade in CySSR inhibitory effects on NO production. Together, these results suggest mercaptocysteines exert their anti-inflammatory effects primarily through the IKKα/β/NF-κB axis. Further work is necessary to confirm these findings by investigating the levels of phosphorylated substrates of the kinases used following treatment with CySSR and evaluating levels of other pro-inflammatory mediators such as cytokines TNF-α, IL-6, and IL-1β, COX-2, and iNOS under the conditions of this study.

4.2 Introduction

Inflammation is a tightly regulated immune response to environmental stimuli such as inflammatory cytokines, oxidative stress, and bacterial endotoxins (1). This inflammatory response is necessary for tissue healing and host defense against microbial infection (2,3). However, chronic inflammation can occur through persistent inflammatory re-initiation and dysregulation of this physiological response (4). Prolonged chronic inflammation is tied to the pathogenesis of cancer, cardiovascular diseases, metabolic syndromes, and neurodegeneration (5-9). Therefore, the search for dietary factors that attenuate inflammation is important for developing dietary interventions that reduce the risk of these chronic diseases.

Lipopolysaccharide (LPS), a major component of Gram-negative bacteria outer membranes, activates the inflammatory cascade in macrophage cells through the binding of this bacterial endotoxin to the Toll-like receptor 4 (TLR4), a transmembrane receptor protein involved in the intracellular initiation of the canonical nuclear factor-κB (NF-κB) inflammatory signaling cascade (10). Upon binding, TLR4 recruits a group of adaptor proteins to form a transmembrane complex that activates tumor necrosis factor (TNF) receptor-associated factor 6, which further induces the activation of transforming growth factor-β-activated kinase 1 (TAK1) (11,12). TAK1 is a major activator of the IκB kinase (IKK) signaling pathway, which is involved in the activation of the NF-κB pathway, as well as mitogen-activated protein kinase (MAPK) cascades (13,14). As such, TAK1 is a central regulator of inflammatory signaling **(Fig. 4.1)**.

MAPKs are a family of highly conserved protein kinases that play a prominent role in regulating proliferation, metabolism, inflammation, and programmed cell death (15). MAPKs integrate and process multiple extracellular signals and serve as primary components of intracellular signaling circuitry (16). The three major subfamilies of MAPKs include

extracellular signal-regulated kinases, ERK1 and 2, the c-Jun NH_2-terminal kinases, JNK, and the p38 kinases (17). TAK1 transduces signals to the MAPKs through the activation of several mitogen-activated protein kinase kinases (MAPKKs) (18). MAPKs can phosphorylate IKKs *in vitro*, activating NF-κB outside of the TLR4/NF-κB axis (19). IKKβ can also activate MAPKs independently of NF-κB, providing possible crosstalk between the NF-κB and MAPK pathways. MAPKs play potential roles in the pathophysiology of inflammatory disease and the inhibition of MAPKs is an important target of pharmacological research (20-22).

Evidence shows the anti-inflammatory effects of *Allium*-derived dietary components may be tied to their ability to modulate the MAPK signaling pathway. Diallyl disulfide (DADS), a component of garlic oil, was shown to block LPS-stimulated phosphorylation of p38, ERK, and JNK in microglial cells (23). Alliin, a cysteine sulfoxide found in garlic tissues, inhibits LPS-induced expression of pro-inflammatory IL-6 and TNF-α in 3T3-L1 adipocytes through the inhibition of ERK1/2 activation (24). Garlic-derived CySSA has been shown to reduce TNF-α and IL-1β with concomitant reductions in p38 and JNK phosphorylation in Sprague-Dawley female rats fed a high-fat diet (25).

Allium vegetables are important components of the human diet and their consumption is potentially linked to the risk reduction of several diseases including cancer (26), cardiovascular disease (27-29), and obesity (29,30). Of these vegetables, garlic and onions are the most widely consumed and studied *Allium* species. *Allium*-derived *S*-alk(en)ylmercaptocysteines (CySSRs) are putative secondary metabolites rapidly formed from the conjugation of these thiosulfinates with cysteine (31-33). Transformation products of thiosulfinates derived from garlic (*S*-allylmercaptocysteine, CySSA) and onion (*S*-1-propenylmercaptocysteine, CySSPe), have been studied for the cytoprotective properties they confer against inflammation (33-36). CySSR may

inhibit biological targets by undergoing disulfide exchange with cysteinyl residues of proteins resulting in a protein-mixed disulfide (37). Previous reports and the work conducted in chapter 2 of this dissertation also suggest CySSR are substrates of β-lyases cystathionine-β-synthase (CBS) and cystathionine-γ-lyase (CSE) and may evolve persulfides and H_2S from this enzymatic activity (37,38). TAK1 contains a reactive cysteine in its active site, the target of several TAK1 covalent inhibitors, which could be inhibited via post-translational modification by persulfide or disulfide exchange (39,40). While inhibition of the NF-κB signaling pathway by CySSR was previously reported (35), the modulation of MAPKs as an alternative pathway by which CySSR ameliorate inflammation has yet to be explored.

A more thorough understanding of the biochemical mechanisms by which CySSRs exert their anti-inflammatory effects could support more targeted investigations into the therapeutic potential of CySSRs against inflammatory diseases. The aim of this study was to evaluate which kinases are important molecular targets in respect to the anti-inflammatory effects of CySSRs in these cells. The present study analyzes the differential impact of CySSRs on MAPKs, IKK, and the upstream kinase TAK1 signaling pathways and evaluate the role of MAPKs in activating NF-κB in LPS-activated macrophages using NO as a biomarker of inflammation.

4.3 Materials and Methods

4.3.1 Chemicals and General Procedures

LPS (*E. coli* serotype O127:B8), Bay 11-7082, FR180204, takinib, dimethyl sulfoxide (DMSO), 3-4,5-(dimethylthiazol-2-yl)-2,5-diphenyltetrazolium bromide (MTT), were purchased from Millipore Sigma (Burlington, MA, USA). SCIO 469 hydrochloride was purchased from Tocris Bioscience (Minneapolis, MN, USA) and bentamapimod was purchased from Cayman Chemical (Ann Arbor, MI, USA). All other chemicals were obtained from Millapore Sigma

unless otherwise noted. All solvents used for extraction or HPLC analysis were purchased from Fisher Scientific (Hampton, NH) or Millapore Sigma. Onion and garlic were procured from a local grocery store in Madison, WI. Analytical HPLC was conducted using 250 x 4.6 mm, 5 μM, Discovery C18 column (Supelco, Bellefonte, PA) on an Ultimate 3000 HPLC System (Thermo Fisher Scientific, Madison, WI) equipped with a diode array detector. Semi-preparative HPLC was carried out using a 250 x 21.2 mm, 5 μM, Discovery C18 (Supelco, Bellefonte, PA) on a Reveleris Prep purification system (Grace Co., Columbia, MD).

4.3.2 Preparation and Isolation of CySSR

CySSA and CySSPe were prepared according to protocols previously outlined, with modifications (33). Approximately 500 g of whole white onions were halved and heated in the microwave for 5 to 8 min (700 W) and cooled to room temperature. The cooled onion tissue was juiced to give 200 to 300 mL of liquid. The crude onion juice was homogenized with approximately 50 g peel fresh garlic and 100 mL deionized water for 1 to 2 min at 4 ºC. The homogenate was left to incubate at room temperature for 45 to 60 min. After the incubation period, the mixture was centrifuged at 12,000 x g for 15 min at 4 ºC and the supernatant collected, discarding the pellet. The supernatant was extracted three times with 100 mL CH_2Cl_2. The organic phase was separated, collected, and dried over anhydrous $MgSO_4$.

The solvent was evaporated under a stream of nitrogen gas until an oily residue of crude thiosulfinates remained. The crude material was resuspended in 5 to 10 mL of ddH_2O and reacted with 0.5 to 1.0 g of cysteine-hydrochloride hydrate for 30 min with stirring. The solution was filtered through a 0.2 μm Whatman filter and separated using a Reveleris® Prep purification system. Separation was conducted on a 25 cm x 21.2 mm, 5 μM Discovery® C18 column with isocratic elution using MeOH:water (30:70) at a flow rate of 12 mL/min over 25 min. Peak

resolution was monitored by UV (254 and 210 nm). These fractions were combined and evaporated under vacuum at 25 ºC to remove excess MeOH. The remaining aqueous solution was frozen at -20 ºC overnight, then freeze dried over three days. Isolated solid compounds were analyzed via HPLC and identified via their MS, ^{1}H NMR and ^{13}C NMR spectra **(Appendix A.2)**, as previously reported (33,34).

4.3.3 Cell Culture Protocols

Murine macrophage RAW 264.7 cells (ATCC® TIB-71) were obtained from ATCC (Manassas, VA). Cell cultures were maintained in 75-cm^2 tissue culture flasks in phenol red-free Dulbecco's Modified Eagle Medium (DMEM, Invitrogen) supplemented with 10% fetal bovine serum (FBS), streptomycin (100 µg/mL), penicillin (100 U/mL), and incubated at 37 ºC with 5% CO_2 humidified atmosphere. Cells (80-90% confluence) were subcultured every 2 to 3 days, passaging at a 1:10 split ratio and cell passages 5 to 16 were used for all experiments. The medium was replaced with fresh DMEM medium containing test compounds and the cells were incubated for 24 h.

4.3.4 Griess Nitric Oxide Assay for Endotoxin-Stimulated RAW 264.7 Cells

RAW 264.7 cells were grown over 24 h in 96-well plates (2 x 10^4 cells per well) in 200 µL of phenol red-free DMEM supplemented with 10% FBS, streptomycin (100 µg/mL), penicillin (100 U/mL), and incubated at 37 ºC with 5% CO_2 humidified atmosphere. The medium was then replaced with fresh medium containing vehicle, mercaptocysteines, and/or chemical inhibitors, and 1 µg/mL lipopolysaccharide (LPS), and plates were incubated for an additional 24 h. A 100 µL sample was removed from the culture supernatant of each well and mixed with an equal amount of fresh prepared Griess reagent, incubated for 10 min, and then the

absorbance at 540 nm was measured using a Spectra Max Absorbance Microplate Reader (Molecular Devices, Sunnyvale, CA).

Cell viability was measured in duplicate 96-well plates using the MTT assay protocol. The medium from the duplicate microplate was aspirated and 100 μL of 3-(4,5-dimethylthiazol-2-yl)-2,5-diphenyltetrazolium bromide (MTT) (0.2% in 2% EtOH) was added to each well and incubated for 4 h in a humidified atmosphere at 37 ºC and 5% CO_2. The MTT solution was aspirated from the wells of the microplate and replaced with 50 μL DMSO (anhydrous). The microplate was allowed to incubate at room temperature for 15 min. The microplate was shaken for 5 min and the absorbance was measured at 570 – 590 nm by microplate reader. The absorbance values of the blanks were subtracted from the controls and treated sample wells.

4.3.5 Combinatorial Analysis

To gain additional insight into the trends observed in these combinatorial experiments, the differences of each combination of kinase inhibitors with or without CySSR treatment was evaluated **(Eq. 4.1A and Fig. 4.2A)**. The NO output for the inhibition of all four kinases was set as the zero point, extrapolated from the ternary inhibition of JNK/p38/IKKα/β and p38/IKKα/β/TAK1, both of which resulted in zero or near zero NO released. It was presumed that inhibition of all four kinases would similarly give zero NO, as the treatment of RAW 264.7 cells with all four kinase inhibitors and LPS resulted in extensive cell death (data not shown). The change in NO was calculated as the difference between the NO released from each of the four ternary combinations with vehicle and the six secondary combinations.

The difference between the NO released from each secondary combination with CySSA or CySSPe versus the ternary combinations with CySSA or CySSPe was also calculated, to give the change in NO output (Δ%NO) of vehicle, CySSA, and CySSPe and represented the change in

NO if one kinase pathway was unimpeded by the presence of its chemical inhibitor. This calculated delta value was assigned to each kinase pathway that was not inhibited in each combination. These delta values were further calculated between the binary and four unary combinations, and subsequently between unary combinations and LPS alone with vehicle, CySSA, or CySSPe. Finally, the Δ%NO values released from the presence of vehicle was subtracted from the Δ%NO released in the presence of CySSA or CySSPe for all sets of combinations to give the difference in Δ%NO (dΔ%NO), summed together for each kinase pathway and either CySSA or CySSPe (∑dΔ%NO), and set relative to the highest value, representing the relative effect each mercaptocysteine has on each kinase pathway **(Eq. 4.1B,C and Fig. 4.2B)**.

4.3.6 Statistical Analysis

Statistical analyses were performed using SigmaPlot 13 software (Systat Software, Inc., San Jose, CA). Results were expressed as mean values ± SD of at least three independent experiments. Difference in the means were evaluated by one-way ANOVA followed by Tukey's HSD test, and differences of $P \leq 0.05$ were deemed significant.

4.4 Results & Discussion

The mitogen-activated protein kinase (MAPK) pathway is a parallel signaling pathway involved in LPS-induced inflammation **(Fig. 4.1)**. The LPS-stimulated immune response is triggered by binding with TLR4 and activation of TAK1, which regulates the IKK-dependent signal to the canonical NF-κB pathway as well as the MAPKs p38, JNK, and ERK1/2 (13,14). To evaluate the magnitude to which kinase pathways contribute to the release of NO, pharmacological inhibitors Bay 11-7082 (IKKα/β inhibitor), SCIO 469 (p38 inhibitor), bentamapimod (JNK inhibitor), takinib (TAK1 inhibitor), and FR180204 (ERK1/2 inhibitor)

were incubated in LPS-stimulated RAW 264.7 cells. The chemical inhibition of IKKα/β, p38, JNK, or TAK1 led to a reduction in NO output in the 2.5 μM to 20 μM range **(Fig. 4.3-4.6)**. However, chemical inhibition of ERK1/2 did not lead to NO inhibition in the same dose range, and therefore was excluded in further inhibition studies **(Fig. 4.7)**. Inhibitor doses were selected at concentrations that led to partial inhibition of NO output (~25 to 50%) and did not induce significant cell death.

CySSA and CySSPe alone inhibit NO output in a dose-dependent manner **(Fig. 4.8)**. Concentrations of CySSA at 100 μM and CySSPe at 25 μM were used for partial inhibition of NO without significant cell death to further probe the effect of kinase chemical inhibitors on CySSR-dependent NO inhibition. Partial inhibition of NO production by the four inhibitors co-incubated with CySSR led to further reduction in NO at 25 μM for CySSPe and 100 μM for CySSA **(Fig. 4.9-4.12)**, except when CySSA was co-incubated with IKKα/β inhibitor, Bay 11-7082, which led to an increase in NO released **(Fig. 4.9)**. Co-incubation of CySSR with inhibitors for either MAP kinases p38 (SCIO 469) or JNK (bentamapimod) led to equal levels of NO reduction by both CySSR compared to the chemical inhibitors alone. On the other hand, combined treatment of CySSPe with TAK1 inhibitor, takinib, resulted in a greater decrease in NO versus CySSA with takinib. These two results suggest CySSA and CySSPe differentially impact these kinase pathways. All treatments exhibited a cell viability of >85%, and so NO reductions were attributed to these treatments.

Multiple chemical inhibitors were combined with CySSR to inhibit multiple targets and evaluate the modulating effects of CySSR on each kinase pathway, as CySSR may inhibit other pathways while a single kinase is inhibited by a single chemical inhibitor. Binary inhibition of IKKα/β/JNK **(Fig. 4.13)**, IKKα/β/p38 **(Fig. 4.14)**, and p38/TAK1 **(Fig. 4.15)** blocked further

inhibition of NO by CySSR. Interestingly, inhibition of IKKα/β/p38 and IKKα/β/TAK1 **(Fig. 4.16)** led to an increase in NO upon co-treatment with CySSA, which suggests the unimpeded JNK pathway may be involved in the inflammatory effect by NO. Additional inhibition of NO by both CySSA and CySSPe was seen when p38/JNK **(Fig. 4.17)** and TAK1/JNK **(Fig. 4.18)** were inhibited compared to vehicle, and so NO production may be attenuated by these two CySSR through inhibition of IKKα/β. Ternary inhibition of p38/JNK/IKKα/β **(Fig. 4.19)** and p38/TAK1/IKKα/β **(Fig. 4.20)** kinases resulted in complete inhibition of NO with and without CySSR, whereas ternary inhibition of kinases JNK/p38/TAK1 **(Fig. 4.21)** and IKKα/β/JNK/TAK1 **(Fig. 4.22)** did not, even in the presence of CySSR.

The change in NO inhibition (Δ%NO) between the absence and presence of a single chemical inhibitor across each combination, with or without CySSR, was calculated to isolate the inhibitory effect of CySSR on each kinase **(Eq. 4.1A)**. The results of this analysis are summarized in **Figure. 4.23**. The corresponding Δ%NO output between vehicle and CySSA or CySSPe over these combinations were further calculated, summed, and set relative to the highest value (CySSPe on IKKα/β) **(Eq. 4.1B,C)** to evaluate the relative effect of each mercaptocysteine on these kinase pathways **(Fig. 4.24)**. These results show that both CySSA and CySSPe strongly inhibit NO release through the IKK signaling pathway. The sum total relative inhibitory effect on NO release was highest for CySSA (93% relative effect) and CySSPe (100% relative effect) in combinations when IKKα/β was uninhibited chemically, which suggests both CySSA and CySSPe act nearly equally on the IKK signaling pathway at the concentrations used here. The remaining inhibitory effect on NO seen by CySSR was exerted through the p38 signaling pathway, especially by CySSPe (~67% relative effect).

However, CySSR does exhibit a partial inhibitory effect on NO output by inhibiting the p38 and JNK MAPK pathways and may modulate these pathways through an H_2S-dependent sulfhydration mechanism. Previous work (38) and the results of chapter 2 suggest that CySSPe evolves H_2S *in vitro*. Endogenous H_2S has been shown to suppress the phosphorylation of p38 and JNK MAPK in rat cardiomyocytes by sulfhydrating and modifying the nitrated cyclic nucleotide, 8-nitroguanisine 3',5'-cyclic monophosphate (8-nitro-cGMP), which normally mediates the activation of these MAP kinases (41).

The inhibitory effect of CySSR on the MAPK signaling pathways may also modulate pathways associated with other chronic diseases, such as gastric cancer and obesity. In gastric cancers, elevated levels of p38 MAPK is responsible for the chemoresistance of gastric tumor cells (42). Furthermore, increased proliferation of gastric cancer exosomes is associated with the activation and activity of ERK1/2 MAPK (43). During the progression of obesity, adipose tissues expand in size in response to the excess accumulation of lipids through the process of adipogenesis in which fibroblast-like progenitor cells differentiate into adipocytes. ERK, JNK, and p38 MAPK are shown to be activated immediately following adipogenesis in 3T3-L1 pre-adipose cells (44). Genetically altered mice that do not express ERK (ERK-/-) or JNK (JNK-/-) exhibit resistance to obesity, which suggests these MAPKs play a role in the etiology of obesity (45,46). Additionally, a previous study suggests p38 MAPK is an enhancer of adipogenesis and necessary for adipocyte differentiation (47).

Further studies are necessary to evaluate the ability of CySSR, especially CySSPe, to modulate these pathways in addition to the NF-κB inflammatory pathway and exert ameliorative properties in relevant disease models for gastric cancer and obesity. The current study is limited by the lack of data regarding the level of activation or deactivation of the kinases examined. The

inhibitory effect of CySSRs on the IKK/NF-κB signaling axis in activated macrophages was previously investigated through Western blot analysis (35), whereas here the MAPKs were not similarly analyzed. To confirm the inhibitory effects on different signaling pathways shown here, future experiments should evaluate if p38, JNK, and TAK1 phosphorylation activity on their target proteins is diminished in the presence of CySSR via Western blot analysis of phosphorylated proteins levels following CySSR treatment.

Additionally, chemical inhibitors can exhibit broad specificity at various concentrations. For example, the IKKα/β inhibitor, Bay 11-7802, has multiple kinase targets and suppresses MyD88-dependent signaling (48). It is possible that other kinases and regulatory pathways involved in the inflammatory process, that were not specifically studied here, have been impeded and their contribution is not accounted for. Furthermore, the study also did not evaluate the effect of inhibitory combinations on other relevant inflammatory mediators (iNOS, TNF-α, IL-1β, IL-6). A thorough analysis of the combinatorial effects of CySSRs with the chemical inhibitors used in this study across other inflammatory biomarkers may provide a more comprehensive understanding of the inhibitory effects CySSRs exert on these kinase pathways and their relationship to inflammation.

In conclusion, CySSR exerted NO suppression predominantly through the inhibition of the IKKα/β and p38 signaling pathways in an LPS-activated murine macrophage model. CySSR-dependent inhibition of the upstream kinase TAK1 signaling pathway was not a major contributor to the modulating effects of CySSR on NO production. Previous work on the anti-inflammatory properties of CySSR in LPS-activated macrophages demonstrated that both mercaptocysteines act on the IKK/NF-κB signaling axis but did not investigate the modulating effect of CySSR on the MAPK pathway activated by the inflammatory response (35). The

current study demonstrates that the IKK/NF-κB axis is the major signaling pathway by which CySSR exert their anti-inflammatory effects relative to the MAP kinase pathways investigated.

4.5 Figures and Tables

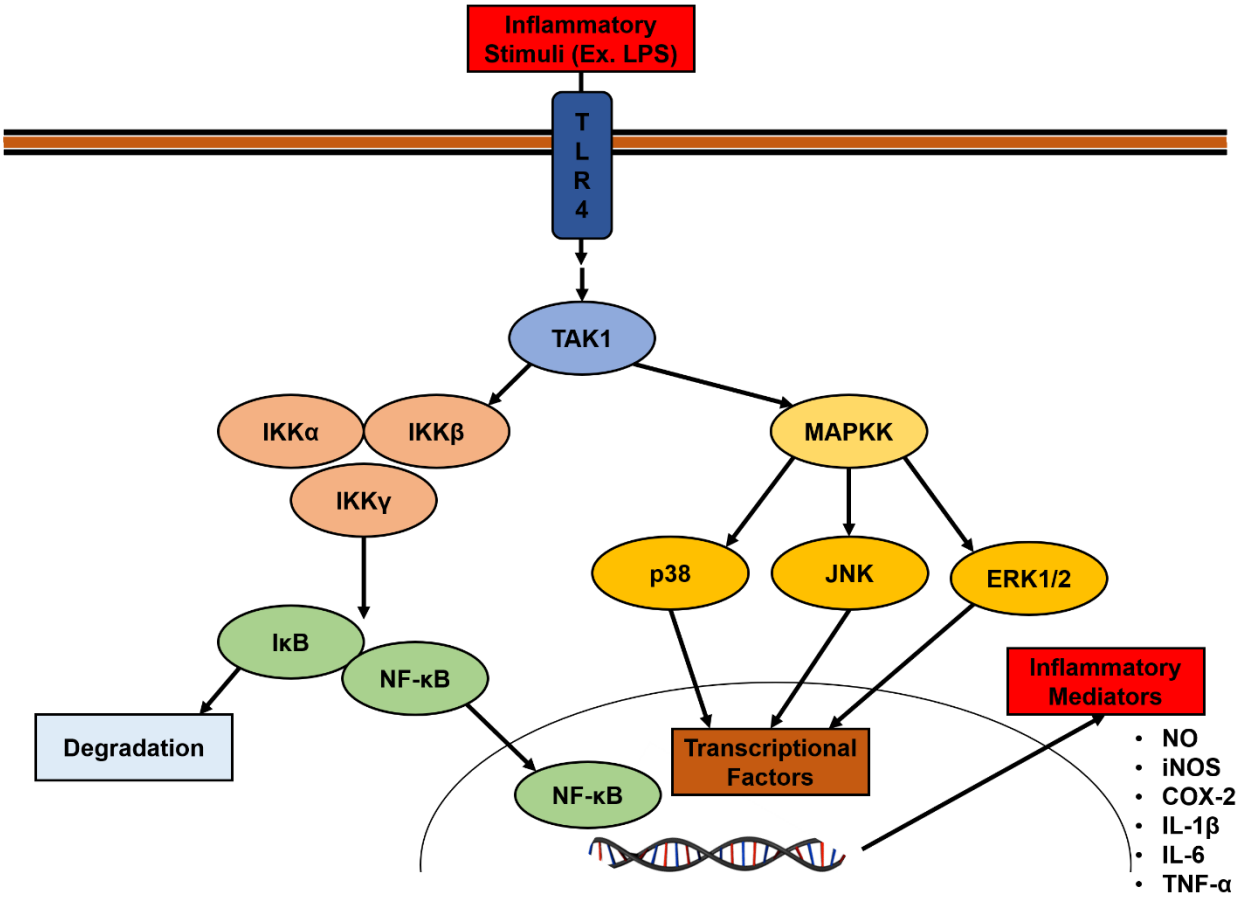

Figure 4.1. Schematic diagram of the canonical NF-κB and MAP kinase pathways involved in the inflammatory response. Adapted from (10).

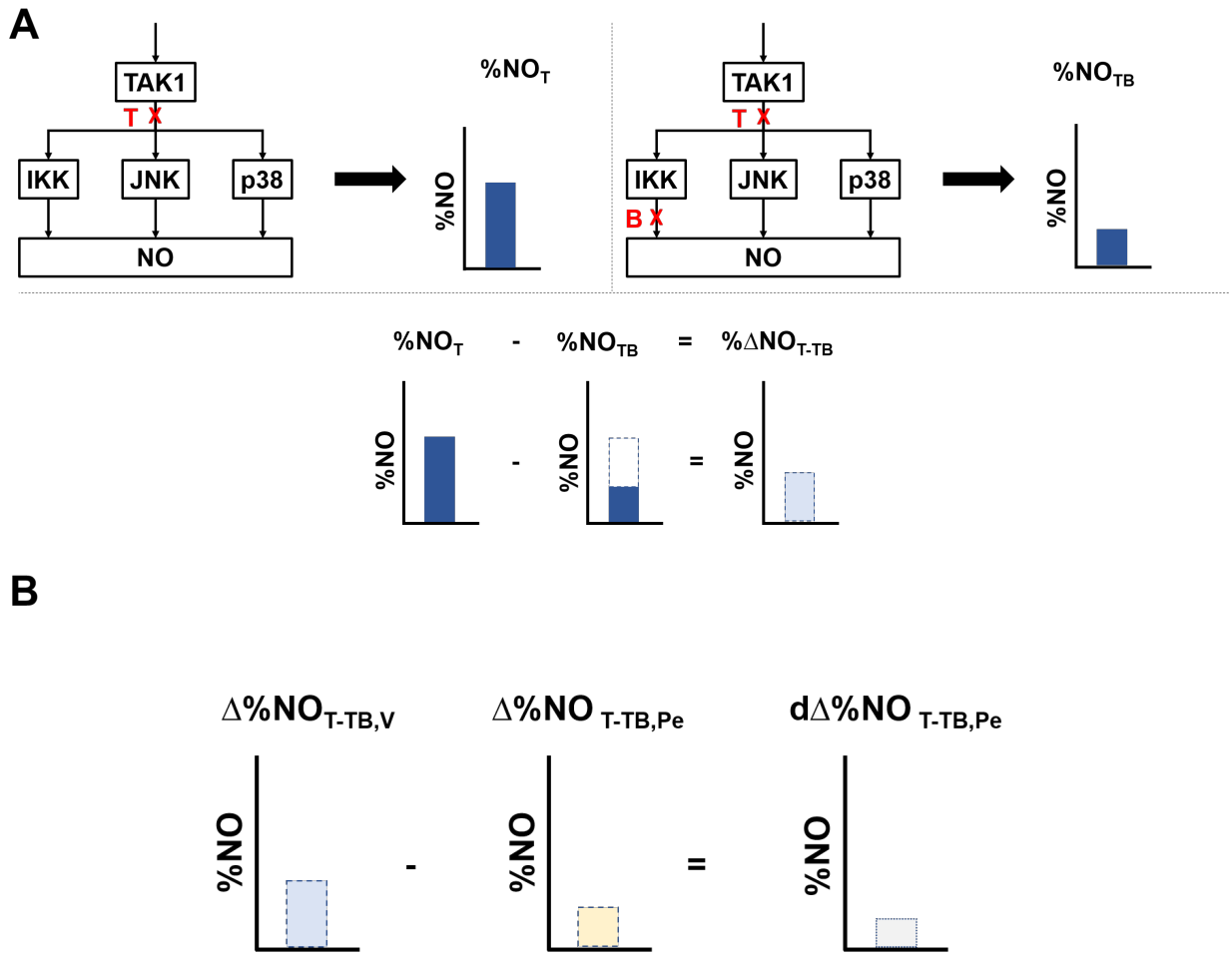

Figure 4.2. Visual diagram of combinatorial calculation for Δ%NO and dΔ%NO**. (A)** Change in NO (Δ%NO) output between macrophages inhibited with takinib alone versus a combination of takinib and Bay-11-7082 (T-TB) and **(B)** example diagram of calculation for differences in Δ%NO output (dΔ%NO) between vehicle alone ($\%\Delta NO_V$) and in the presence of CySSPe ($\%\Delta NO_{Pe}$). T = takinib (TAK1 inhibitor), B = Bay-11-7082 (IKKα/β inhibitor), V = vehicle, Pe = CySSPe.

Eq. 4.1A. $\Delta\%NO_{Combo\ x1\ -\ Combo\ z1,Vehicle} = \%NO_{Combo\ x1,Vehicle} - \%NO_{Combo\ z1,Vehicle}$

Ex. 4.1A. $\Delta\%NO_{T\text{-}TB,V} = \%NO_{T,V} - \%NO_{TB,V}$
$\Delta\%NO_{T\text{-}TB,V} = 54.9\% - 20.6\% = 34.3\%$

Eq. 4.1B. $d\Delta\%NO_{CySSR} = \Delta\%NO_{Combo\ x1\ -\ Combo\ z1,Vehicle} - \Delta\%NO_{Combo\ x1\ -\ Combo\ z1,CySSR}$

Ex. 4.1B. $d\Delta\%NO_{T\text{-}TB,Pe} = \Delta\%NO_{T\text{-}TB,V} - \Delta\%NO_{T\text{-}TB,Pe}$
$d\Delta\%NO_{T\text{-}TB,Pe} = 34.3\% - 4.0\% = 30.3\%$

Eq. 4.1C. $\sum d\Delta\%NO_{Inhibitor,CySSR} = d\Delta\%NO_{Combo\ x1\ -\ Combo\ y1,CySSR} + d\Delta\%NO_{Combo\ x2\ -\ Combo\ y2,CySSR}\cdots$

Ex. 4.1C. $\sum d\Delta\%NO_{B,Pe} = d\Delta\%NO_{T\text{-}TB,Pe} + d\Delta\%NO_{S\text{-}SB,Pe} + d\Delta\%NO_{TS\text{-}TSB,Pe}\cdots$
$\sum d\Delta\%NO_{B,Pe} = 19.4\% + 30.3\% + 39.7\% + 34.5\% + 2.3\% + 30.5\% + 43.1\%$
$\sum d\Delta\%NO_{B,Pe} = 199.7\%$

Equations 4.1. Summary of equations and examples used to calculate isolated effects of each chemical inhibitor when used alone or in combination to inhibit kinase pathways with or without CySSR. T = takinib (TAK1 inhibitor), B = Bay-11-7082 (IKKα/β inhibitor), V = vehicle, Pe = CySSPe.

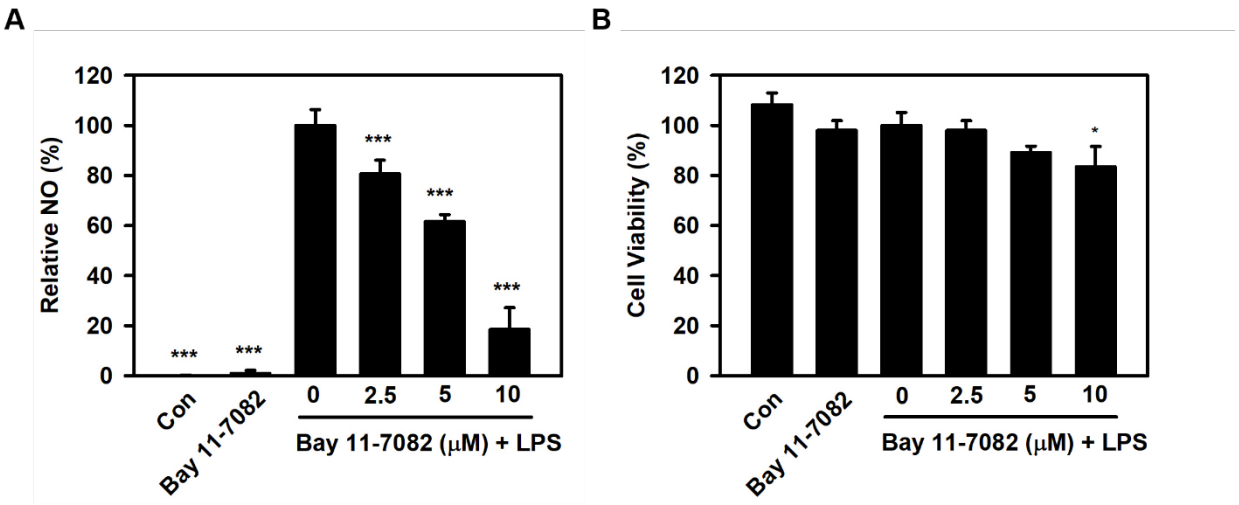

Figure 4.3. NO output and cell viability of activated RAW 264.7 cells treated with Bay 11-7082. Cells were co-treated with 1 μg/mL LPS and Bay 11-7082 (IKKα/β inhibitor) from 0 to 10 μM, then assayed for **(A)** NO release and **(B)** cell viability. Bay 11-7082 alone at 5 μM. Cell viabilility dropped below 50% at 20 μM. Statistical significance was determined by one-way ANOVA with Tukey's post-test. * = $P < 0.05$ and *** = $P < 0.001$ versus LPS only (0 μM inhibitor).

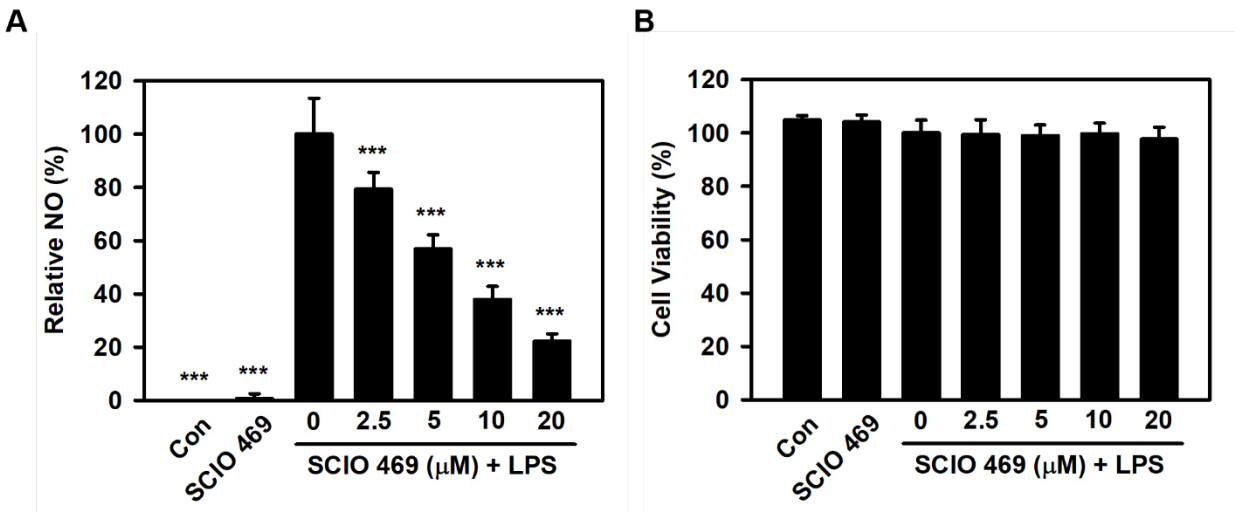

Figure 4.4. NO output and cell viability of activated RAW 264.7 cells treated with SCIO 469. Cells were co-treated with 1 μg/mL LPS and SCIO 469 (p38 inhibitor) from 0 to 20 μM, then assayed for **(A)** NO release and **(B)** cell viability. SCIO 469 alone at 20 μM. Statistical significance was determined by one-way ANOVA with Tukey's post-test. *** = $P < 0.001$ versus LPS (0 μM inhibitor).

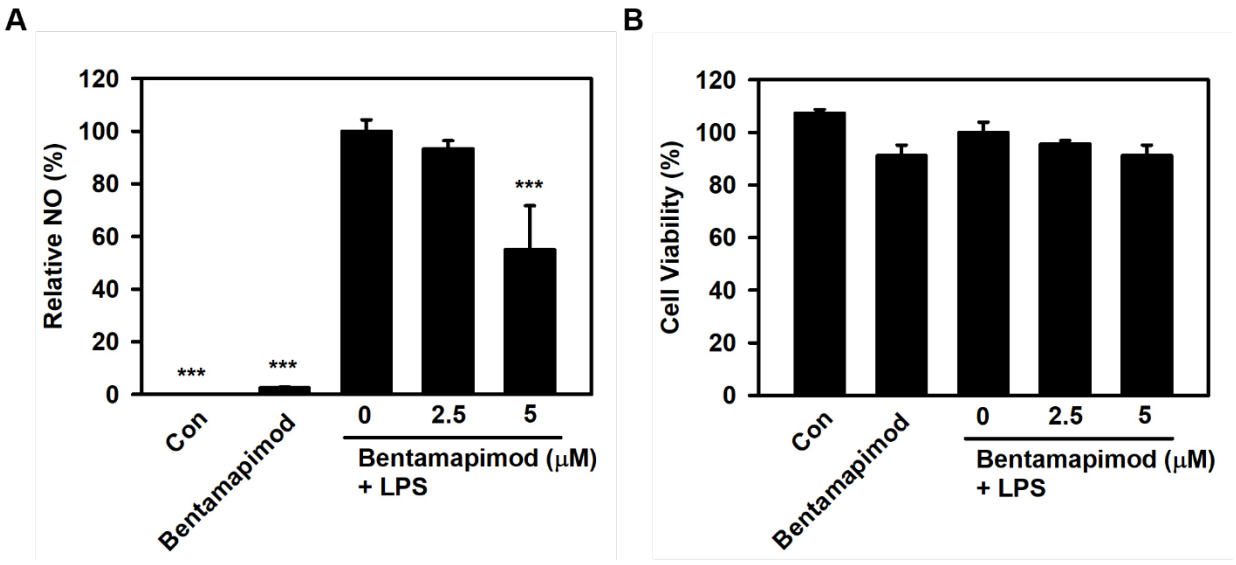

Figure 4.5. NO output and cell viability of activated RAW 264.7 cells treated with bentamapimod. Cells were co-treated with 1 μg/mL LPS and bentamapimod (JNK inhibitor) from 0 to 20 μM, then assayed for **(A)** NO release and **(B)** cell viability. Bentamapimod alone was at 5 μM and concentrations above 10 μM exhibited cell viabilities below 50%. Statistical significance was determined by one-way ANOVA with Tukey's post-test. *** = $P < 0.001$ versus LPS (0 μM inhibitor + LPS).

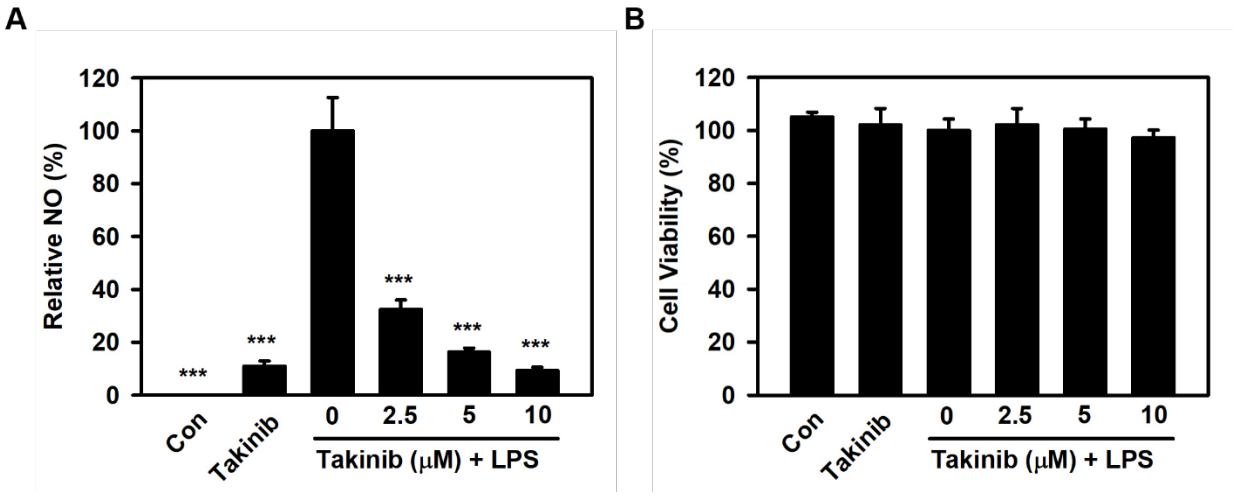

Figure 4.6. NO output and cell viability of activated RAW 264.7 cells treated with takinib. Cells were co-treated with 1 μg/mL LPS and takinib (TAK1 inhibitor) from 0 to 10 μM, then assayed for **(A)** NO release and **(B)** cell viability. Takinib alone was at 2.5 μM, and cell viability was <50% at 20 μM. Statistical significance was determined by one-way ANOVA with Tukey's post-test. *** = $P < 0.001$ versus LPS (0 μM inhibitor + LPS).

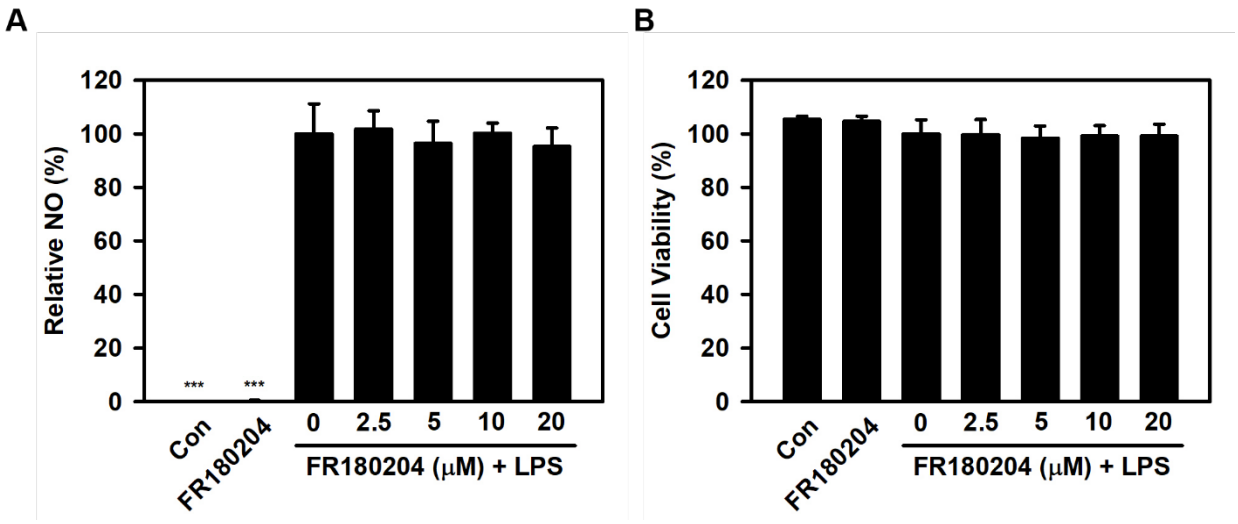

Figure 4.7. NO output and cell viability of activated RAW 264.7 cells treated with FR180204. Cells were co-treated with 1 μg/mL LPS and FR180204 (ERK1/2 inhibitor) from 0 to 20 μM, then assayed for **(A)** NO release and **(B)** cell viability. FR180204 alone at 20 μM. Statistical significance was determined by one-way ANOVA with Tukey's post-test. *** = $P < 0.001$ versus LPS (0 μM inhibitor + LPS).

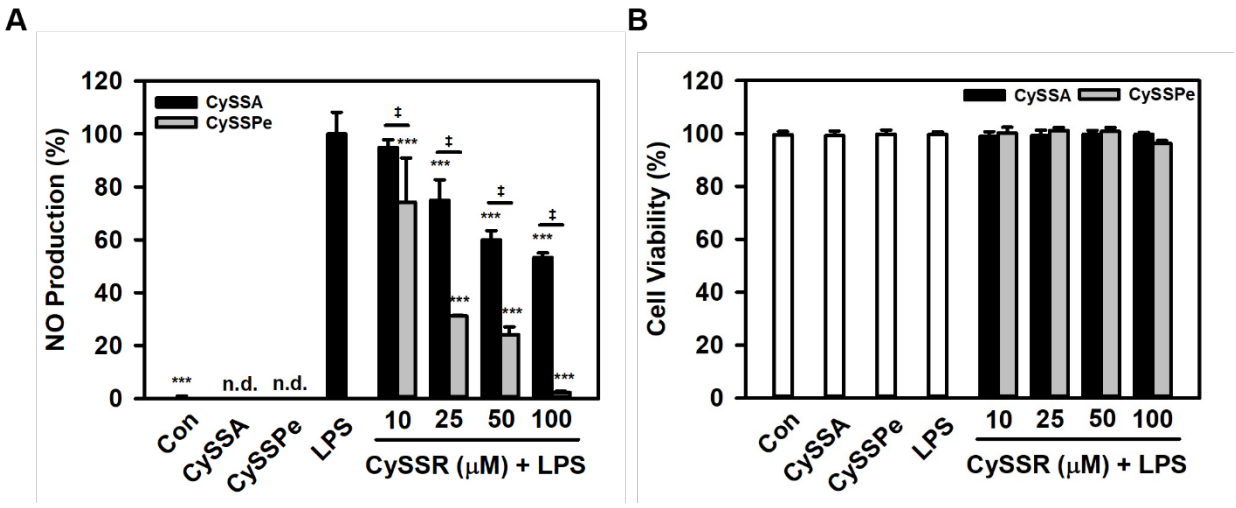

Figure 4.8. NO output and cell viability of activated RAW 264.7 cells treated with CySSR. Cells were co-treated with 1 μg/mL LPS and CySSA or CySSPe from 0 to 100 μM, then assayed for **(A)** NO release and **(B)** cell viability. Statistical significance was determined by one-way ANOVA with Tukey's post-test. *** = $P < 0.001$ versus LPS. Bars bearing ‡ = $P < 0.001$, n.d. = not detectable.

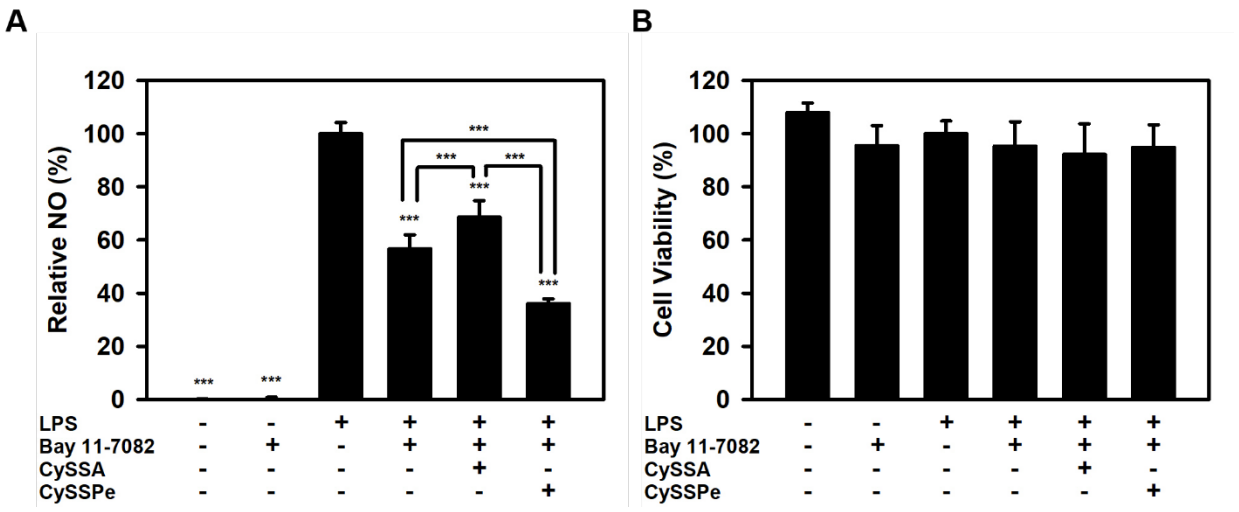

Figure 4.9. NO output and cell viability of activated RAW 264.7 cells co-treated with Bay 11-7082 and CySSR. Cells were activated with LPS, treated with 5 μM Bay 11-7082 and vehicle, CySSA (100 μM) or CySSPe (25 μM), then assayed for **(A)** NO release and **(B)** cell viability. Statistical significance was determined by one-way ANOVA with Tukey's post-test. *** = $P < 0.001$ versus LPS.

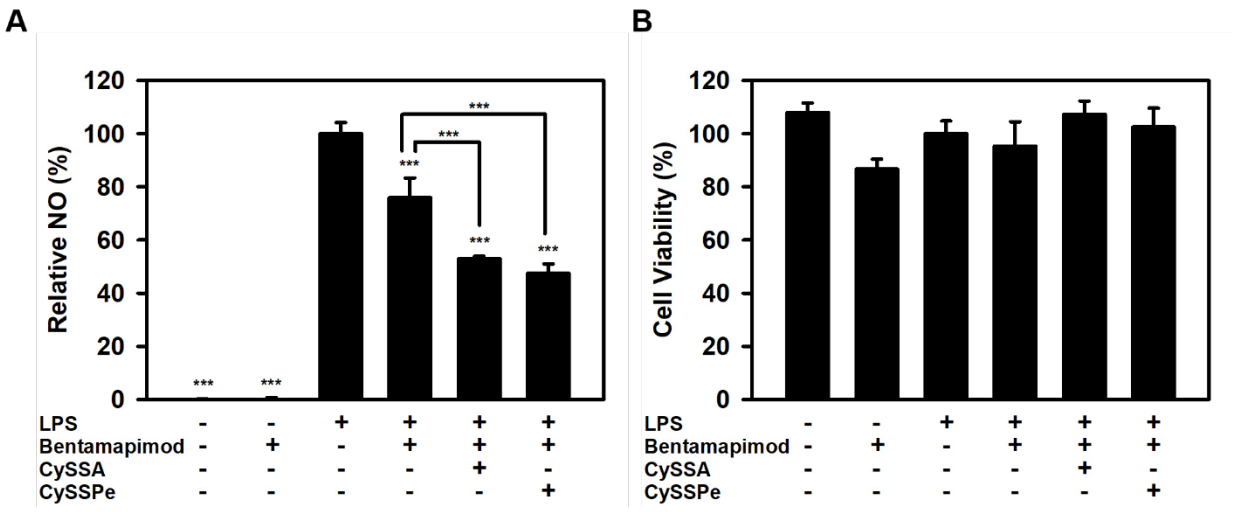

Figure 4.10. NO output and cell viability of activated RAW 264.7 cells treated with bentamapimod and CySSR. Cells were activated with LPS, treated with 5 μM bentamapimod and vehicle, CySSA (100 μM) or CySSPe (25 μM), then assayed for **(A)** NO release and **(B)** cell viability. Statistical significance was determined by one-way ANOVA with Tukey's post-test. *** = $P < 0.001$ versus LPS.

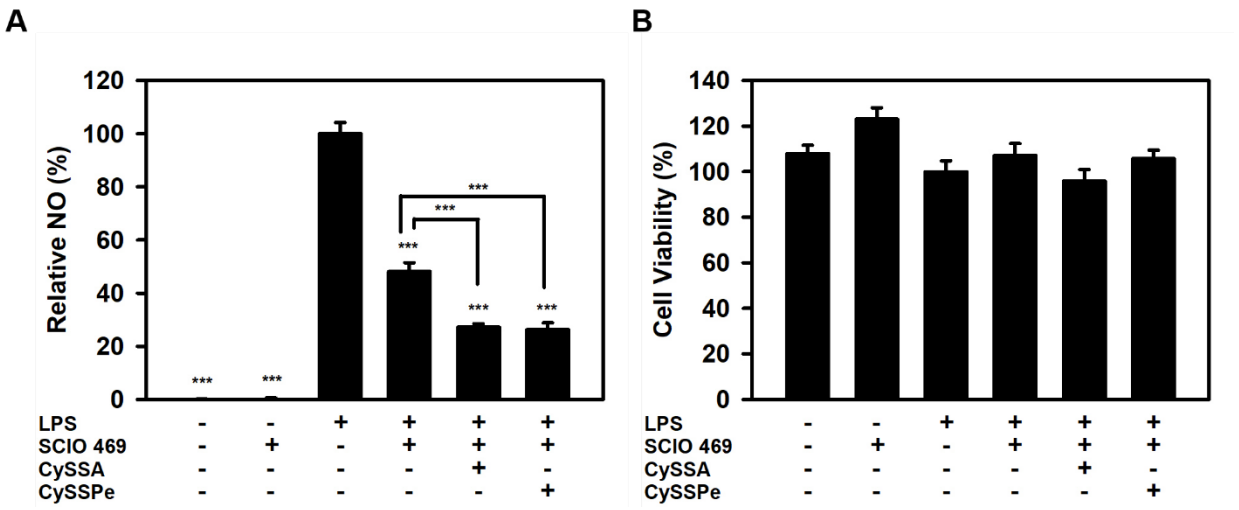

Figure 4.11. NO output and cell viability of activated RAW 264.7 cells treated with SCIO 469 and CySSR. Cells were activated with LPS, treated with 5 μM SCIO 469 and vehicle, CySSA (100 μM) or CySSPe (25 μM), then assayed for **(A)** NO release and **(B)** cell viability. Statistical significance was determined by one-way ANOVA with Tukey's post-test. *** = $P < 0.001$ versus LPS.

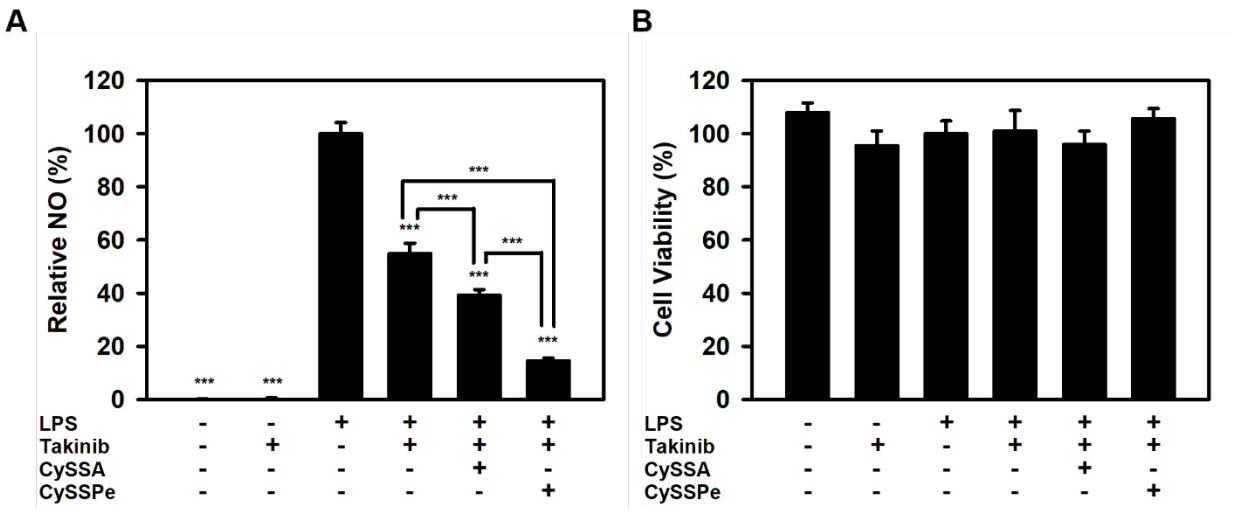

Figure 4.12. NO output and cell viability of activated RAW 264.7 cells treated with takinib and CySSR. Cells were activated with LPS, treated with 2.5 μM takinib and vehicle, CySSA (100 μM) or CySSPe (25 μM), then assayed for **(A)** NO release and **(B)** cell viability. Statistical significance was determined by one-way ANOVA with Tukey's post-test. *** = $P < 0.001$ versus LPS.

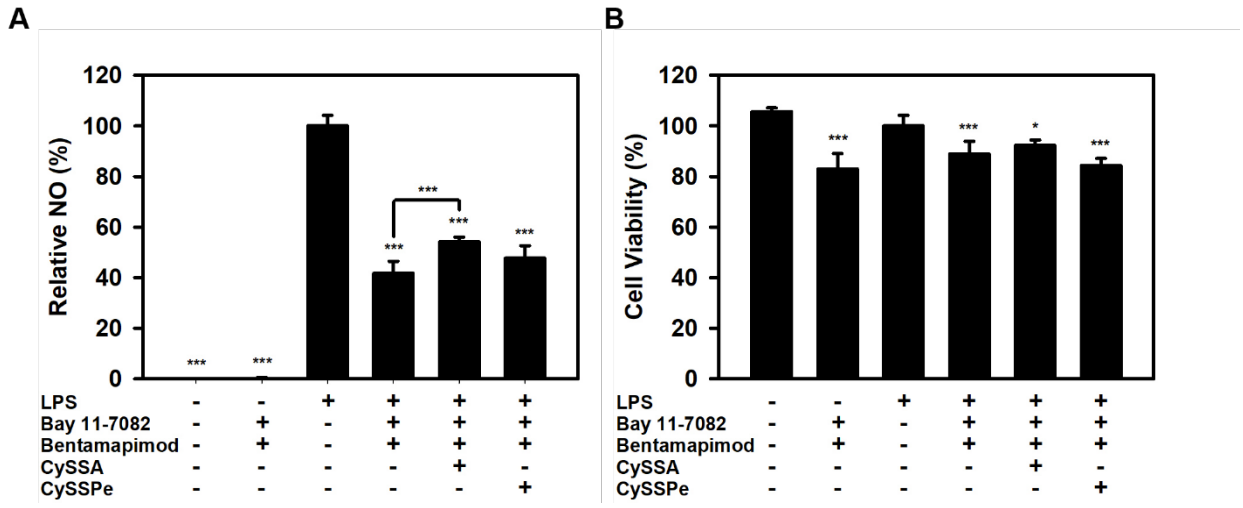

Figure 4.13. NO output and cell viability of activated RAW 264.7 cells co-treated with Bay 11-7082, bentamapimod and CySSR. Cells were activated with LPS, cotreated with 5 μM Bay 11-7082 and 5 μM bentamapimod with vehicle, CySSA (100 μM) or CySSPe (25 μM), then assayed for **(A)** NO release and **(B)** cell viability. Statistical significance was determined by one-way ANOVA with Tukey's post-test. * = $P < 0.05$ and *** = $P < 0.001$ versus LPS.

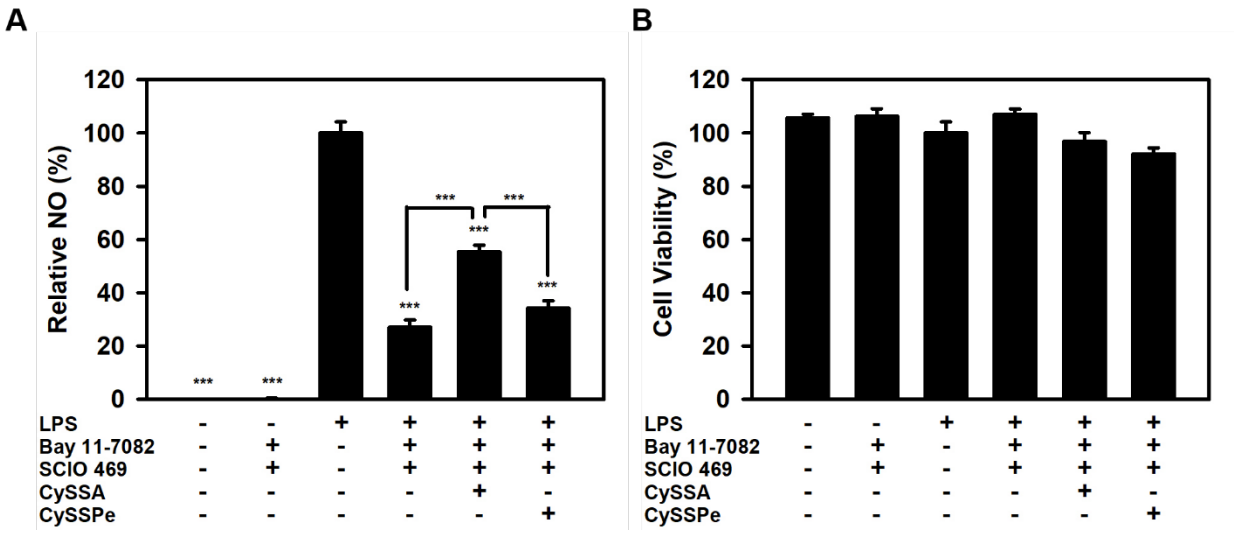

Figure 4.14. NO output and cell viability of activated RAW 264.7 cells co-treated with Bay 11-7082, SCIO 469 and CySSR. Cells were activated with LPS, cotreated with 5 μM Bay 11-7082 and 5 μM SCIO 469 with vehicle, CySSA (100 μM) or CySSPe (25 μM), then assayed for **(A)** NO release and **(B)** cell viability. Statistical significance was determined by one-way ANOVA with Tukey's post-test. *** = $P < 0.001$ versus LPS.

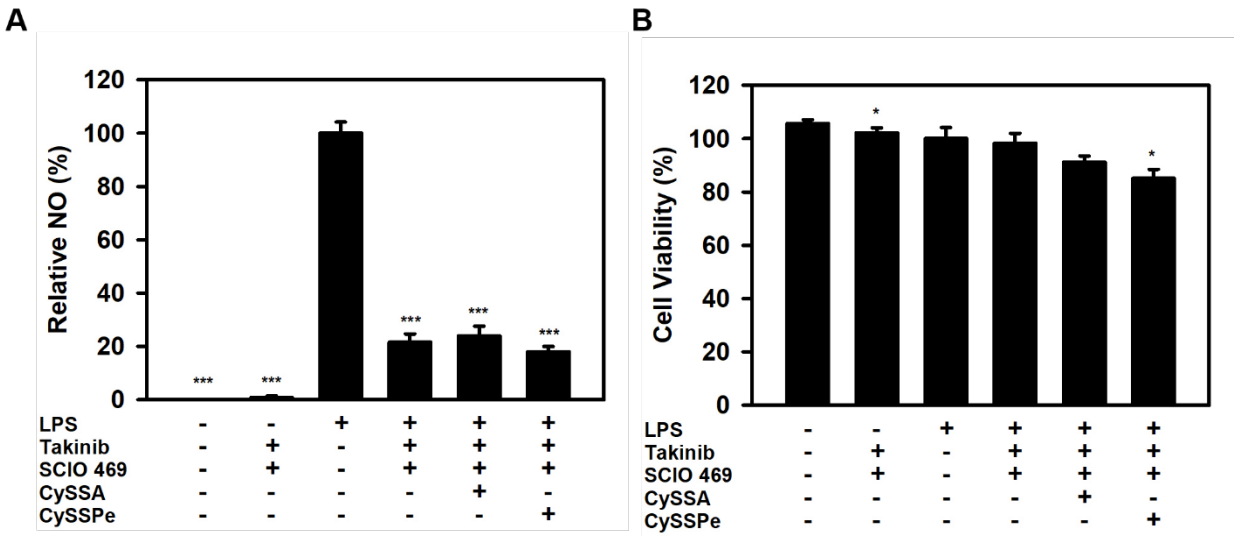

Figure 4.15. NO output and cell viability of activated RAW 264.7 cells co-treated with takinib, SCIO 469 and CySSR. Cells were activated with LPS, cotreated with 2.5 μM takinib and 5 μM SCIO 469 with vehicle, CySSA (100 μM) or CySSPe (25 μM), then assayed for **(A)** NO release and **(B)** cell viability. Statistical significance was determined by one-way ANOVA with Tukey's post-test. * = $P < 0.05$ and *** = $P < 0.001$ versus LPS.

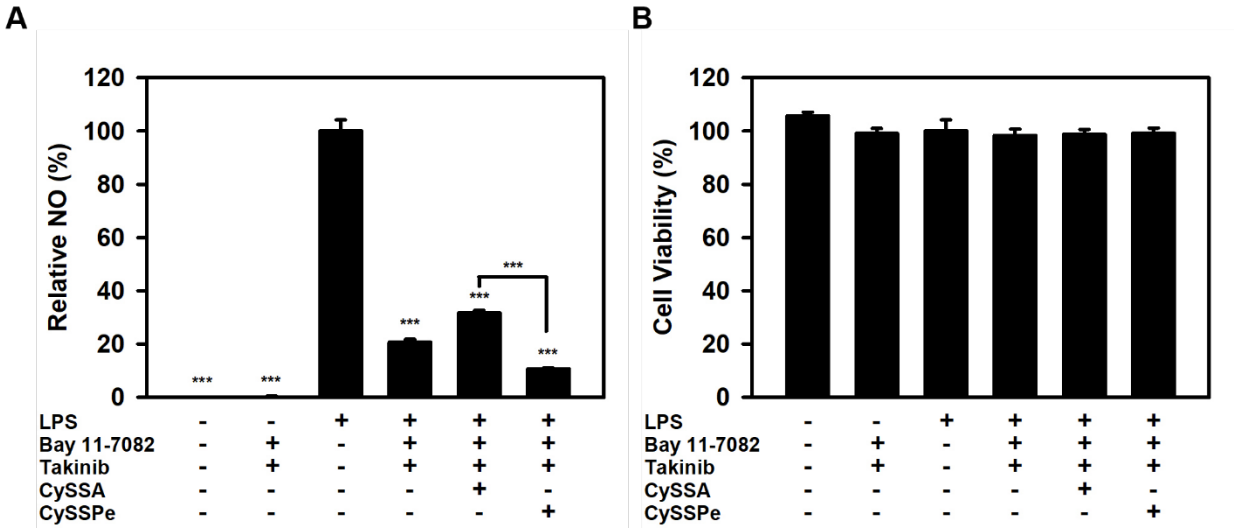

Figure 4.16. NO output and cell viability of activated RAW 264.7 cells co-treated with Bay 11-7082, takinib and CySSR. Cells were activated with LPS, cotreated with 5 μM Bay 11-7082 and 2.5 μM takinib with vehicle, CySSA (100 μM) or CySSPe (25 μM), then assayed for **(A)** NO release and **(B)** cell viability. Statistical significance was determined by one-way ANOVA with Tukey's post-test. *** = $P < 0.001$ versus LPS.

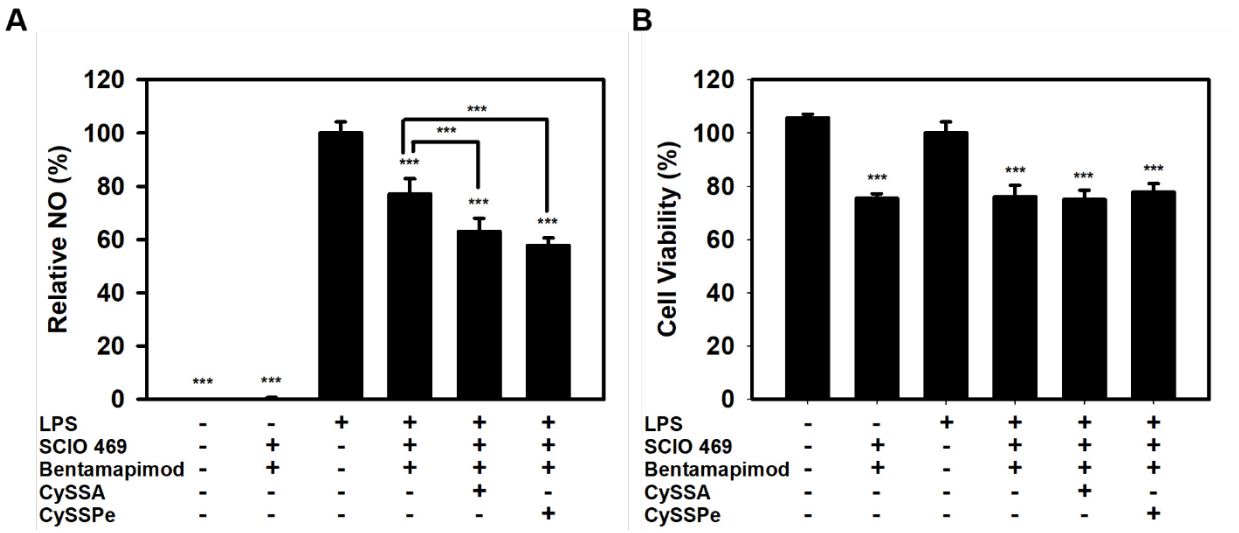

Figure 4.17. NO output and cell viability of activated RAW 264.7 cells co-treated with SCIO 469, bentamapimod and CySSR. Cells were activated with LPS, cotreated with 5 μM SCIO 469 and 5 μM bentamapimod with vehicle, CySSA (100 μM) or CySSPe (25 μM), then assayed for **(A)** NO release and **(B)** cell viability. Statistical significance was determined by one-way ANOVA with Tukey's post-test. *** = $P < 0.001$ versus LPS.

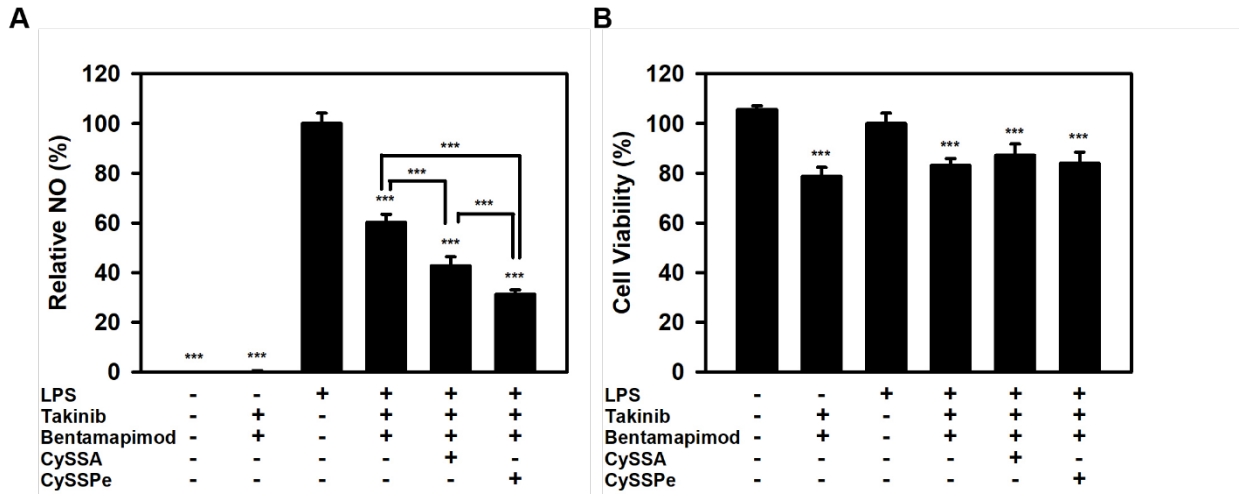

Figure 4.18. NO output and cell viability of activated RAW 264.7 cells co-treated with takinib, bentamapimod and CySSR. Cells were activated with LPS, cotreated with 2.5 μM takinib and 5 μM bentamapimod with vehicle, CySSA (100 μM) or CySSPe (25 μM), then assayed for **(A)** NO release and **(B)** cell viability. Statistical significance was determined by one-way ANOVA with Tukey's post-test. *** = $P < 0.001$ versus LPS.

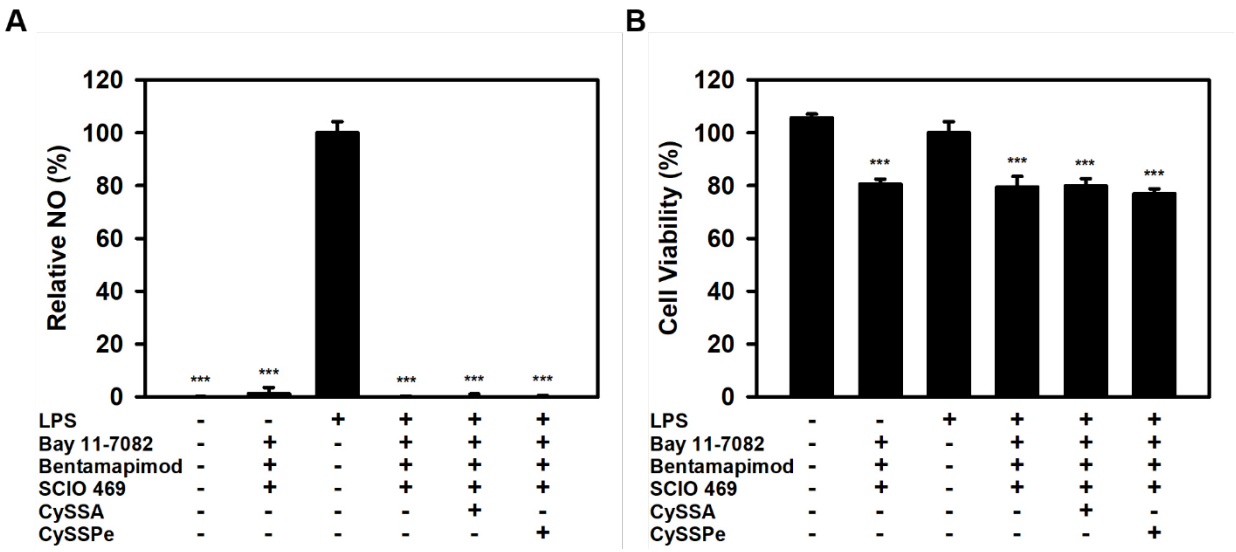

Figure 4.19. NO output and cell viability of activated RAW 264.7 cells co-treated with Bay 11-7082, bentamapimod, SCIO 469 and CySSR. Cells were activated with LPS and cotreated with 5 μM Bay 11-7082, 5 μM bentamapimod, and 5 μM SCIO 469 with vehicle, CySSA (100 μM) or CySSPe (25 μM), then assayed for **(A)** NO release and **(B)** cell viability. Statistical significance was determined by one-way ANOVA with Tukey's post-test. *** = $P < 0.001$ versus LPS.

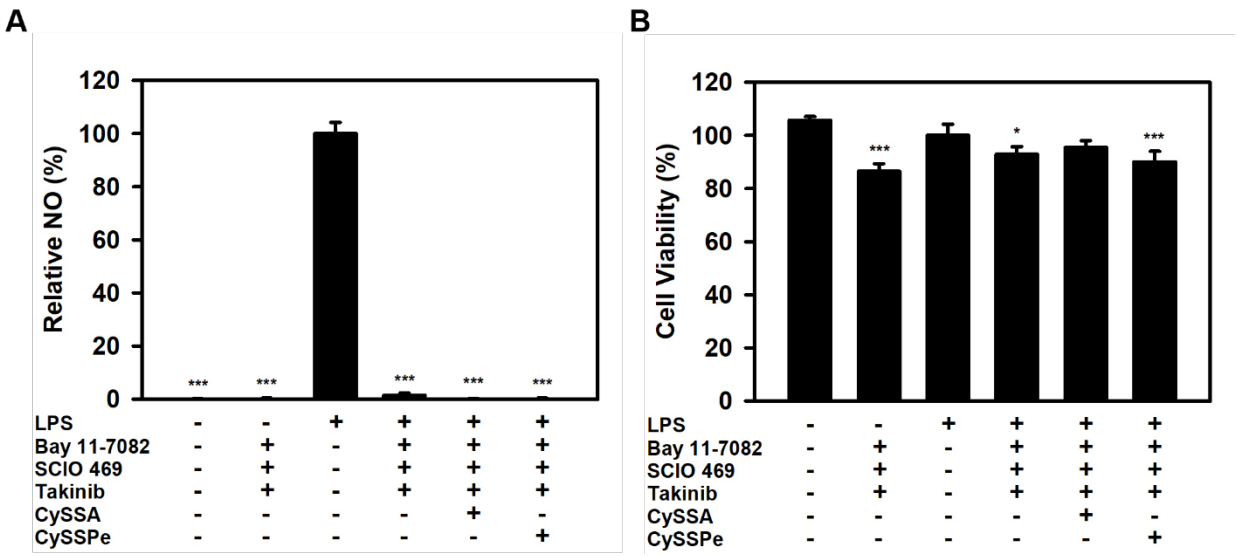

Figure 4.20. NO output and cell viability of activated RAW 264.7 cells co-treated with Bay 11-7082, SCIO 469, takinib and CySSR. Cells were activated with LPS and cotreated with 5 μM Bay 11-7082, 5 μM SCIO 469, and 2.5 μM takinib with vehicle, CySSA (100 μM) or CySSPe (25 μM), then assayed for **(A)** NO release and **(B)** cell viability. Statistical significance was determined by one-way ANOVA with Tukey's post-test. * = $P < 0.05$ and *** = $P < 0.001$ versus LPS.

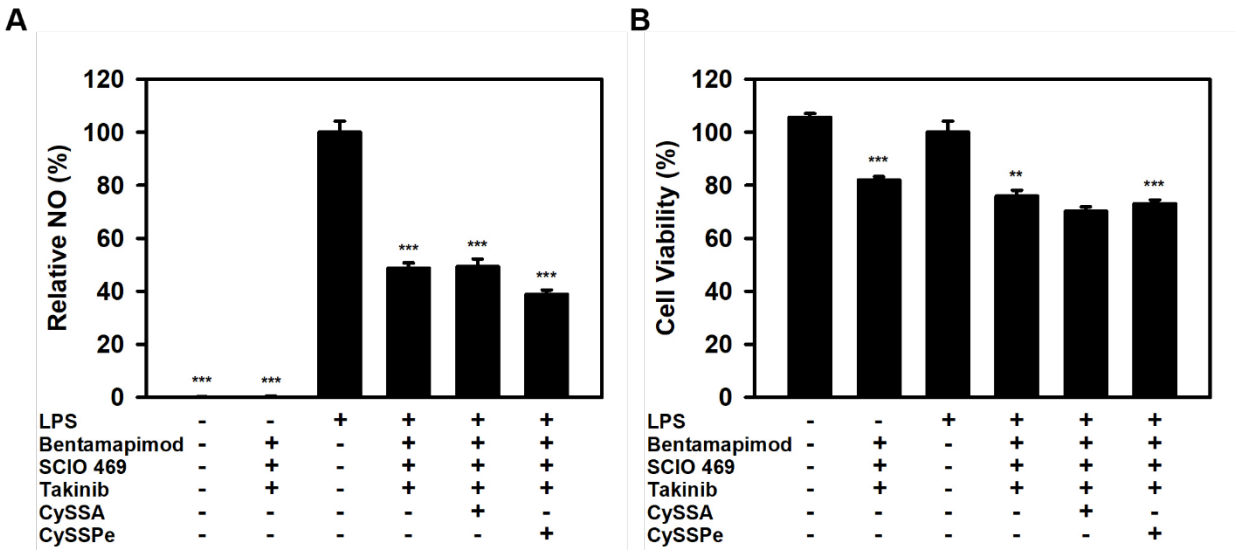

Figure 4.21. NO output and cell viability of activated RAW 264.7 cells co-treated with bentamapimod, SCIO 469, takinib and CySSR. Cells were activated with LPS and cotreated with 5 μM bentamapimod, 5 μM SCIO 469, and 2.5 μM takinib with vehicle, CySSA (100 μM) or CySSPe (25 μM), then assayed for **(A)** NO release and **(B)** cell viability. Statistical significance was determined by one-way ANOVA with Tukey's post-test. ** = $P < 0.01$ and *** = $P < 0.001$ versus LPS.

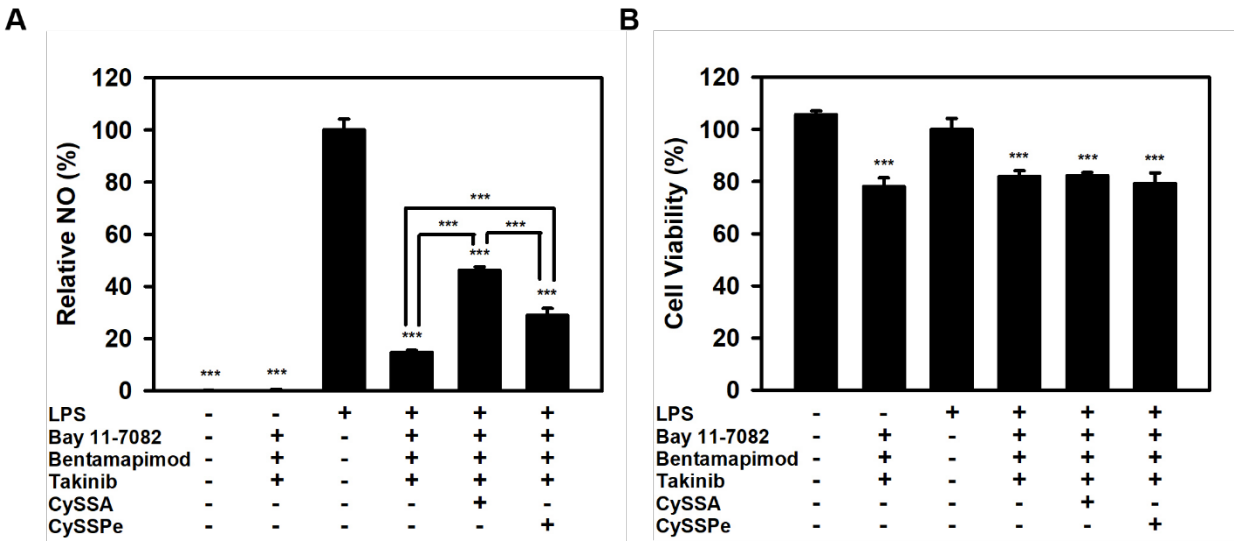

Figure 4.22. NO output and cell viability of activated RAW 264.7 cells co-treated with Bay 11-7082, bentamapimod, takinib and CySSR. Cells were activated with LPS and cotreated with 5 μM Bay 11-7082, 5 μM bentamapimod, and 2.5 μM takinib with vehicle, CySSA (100 μM) or CySSPe (25 μM), then assayed for **(A)** NO release and **(B)** cell viability. Statistical significance was determined by one-way ANOVA with Tukey's post-test. *** = $P < 0.001$ versus LPS.

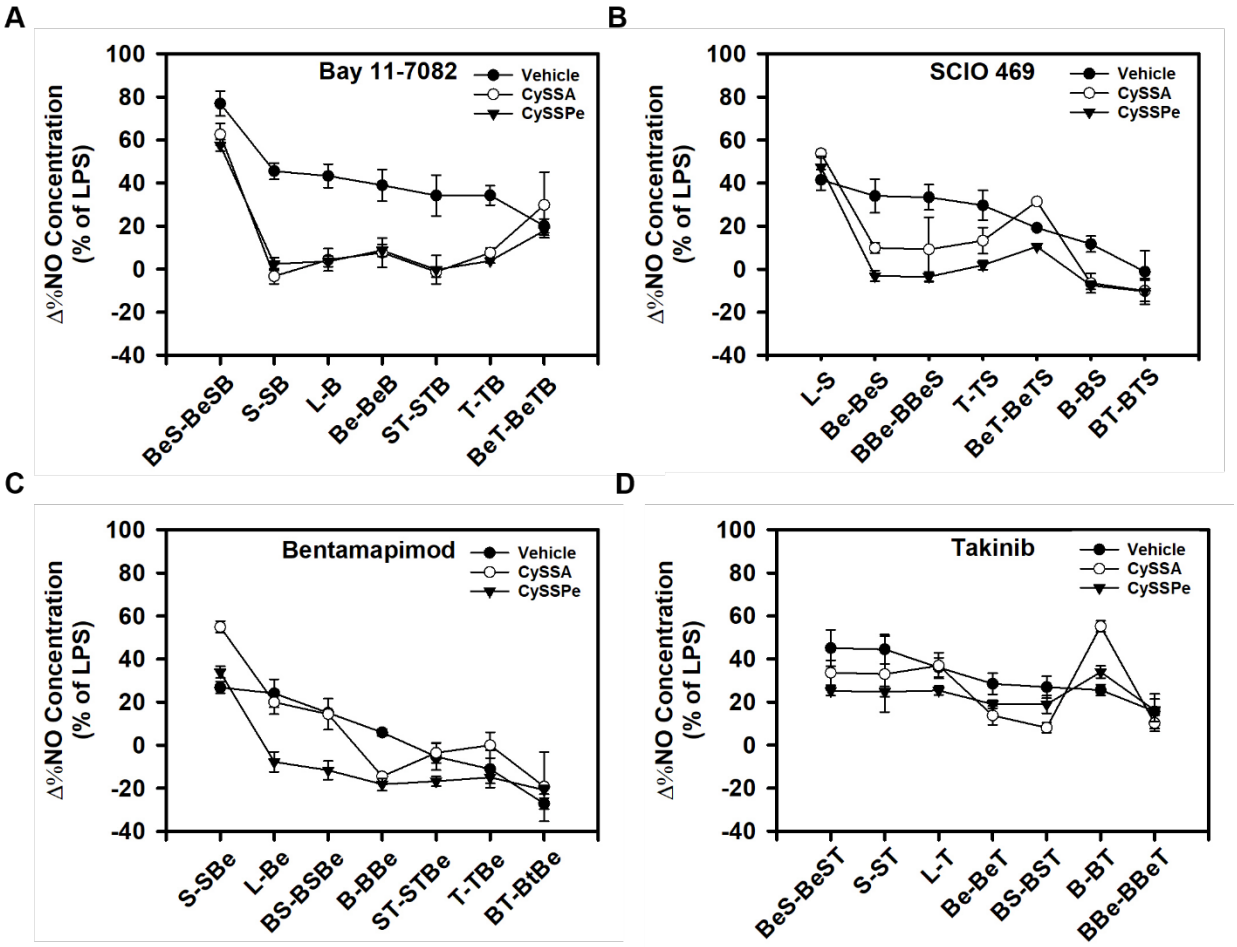

Figure 4.23. Plotted Δ%NO between the absence and presence of chemical inhibitors. **(A) Bay 11-7082**, **(B) SCIO 469**, **(C) bentampaimod**, and **(D) takinib** for all inhibitor permutations with vehicle, CySSA, or CySSPe. Abbreviated x-axis is labeled for the NO output of the combinations used in each calculation. L = LPS only, T = takinib (TAK1 inhibitor), B = Bay-11-7082 (IKKα/β inhibitor), Be = bentamapimod (JNK inhibitor), and S = SCIO 469 (p38 inhibitor).

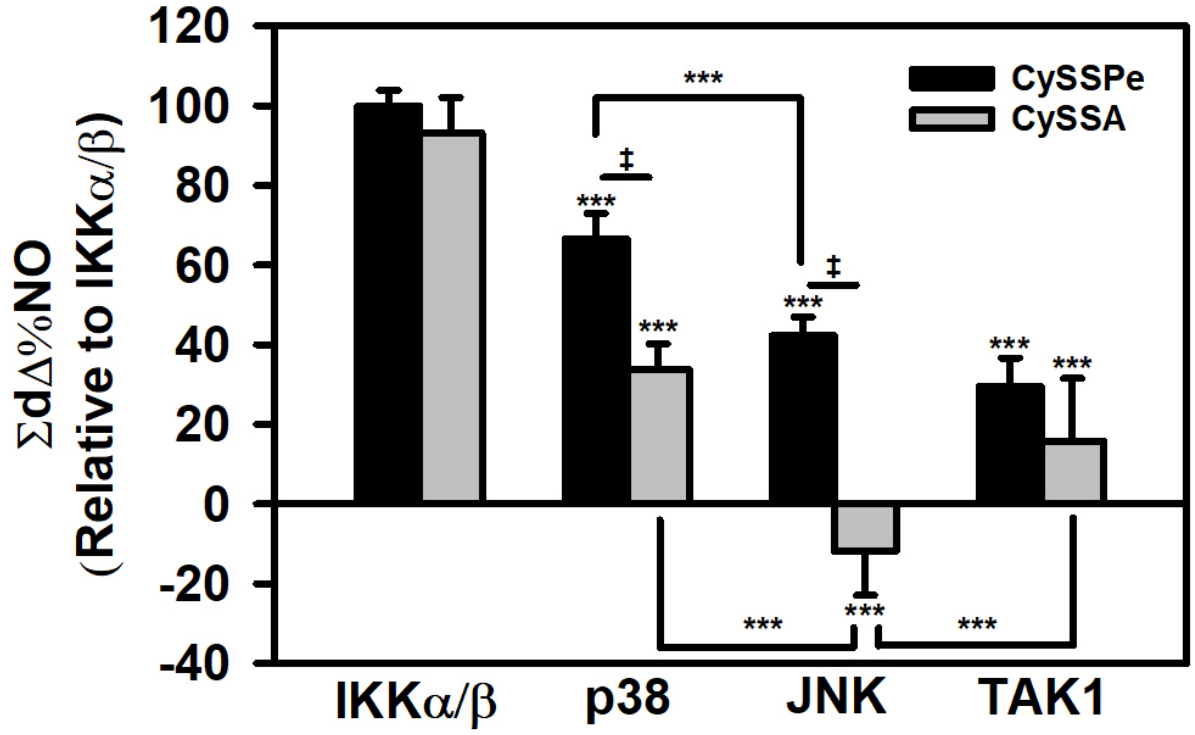

Figure 4.24. Relative total Δ%NO summed for each kinase pathways affected by CySSR. Summed outputs were set relative to IKKα/β for CySSPe. Statistical significance was determined by one-way ANOVA with Tukey's post-test. *** = $P < 0.001$ versus IKKα/β for CySSPe. Bars bearing ‡ = $P < 0.001$.

4.6 References

1. Medzhitov, R. Origin and Physiological Roles of Inflammation. *Nature* **2008**, *454*, 428-435.

2. Karin, M., Clevers, H. Reparative Inflammation Takes Charge of Tissue Repair. *Nature* **2016**, *529*, 307-315.

3. Muralidharan, S., Mandrekar, P. Cellular Stress Response and Innate Immune Signaling: Integrating Pathways in Host Defense and Inflammation. *J. Leukoc. Biol.* **2013**, *94*, 1167-1184.

4. Schett, G., Neurath, M.F. Resolution of Chronic Inflammatory Disease: Universal and Tissue-Specific Concepts. *Nat. Commun.* **2018**, *9*, 1-8.

5. Grivennikov, S.I., Greten, F.R., Karin, M. Immunity, Inflammation, and Cancer. *Cell* **2010**, *140*, 883-899.

6. Libby, P. Inflammation in Atherosclerosis. *Arterioscler. Thromb. Vasc. Biol.* **2012**, *32*, 2045-2051.

7. Ouchi, N., Parker, J.L., Lugus, J.J., Walsh, K. Adipokines in Inflammation and Metabolic Disease. *Nat. Rev. Immunol.* **2011**, *11*, 85-97.

8. Glass, C.K., Saijo, K., Winner, B., Marchetto, M.C., Gage, F.H. Mechanisms Underlying Inflammation in Neurodegeneration. *Cell* **2010**, *140*, 918-934.

9. Maury, E., Brichard, S.M. Adipokine Dysregulation, Adipose Tissue Inflammation and Metabolic Syndrome. *Mol. Cell. Endocrinol.* **2010**, *314*, 1-16.

10. Kawai, T., Akira, S. The Role of Pattern-Recognition Receptors in Innate Immunity: Update on Toll-Like Receptors. *Nat. Immunol.* **2010**, *11*, 373-384.

11. Lin, S.-C., Lo, Y.-C., Wu, H. Helical Assembly in the MyD88-IRAK4-IRAK2 Complex in TLR/IL-1R Signalling. *Nature* **2010**, *465*, 885-890.

12. Ajibade, A.A., Wang, H.Y., Wang, R.-F. Cell Type-Specific Function of TAK1 in Innate Immune Signaling. *Trends Immunol.* **2013**, *34*, 307-316.

13. Chen, Z.J. Ubiquitination in Signaling to and Activation of IKK. *Immunol Rev.* **2012**, *246*, 95-106.

14. Ninomiya-Tsuji, J., Kishimoto, K., Hiyama, A., Inoue, J.-I., Cao, Z., Matsumoto, K. The Kinase TAK1 Can Activate the NIK-Iκb as well as the MAP Kinase Cascade in the IL-1 Signalling Pathway. *Nature* **1999**, *398*, 252-256.

15. Morrison, D.K. MAP Kinase Pathways. *CSH Perspect. Biol.* **2012**, *4*, 1-5.

16. Bardell, L. Mechanisms of MAPK Signalling Specificity. *Biochem. Soc. Trans.* **2006**, *34*, 837-841.

17. Johnson, G.L., Lapadat, R. Mitogen-Activated Protein Kinase Pathways Mediated by ERK, JNK, and P38 Protein Kinases. *Science* **2002**, *298*, 1911-1912.

18. Sabio, G., Davis, R.J. TNF and MAP Kinase Signalling Pathways. *Semin. Immunol.* **2014**, *26*, 237-245.

19. Oeckinghaus, A., Hayden, M.S., Ghosh, S. Crosstalk in NF-κB Signaling Pathways. *Nat. Immunol.* **2011**, *12*, 695-708.

20. Kumar, S., Boehm, J., Lee, J.C. p38 MAP Kinases: Key Signalling Molecules as Therapeutic Targets for Inflammatory Diseases. *Nat. Rev. Drug Discov.* **2003**, *2*, 717-726.

21. Cuenda, A., Rousseau, S. p38 MAP-Kinases Pathway Regulation, Function and Role in Human Diseases. *Biochim. Biophys. Acta Mol. Cell Res.* **2007**, *1773*, 1358-1375.

22. Kim, E.K., Choi, E.-J. Compromised MAPK Signaling in Human Diseases: An Update. *Arch. Toxicol.* **2015**, *89*, 867-882.

23. Park, H.Y., Kim, N.D., Kim, G.-Y., Hwang, H.J., Kim, B.-W., Kim, W.J., Choi, Y.H. Inhibitory Effects of Diallyl Disulfide on the Production of Inflammatory Mediators and Cytokines in Lipopolysaccharide-Activated BV2 Microglia. *Toxicol. App. Pharmacol.* **2012**, *262*, 177-184.

24. Quintero-Fabián, S., Ortuño-Sahagún, D., Vázquez-Carrera, M., López-Roa, R.I. Alliin, a Garlic (*Allium sativum*) Compound, Prevents LPS-Induced Inflammation in 3T3-L1 Adipocytes. *Mediators Inflamm.* **2013**, *2013*, 1-11.

25. Xiao, J., Ching, Y.P, Liong, E.C., Nanji, A.A., Fung, M.L., Tipoe, G.L. Garlic-Derived *S*-Allylmercaptocysteine is a Hepato-Protective Agent in Non-Alcoholic Fatty Liver Disease In Vivo Animal Model. *Eur. J. Nutr.* **2013**, *52*, 179-191.

26. Powolny, A.A., Singh, S.V. Multitargeted Prevention and Therapy of Cancer by Diallyl Trisulfide and Related *Allium* Vegetable-Derived Organosulfur Compounds. *Canc. Lett.* **2008**, *269*, 305-314.

27. Blekkenhorst, L.C., Bondonno, C.P., Lewis, J.R., Devine, A., Zhu, K., Lim, W.H., Woodman, R.J., Beilin, L.J., Prince, R.L., Hodgson, J.M. Cruciferous and Allium Vegetable Intakes are Inversely Associated with 15-Year Atherosclerotic Vascular Disease Deaths in Older Adult Women. *J. Am. Heart. Assoc.* **2017**, *6*, 1-15.

28. Varshney, R., Budoff, M.J. Garlic and Heart Disease. *J. Nutri*. **2016**, *146*, 416S-421S.

29. Hosseini, A., Hosseinzadeh, H. A Review on the Effects of *Allium Sativum* (Garlic) in Metabolic Syndrome. *J. Endocrinol. Invest.* **2015**, *38*, 1147-1157.

30. Yang, C., Li, L., Yang, L., Lǔ, H., Wang, S., Sun, G. Anti-Obesity and Hypolipidemic Effects of Garlic Oil and Onion Oil in Rats Fed a High-Fat Diet. *Nutr. Metab.* **2018**, *15*, 1-8.

31. Miron, T., Rabinkov, A., Mirelman, D., Wilchek, M., Weiner, L. The Mode of Action of Allicin: Its Ready Permeability through Phospholipid Membranes May Contribute to Its Biological Activity. *Biochim. Biophys. Acta Biomembr.* **2000**, *1463*, 20-30.

32. Rabinkov, A., Miron, T., Mirelman, D., Wilchek, M., Glozman, S., Yavin, E., Weiner, L. *S*-allylmercaptoglutathione: The Reaction Product of Allicin with Glutathione Possesses SH-Modifying and Antioxidant Properties. *BBA-Mol. Cell Res.* **2000**, *1499*, 144-153.

33. Zhang, G., Parkin, K.L. A Tissue Homogenate Method to Prepare Gram-Scale *Allium* Thiosulfinates and Their Disulfide Conjugates with Cysteine and Glutathione. *J. Agric. Food Chem.* **2013**, *61*, 3030-3038.

34. Zhang, G., Parkin, K.L. *S*-Alk(en)ylmercaptocysteine: Chemical Synthesis, Biological Activities, and Redox-Related Mechanism. *J. Agric. Food Chem.* **2013**, *61*, 3030-3038.

35. Tocmo, R., Parkin, K. *S*-Alk(en)ylmercaptocysteine Suppresses LPS-Induced Pro-Inflammatory Responses in Murine Macrophages through Inhibition of NF-κB Pathway and Modulation of Thiol Redox Status. *Free Rad. Biol. Med.* **2018**, *129*, 548-558.

36. Xiao, J., Liong, E.C., Ling, M.-T., Ching, Y.-P., Fung, M.-L., Tipoe, G.L. *S*-Allylmercaptocysteine Reduces Carbon Tetrachloride-Induced Hepatic Oxidative Stress and Necroinflammation via Nuclear Factor Kappa B-Dependent Pathways in Mice. *Eur. J. Nutr.* **2012**, *51*, 323-333.

37. Pinto, J.T., Krasnikov, B.F., Cooper, A.J.L. Redox-Sensitive Proteins are Potential Targets of Garlic-Derived Mercaptocysteine Derivatives. *J. Nutr.* **2006**, *136*, 835S-841S.

38. Tocmo, R., Parkin, K. *S*-1-propenylmercaptocysteine Protects Murine Hepatocytes Against Oxidative Stress via Persulfidation of Keap1 and Activation of Nrf2. *Free Rad. Biol. Med.* **2019**, *143*, 164-175.

39. Kilty, I., Jones, L.H. TAK1 Selective Inhibition: State of the Art and Future Opportunities. *Future Med. Chem.* **2015**, *7*, 23-33.

40. Ida, T., Sawa, T., Ihara, H., Tsuchiya, Y., Watanabe, Y., Kumagai, Y., Suematsu, M., Motohashi, H., Fujii, S., Matsunaga, T., Yamamoto, M., Ono, K. Devarie-Baez, N.O., Xian, M., Fukuto, J.M., Akaike, T. Reactive Cysteine Persulfides and S-Polythiolation

Regulate Oxidative Stress and Redox Signaling. *Proc. Natl. Acad. Sci. USA* **2014**, *111*, 7606-7611.

41. Nishida, M., Sawa, T., Kitajima, N., Ono, K., Inoue, H., Ihara, H., Motohashi, H., Yamamoto, M., Suematsu, M., Kurose, H., van der Vliet, A., Freeman, B.A., Shibata, T., Uchida, K., Kumagai, Y., Akaike, T. Hydrogen Sulfide Anion Regulates Redox Signaling Via Electrophile Sulfhydration. *Nat. Chem. Biol.* **2012**, *8*, 714-724.

42. Guo, X., Ma, N., Wang, J., Song, J., Bu, X., Cheng, Y., Sun, K., Xiong, H., Jiang, G., Zhang, B., Wu, M., Wei, L. Increased p38-MAPK is Responsible for Chemotherapy Resistance in Human Gastric Cancer Cells. *BMC Cancer* **2008**, *8*, 1-9.

43. Qu, J.-L., Qu, X.-J., Zhao, M.-F., Teng, Y.-E., Zhang, Y., Hou, K.-Z., Jiang, Y.-H., Yang, X.-H., Liu, Y.-P. Gastric Cancer Exosomes Promote Tumour Cell Proliferation Through PI3K/Akt and MAPK/ERK Activation. *Digest. Liver Dis.* **2009**, *41*, 875-880.

44. Bost, F., Aouadi, M., Binétruy, B. The Role of MAPKs in Adipocyte Differentiation and Obesity. *Biochimie* **2005**, *87*, 51-56.

45. Bost, F., Aouadi, M., Caron, L., Even, P., Belmonte, N., Prot, M., Dani, C., Hofman, P., Pagès, Pouysségur, J., Marchand-Brustel, Y.L., Binétruy, B. The Extracellular Signal-Regulated Kinase Isoform ERK1 is Specifically Required for In Vitro and In Vivo Adipogenesis. *Diabetes* **2005**, *54*, 402-411.

46. Hirosumi, J., Tuncman, G., Chang, L., Görgün, C.Z., Uysal, K.T., Maeda, K., Karin, M., Hotamisligil, G.S. A Central Role for JNK in Obesity and Insulin Resistance. *Nature* **2002**, *420*, 333-336.

47. Aouadi, M., Jager, J., Laurent, K., Gonzalez, T., Cormont, M., Binétruy, Marchand-Brustel, Y.L., Tanti, J.-F., Bost, F. p38MAP Kinase Activity is Required for Human Primary Adipocyte Differentiation. *FEBS Lett.* **2007**, *581*, 5591-5596.

48. Strickson, S., Campbell, D.G., Emmerich, C.H., Knebel, A., Plater, L., Ritorto, M.S., Shpiro, N., Cohen, P. The Anti-Inflammatory Drug BAY 11-7082 Suppresses the MyD88-Dependent Signalling Network by Targeting the Ubiquitin System. *Biochem. J.* **2013**, *451*, 427-437.

Chapter 5

Attenuation of Inflammation by *S*-1-Propenylmercaptocysteine in a Mouse Model of Obesity

Bryan Le of the Parkin Lab at the University of Wisconsin, Madison contributed to the current work by obtaining food consumption and body weight data, collecting blood and liver samples, obtaining hepatic glutathione and cytokine data, and analyzing results. Dr. Jee-Hwan Oh of the van Pijkeren Lab at the University of Wisconsin, Madison contributed to the current work by collecting blood and liver samples and obtaining lipid, adipokine, liver enzyme, and LPS biomarker data from these samples. Laura Alexander of the van Pijkeren Lab at the University of Wisconsin, Madison contributed by assisting in obtaining food consumption and body weight data.

5.1 Abstract

The objective of this study was to evaluate the anti-obesity effects of onion-derived *S*-1-propenylmercaptocysteine (CySSPe) on a diet-induced mouse model of obesity. Mice were fed a high-fat/high-carbohydrate diet (HFHCD) over 8 weeks to induce obesity. One hundred μL CySSPe at 10 mM in 0.1 M PBS was administered daily via oral gavage while diets continued for an additional 8 weeks. CySSPe decreased HFHCD-induced elevation of liver triglycerides, attenuated elevated levels of pro-inflammatory cytokines TNF-α and IL-6 in plasma, and TNF-α, IL-6, and IL-1β in liver tissue, and restored total liver glutathione to the same level as the mice fed the regular diet. HFHCD increased liver, fat pad, and body weight, high-density lipoprotein (HDL) and very-low-density lipoprotein (VLDL) cholesterol, liver enzyme activity, and leptin levels, while decreasing adiponectin levels; CySSPe supplementation did not modulate these morphometric and serum biomarkers. Further work is necessary to understand the molecular mechanisms underlying the *in vivo* anti-inflammatory effects of CySSPe in obesity animal models.

5.2 Introduction

Obesity is a growing global epidemic that increases the risk of other chronic diseases, including cardiovascular disease, diabetes mellitus, and various cancers (1). Obesity is most commonly caused by excess energy consumption relative to energy expenditure, but may also include genetic, physiological, and environmental factors (2). The increased consumption of fruits and vegetables is inversely associated with weight gain and is a potential intervention for obesity (3,4). Many fruits and vegetables are water-rich, high-fiber, low-glycemic foods that help suppress appetite and displace high calorie foods in the diet (5). Fruits and vegetables also contain dietary phytochemicals, which include terpenoids, organosulfurs, phytosterols, and polyphenols, that suppress obesity-associated oxidative stress, inflammation, and lipid accumulation (6).

Obesity is initiated by the excess accumulation of triglycerides and fatty acids by fat storage depots and adipose tissues, which are primarily composed of adipocytes (7). Adipose tissues grow to accommodate high levels of lipids from alimentary sources by expanding in cell size through hypertrophic growth. Hypertrophic adipose tissue growth generates localized hypoxic conditions and subsequent cell death, initiating the release of pro-inflammatory adipokines and cytokines that leads to the recruitment of M1 macrophage cells (8,9). These macrophages, in turn, further produce pro-inflammatory cytokines and mediators that exacerbates the inflammatory and oxidative status of adipose tissues, increasing the risk of insulin resistance, type 2 diabetes mellitus, and metabolic syndrome (10).

Attenuation of lipogenesis and increased fatty acid oxidation are two metabolic pathways by which obesity-induced weight gain is inhibited. Several factors are involved in adipocyte lipogenesis, lipolysis, and cellular bioenergetics (11), which can be modulated by H_2S, a product

of dietary organosulfur metabolism (12). The peroxisome proliferators-activated receptors (PPAR) are a family of ligand-activated transcription factors involved in the regulation of metabolism and energy homeostasis in adipose tissues (13). These factors control the peroxisomal β-oxidation pathway of fatty acids by regulating acyl-CoA oxidase, serving as activators of fatty acid oxidation and fat burning (14). H_2S endogenously generated by cystathinione γ-lyase has been shown to increase PPARγ activity via sulfhydration of C139 in adipocytes (15). H_2S also stimulates mitochondrial bioenergetics by *S*-sulfhydration of ATP synthase (ATP5A1) at Cys244 and Cys294, thereby increasing the synthesis of ATP and supporting lipid metabolism (16). Additionally, H_2S reduces the accumulation of lipids in the liver of obese mice by reducing the expression of hepatic fatty acid synthase (FAS) (17).

Allium vegetables, which include onions, garlic, shallots, chives, and so forth, generate bioactive organosulfur compounds through an alliinase-dependent mechanism (18). Upon tissue maceration, alliinase is released and degrades endogenous cysteine sulfoxides to rapidly form thiosulfinates. These thiosulfinates are unstable and readily degrade to a plurality of sulfur-rich compounds, including disulfides, trisulfides, ajoene, vinyldithiins, and zwiebelanes (18-20). Thiosulfinates also conjugate to cysteine or cysteine-containing molecules, such as glutathione, to form *S*-alk(en)ylmercaptocysteines (CySSR) and analogues (21). Several of these *Allium* organosulfur compounds have demonstrated H_2S-releasing characterstics *in vitro*, including diallyl disulfide (DADS) (22), diallyl trisulfide (DATS) (23), and *S*-1-propenylmercaptocysteine (CySSPe) (24).

These *Allium* organosulfur compounds exhibit anti-obesity effects in vitro and in vivo. 1,2-Vinyldithiin, a garlic-derived organosulfur, was found to inhibit adipocyte differentiation, lipid accumulation, and inflammatory adipokine secretion in human preadipocyte cells (25).

DATS, another garlic-derived organosulfur compound, blocked differentiation of 3T3-L1 preadipocytes into adipocytes by activating ERK1/2 and downregulating adipogenic genes (26). In another study, garlic essential oil and its primary component, DADS, reduced biomarkers and pro-inflammatory cytokines associated with a nonalcoholic fatty liver disease (NAFLD) model induced with a high fat diet (HFD) in C57BL/6J mice (27). Fresh powdered garlic ameliorated HFD-induced weight gain and reduced fat-accumulating gene expression in C57BL/6 mice, possibly through its *S*-allyl cysteine sulfoxide content (28). Garlic extract reduced adipose tissue mass, serum obesity biomarkers, and mRNA expression levels of adipogenic genes in Sprague-Dawley rats on an HFD (29). DADS and DATS both suppressed symptoms of obesity in combination with green tea or Orlistat, respectively, in vivo (30,31). *S*-allylmercaptocysteine (CySSA), the cysteine conjugate of major garlic thiosulfinate allicin, was previously shown to downregulate the transcription of inflammatory mediators in an HFD-induced Sprague-Dawley rats NAFLD animal model (32). Garlic and onion oil were both found to reduce diet-induced weight gain, adipose tissue weight, and serum lipids (33). However, as illustrated by the previous articles, most investigations into the anti-obesity properties of *Allium* involve garlic or garlic-based compounds with comparatively few studies on specific compounds derived from onion.

Obesity is associated with metabolic dysregulation and chronic, low-grade inflammation triggered by the recruitment of macrophages to white adipose tissue through the secretion of inflammatory factors and adipokines (34). Dietary components that possess anti-inflammatory effects have been proposed as potential intervention for obesity (35). Structure-bioactivity studies on CySSR revealed the predominant onion conjugated derivative, CySSPe, and CySSA possessed more potent inhibitory effects against NO production than saturated analogues in LPS-activated macrophages (21,36). Another study showed both CySSPe and CySSA inhibited

upregulation of pro-inflammatory mediators nitric oxide (NO), inducible NO synthase (iNOS), TNF-α, IL-1β, and IL-6 by suppressing NF-κB signaling pathway in LPS-stimulated RAW cells, with CySSPe demonstrating more potent bioactivities compared to CySSA (37). CySSPe was also shown to exert cytoprotective effects against oxidative stress in Hepa1c1c7 hepatocytes through the activation of Nrf2 via an *S*-sulfhydration mechanism (24).

The aim of the present study was to evaluate the anti-obesity effects of onion-derived CySSPe in an HFHCD-induced murine model of obesity. Given the H_2S-releasing properties exhibited by CySSPe in previous work (24) and chapter 2, it was hypothesized that CySSPe could exhibit anti-obesity properties by reducing triglyceride levels, weight gain, and obesity-induced inflammation in obese mice through the release of H_2S *in vivo*. Determining if CySSPe possesses anti-obesity effects could support the design of *Allium* conjugate-based dietary interventions or functional foods targeted to reduce the risk of obesity.

5.3 Materials and Methods

5.3.1 Chemicals and Reagents

All chemicals were obtained from Sigma-Aldrich (Milwaukee, WI) unless otherwise noted. All solvents used for fraction collection or HPLC analysis were purchased from Thermo Fisher Scientific (Madison, WI) unless otherwise noted. Garlic and onion were purchased from a local retailer in Madison, WI. Glutathione assay kit was purchased from Cayman Chemical (Ann Arbor, MI). TNF-α, IL-1β, and IL-6 ELISA kits were purchased from Thermo Fisher Scientific. Leptin and adiponectin quantikine ELISA kits were purchased from R&D Systems (Minneapolis, MN). Aspartate transaminase (AST) and alanine transaminase (ALT) enzyme activity assay kits were purchased from Sigma-Aldrich (Milwaukee, WI). HDL and LDL/VLDL cholesterol assay

kits were purchased from Abcam (Cambridge, MA). Lipopolysaccharide (LPS) endotoxin chromogenic quantitative assay kits were purchased from Thermo Fisher Scientific.

5.3.2 Enzymatic Preparation of *S*-1-Propenylmercaptocysteine (CySSPe)

A modified version of a previously published CySSPe preparation was developed (21). Approximately 50 kg of yellow onions were heat treated in 2 kg batches in the microwave (700 W) for 7 – 8 min, left to cool, and juiced. The onion juice was placed in the refrigerator to further cool at 4 ºC. The cooled onion juice was homogenized with 2.5 kg peeled fresh garlic in batches of 100 g for 1 – 2 min and allowed to incubate for 45 minutes. The homogenized mixture was centrifuged at 15,000 x g for 10 to 15 min at room temperature. The supernatant was collected and combined, and the vegetable tissue pellet was discarded. The supernatant was extracted 5 – 8 times with 125 mL dichloromethane and the solvent-aqueous phase emulsions collected via separatory funnel. The emulsions were centrifuged at 10,000 x g for 5 min and the organic phases separated, collected, and combined. The organic phase was dried under a gentle N_2 stream and the residue was resuspended in water.

Cysteine hydrochloride monohydrate (1.0 g) was dissolved in 10 mL MeOH per 2 kg onion batch of residue. The methanolic cysteine solution was added to aqueous extract and allowed to stir for 30 min. The crude solution was diluted to 50 mL with HPLC-grade water and separated using a Reveleris® Prep purification system (Grace Co., Columbia, MD). Separation was conducted on a 25 cm x 21.2 mm, 5 µM Discovery® C18 column (Supelco, Bellefonte, PA) with isocratic elution using MeOH:H_2O (30:70) at a flow rate of 12 mL/min over 25 min. Peak resolution was monitored by UV (254 and 210 nm). Isolated fractions were combined and slowly evaporated under vacuum at 25 ºC to minimize thermal decomposition to give ~3 to 5 mg of purified CySSPe per 2 kg onion/100 g garlic batch. The isolated compound was analyzed by

HPLC **(Appendix A.2.)**. The purified CySSPe was immediately dissolved in Dulbecco's PBS (Sigma-Aldrich, St. Louis, MO) in 1.5 mL aliquots and stored at -20 ^{o}C until use.

5.3.3 Mice and Housing

Mice (C57BL/6J, male, 6 weeks old from The Jackson Laboratory, Bar Harbor, ME) were housed under controlled environmental conditions with a 12-h light-dark cycle at the University of Wisconsin-Madison Department of Animal Sciences. Mice were housed in caging (n=4 per cage) containing bedding and given unlimited access to rodent chow pellets (Teklad Rodent Diet, Cat. #8604, Envigo, Madison, WI) or specially formulated high-fat/high-carbohydrate pellets with ~47% kcal from fat and ~30% kcal from sucrose (Teklad Custom Diet, Cat. #TD.08811, Envigo, Madison, WI) and water. All experiments were reviewed and approved by the Institutional Animal Care and Use Committee at the University of Wisconsin-Madison.

A sham regular chow diet group (n=12) was fed a regular chow diet for the duration of the experiment. Obesity was induced in the sham high-fat/high carbohydrate "Western" diet (HFHCD) group (n=12) and the CySSPe treatment group (n=12) by providing unrestricted access to high-fat/high-carbohydrate pellets for 8 weeks. During the course of this phase, one mouse prematurely died from the treatment group, reducing this group to n=11. Following the induction of obesity, the sham regular chow diet group and the sham HFHCD group were orally gavaged using a ball-tipped 18-gauge feeding needle with 100 µL of 0.1 M phosphate-buffered saline (PBS) daily for 8 weeks. The CySSPe treatment group was orally gavaged with 100 µL of 10 mM CySSPe in PBS. This dose is equivalent to a 60 kg adult consuming 1 medium-sized onion (200 g) per day. The dose was calculated according to the method outlined by Reagan-Shaw et al. (38) and extrapolating the average potential molar equivalent of asymmetric methyl 1-propenyl thiosulfinates generated from 200 g of onion. Symmetrical di-1-propenyl

thiosulfinates rapidly convert to zwiebelanes and do not contribute 1-propenyl molar equivalents (20). Food intake and body weights of mice were recorded for the duration of the experiment. After 8 weeks, the mice were euthanized using CO_2 overdose according to protocols outlined by the Institutional Animal Care and Use Committee. Upon sacrifice, the liver was excised and weighed. A portion of the liver tissue was snap frozen in liquid nitrogen and stored at -80 ºC for later use. Fat pad tissue was also excised and weighed. All mouse experiments were performed in accordance with NIH Office of Laboratory Animal Welfare guidelines, the Animal Welfare Act, and United States federal law and were approved by the Application Review for Research Oversight at Wisconsin (ARROW) committee and overseen by the IACUC under protocol ID A006078-A02.

5.3.4 Lipid Triglyceride Measurements

Lipid triglyceride levels were measured according to previously reported procedures (39). One hundred to 300 mg of liver was pre-weighed and mixed with 350 µL ethanolic KOH (2 EtOH:1 30% aqueous KOH v/v). The mixture was saponified overnight at 55 ºC with occasional vortexing to completely digest the tissues. Six hundred fifty µL H_2O/EtOH (1:1 v/v) was added and the solution was centrifuged at 15,000 x g for 5 min. The supernatant was collected and diluted to 1.2 mL with H_2O/EtOH (1:1 v/v). Two hundred µL of the solution was transferred to a new centrifuge tube and 215 µL of 1 M aqueous $MgCl_2$ was vortexed with the solution. The solution was allowed to stand for 10 min at 4 ºC to precipitate free fatty acids. The cloudy mixture was microfuged for 5 min and the supernatant containing free glycerol was collected.

Triglyceride (GPO Trinder) Reagent A (Sigma-Aldrich, Milwaukee, WI) used for quantitative enzymatic determination of free glycerol was reconstituted to manufacturer's instructions. One mL of the reconstituted reagent A was added to centrifuge tubes. Thirty µL of

sample was added to each tube and shaken. Two hundred μL of each sample mixture was transferred to a 96-well plate and allowed to incubate at room temperature for 15 min. The absorbance of each sample was spectroscopically determined at 540 nm. Glycerol standards were measured to generate a standard curve under the same conditions outlined above.

5.3.5 Blood Collection and Adipokine ELISA

Blood (~100 μL) was collected from each mouse using heparin-coated capillary tubes (Thermo Fischer Scientific, Madison, WI) at the 0, 4, and 8-week time points via retro-orbital puncture. Plasma was isolated from the whole blood sample by centrifugation at 2,000 x g for 15 min at 4 ^{o}C, and the plasma fraction was stored at -20 ^{o}C until further use.

Adiponectin and leptin plasma levels were measured using commercially available ELISA kits. Plasma samples were diluted 4,000-fold for adiponectin analysis and 40-fold for leptin analysis. Each standard or sample (100 μL) was added to 96-well plates pre-coated with capture antibodies and incubated at room temperature for 2.5 h. The solution was discarded, rinsed 4 times with a washing buffer (10 mM phosphate buffer, pH 7.4, 150 mM NaCl, 0.05% Tween-20, 0.1% sodium azide), and blotted dry. Biotinylated adiponectin or leptin detection antibody (100 μL) was added to each well and incubated for 1 h at room temperature with gentle shaking. The solution was aspirated, washed 4 times with washing buffer, and blotted dry. One hundred μL of horseradish peroxidase (HRP)-streptavidin solution was added to each well and incubated for 45 min at room temperature with gentle shaking. The HRP-streptavidin solution was aspirated, washed 4 times with washing buffer, and again blotted dry. One hundred μL of a tetramethylbenzidine (TMB) peroxide-substrate solution (0.005% TMB, 0.006% H_2O_2, 0.01 M acetate buffer, pH 3.3, 0.05% sodium nitroprusside) was added to each well and incubated for 30 min at room temperature in the dark with gentle shaking. Fifty μL of 0.16 M sulfuric acid was

added to each well to stop the reaction. The microplates were immediately read at a wavelength of 450 nm with a UV-Visible SpectraMax spectrophotometer. A standard curve was generated from the standard solutions provided and adiponectin or leptin concentrations were calculated from this curve

5.3.6 Cholesterol Profile

HDL and VLDL cholesterol levels were evaluated using a commercial kit and assayed via manufacturer's instructions. HDL and VLDL fractions were first separated by the addition of 100 µL plasma sample to 100 µL precipitation buffer (100 g/L polyethylene glycol, pH 8.0) and incubated for 10 min at room temperature. The sample was centrifuged for 10 min at room temperature at 2,000 x g, the HDL fraction (supernatant) was collected, and the precipitate was resuspended in 200 µL PBS to give the VLDL fraction. Lipoprotein fractions were diluted 20-fold for both HDL and VLDL cholesterol analysis. Fifty µL of the diluted samples and standards were added to each well of a 96-well microplate. Fifty µL of cholesterol esterase and buffer reaction solution was added to each well, mixed by lightly pipetting, and incubated at 37 ºC for 60 min in the dark to evaluate total cholesterol. The microplate absorbance was measured at a wavelength of 570 nm with a UV-Visible SpectraMax spectrophotometer. A standard curve was generated using the standards supplied by the commercial kit and used to calculate HDL and VLDL concentrations.

5.3.7 Liver Enzyme Activity

AST and ALT enzyme activities in plasma were assayed according to the manufacturer's instructions. Plasma samples were diluted 5-fold for both ALT and AST activity analysis. Twenty µL of standards and diluted samples was added to the wells of a 96-well microplate. One hundred µL of ALT or AST enzyme and substrate in buffer (100 mM Tris-HCl, pH 7.8, 10 mM

sodium bicarbonate, 0.1 mM pyridoxal-5-phosphate, 0.01% sodium azide, L-alanine, 150 mM α-ketoglutarate) was added to each well and incubated at room temperature for 60 min at 37 ^{o}C protected from light. The absorbance was measured at 570 nm using a UV-Visible SpectraMax spectrophotometer. A standard curve was generated using pyruvate standards supplied by the manufacturer and enzyme activity was calculated from the curve.

5.3.8 Total Glutathione and GSH/GSSG Ratio

Liver tissue samples were homogenized in ice cold GSH MES buffer (0.4 M 2-(N-morpholino)ethanesulphonic acid, 0.1 M phosphate, pH 6.0, 2 mM EDTA diluted by equal volumes of HPLC-grade water). The homogenate was centrifuged at 10,000 x g for 15 min at 4 ^{o}C and the supernatant collected and kept on ice. The samples were deproteinated by adding equal volumes of aqueous metaphosphoric acid solution (0.5 g/mL), vortexing, and allowing to stand at room temperature for 5 min. The mixture was centrifuged at 2,000 x g for 2 min and the supernatant was carefully collected. Fifty µL of 4 M triethanolamine in water was added per mL of supernatant and vortexed. Fifty µL of sample was assayed with 150 µL Assay Cocktail (MES Buffer, distilled water, $NADP^{+}$, glucose-6-phosphate, glutathione reductase, glucose-6-phosphate dehydrogenase, DNTB) using the Cayman Chemical Glutathione Assay kit according to the manufacturer's protocols. A standard curve of GSH was generated using the standards that came with the assay kit.

For the quantification of oxidized glutathione, 10 µL of 1 M 2-vinylpyridine (100% EtOH) was added to the deproteinated solution prior to the addition of triethanolamine. The samples were vortexed and incubated at room temperature for 60 minutes. The samples were assayed in the same manner as outlined above for total glutathione. A standard curve for GSSG was generated using the standards provided by the assay kit.

5.3.9 Measurement of Pro-Inflammatory Cytokines

Liver tissues were homogenized in cold RIPA lysis buffer (ThermoFisher Scientific, Madison, WI) with 1% ProteaseArrest Inhibitor Cocktail (G-Biosciences, St. Louis, MO) and 1% PhosphataseArrest Inhibitor Cocktail (G-Biosciences, St. Louis, MO), incubated for 1 hr at 4 ^{o}C, and sonicated for 1 min at 4 ^{o}C. The homogenate was centrifuged at 14,000 x g for 15 min at 4 ^{o}C. The supernatant was collected and stored at -20 ^{o}C for later analysis. Mouse IL-1β, mouse TNF-α, and mouse IL-6 ELISAs (Invitrogen, Carlsbad, CA) were conducted according to manufacturer's instructions. Protein concentrations were measured using the Bradford Protein Assay (Bio-Rad, Hercules, CA) according to manufacturer's instructions and cytokine concentrations were set relative to protein levels.

5.3.10 Statistical Analysis

Statistical analyses were performed using SigmaPlot 13 software (Systat Software, Inc., San Jose, CA). Outlier analyses were conducted using JMP Pro 15 software (SAS Institute, Cary, NC) and evaluated by the Quantile Range Outliers method of outlier detection. Results were expressed as mean values ± SD. Difference in the means were evaluated by one-way ANOVA followed by Tukey's HSD test, and differences of $P \leq 0.05$ were considered significant.

5.4 Results

5.4.1 Effect of CySSPe treatment on HFHCD-induced obesity and serum biochemistry

HFHCD-induced obesity is known to alter morphometric measurements and serum lipid and adipokine biomarkers. Body weight gains were significantly higher in mice consuming HFHCD in comparison to those eating the control diet following the 8-week obesity induction period ($P < 0.001$) **(Fig. 5.1A)**. The CySSPe treatment group exhibited a marginal increase in food consumption over the HFHCD group **(Fig. 5.1B)**, however, the body weight gain, percent

fat pad weight, and percent liver weight between the HFHCD and treatment groups were not significantly different **(Fig. 5.1A and 5.2)**. CySSPe treatment reduced liver triglyceride levels relative to the HFHCD group **(Fig. 5.3)**, whereas adiponectin, leptin, and high-density lipoprotein (HDL) and very-low-density lipoprotein (VLDL) cholesterol were unaffected **(Fig. 5.4-5.7)**. The adiponectin levels between HFHCD/treatment groups were initially elevated compared to the sham chow group (T = 0 weeks) but were not significantly different at the end of the 8-week treatment period **(Fig. 5.4)**.

5.4.2 Effect of CySSPe treatment on liver enzyme activity

Activity levels of alanine transaminase (ALT) and aspartate transaminase (AST) in plasma are known to be elevated from obesity-associated non-alcoholic fatty liver disease (NAFLD) (40), however, CySSPe treatment did not affect ALT and AST activity over the treatment period relative to the sham HFHCD group **(Fig. 5.8)**.

5.4.3 CySSPe restored total glutathione levels but not GSH/GSSG ratio

HFHCD-induced obesity suppresses levels of hepatic antioxidant enzymes and glutathione in rodents (41). HFHCD-induced obesity reduced total hepatic glutathione species (GSH + GSSG) compared to the control diet and CySSPe administration restored total glutathione ($P < 0.05$) **(Fig. 5.9A)**. However, the differences in hepatic redox status (GSH/GSSG) as an index of oxidative stress between the three groups were not statistically different **(Fig. 5.9B)**.

5.4.4 CySSPe suppressed elevated inflammatory cytokines from HFHCD-induced obesity

Obesity induced by HFHCD is associated with low-grade inflammation triggered by inflammatory cytokines released from white adipose tissues, macrophages recruited to adipose tissue, and lipopolysaccharides (LPS) leaked into the bloodstream from gut microbiota (42). LPS

was not significantly different between the three groups at T = 0 **(Fig. 5.10)**. At T = 4 weeks, the CySSPe treatment group decreased LPS levels compared to control. Mice consuming the HFHCD exhibited elevated levels of inflammatory cytokines TNF-α and IL-6 in plasma and TNF-α, IL-1β, and IL-6 in liver tissue compared to the control chow diet, which were significantly reduced by CySSPe treatment after 8 weeks (**Fig. 5.11 and 5.12)**.

5.5 Discussion

CySSPe treatment reduced HFHCD-induced elevated triglyceride levels in the liver ($P < 0.05$) **(Fig. 5.3.)**. Excess triglycerides accumulate in the liver during the progression of NAFLD, a liver disease closely associated with obesity (43). Elevated triglyceride storage and de novo biosynthesis from excess caloric intake impairs mitochondrial function and increases oxidative damage, hepatocyte death, and inflammation (44). H_2S (administered as NaHS) has previously been shown to reduce expression of fatty acid synthase (FAS), a multi-enzyme protein complex that controls lipid synthesis, and increase expression of carnitine palmitoyltransferase-1 (CPT-1), an enzyme that regulates energy expenditure, in C57BL/6 mice fed a HFD (17). Adipose tissues exhibit decreased expression of H_2S synthesizing enzymes and lowered H_2S levels in both genetic and HFD-induced mouse models of obesity (45). In another animal study, CSE in the liver and lung tissues was found to be downregulated in HFD-fed mice, with concomitant reduction in biosynthesis of H_2S in these tissues (46). Lipid accumulation may be reduced by the H_2S formed from CySSPe treatment, as shown in chapter 2, which would reverse decreases in H_2S caused by the HFHCD (24,45).

While the HFHCD induced significant changes in morphometric measurements, serum lipid biochemistry, and enzyme activity levels, the findings in the present study suggest CySSPe had no effect on the obesity-induced changes of these markers. In contrast, Sprague-Dawley rats

gavaged with CySSA (200 mg/kg) decreased body weight, fat mass, and ALT activity (32). Additionally, intraperitoneal injection of NaHS (50 μmol/kg) for 4 weeks significantly decreased liver weight and hepatic total cholesterol in HFHCD mice (17). The CySSPe dose used in this study (9.8 mg/kg or ~50 μmol/kg) may not have reached sufficient physiological levels to directly affect or release the level of H_2S necessary to modulate these parameters, as CySSPe releases H_2S stoichiometrically at a 1:5 (H_2S/CySSPe) ratio *in chemico* (as shown in chapter 2 of this dissertation).

Glutathione is the most abundant non-enzymatic antioxidant in liver tissues and plays an important role in cytoprotection by conjugating with xenobiotics, directly quenching reactive oxygen species (ROS), serving as a substrate for antioxidant enzymes to detoxify oxidative stress, and maintaining redox homeostasis (47). In this study, CySSPe restored HFHCD-induced reduction of total glutathione levels in the liver to control levels but did not modulate the GSH/GSSG ratio **(Fig. 5.9)**. Glutathione was found to be lowered in the liver and renal tissues of rats fed an HFD by the excess lipid peroxides and free radicals generated by hypertrophic adipose tissues (41). Previous cell studies showed CySSPe mitigated oxidative damage by increasing the production of glutathione in murine hepatocytes and macrophages through the upregulation of γ-glutamylcysteine ligase (GCL), a rate-limiting enzyme in glutathione biosynthesis (24,37). Restoration of hepatic glutathione levels and GSH/GSSG redox ratio with a novel cystine compound has been shown to ameliorate the oxidative stress characterized by diet-induced obesity (48).

Obesity is strongly associated with mild, chronic inflammation, partially mediated by the recruitment of pro-inflammatory M1 macrophages to adipose tissues (49). CySSPe treatment inhibited the elevated levels of inflammatory cytokines in plasma and liver induced by diet-

induced obesity, which suggests CySSPe possesses anti-inflammatory properties *in vivo* **(Fig. 5.11 and 5.12)**. In rats with diet-induced NAFLD, CySSA attenuated elevated TNF-α and IL-1β production. (Fig. 4 in (18)). Furthermore, both CySSA and CySSPe have been shown to decrease TNF-α, IL-6, and IL-1β production by LPS-activated macrophages by inhibiting the NF-κB signaling pathway (37). In chapter 3 of this dissertation, it was shown that the Nrf2/ARE signaling pathway is upregulated by CySSR in activated macrophages and Nrf2-silencing restores nitric oxide (NO) biosynthesis after CySSR treatment. Mechanistically, CySSPe may suppress pro-inflammatory cytokine synthesis by upregulating Nrf2 and antioxidant response element (ARE) enzymes, which support the biosynthesis of glutathione and scavenging of ROS associated with the inflammatory state (24,37). ROS, including H_2O_2, is a necessary factor for proper Toll-like receptor 4 (TLR4) oligomerization and lipid raft complex assembly, a required step for NF-κB inflammatory signaling (50,51). CySSR modulate the thiol redox status by elevating GSH concentrations, which may impede NF-κB initiation by countering these elevated levels of H_2O_2 (37). Elevated levels of the previously mentioned cytokines can lead to prolonged inflammation, aggravating obesity comorbidities (52). Inhibition of obesity-induced inflammation, including inhibiting pro-inflammatory cytokine production, is a potential target for resolving metabolic diseases and symptoms associated with obesity, such as insulin resistance, metabolic syndrome, and diabetes mellitus (53).

The calculated dose used here was based on the human equivalent dose conversion of one average medium onion (200 g) for a 60 kg human adult to a 20 g mouse. The molar amount of 1-propenylmercapto equivalents from methyl 1-propenyl thiosulfinate, a stable, 1-propenyl-containing thiosulfinate generated from onion, is 0.31 mmol (20,54), giving an equivalent mouse dose of 12.3 mg/kg per day (38). The daily dose of 9.8 mg/kg CySSPe used in this study

dispersed in an average mouse would yield 250 μM CySSPe (55), which is sufficient to elicit relevant biological responses in cell cultures (21,24,37). However, the derivative CySSA appears to be rapidly metabolized ($t_{1/2}$ = 3.8 min) following intravenous injection in rats (56), and so the CySSPe pool could be quickly depleted during gastrointestinal absorption and metabolism. Therefore, investigations into the pharmacokinetics of CySSPe may be important for future experimental work involving animal models.

In conclusion, CySSPe treatment offered some protection against obesity-associated inflammation in an HFHCD-induced mouse model of obesity. These results suggest the anti-obesity effects of CySSPe are limited. Further studies into the ability of CySSPe to increase H_2S levels and enhance H_2S biosynthesis enzyme capacity, inhibit NF-κB signaling, and upregulate Nrf2 and Nrf2-associated antioxidant proteins *in vivo* as possible mechanisms for the anti-inflammatory effects exhibited by CySSPe are warranted under the conditions of this study. Investigating the potential inhibitory effect of CySSPe on p38 mitogen-activated protein kinases (MAPK) could also contribute to an understanding of the anti-inflammatory properties of CySSPe. Additionally, a dose-response analysis could be conducted to evaluate the optimal intraperitoneal dose concentration of CySSPe needed to suppress pro-inflammatory cytokine production in obese mice.

5.6 Figures and Tables

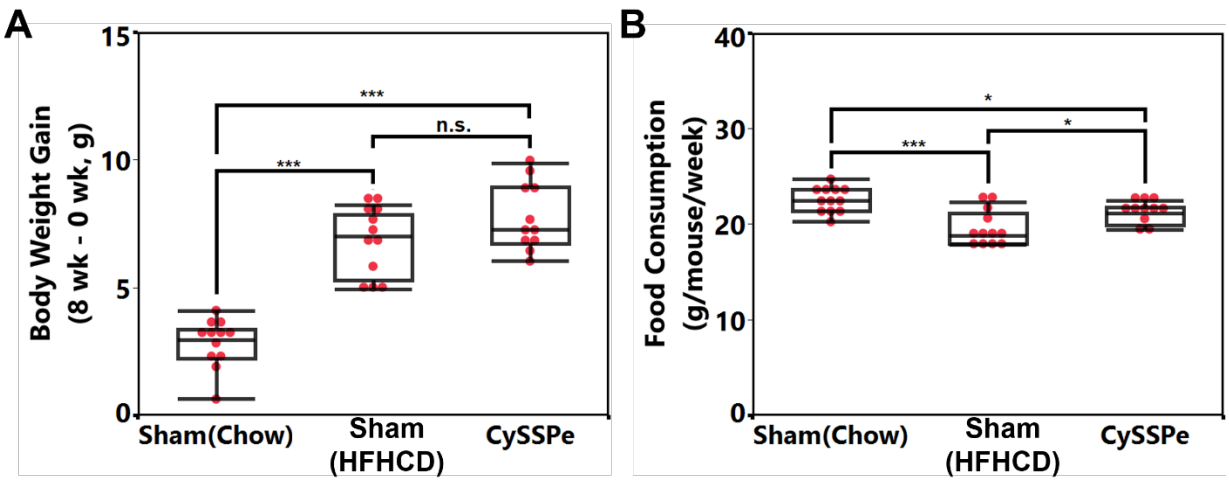

Figure 5.1. Total body weight gain and food consumption of C57BL/6J mice**. (A)** Total body weight gain following obesity induction period and **(B)** weight of food consumption per mouse per week. N = 12 for sham, n = 11 for treatment group. Difference in the means were evaluated by one-way ANOVA followed by Tukey's HSD test. * = $P < 0.05$, *** = $P < 0.001$, n.s. = not significant

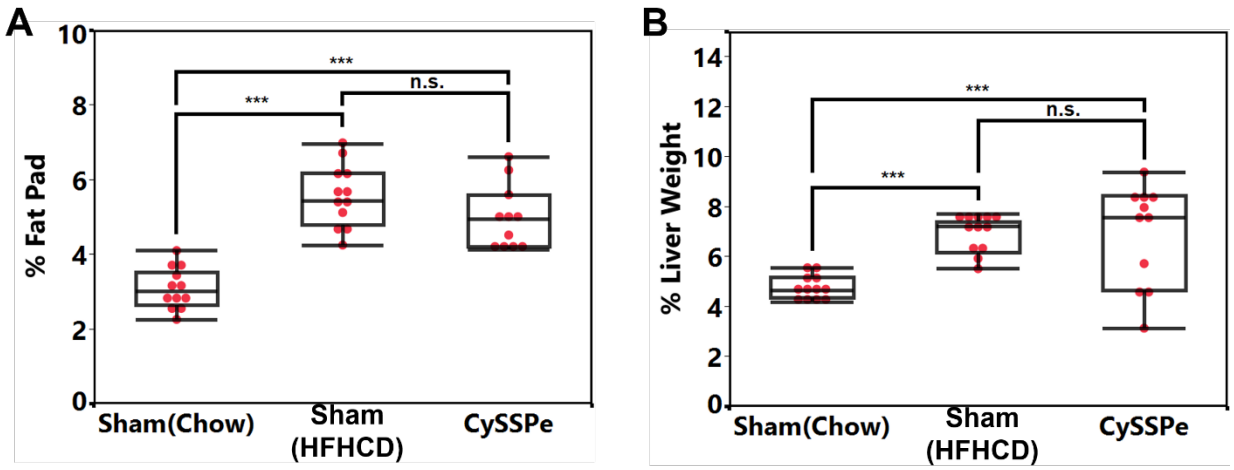

Figure 5.2. Fat pad and liver weight of C57BL/6J mice at sacrifice**. (A)** Fat pad weight as a percentage of final body weight and **(B)** liver weight as a percentage of final body weight. N = 12 for sham, n = 11 for CySSPe treatment group. Difference in the means were evaluated by one-way ANOVA followed by Tukey's HSD test. *** = $P < 0.001$, n.s. = not significant

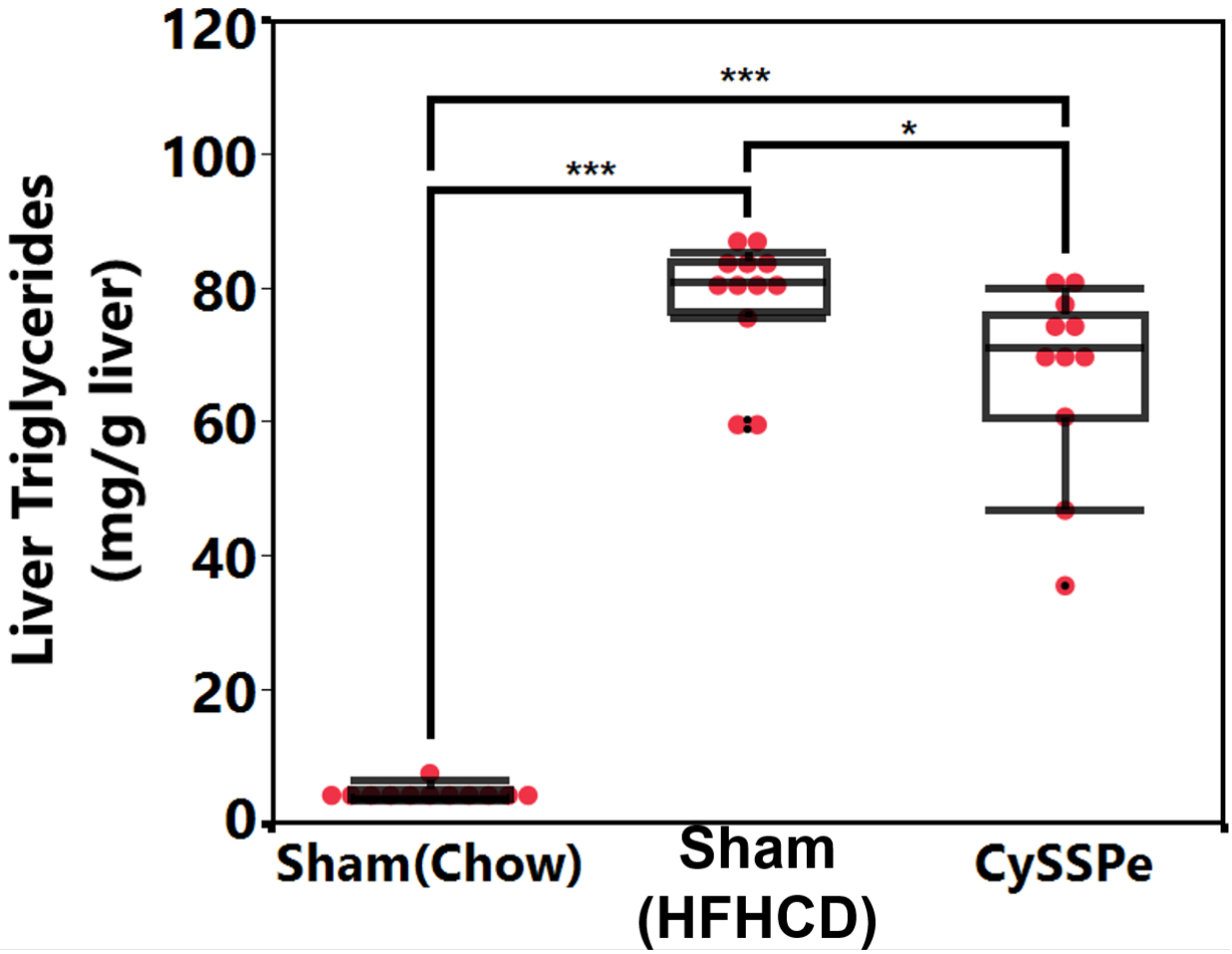

Figure 5.3. Total liver triglycerides in C57BL/6J mice after CySSPe treatment. N = 12 for sham, n = 11 for CySSPe treatment group. Red and black points represent outliers evaluated by Quantile Range Outliers method of outlier detection. Difference in the means were evaluated by one-way ANOVA followed by Tukey's HSD test. * = $P < 0.05$, *** = $P < 0.001$

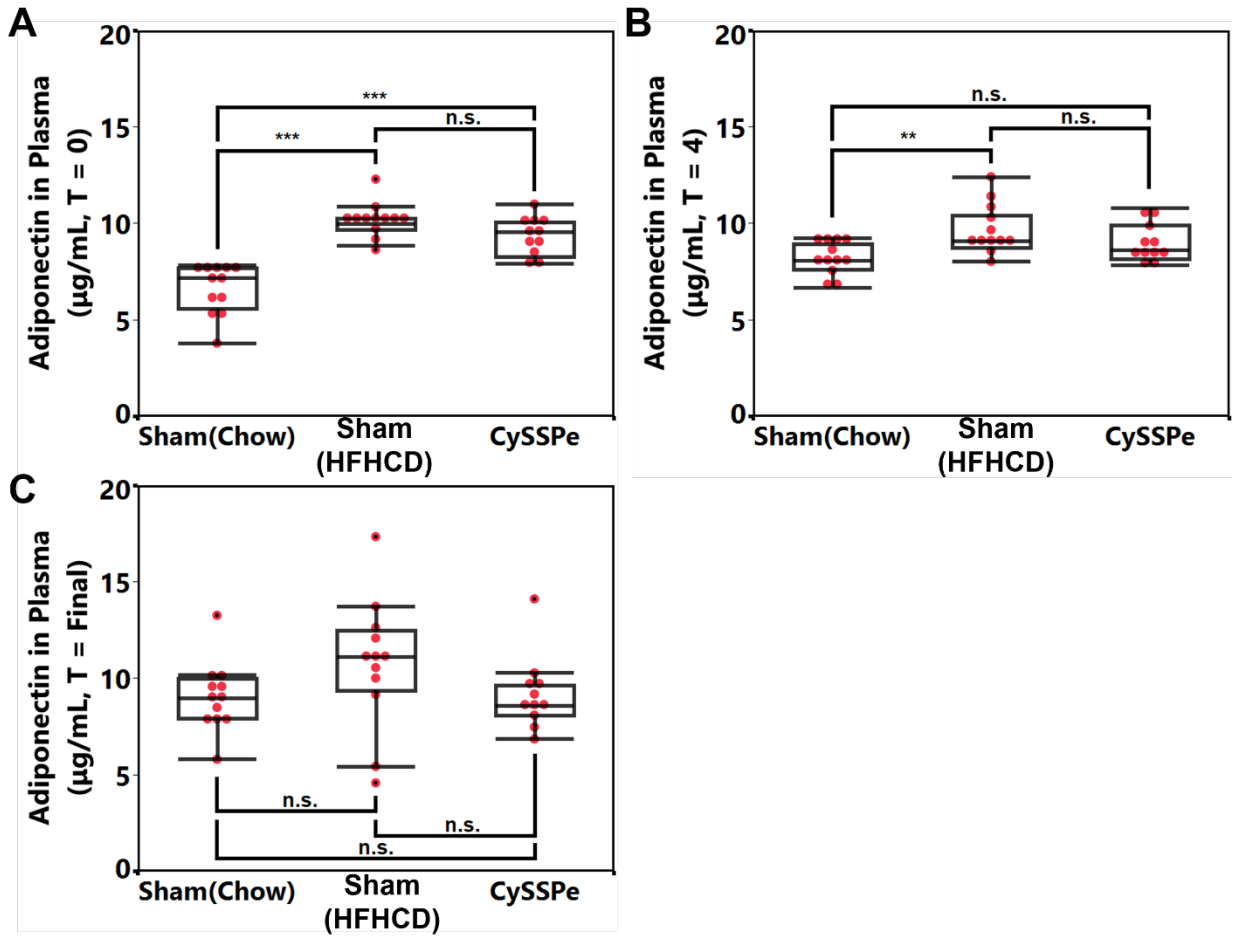

Figure 5.4. Adiponectin levels in blood plasma at 0, 4 and 8 weeks of CySSPe treatment. **(A)** Week 0, **(B)** week 4, and **(C)** week 8 of treatment. N = 12 for sham, n = 11 for CySSPe treatment group. Red and black points represent outliers evaluated by Quantile Range Outliers method of outlier detection. Difference in the means were evaluated by one-way ANOVA followed by Tukey's HSD test. ** = $P < 0.01$, *** = $P < 0.001$, n.s. = not significant

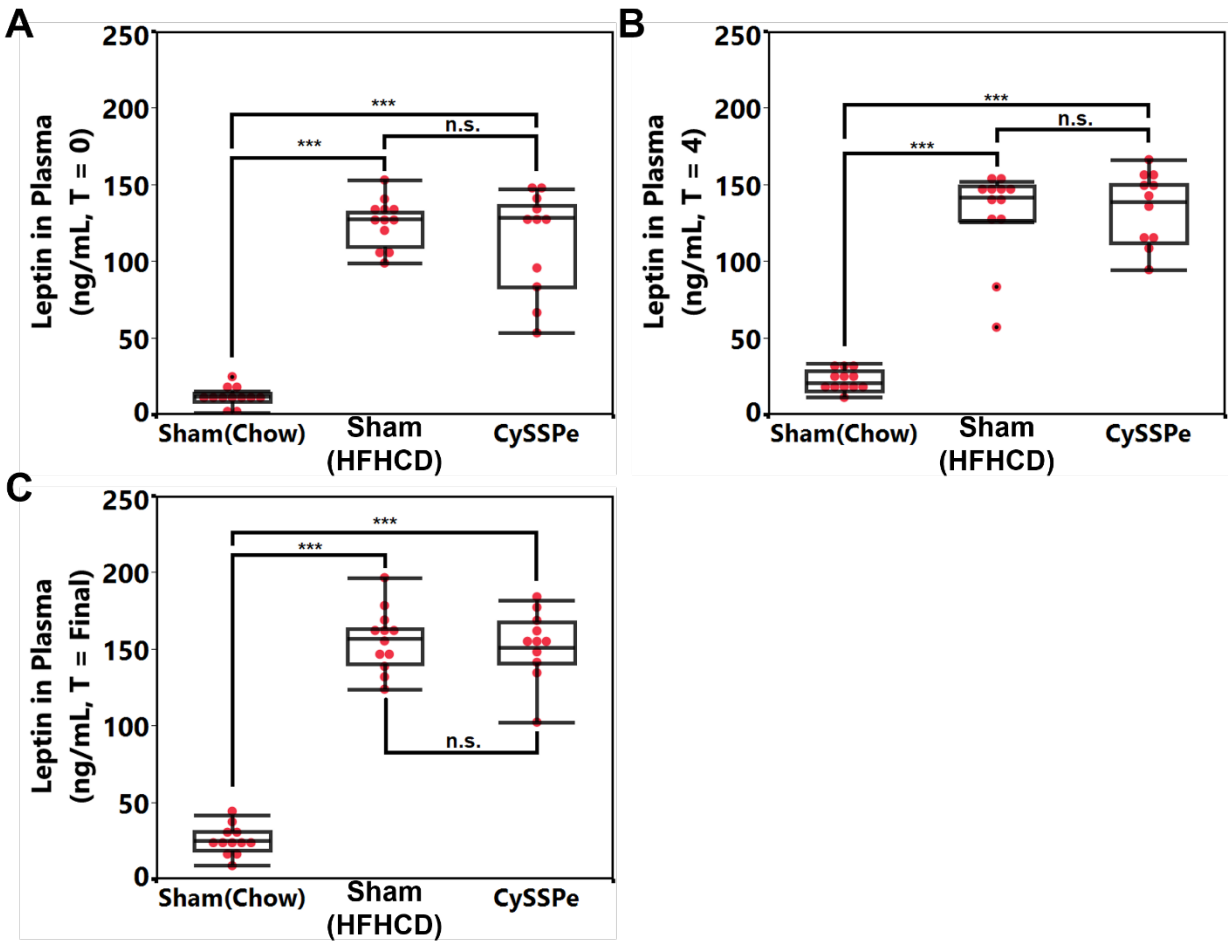

Figure 5.5. Leptin levels in blood plasma at 0, 4 and 8 weeks of CySSPe treatment. **(A)** Week 0, **(B)** week 4, and **(C)** week 8 of treatment. N = 12 for sham, n = 11 for CySSPe treatment group. Red and black points represent outliers evaluated by Quantile Range Outliers method of outlier detection. Difference in the means were evaluated by one-way ANOVA followed by Tukey's HSD test. *** = $P < 0.001$, n.s. = not significant

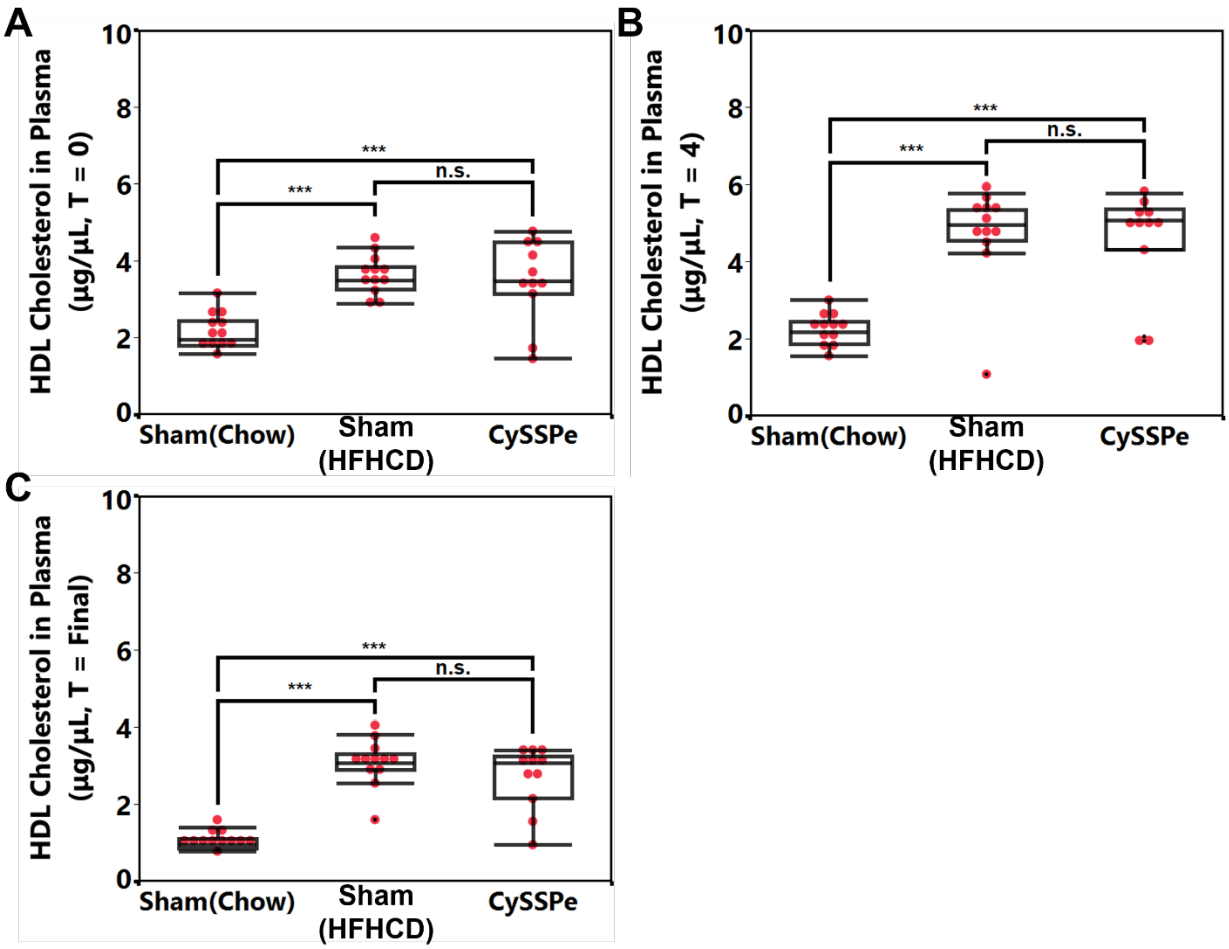

Figure 5.6. HDL cholesterol levels in blood plasma at 0, 4 and 8 weeks of CySSPe treatment. **(A)** Week 0, **(B)** week 4, and **(C)** week 8 of treatment. N = 12 for sham, n = 11 for CySSPe treatment group. Red and black points represent outliers evaluated by Quantile Range Outliers method of outlier detection. Difference in the means were evaluated by one-way ANOVA followed by Tukey's HSD test. *** = $P < 0.001$, n.s. = not significant

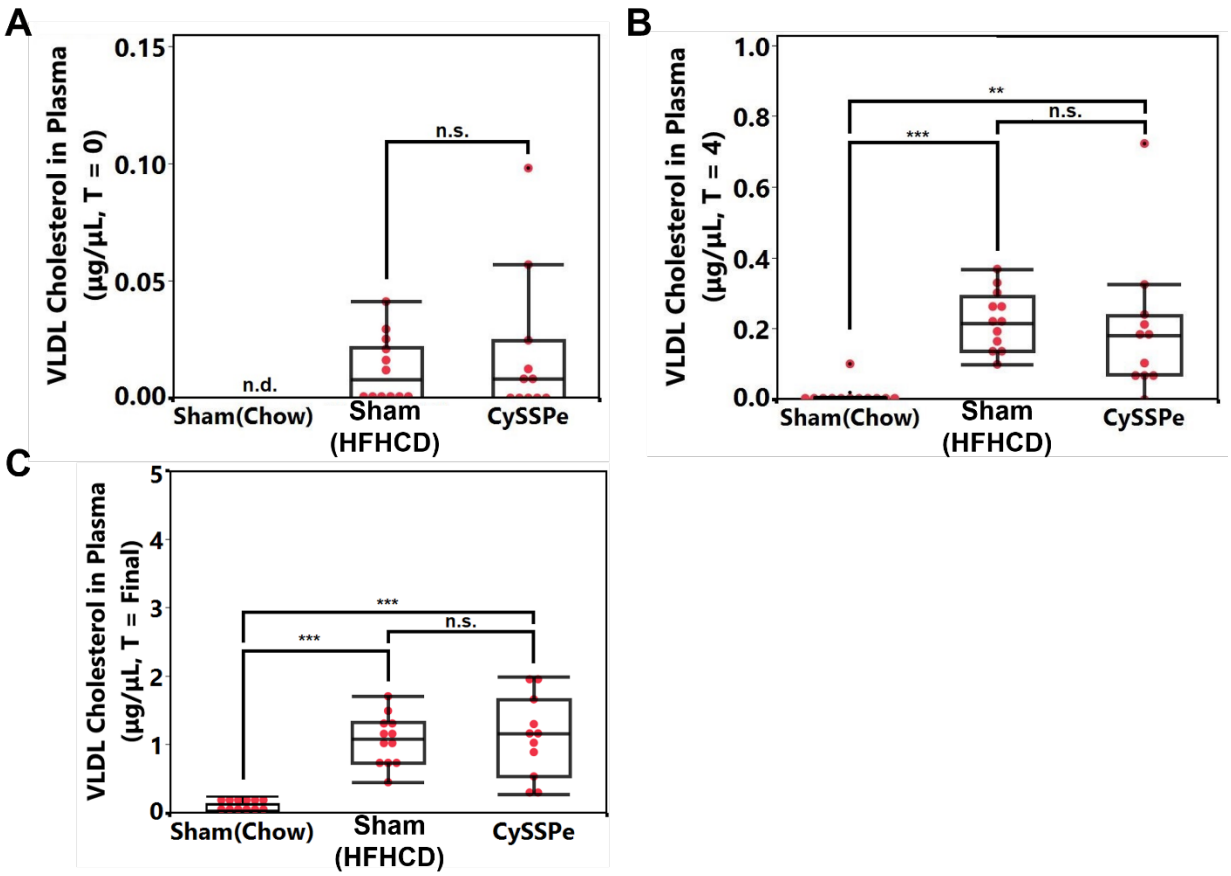

Figure 5.7. VLDL cholesterol levels in blood plasma at 0, 4 and 8 weeks of CySSPe treatment. **(A)** Week 0, **(B)** week 4, and **(C)** week 8 of treatment. Red and black points represent outliers evaluated by Quantile Range Outliers method of outlier detection. Difference in the means were evaluated by one-way ANOVA followed by Tukey's HSD test. ** = $P < 0.01$, *** = $P < 0.001$, n.d. = not detectable, n.s. = not significant

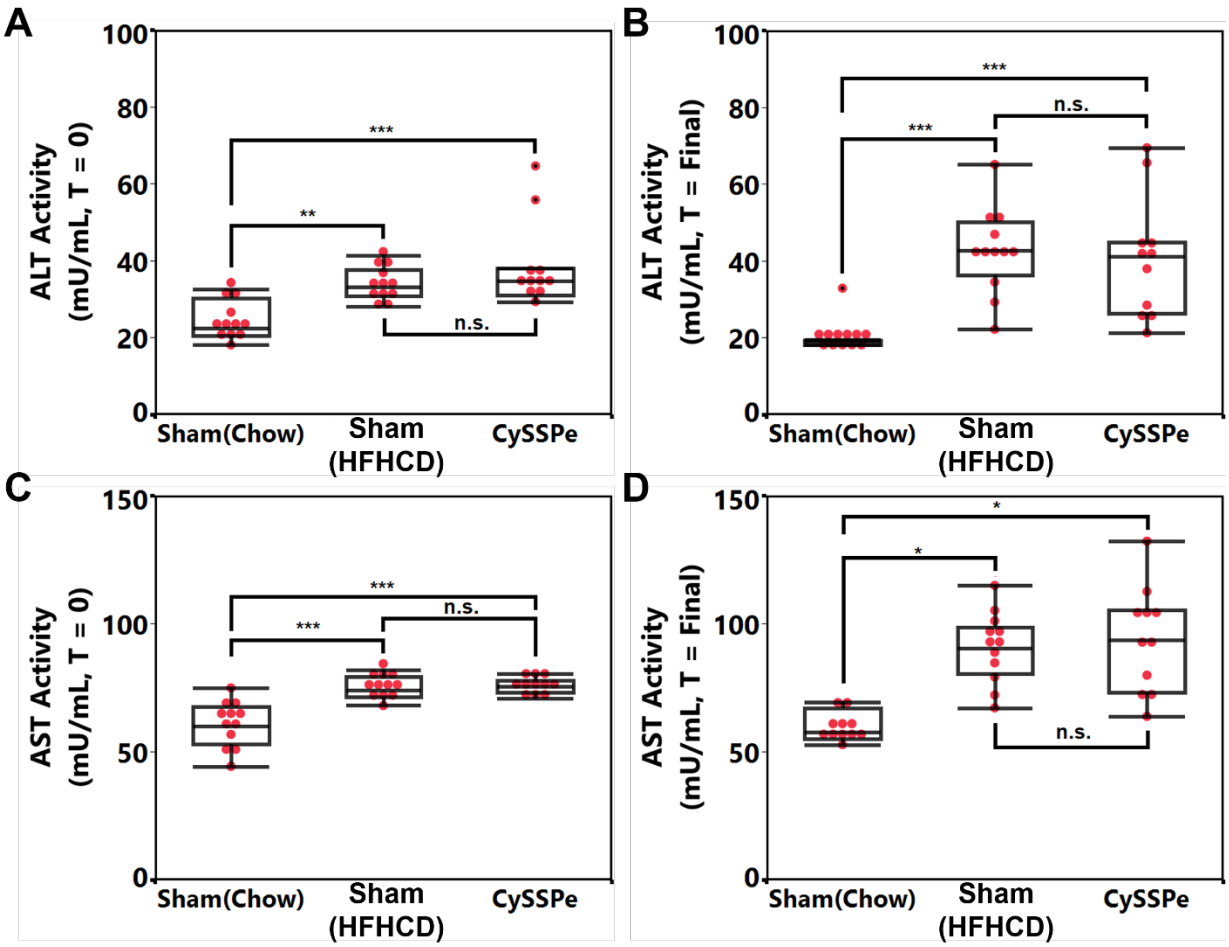

Figure 5.8. ALT and AST activities levels in serum at 0 and 8 weeks of CySSPe treatment. Alanine transaminase (ALT) at **(A)** week 0 and **(B)** week 8 and aspartate transaminase (AST) at **(C)** week 0 and **(D)** week 8 of treatment. Red and black points represent outliers evaluated by Quantile Range Outliers method of outlier detection. Difference in the means were evaluated by one-way ANOVA followed by Tukey's HSD test. * = $P < 0.05$, ** = $P < 0.01$, *** = $P < 0.001$, n.s. = not significant

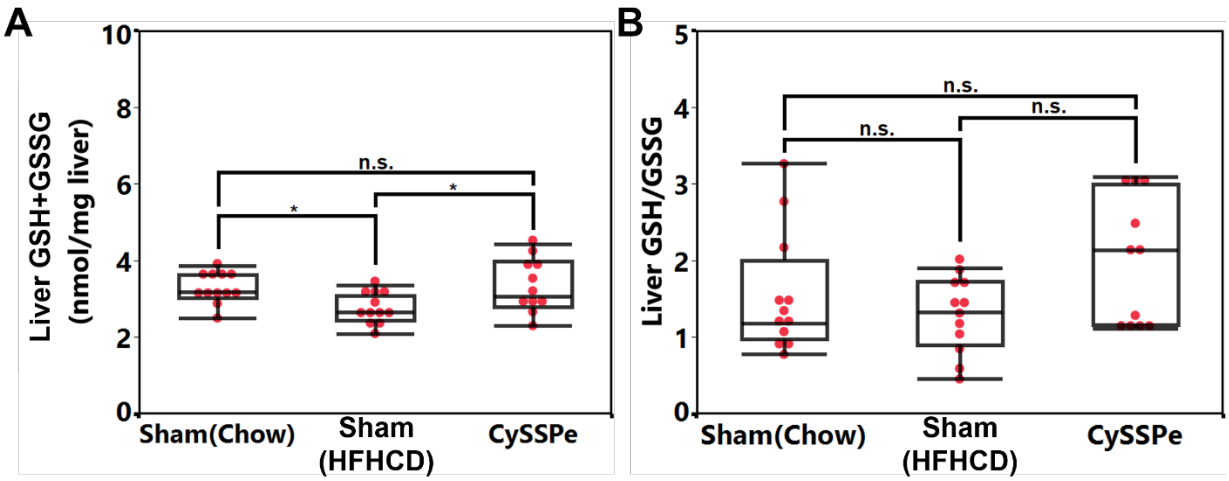

Figure 5.9. Hepatic glutathione levels and redox status. **(A)** Total liver glutathione species per mass of liver and **(B)** reduced glutathione/oxidized glutathione ratio in the liver. Red and black points represent outliers evaluated by Quantile Range Outliers method of outlier detection. Difference in the means were evaluated by one-way ANOVA followed by Tukey's HSD test. * = $P < 0.05$, n.s. = not significant

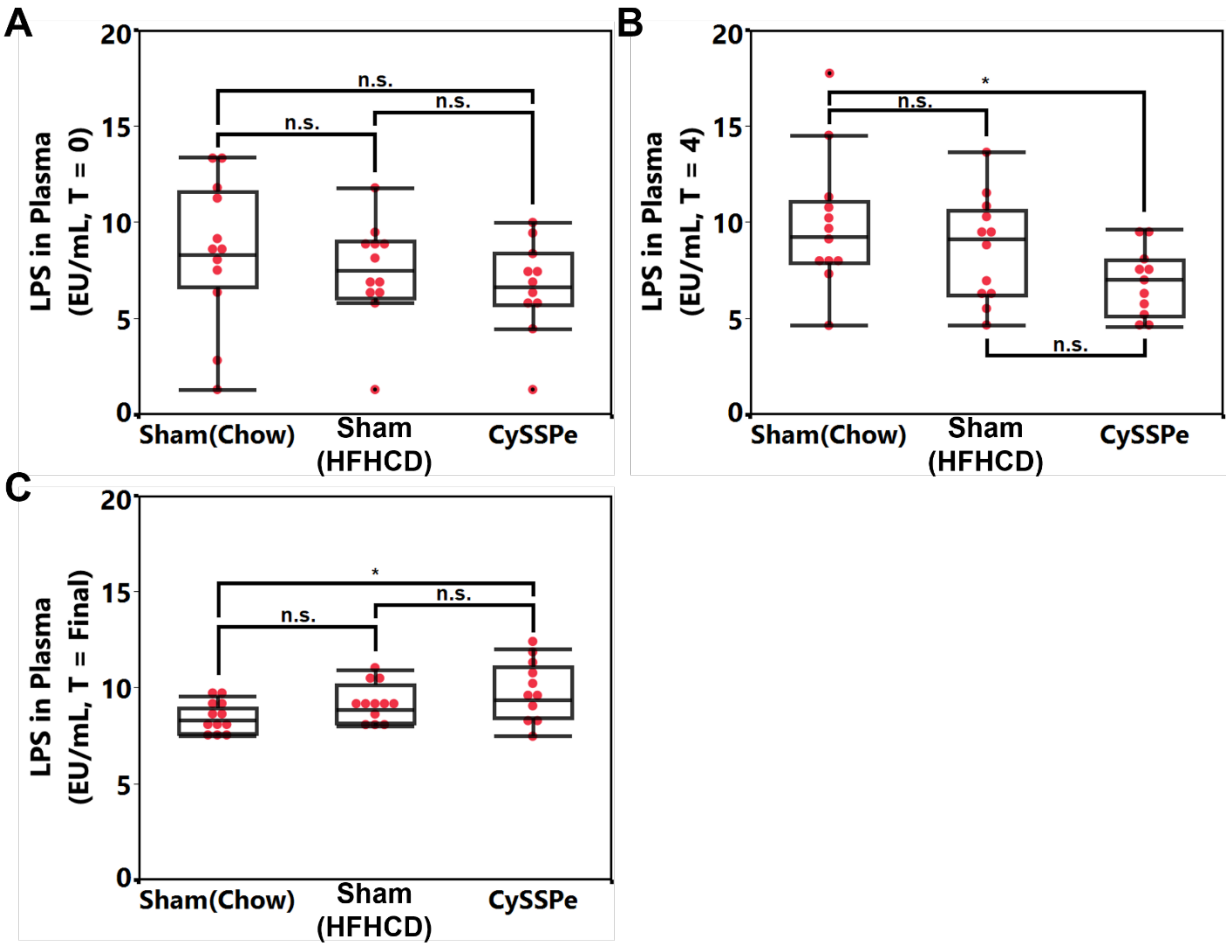

Figure 5.10. LPS levels in blood plasma at 0, 4, and 8 weeks of CySSPe treatment. **(A)** Week 0, **(B)** week 4, and **(C)** week 8 of treatment. Red and black points represent outliers evaluated by Quantile Range Outliers method of outlier detection. Difference in the means were evaluated by one-way ANOVA followed by Tukey's HSD test. * = $P < 0.05$, n.s. = not significant

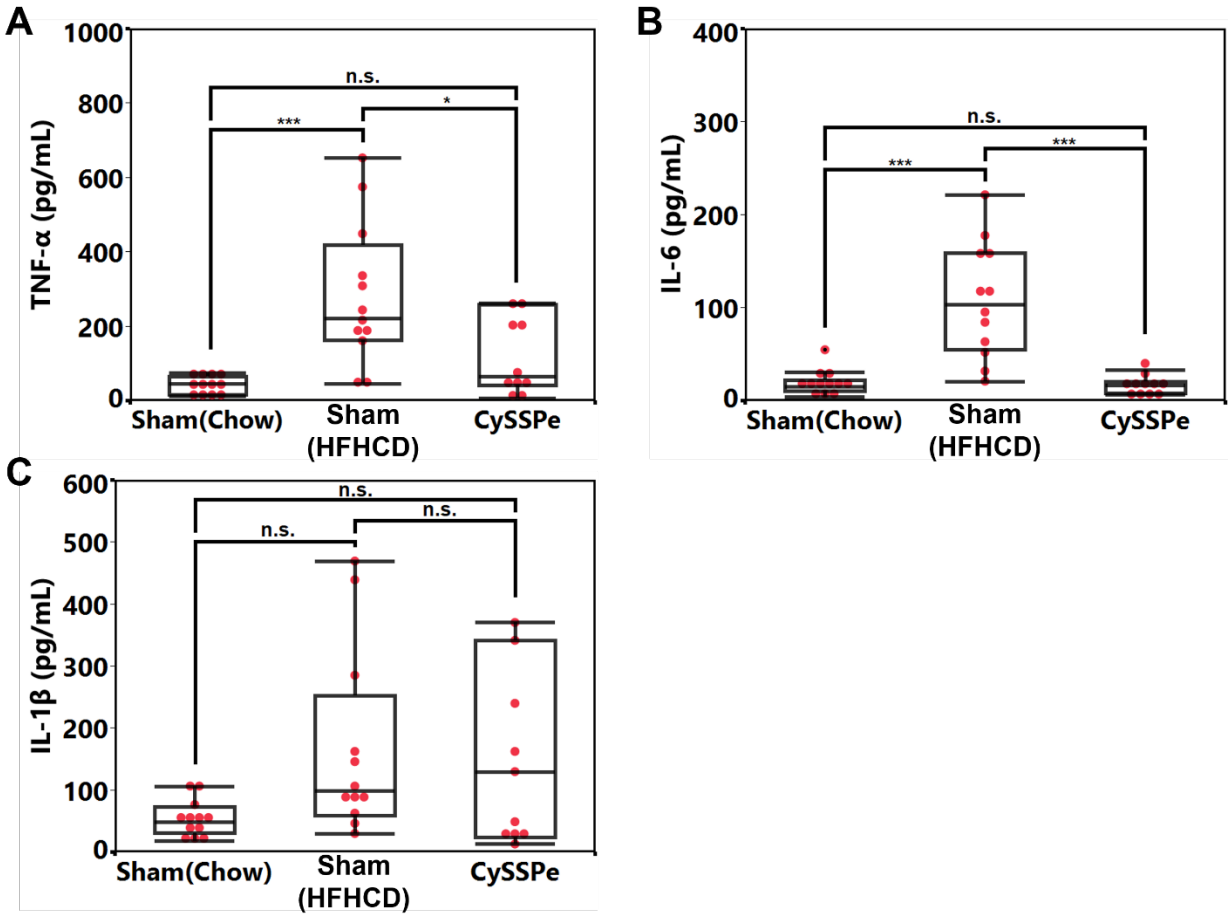

Figure 5.11. Concentration of IL-1β, IL-6, and TNF-α in blood plasma at 8 weeks of CySSPe treatment. Concentration of inflammatory cytokines **(A)** IL-1β, **(B)** IL-6, and **(C)** TNF-α. Difference in the means were evaluated by one-way ANOVA followed by Tukey's HSD test. * = $P < 0.05$, *** = $P < 0.001$, n.s. = not significant

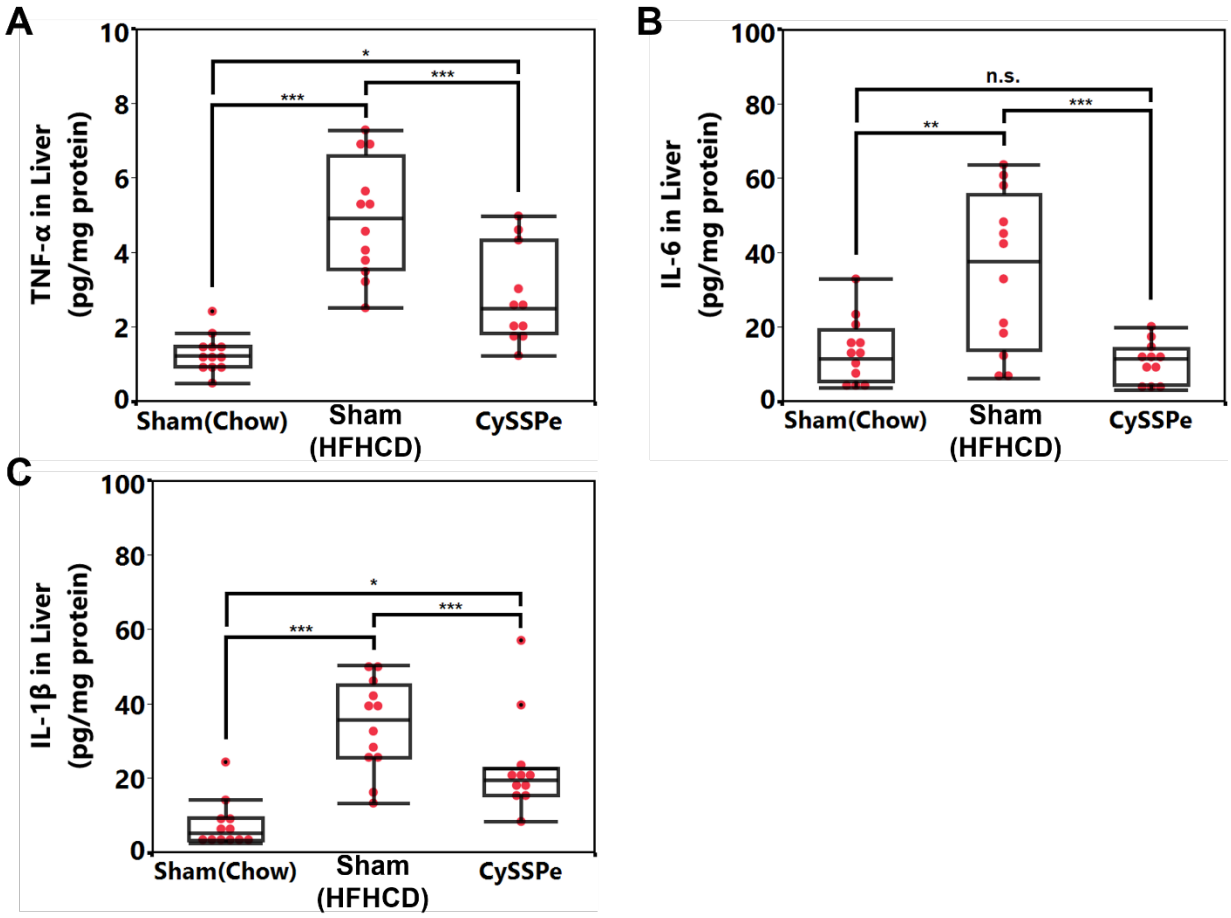

Figure 5.12. Concentration of IL-1β, IL-6, and TNF-α in liver at 8 weeks of CySSPe treatment. Concentration of inflammatory cytokines **(A)** IL-1β, **(B)** IL-6, and **(C)** TNF-α in liver, set relative to protein levels. Red and black points represent outliers evaluated by Quantile Range Outliers method of outlier detection. Difference in the means were evaluated by one-way ANOVA followed by Tukey's HSD test. * = $P < 0.05$, ** = $P < 0.01$, *** = $P < 0.001$, n.s. = not significant

5.7 References

1. GBD 2015 Obesity Collaborators. Health Effects of Overweight and Obesity in 195 Countries Over 25 Years. *N. Engl. J. Med.* **2017**, *377*, 13-27.

2. Wright, S.M., Aronne, L.J. Causes of Obesity. *Abdom. Radiol.* **2012**, *37*, 730-732.

3. Buijsse, B., Feskens, E.J.M., Schulze, M.B., Forouhi, N.G., Wareham, N.J., Sharp, S., Palli, D., Tognon, G., Halkjaer, J., Tjønneland, A., Jakobsen, M.U., Overvad, K., van der A, D.L., Du, H., Sørensen, T.I.A., Boeing, H. Fruit and Vegetable Intakes and Subsequent Changes in Body Weight in European Populations: Results from the Project on Diet, Obesity, and Genes (DiOGenes). *Am. J. Clin. Nutr.* **2009**, *90*, 202-209.

4. He, K., Hu, F.B., Colditz, G.A., Manson, J.E., Willett, W.C., Liu, S. Changes in Intake of Fruits and Vegetables in Relation to Risk of Obesity and Weight Gain Among Middle-Aged Women. *IJO* **2004**, *28*, 1569-1574.

5. Rolls, B.J., Ello-Martin, J.A., Tohill, B.C. What Can Intervention Studies Tell Us about the Relationship between Fruit and Vegetable Consumption and Weight Management? *Nutr. Rev.* **2004**, *62*, 1-17.

6. González-Castejón, M., Rodriguez-Casado, A. Dietary Phytochemicals and Their Potential Effects on Obesity: A Review. *Pharmacol. Res.* **2011**, *64*, 438-455.

7. Otto, T.C., Lane, M.D. Adipose Development: From Stem Cell to Adipocyte. *Crit. Rev. Biochem. Mol. Biol.* **2005**, *40*, 229-242.

8. Hosogai, N., Fukuhara, A., Oshima, K., Miyata, Y., Tanaka, S., Segawa, K., Furukawa, S., Tochino, Y., Komuro, R., Matsuda, M., Shimomura, I. Adipose Tissue Hypoxia in Obesity and Its Impact on Adipocytokine Dysregulation. *Diabetes* **2007**, *56*, 901-911.

9. Ye, J. Emerging Role of Adipose Tissue Hypoxia in Obesity and Insulin Resistance. *Int. J. Obes.* **2009**, *33*, 54-66.

10. Jung, U.J., Choi, M.-S. Obesity and Its Metabolic Complications: The Role of Adipokines and the Relationship between Obesity, Inflammation, Insulin Resistance, Dyslipidemia and Nonalcoholic Fatty Liver Disease. *Int. J. Mol. Sci.* **2014**, *15*, 6184-6223.

11. Beltowski, J., Jamroz-Wiśniewska, A. Hydrogen Sulfide in the Adipose Tissue-Physiology, Pathology, and a Target for Pharmacotherapy. *Molecules* **2017**, *22*, 1-16.

12. Melino, S., Leo, S., Papajani, V.T. Natural Hydrogen Sulfide Donors from *Allium* sp. As a Nutraceutical Approach in Type 2 Diabetes Prevention and Therapy. *Nutrients* **2019**, *11*, 1-25.

13. Evans, R.M., Barish, G.D., Wang, Y.-X. PPARs and the Complex Journey to Obesity. *Nat. Med.* **2004**, *10*, 355-361.

14. Cheung, S.H., Lau, J.Y.W. Hydrogen Sulfide Mediates Athero-Protection Against Oxidative Stress via *S*-Sulfhydration. *PLoS One* **2018**, *13*, 1-20.

15. Cai, J., Shi, X., Wang, H., Fan, J., Feng, Y., Lin, X., Yang, J., Cui, Q., Tang, C., Xu, G., Geng, B. Cystathionine γ Lyase-Hydrogen Sulfide Increases Peroxisome Proliferator-Activated Receptor γ Activity by Sulfhydration at C139 Site Thereby Promoting Glucose Uptake and Lipid Storage in Adipocytes. *BBA-Mol. Cell Biol. L.* **2016**, *1861*, 419-429.

16. Módis, K., Ju, Y., Ahmad, A., Untereiner, A.A., Altaany, Z., Wu, L., Szabo, C., Wang, R. *S*-Sulfhydration of ATP Synthase by Hydrogen Sulfide Stimulates Mitochondrial Bioenergetics. *Pharmacol. Res.* **2016**, *113*, 116-124.

17. Wu, D., Zheng, N., Qi, K., Cheng, H., Sun, Z., Gao, B., Zhang, Y., Pang, W., Huangfu, C., Ji, S., Xue, M. Exogenous Hydrogen Sulfide Mitigates the Fatty Liver in Obese Mice Through Improving Lipid Metabolism and Antioxidant Potential. *Med. Gas Res.* **2015**, *5*, 1-8.

18. Block, E. The Organosulfur Chemistry of the Genius *Allium* – Implications for the Organic Chemistry of Sulfur. *Angew. Chem. Int. Ed.* **1992**, *31*, 1135-1178.

19. Block, E., Ahmad, S., Catalfamo, J.L., Jain, M.K., Apitz-Castro, R. Antithrombotic Organosulfur Compounds from Garlic: Structural, Mechanistic, and Synthetic Studies. *J. Am. Chem. Soc.* **1986**, *108*, 7045-7055.

20. Bayer, T., Wagner, H., Block, E., Grisoni, S., Zhao, S.H., Neszmelyi, A. Zwiebelanes: Novel Biologically Active 2,3-Dimethyl-5,6-dithiabicyclo[2.1.1]hexane 5-Oxides from Onion. *J. Am. Chem. Soc.* **1989**, *111*, 3085-3086.

21. Zhang, G., Parkin, K.L. A Tissue Homogenate Method to Prepare Gram-Scale *Allium* Thiosulfinates and Their Disulfide Conjugates with Cysteine and Glutathione. *J. Agric. Food Chem.* **2013**, *61*, 3030-3038.

22. Benavides, G.A., Squadrito, G.L., Mills, R.W., Patel, H.D., Isbell, T.S., Patel, R.P., Darley-Usmar, V.M., Doeller, J.E., Kraus, D.W. Hydrogen sulfide mediates the vasoactivity of garlic. *Proc. Natl. Acad. Sci. U.S.A.* **2007**, *104*, 17977-17982.

23. Liang, D., Wu, H., Wong, M.W., Huang, D. Diallyl Trisulfide Is a Fast H_2S Donor, but Diallyl Disulfide Is a Slow One: The Reaction Pathways and Intermediates of Glutathione with Polysulfides. *Org. Lett.* **2015**, *17*, 4196-4199.

24. Tocmo, R., Parkin, K. *S*-Alk(en)ylmercaptocysteine Suppresses LPS-Induced Pro-Inflammatory Responses in Murine Macrophages through Inhibition of NF-κB Pathway and Modulation of Thiol Redox Status. *Free Rad. Biol. Med.* **2018**, *129*, 548-558.

25. Keophiphath, M., Priem, F., Jacquemond-Collet, I., Clement, K., Lacasa, D. 1,2-Vinyldithiin from Garlic Inhibits Differentiation and Inflammation of Human Preadipocytes. *J. Nutr.* **2009**, *139*, 2055-2060 (2009).

26. Lii, C.-K., Huang, C.-Y., Chen, H.-W., Chow, M.-Y., Lin, Y.-R., Huang, C.-S., Tsai, C.-W. Diallyl Trisulfide Suppresses the Adipogenesis of 3T3-L1 Preadipocytes through ERK Activation. *Food Chem. Toxicol.* **2012**, *50*, 478-484.

27. Lai, Y.-S., Chen, W.-C., Ho, C.-T., Lu, K.-H., Lin, S.-H., Tseng, H.-C., Lin, S.-Y., Sheen, L.-Y. Garlic Essential Oil Protects against Obesity-Triggered Nonalcoholic Fatty Liver Disease through Modulation of Lipid Metabolism and Oxidative Stress. *J. Agric. Food Chem.* **2014**, *62*, 5897-5906.

28. Kim, M., Kim, H. Effect of Garlic on High Fat Induced Obesity. *Acta Biol. Hung.* **2011**, *62*, 244-254.

29. Joo, H., Kim, C.-T., Kim, I.-H., Kim, Y. Anti-Obesity Effects of Hot Water Extract and High Hydrostatic Pressure Extract of Garlic in Rats Fed a High-Fat Diet. *Food Chem. Toxicol.* **2013**, *55*, 100-105.

30. Bae, J., Kumazoe, M., Fujimura, Y., Tachibana, H. Diallyl Disulfide Potentiates Anti-Obesity Effect of Green Tea in High-Fat/High-Sucrose Diet-Induced Obesity. *J. Nutr. Biochem.* **2019**, *64*, 152-161.

31. Annamalai, S., Mohanam, L., Raja, V., Dev, A., Prabhu, V. Antiobesity, Antioxidant and Hepatoprotective Effects of Diallyl Trisulphide (DATS) Alone or in Combination with Orlistat on HFD Induced Obese Rats. *Biomed. Pharmacother.* **2017**, *93*, 81-87.

32. Xiao, J., Ching, Y.P., Liong, E.C., Nanji, A.A., Fung, M.L., Tipoe, G.L. Garlic-Derived *S*-Allylmercaptocysteine is a Hepato-Protective Agent in Non-Alcoholic Fatty Liver Disease In Vivo Animal Model. *Eur. J. Nutr.* **2013**, *52*, 179-191.

33. Yang, C., Li, L., Yang, L., Lǔ, H., Wang, S., Sun, G. Anti-Obesity and Hypolipidemic Effects of Garlic Oil and Onion Oil in Rats Fed a High-Fat Diet. *Nutr. Metab.* **2018**, *15*, 1-8.

34. Shoelson, S.E., Herrero, L., Naaz, A. Obesity, Inflammation, and Insulin Resistance. *Gastroenterology* **2007**, *132*, 2169-2180.

35. Sears, B., Ricordi, C. Anti-Inflammatory Nutrition as a Pharmacological Approach to Treat Obesity. *J. Obes.* **2010**, *2011*, 1-14.

36. Zhang, G., Parkin, K.L. *S*-Alk(en)ylmercaptocysteine: Chemical Synthesis, Biological Activities, and Redox-Related Mechanism. *J. Agric. Food Chem.* **2013**, *61*, 1896-1903.

37. Tocmo, R., Parkin, K. *S*-Alk(en)ylmercaptocysteine Suppresses LPS-Induced Pro-Inflammatory Responses in Murine Macrophages through Inhibition of NF-κB Pathway and Modulation of Thiol Redox Status. *Free Rad. Biol. Med.* **2018**, *129*, 548-558.

38. Reagan-Shaw, S., Nihal, M., Ahmad, N. Dose Translation from Animal to Human Studies Revisited. *FASEB J.* **2008**, *22*, 659-661.

39. Jouihan, H. Measurement of Liver Triglyceride Content. *Bio-protocol* **2012**, *2*, e223.

40. Neuman, M.G., Cohen, L.B., Manau, R.M. Biomarkers in Nonalcoholic Fatty Liver Disease. *Can. J. Gastroenterol. Hepatol.* **2014**, *28*, 607-618.

41. Noeman, S.A., Hamooda, H.E., Baalash, A.A. Biochemical Study of Oxidative Stress Markers in the Liver, Kidney and Heart of High Fat Diet Induced Obesity in Rats. *Diabetol. Metab.* **2011**, *3*, 1-8.

42. Hersoug, L.-G., Møller, P.; Loft, S. Role of Microbiota-Derived Lipopolysaccharide in Adipose Tissue Inflammation, Adipocyte Size and Pyroptosis During Obesity. *Nutr. Res. Rev.* **2018**, *31*, 153-163.

43. Furukawa, S., Fujita, T., Shimabukuro, M., Iwaki, M., Yamada, Y., Nakajima, Y., Nakayama, O., Makishima, M., Matsuda, M., Shimomura, I. Increased Oxidative Stress in Obesity and Its Impact on Metabolic Syndrome. *J. Clin. Invest.* **2017**, *114*, 1752-1761.

44. Parekh, S., Anania, F.A. Abnormal Lipid and Glucose Metabolism in Obesity: Implications for Nonalcoholic Fatty Liver Disease. *Gastroenterology* **2007**, *132*, 2191-2207.

45. Peh, M.T., Anwar, A.B., Ng, D.S., Atan, M.S.B.M., Kumar, S.D., Moore, P.K. Effect of Feeding a High Fat Diet on Hydrogen Sulfide (H_2S) Metabolism in the Mouse. *Nitric Oxide* **2014**, *41*, 138-145.

46. Katsouda, A., Szabo, C., Papapetropoulos, A. Reduced Adipose Tissue H_2S in Obesity. *Pharmacol. Res.* **2018**, *128*, 190-199.

47. Forman, H.J., Zhang, H., Rinna, A. Glutathione: Overview of Its Protective Roles, Measurement, and Biosynthesis. *Mol. Aspects Med.* **2009**, *30*, 1-12.

48. Sinha-Hikim, I., Sinha-Hikim, A.P., Shen, R., Kim, H., French, S.W., Vaziri, N.D., Crum, A., Rajavashisth, T.B., Norris, K.C. A Novel Cystine Based Antioxidant Attenuates Oxidative Stress And Hepatic Steatosis In Diet-Induced Obese Mice. *Exp. Mol. Pathol.* **2011**, *91*, 419-428.

49. Makki, K., Froguel, P., Wolowczuk, I. Adipose Tissue in Obesity-Related Inflammation and Insulin Resistance: Cells, Cytokines, and Chemokines. *Int. Sch. Res. Notices* **2013**, *2013*, 1-12.

50. Wong, S.W., Kwong, M.J., Choi, A.M.K., Kim, H.P., Nakahira, K., Hwang, D.H. Fatty Acids Modulate Toll-Like Receptor 4 Activation Through Regulation of Dimerization and Recruitment into Lipid Rafts in a Reactive Oxygen Species-Dependent Manner. *J. Biol. Chem.* **2009**, *284*, 27384-27392.

51. Lu, S.-P., Feng, M.-H.L., Huang, H.-L., Huang, Y.-C., Tsou, W.-I., Lai, M.-Z. Reactive Oxygen Species Promote Raft Formation in T Lymphocytes. *Free. Radic. Biol. Med.* **2007**, *42*, 936-944.

52. Pereira, S.S., Alvarez-Leite, J.I. Low-Grade Inflammation, Obesity, and Diabetes. *Curr. Obes. Rep.* **2014**, *3*, 422-432.

53. Reilly, S.M., Saltiel, A.R. Adapting to Obesity with Adipose Tissue Inflammation. *Nat. Rev. Endocrinol*. **2017**, *13*, 633-643.

54. Thomas, D.J., Parkin, K.L. Quantification of Alk(en)yl-L-cysteine Sulfoxides and Related Amino Acids in Alliums by High-Performance Liquid Chromatography. *J. Agric. Food Chem.* **1994**, *42*, 1632-1638.

55. Chapman, M.E., Hu, L., Plato, C.F., Kohan, D.E. Bioimpedance Spectroscopy for the Estimation of Body Fluid Volumes in Mice. *Am. J. Physiol. Renal Physiol.* **2010**, *299*, F280-F283.

56. Yang, M., Dong, Z., Jiang, X., Zhao, Z., Zhang, J., Cao, X., Zhang, D. Determination of *S*-Allylmercaptocysteine in Rat Plasma by LC-MS/MS and Its Application to a Pharmacokinetics Study. *J. Chromatogr. Sci.* **2018**, *56*, 396-402.

Chapter 6

Conclusions and Future Work

The current research examined the two major asymmetric cysteine conjugates of *Allium* organosulfur species that exhibit potent biological effects, *S*-allylmercaptocysteine (CySSA) and *S*-1-propenylmercaptocysteine (CySSPe). These mercaptocysteines are known to be transformation products of cysteine and cysteine-containing compounds with thiosulfinates and other *Allium* organosulfur compounds (1-3). Research on these compounds has largely focused on the garlic derivative, CySSA, previously shown to attenuate oxidation (4,5), inflammation (5), and carcinogenesis (6). However, the major onion derivative CySSPe exerts similar or more potent chemoprotective and anti-inflammatory properties in Hepa1c1c7 hepatocytes and RAW 264.7 macrophage cells compared to CySSA (1,7). Furthermore, CySSPe appears to modulate oxidative stress and inflammation through a glutathione-dependent mechanism involving the upregulation of Nrf2 and several antioxidant enzymes (8). However, there remains few studies that have been conducted to examine the biological properties of CySSPe *in vitro* and none *in vivo*. The work described in this dissertation extends knowledge regarding CySSA and primarily the less well-studied CySSPe regarding their biological effects and mechanisms of action in cell culture. Additionally, the work here describes what is believed to be the first animal study conducted to evaluate the *in vivo* biological effects of CySSPe.

In this work, CySSPe was shown to exhibit higher hydrogen sulfide (H_2S)-releasing properties in comparison to CySSA from *in chemico* studies with glutathione and cell culture incubations. H_2S may be a marker of persulfide formation (9) and these results could indicate that CySSPe is more readily metabolized to persulfides via a glutathione and enzyme-dependent mechanism versus CySSA. Previous work confirmed CySSPe treatment of hepatocytes leads to elevated persulfide levels (8). Persulfides are highly reactive organosulfur species that can rapidly quench reactive oxygen species (ROS) and modulate signaling pathways, including Nrf2-

Keap1 (10). More rapid metabolism of CySSPe to persulfide and H_2S may be linked to the enhanced bioactivities demonstrated by CySSPe over other mercaptocysteines.

The research work described supports the inclusion of onions and onion-derived compounds in the diet as an intervention for inflammation. Studies have shown an inverse correlation between fruit and vegetable intake and inflammatory markers tumor necrosis factor alpha (TNF-α) and interleukin 6 (IL-6) in the serum (11,12). Furthermore, the inclusion of *Allium* vegetables in the diet has been correlated with reductions in gastric cancer and cardiovascular disease risk (13-15). The preclinical study described in chapter 5 used physiologically attainable doses of compounds that could be generated in whole foods and suggests that the anti-inflammatory effects from onion 1-propenylmercapto equivalents occurs at levels reached through routine consumption. CySSPe was shown to suppress pro-inflammatory cytokines TNF-α and IL-6 in the plasma and TNF-α, IL-6, and IL-1β in liver, which is consistent with in vitro evidence from the literature (7). Both CySSA and CySSPe were also shown to act on the IKKα/β/NF-κB axis alongside the p38 MAPK pathway in inhibiting LPS-induced NO production in macrophages. Therefore, the *in vivo* anti-inflammatory effects of CySSPe may be mediated by inhibition of both NF-κB and p38 signaling as part of their mechanisms of action, and experiments could be carried out to evaluate if CySSPe treatment decreases the protein levels of these transcriptional regulators and the (de)phosphorylation activities of kinases upstream or downstream of these pathways in animals.

In this research, CySSPe conjugate species were shown to generate H_2S in the presence of biologically relevant thiols and in cell culture. The ability of CySSPe to release H_2S in biological settings could be further investigated as a therapeutic compound in conditions where other H_2S donors has been shown to suppress inflammation and oxidative stress (16,17). Several

pharmacological agents have been designed to release H_2S under physiological conditions and shown to suppress inflammation. These H_2S donors inhibit the activation of NF-κB, infiltration of leukocytes, and pro-inflammatory cytokine synthesis. Elevated levels of H_2S can also rescue cells from oxidative stress by activating Nrf2 through the *S*-sulfhydration of Keap1 (18). Proteome-wide analysis of five human cell lines revealed 994 proteins are persulfidated following treatment with H_2S (19). These persulfide-modified proteins are collective grouped as the persulfidome, and a detailed portion of these proteins can be found in the supplemental materials Supplementary Data Set 1 and 2 of reference 20 and Table S1 and Data S5 of reference 21. Additionally, the presence of H_2S biosynthesis enzymes cystathionine β-lyase (CBS) and cystathionine γ-synthase (CSE) may be important mediators of CySSPe bioactivity. It would be interesting to compare the H_2S and H_2S-evolving enzyme levels between animals treated with CySSPe and CySSA. An investigation into whether or not CBS and CSE knockout mice exhibit attenuated suppression of pro-inflammatory cytokines production by CySSPe could provide a link between the anti-inflammatory effects exerted by CySSPe and H_2S/H_2S synthesizing enzymes. Furthermore, proteomic mapping of persulfidated sites following *in vitro* and *in vivo* treatment with CySSPe could be investigated to evaluate if CySSPe persulfidates multiple protein targets involved in glycolysis, NF-κB signaling, and redox regulatory processes (19-21). Proteomic network analysis of the global protein expression from lipopolysaccharide (LPS)-activated RAW 264.7 cells was previously conducted (22,23), and analysis of the overlap between the previously mentioned persulfidome and this inflammatory proteome could be applied to determine which proteins may be potential targets of CySSPe-mediated persulfidation following inflammatory challenge and CySSPe treatment. In light of the results of this study and previous research, H_2S is likely to be merely a biomarker of persulfide thiol-exchange, and that

the primary bioactive intermediate that exerts the bioactivity of mercaptocysteines are their persulfide metabolites.

The work herein also demonstrated that CySSA and CySSPe activate Nrf2 and upregulate antioxidant proteins in activated macrophages. LPS-dependent inflammatory signaling is triggered by binding of LPS to the Toll-like receptor 4 (TLR4) and the recruitment of NADPH oxidase 4 (NOX4), a membrane-bound oxidative stress sensor (24). Suppression of oxidative stress by CySSPe-induced Nrf2 activation and subsequent upregulation of associated cytoprotective proteins, which would impede TLR4 signaling and downstream activation of NF-κB, could be one mechanism by which these compounds exhibits its anti-inflammatory properties. Given that CySSPe activates Nrf2 through a persulfide-related mechanism (8), an important line of research could include evaluating if CySSPe upregulates Nrf2 and improves antioxidant defenses *in vivo* as a mechanism by which CySSPe suppresses inflammation. It would be important to evaluate if Nrf2-linked antioxidant enzyme levels, such as thioredoxin reductase (TrxR), heme oxygenase-1 (HO-1), cysteine glutamate ligase (CGL), and quinone reductase (QR), are elevated in liver tissues following treatment of animals with CySSPe. Glutathione-dependent enzymes and proteins, such as glutathione reductase (GR), glutathione-S-transferase (GST), glutaredoxins (Grx) and glutathione peroxidase (GPx), are of particular interest as enzymes of the cellular protective systems against oxidative stress.

Previous work has shown that CySSR are imported into cells by the xCT cysteine transporter and reduced by a Grx-dependent process to give cysteine and alkyl mercaptans (25). Allyl mercaptan from garlic derivative CySSA has been shown to be subsequently methylated and oxidized to give allyl methyl sulfone *in vivo* (26,27). CySSA is rapidly metabolized with a half-life of less than 5 minutes when administered intraperitoneally (28). However, it is unclear

what metabolic transformations occur with CySSPe and its thiol product, 1-propenyl mercaptan, which may also be rapidly metabolized and not reach therapeutically effective blood and tissue concentrations. Studying the *in vivo* pharmokinetics of CySSPe would provide insight into if physiological concentrations of CySSPe reach the levels necessary to activate Nrf2 and inhibit NF-κB at the doses used in this and previous work (7,8).

References

1. Zhang, G., Li, B., Lee, C.-H., Parkin, K.L. Cysteine and Glutathione Mixed-Disulfide Conjugates of Thiosulfinates: Chemical Synthesis and Biological Activities. *J. Agric. Food Chem.* **2010**, *58*, 1564-1571.

2. Zhang, G., Parkin, K.L. A Tissue Homogenate Method To Prepare Gram-Scale *Allium* Thiosulfinates and Their Disulfide Conjugates with Cysteine and Glutathione. *J. Agric. Food Chem.* **2013**, *61*, 3030-3038.

3. Liang, D., Wu, H., Wong, M.W., Huang, D. Diallyl Trisulfide Is a Fast H_2S Donor, but Diallyl Disulfide Is a Slow One: The Reaction Pathways and Intermediates of Glutathione with Polysulfides. *Org. Lett.* **2015**, *17*, 4196-4199.

4. Xiao, J., Liong, E.C., Ling, M.-T., Ching, Y.-P., Fung, M-L., Tipoe, G.L. *S*-Allylmercaptocysteine Reduces Carbon Tetrachloride-Induced Hepatic Oxidative Stress and Necroinflammation via Nuclear Factor Kappa B-Dependent Pathways in Mice. *Eur. J. Nutr.* **2012**, *51*, 323-333.

5. Zhu, X., Jiang, X., Li, A., Zhao, Z., Li, S. *S*-Allylmercaptocysteine Attenuates Cisplatin-Induced Nephrotoxicity through Suppression of Apoptosis, Oxidative Stress, and Inflammation. *Nutrients* **2017**, *9*, 1-16.

6. Zhu, X., Jiang, X., Li, A., Sun, Y., Liu, Y., Sun, X., Feng, X., Li, S., Zhao, Z. *S*-Allylmercaptocysteine Suppresses the Growth of Human Gastric Cancer Xenografts through Induction of Apoptosis and Regulation of MAPK and PI3K/Akt Signaling Pathways. *Biochem. Biophys. Res. Commun.* **2017**, *491*, 821-826.

7. Tocmo, R., Parkin, K. *S*-Alk(en)ylmercaptocysteine Suppresses LPS-Induced Pro-Inflammatory Responses in Murine Macrophages through Inhibition of NF-Kb Pathway and Modulation of Thiol Redox Status. *Free Rad. Biol. Med.* **2018**, *129*, 548-558.

8. Tocmo, R., Parkin, K. *S*-1-Propenylmercaptocysteine Protects Murine Hepatocytes Against Oxidative Stress via Persulfidation of Keap1 and Activation of Nrf2. *Free Rad. Biol. Med.* **2019**, *143*, 164-175.

9. Ida, T., Sawa, T., Ihara, H., Tsuchiya, Y., Watanabe, Y., Kumagai, Y., Suematsu, M., Motohashi, H., Fujii, S., Matsunaga, T., Yamamoto, M., Ono, K. Devarie-Baez, N.O., Xian, M., Fukuto, J.M., Akaike, T. Reactive Cysteine Persulfides and *S*-Polythiolation Regulate Oxidative Stress and Redox Signaling. *Proc. Natl. Acad. Sci. USA* **2014**, *111*, 7606-7611.

10. Filipovic, M.R., Zivanovic, J., Alvarez, B., Banerjee, R. Chemical Biology of H_2S Signaling through Persulfidation. *Chem. Rev.* **2018**, *118*, 1253-1337.

11. Holt, E.M., Steffen, L.M., Moran, A., Basu, S., Steinberger, J., Ross, J.A., Hong, C.-P., Sinaiko, A.R. Fruit and Vegetable Consumption and Its Relation to Markers of Inflammation and Oxidative Stress in Adolescents. *J. Am. Diet. Assoc.* **2009**, *109*, 414-421 (2009).

12. Root, M.M., McGinn, M.C., Nieman, D.C., Henson, D.A., Heinz, S.A., Shanely, R.A., Knab, A.M., Jin, F. Combined Fruit and Vegetable Intake is Correlated with Improved Inflammatory and Oxidant Status from a Cross-Sectional Study in a Community Setting. *Nutrients* **2012**, *4*, 29-41.

13. Zhou, Y., Zhuang, W., Hu, W., Liu, G.-J., Wu, T.-X., Wu, X.-T. Consumption of Large Amounts of *Allium* Vegetables Reduces Risk for Gastric Cancer in a Meta-Analysis. *Gastroenterology* **2011**, *141*, 80-89.

14. Blekkenhorst, L.C., Bondonno, C.P., Lewis, J.R., Devine, A., Zhu, K., Lim, W.H., Woodman, R.J., Beilin, L.J., Prince, R.L., Hodgson, J.M. Cruciferous and Allium Vegetable Intakes are Inversely Associated with 15-Year Atherosclerotic Vascular Disease Deaths in Older Adult Women. *J. Am. Heart Assoc.* **2017**, *6*, 1-15.

15. Bahadoran, Z., Mirmiran, P., Momenan, A.A., Azizi, F. Allium Vegetable Intakes and Incidence of Cardiovascular Disease, Hypertension, Chronic Kidney Disease, and Type 2 Diabetes in Adults: A Longitudinal Follow-Up Study. *J. Hypertens.* **2017**, *35*, 1909-1916.

16. Wallace, J.L. Hydrogen Sulfide-Releasing Anti-Inflammatory Drugs. *Trends Pharmacol Sci.* **2007**, *28*, 501-505.

17. Powell, C.R., Dillon, K.M., Matson, J.B. A Review of Hydrogen Sulfide (H_2S) Donors: Chemistry and Potential Therapeutic Applications. *Biochem. Pharmacol.* **2018**, *149*, 110-123.

18. Yang, G., Zhao, K., Ju, Y., Mani, S., Cao, Q., Puukila, S., Khaper, N., Wu, L., Wang, R. Hydrogen Sulfide Protects Against Cellular Senescence *via S*-Sulfhydration of Keap1 and Activation of Nrf2. *Antioxid. Redox Signal.* **2013**, *18*, 1906-1919.

19. Fu, L., Liu, K., He, J., Tian, C., Yu, X., Yang, J. Direct Proteomic Mapping of Cysteine Persulfidation. *Antioxid. Redox Signal.* [Online early access]. DOI: 10.1089/ars.2019.7777. Published Online: Sept 9, 2019. https://www.liebertpub.com/doi/full/10.1089/ars.2019.7777 (accessed July 8, 2020).

20. Wu, Q., Zhao, B., Weng, Y., Shan, Y., Li, X., Hu, Y., Liang, Z., Yuan, H., Zhang, L., Zhang, Y. Site-Specific Quantification of Persulfidome by Combining an Isotope-Coded Affinity Tag with Strong Cation-Exchange-Based Fractionation. *Anal. Chem.* **2019**, *91*, 14860-14864.

21. Zivanovic, J., Kouroussis, E., Kohl, J.B., Adhikari, B., Bursac, B., Schott-Roux, S., Petrovic, D., Miljkovic, J.L., Thomas-Lopez, D., Jung, Y., Miler, M., Mitchell, S.,

Milosevic, V., Gomes, J.E., Benhar, M., Gonzalez-Zorn, B., Ivanovic-Burmazovic, I., Torregrossa, R., Mitchell, J.R., Whiteman, M., Schwarz, G., Snyder, S.H., Paul, B.D., Carroll, K.S., Filipovic, M.R. Selective Persulfide Detection Reveals Evolutionary Conserved Antiaging Effects of *S*-Sulfhydration. *Cell Metab.* **2019**, *30*, 1152-1170.

22. Kamal, A.H.M., Chakrabarty, J.K., Udden, S.M.N., Zaki, M.H., Chowdhury, S.M. Inflammatory Proteomic Network Analysis of Statin-Treated and Lipopolysaccharide-Activated Macrophages. *Sci. Rep.* **2018**, *8*, 1-13.

23. Kamal, A.H.M., Fessler, M.B., Chowdhury, S.M. Comparative and Network-Based Proteomic Analysis of Low Dose Ethanol- and Lipopolysaccharide-Induced Macrophages. *PLoS One* **2018**, *13*, 1-22.

24. Brandes, R.P., Weissmann, N., Schröder, K. Nox Family NADPH Oxidases: Molecular Mechanisms of Activation. *Free Rad. Biol. Med.* **2014**, *76*, 208-226.

25. Zhang, G., Parkin, K.L. *S*-Alk(en)ylmercaptocysteine: Chemical Synthesis, Biological Activities, and Redox-Related Mechanism. *J. Agric. Food Chem.* **2013**, *61*, 1896-1903.

26. German, E., Auger, J., Ginies, C., Siess, M.-H., Teyssier, C. In Vivo Metabolism of Diallyl Disulphide in the Rat: Identification of Two New Metabolites. *Xenobiotica* **2002**, *32*, 1127-1138.

27. Scheffler, L., Sauermann, Y., Heinlein, A., Sharapa, C., Buettner, A. Detection of Volatile Metabolites Derived from Garlic *(Allium sativum)* in Human Urine. *Metabolites* **2016**, *6*, 1-23.

28. Yang, M., Dong, Z., Jiang, X., Zhao, Z., Zhang, J., Cao, X., Zhang, D. Determination Of S-Allylmercaptocysteine in Rat Plasma by LC-MS/MS and its Application to a Pharmacokinetics Study. *J. Chromatogr. Sci.* **2018**, *56*, 396-402.

Appendix

A.2 Supplemental Materials for Chapter 2

A.2.1 Supplemental Figures

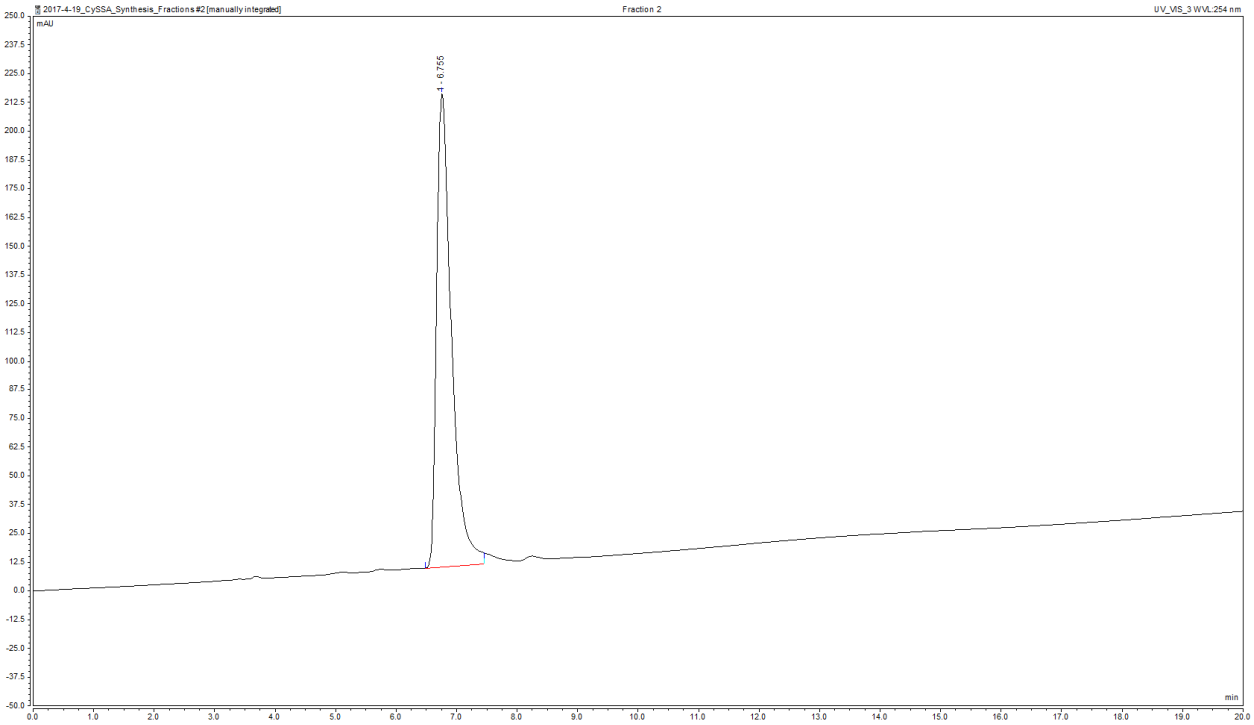

Figure A.2.1.S1. HPLC chromatogram of purified *S*-allylmercaptocysteine (CySSA) with a retention time of 6.76 min, eluted with 30:70 MeOH/H_2O (0.5% acetic acid) on a C18 column and flow rate of 0.8 mL/min.

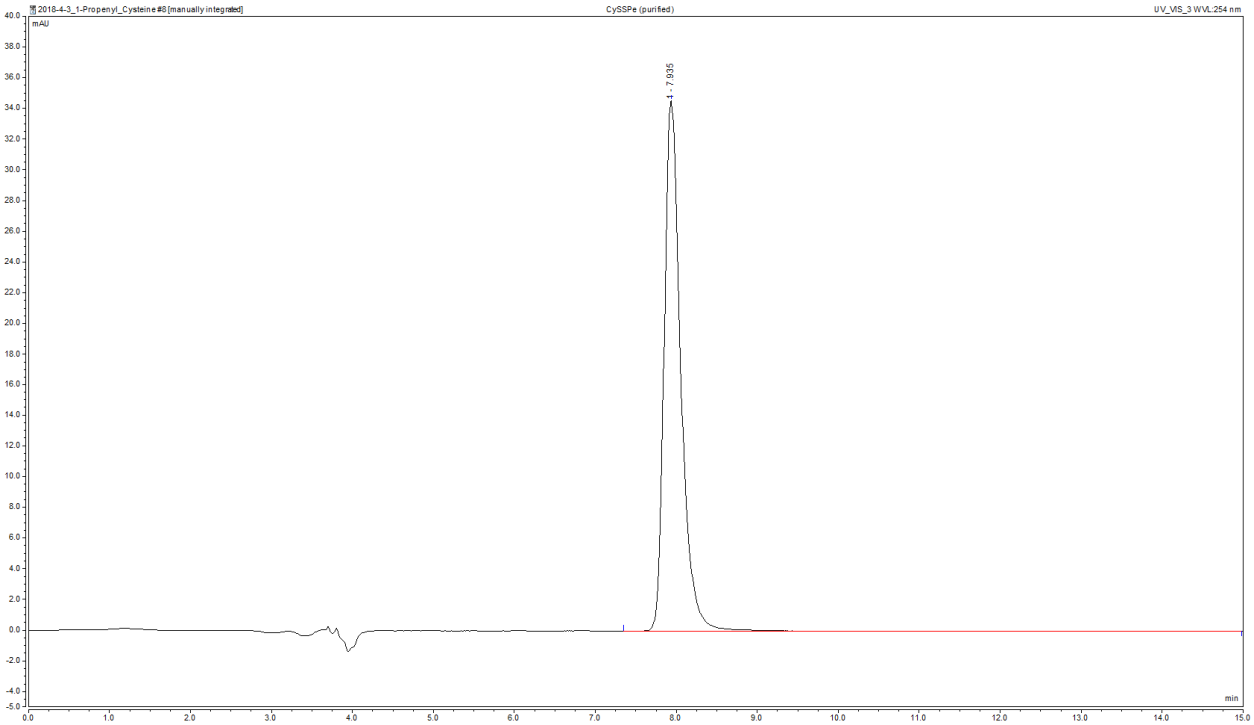

Figure A.2.1.S2. HPLC chromatogram of purified *S*-1-propenylmercaptocysteine (CySSPe) with retention time of 7.94 min, eluted with 30:70 MeOH/H_2O (0.5% acetic acid) on a C18 column and flow rate of 0.8 mL/min.

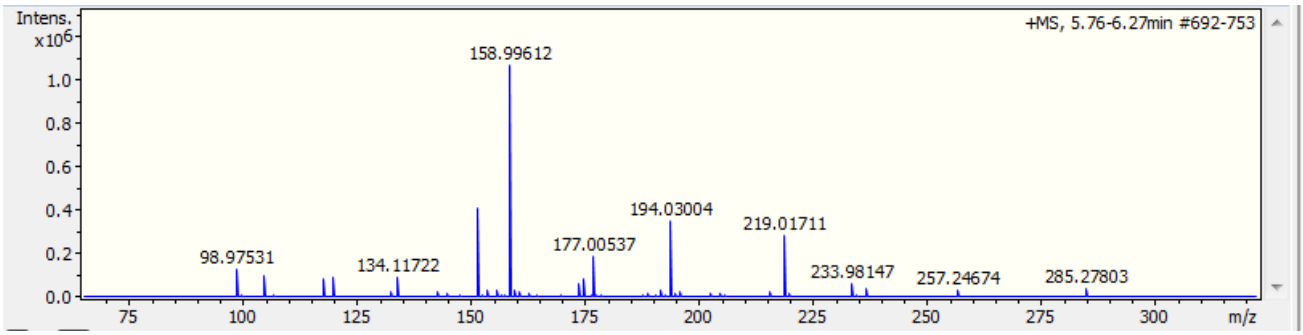

Figure A.2.1.S3. Mass spectrometry chromatogram of CySSA. $[M+H]^+$ m/z calculated = 194.0309, found = 194.03004

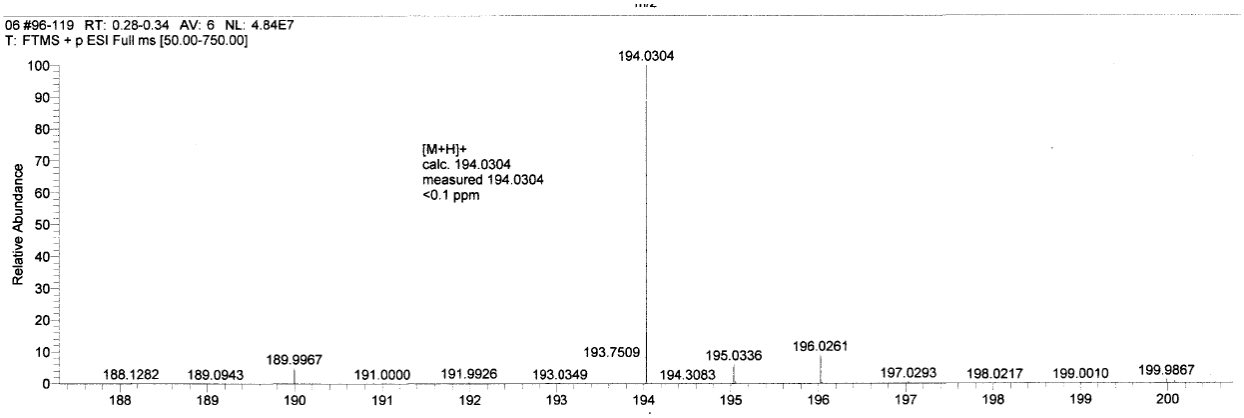

Figure A.2.1.S4. Mass spectrometry chromatogram of CySSPe. $[M+H]^+$ m/z calculated = 194.0304, found = 194.0304

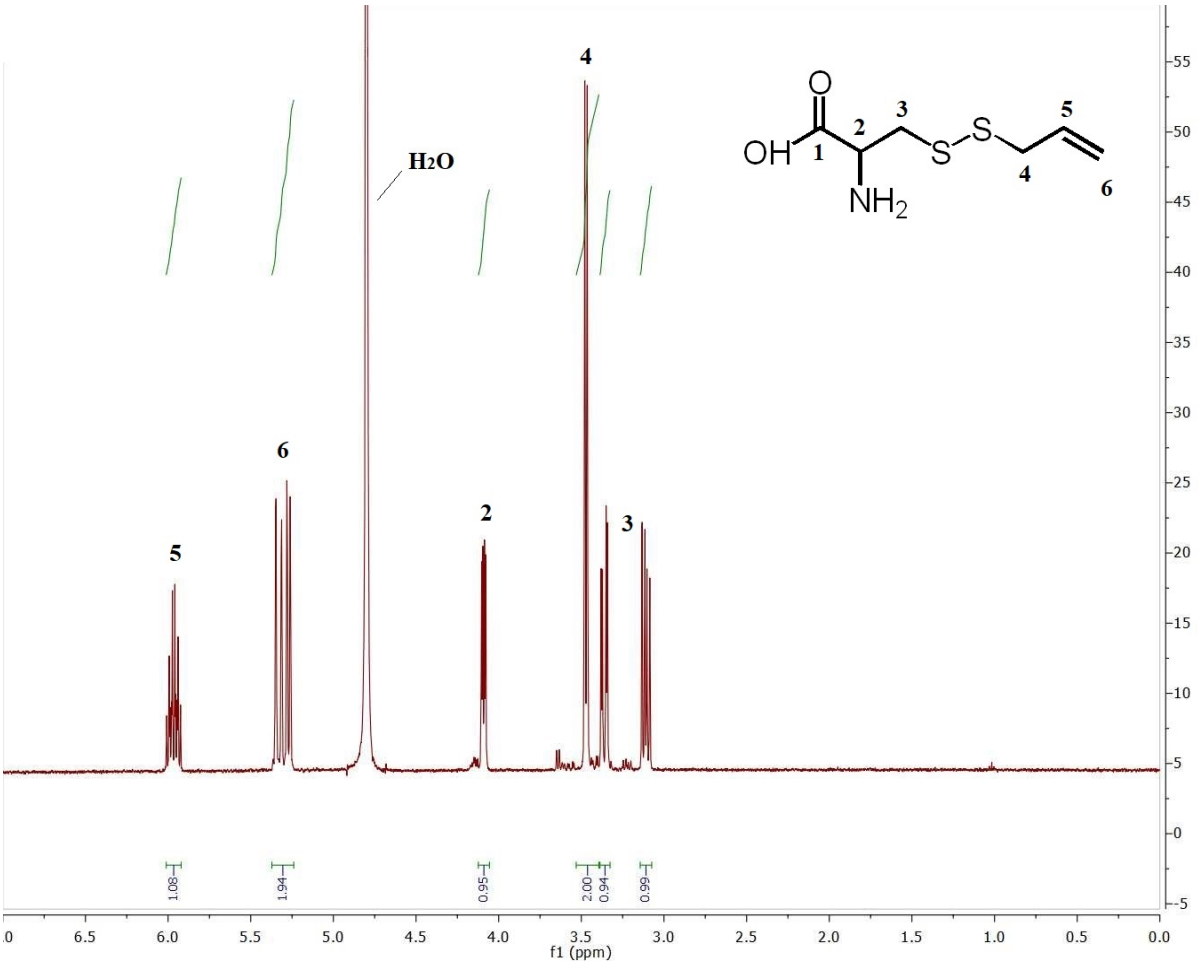

Figure A.2.1.S5. ^{1}H NMR (500 MHz, D_2O) of CySSA.

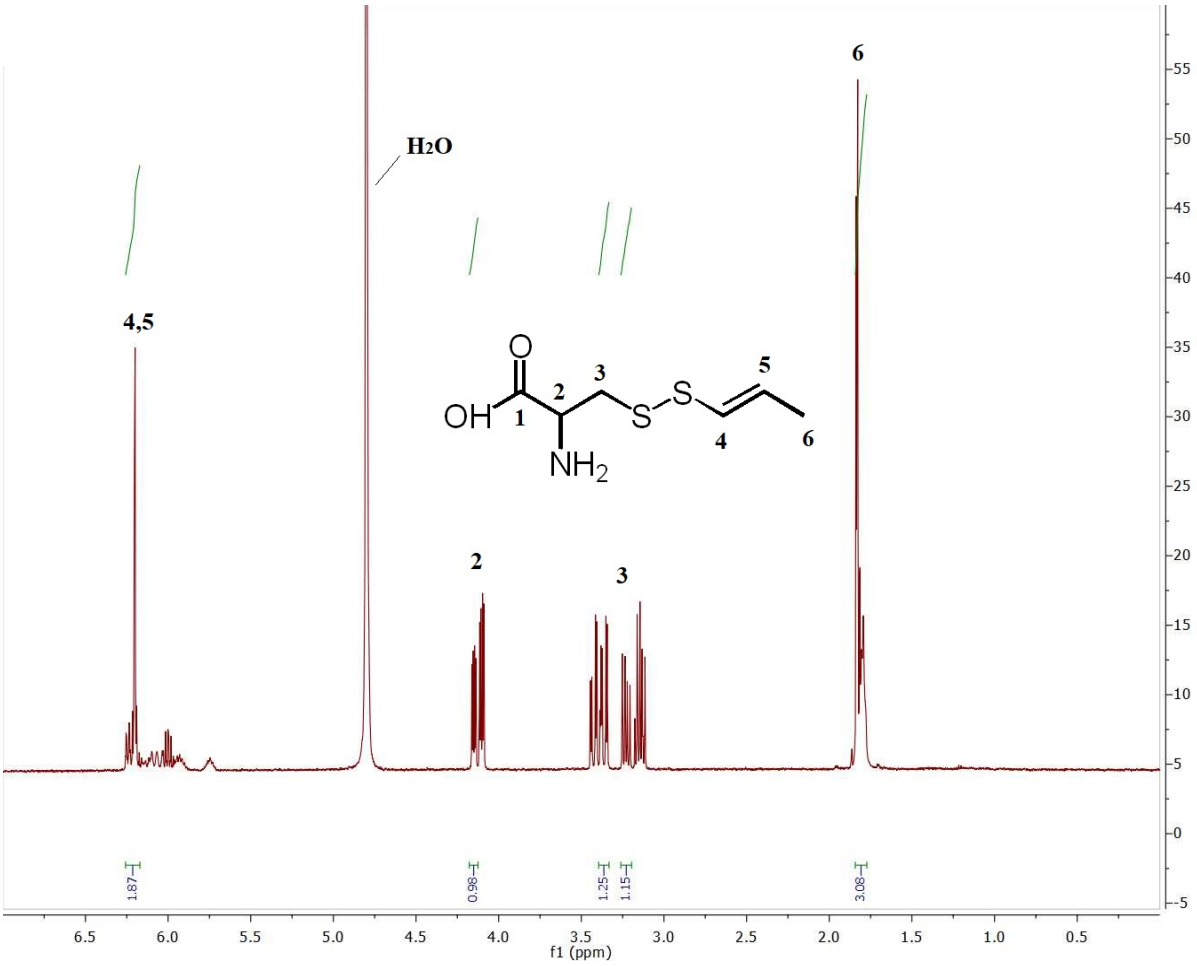

Figure A.2.1.S6. ^{1}H NMR (500 MHz, D_2O) of CySSPe.

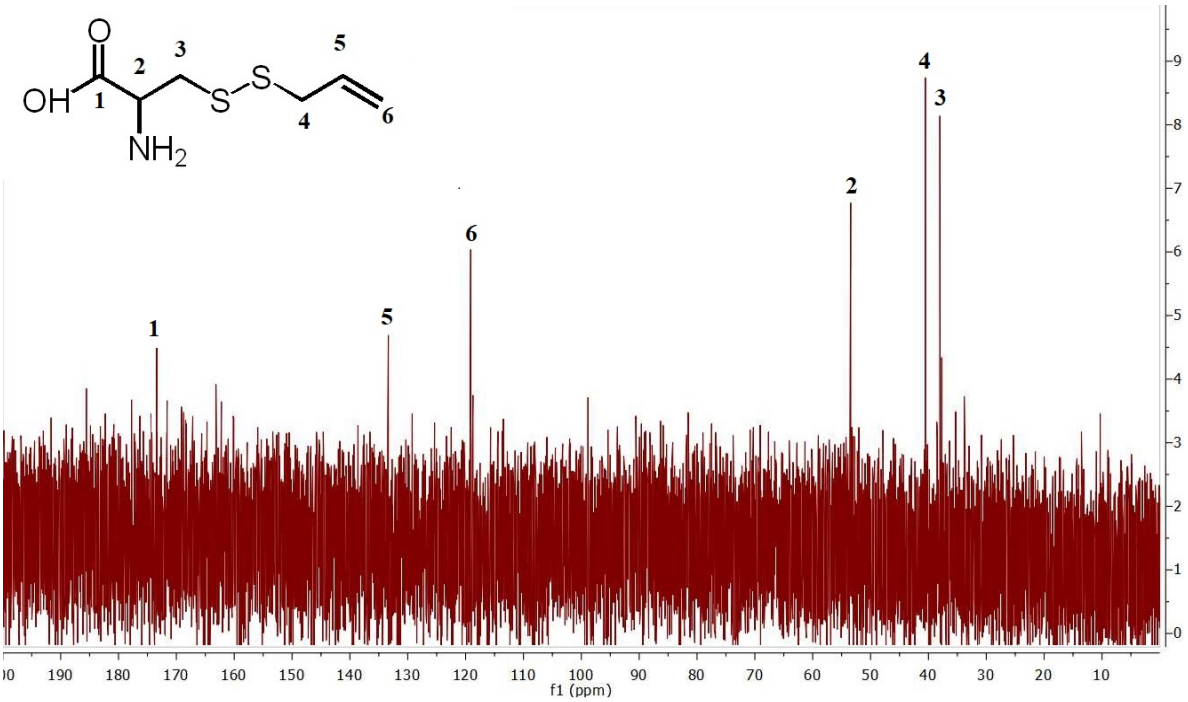

Figure A.2.1.S7. ^{13}C NMR (125 MHz, D_2O) of CySSA.

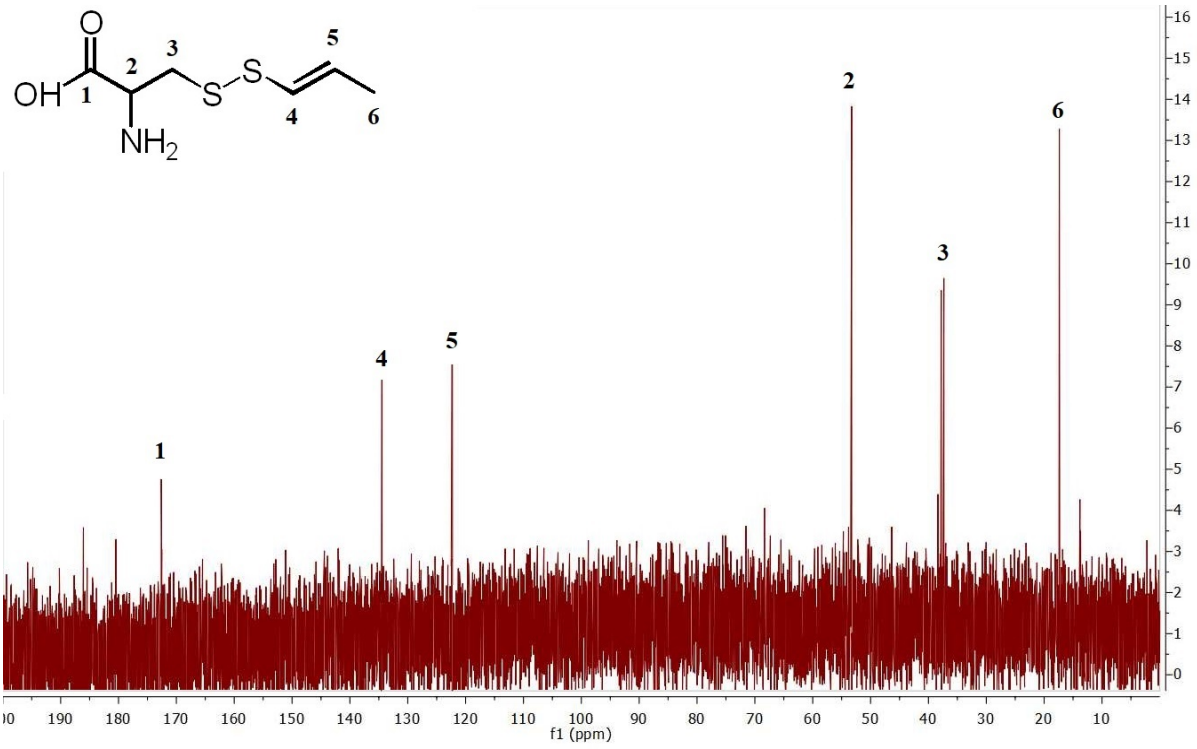

Figure A.2.1.S8. ^{13}C NMR (125 MHz, D_2O) of CySSPe.

A.2.2 Supplemental Tables

Table A.2.2.S1. Tabulated ^{1}H NMR peaks for CySSA and CySSPe (in ppm).

Position	CySSA	CySSPe
2	4.09 (dd, *J* = 8.7, 3.9 Hz, 1H)	4.15 (dd, *J* = 8.2, 3.9 Hz, 1H)
3	3.11 (dd, *J* = 14.8, 8.7 Hz, 1H) 3.36 (dd, *J* = 14.8, 3.9 Hz, 1H)	3.18 (m, 1H) 3.39 (m, 1H)
4	3.47 (d, *J* = 7.4 Hz, 2H)	6.2 (m, 1H)
5	5.97 (ddt, *J* = 17.2, 10.0, 7.4 Hz, 1H)	6.2 (m, 1H)
6	5.30 (m, 2H)	1.83 (m, 3H)

Table A.2.2.S2. Tabulated ^{13}C NMR peaks for CySSA and CySSPe (in ppm).

Position	CySSA	CySSPe
1	173.8	172.8
2	53.4	53.3
3	38.0	37.8
4	40.5	134.6
5	133.4	122.3
6	119.1	17.4